CRYSTAL ENGINEERING STUDIES ON THE MOLECULAR SALTS AND SILVER(I) COORDINATION COMPOUNDS FOR [2 + 2] CYCLOADDITION REACTION IN THE SOLID STATE

GOUTAM KUMAR KOLE

(M.Sc., Indian Institute of Technology Madras, Chennai, India)

A THESIS SUBMITTED

FOR THE DEGREE OF DOCTOR OF PHILOSOPHY

DEPARTMENT OF CHEMISTRY

NATIONAL UNIVERSITY OF SINGAPORE

2011

To all of my Teachers and Well-wishers

Acknowledgements

Thesis Declaration

This work described in this thesis is the original work, performed independently under the supervision of Prof. Jagadese J. Vittal, (in the 'Inorganic Materials and Supramolecular Chemistry' laboratory, S8-05-15), Department of Chemistry, National University of Singapore, between 06 August, 2007 and 05 August, 2011. The content of this thesis has not been submitted for a degree at this or any other university before.

Goutam Kumar Kole	*Goutam Kumar Kole*	15 August, 2011
Name	Signature	Date

Table of Contents

Chapter 1

Chapter 2

Chapter 3

Chapter 8

Abbreviations and Symbols

1 D	One Dimensional
2,2'-bpe	*trans*-1,2-bis(2'-pyridyl)ethylene
3-PAH	*trans*-3-(3'-Pyridyl) acrylic acid
4,4'-bpdb	1,4-Bis(4'-pyridyl)-2,3-diaza-1,3-butadiene
4,4'-bpe or bpe	1,2-Bis(4'-pyridyl)ethylene
4,4'-bpethane	*trans*-1,2-Bis(4'-pyridyl)ethane
4,4'-bpy or bpy	4,4'-Bipyridine
4-AP	4-Aminopyridine
4-PAH	*trans*-3-(4'-Pyridyl) acrylic acid
4-SP	4-styrylpyridine
Å	Angstrom
a. u.	Arbitrary Unit
bta	1,2,3,4-Benzenetetracarboxylic acid
CIF	Crystallographic Information File
CP	Coordination Polymer
cyclohexa	Cyclohexylamine
d	Doublet
DAB	1,4-Diaminobutane
DAP	1,3-Diaminopropane
DBEA	2,2′-Dithiobisethanammonium cation
dd	Doublet of doublet
deg.	Degree
DPA	3,3′-Dipropylaminoamine
dppe	1,2-Bis(diphenylphosphino)ethane
dppm	1,1-Bis(diphenylphosphino)methane
dppp	1,3-Bis(diphenylphosphino)propane
EDA	Ethylenediamine
FT-IR	Fourier Transform Infrared
Guan	Guanidinium cation
h	Hour
H_2SDC	*trans*-4,4'-Stilbenedicarboxylic acid
HH	Head-to-head
HH-3,3-BPCD	1,2-bis(3'-pyridyl)cyclobutane-3,4-dicarboxylic acid
HH-4,4-BCBPCB	1,2-Bis(4'-carboxyphenyl)-3,4-bis(4"-pyridyl)cyclobutane

HH-4,4-BPCD	1,2-bis(4'-pyridyl)cyclobutane-3,4-dicarboxylic acid
HPVBA	4-*trans*-2-(pyrid-4'-yl-vynyl) benzoic acid
HT	Head-to-tail
HT-3,3-BPCD	2,4-bis(3'-pyridyl)cyclobutane-1,3-dicarboxylic acid
HT-4,4-BCBPCB	1,3-Bis(4'-carboxyphenyl)-2,4-bis(4''-pyridyl)cyclobutane
HT-4,4-BPCD	2,4-bis(4'-pyridyl)cyclobutane-1,3-dicarboxylic acid
m	Multiplet
min	Minute
MOF	Metal Organic Framework
NMR	Neuclear Magnetic Resonance
PCP	Porous Coordination Polymer
pcu	Primitive Cubic
Pip	Piperizinium cation
ppm	Parts per million
PXRD	Powder X-ray Diffraction
rctc	*Regio-cis-trans-cis*
rctt	*Regio-cis-trans-trans*
s	Singlet
SCSC	Single crystal to single crystal
t	Triplet
TCCB	1,2,3,4-tetrakis-(4'-Carboxyphenyl)cyclobutane
TFA	Trifluoroacetate
TGA	Thermogravimertic Analysis
UV	Ultra-violet
wt	Weight

Summary

This thesis describes syntheses and characterization of several molecular salts and silver(I) coordination compounds of certain linear olefins. The relative orientations of these olefins in the solid state structures of these molecular salts and silver coordination compounds were analysed in terms of their solid state [2 + 2] cycloaddition reaction to synthesize a particular isomer of the corresponding cyclobutane compounds. These cyclobutane derivatives can serve as potential ligands for making co-crystals and coordination polymers.

The first chapter of this thesis provides the background research in this field briefly and reviews the current interest on molecular salts, co-crystals and polymeric and discrete coordination compounds especially on Ag(I) coordination compounds. It also describes the present challenges on the [2 + 2] cycloaddition reaction in the solid state and scope of this thesis.

Chapter 2 describes several molecular salts of *trans*-4,4'-stilbenedicarboxylic acid (H_2SDC) with various amines. The ionic synthons or charge assisted hydrogen bonding make all these salts very stable. The orientations of SDC^{2-} anions have been analysed and their photoreactivity have been studied. The hydrated molecular salt with 1,3-diaminopropane undergoes quantitative photodimerization, whereas the salts with the analogous bases ethylenediamine and 1,4-diaminobutane do not. Although the SDC^{2-} anions are oriented parallel in a salt with 4-aminopyridine, its photostability has been accounted from Schmidt's distance criteria. The mechanochemical grinding route has also been explored in this chapter to access a new tetracarboxylic acid ligand 1,2,3,4-tetrakis(4′-carboxyphenyl)cyclobutane (TCCB).

In Chapter 3, the solid state photodimerization of *trans*-3-(4'-pyridyl)acrylic acid (4-PAH) and *trans*-3-(3'-pyridyl)acrylic acid (3-PAH) are discussed. The photo-

inert 4-PAH has been made photoreactive by forming molecular salts with various strong acids where the anions present in these salts are found to have tremendous influence on its packing. The monovalent anions like Cl^-, $CF_3CO_2^-$, ClO_4^-, BF_4^- help to align 4-PAH$_2^+$ cations in *head-to-tail* parallel orientation which result in the formation of HT-photodimer 2,4-bis(4'-pyridyl)cyclobutane-1,3-dicarboxylic acid (HT-4,4-BPCD). On the other hand, the presence of both sulphate and bisulphate anions in the hydrated salt obtained with H_2SO_4 makes it very interesting; where 4-PAH$_2^+$ cations are found to orient in infinite *head-to-head* parallel arrangement. The single crystals of this salt undergoes 66% photodimerization, whereas the ground powder which absorbs an extra molecule of water during grinding, undergoes quantitative conversion to HH-photodimer 3,4-bis(4'-pyridyl)cyclobutane-1,2-dicarboxylic acid (HH-4,4-BPCD). The associated structural transformation has been attributed to the absorption of moisture during grinding that changes composition, crystal structure and photoreactivity, which is described in Chapter 3. In short, the stereoselective syntheses of two photodimer of 4-PAH is achieved just by tuning the anions present in the salts.

Unlike 4-PAH, 3-PAH is photoreactive in the solid state and known to undergo 66% photodimerization in *head-to-head* fashion. Therefore, it was a challenge to align 3-PAH in *head-to-tail* fashion in the solid state. By extending our strategy of salt formation, the HT-parallel orientation of 3-PAH$_2^+$ cations has been achieved and the corresponding HT-photodimer 2,4-bis(3'-pyridyl)cyclobutane-1,3-dicarboxylic acid (HT-3,3-BPCD) has been synthesized in quantitative yield. Interestingly, all these pyridyl based cyclobutane compounds undergo isomerisation from *rctt-* (as synthesized form) to *rctc-* forms in the presence of H^+ and the mechanistic details of such isomerisation have been discussed.

Chapter 4 deals with the solid state photodimerization of 4-*trans*-2-(pyrid-4-yl-vynyl) benzoic acid (HPVBA) as the extension of the synthetic strategy that is

presented in chapter 3. H_2PVBA^+ undergoes photodimerization in HT-fashion for ClO_4^-, NO_3^- and also for sulphate-bisulphate. When HPVBA is allowed to react with excess amount of H_2SO_4 in water, the yellow precipitate obtained undergoes photodimerization in HH-fashion. For HPVBA, we also have explored the carboxylic acid functionality to make salts with 1,4-diaminobutane which undergoes 80% photodimerization in HT-fashion. Two photodimers (HH and HT) also undergo isomerisation, as mentioned above for other photodimers, from *rctt-* to *rctc-* forms.

In Chapter 5, the synthesis, structural characterization and photoreactivity of various discrete and polymeric Ag(I) coordination compounds of 3-PAH and 4-PAH are discussed. For the discrete cationic complexes, it is observed that the Ag⋯Ag distances are close to the sum of van der Waal radii of two Ag(I) ions (3.44 Å) and further the weakly interacting BF_4^- and ClO_4^- anions have negligible effect on this preorganisation. Therefore, the parallel alignments of 3-PAH and 4-PAH are the collective result of all possible supramolecular interactions besides weak argentophilic interaction. In neutral polymeric compound of 3-PAH with Ag(I), the infinite parallel arrangement of 1D ribbons due to stronger argentophilic interaction (Ag⋯Ag distance is 3.11 Å) leads to quantitative photodimerization. The photostability of the analogous polymer of 4-PA and absence of such argentophilic interaction are rationalised with the difference in shape of 3-PAH and 4-PAH.
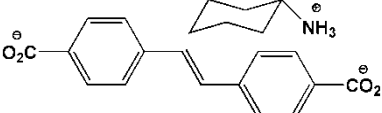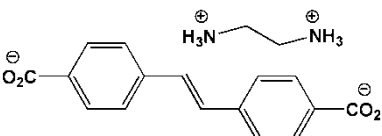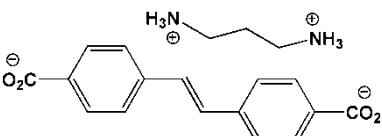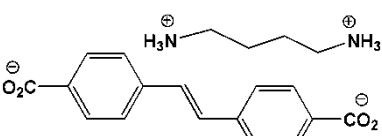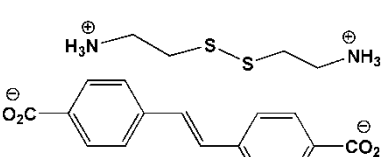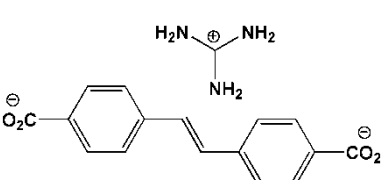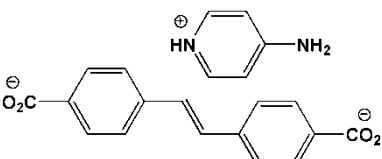
Chapter 6 describes various macrocyclic and polymeric Ag(I) coordination compounds of 3-PA, 4-PA, PVBA and 4-styrylpyridine (4-SP) with various phosphine derived auxiliary ligands like triphenylphosphine, 1,1-bis(diphenylphosphino)methane (dppm), 1,2-bis(diphosphino)ethane (dppe), 1,3-bis(diphosphino)propane (dppp). The dimensionality of these compounds varies from 0D to 3D and the coordination number of Ag(I) varies from 2 to 4. In some cases 3-PA and 4-PA are found to orient in parallel fashion on the same plane, unfavourable

for cycloaddition reaction. However, 4-SP undergoes photodimerization in a discrete cationic complex with AgBF$_4$ and dppm.
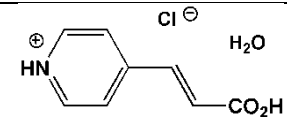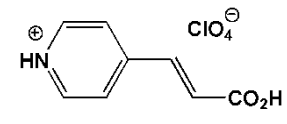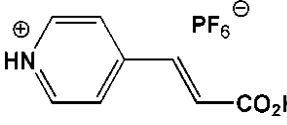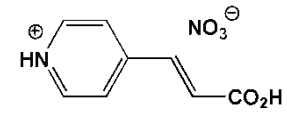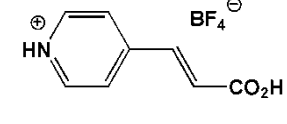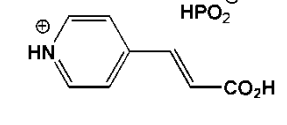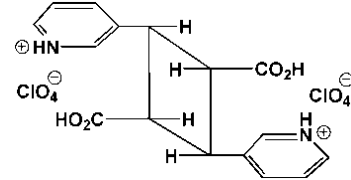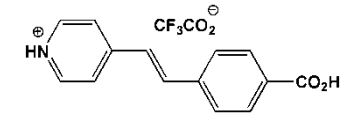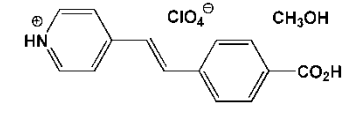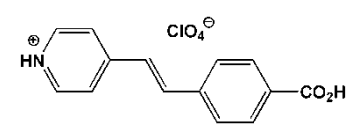
The crystal engineering studies on some of these functional cyclobutane derived compounds, synthesized so far, are discussed in Chapter 7. Many co-crystals and coordination polymers, synthesized from these tetradentate ligands, are described where Zn(II)-TCCB MOF is found to adsorb CO$_2$ gas selectively, indicating it to be a potential candidate for such application.

Finally, this doctoral dissertation ends with an overall conclusion of all the chapters discussed. This also offers a proposal for further investigations that can be extended in this particular area of research.

List of Compounds Synthesized

No.	Compounds	Structural Units
1	Cyclohexylammonium-SDC salt, (cyclohexa)$_2$(SDC)	^-O_2C–...–NH_3^+ (cyclohexyl)... CO_2^-
2	Ethylenediammonium-SDC Salt, (EDA)(SDC)	H_3N^+–CH$_2$CH$_2$–NH_3^+; ^-O_2C–...–CO_2^-
3	1,3-Diammoniumpropane-SDC Salt, (DAP)(SDC)·H$_2$O	H_3N^+–(CH$_2$)$_3$–NH_3^+; ^-O_2C–...–CO_2^-
4	1,4-Diammoniumbutane-SDC salt, (DAB)(SDC)·2H$_2$O	H_3N^+–(CH$_2$)$_4$–NH_3^+; ^-O_2C–...–CO_2^-
5	2,2′-Dithiobis(ethanammonium)-SDC salt, (DBEA)(SDC)	H_3N^+–CH$_2$CH$_2$–S–S–CH$_2$CH$_2$–NH_3^+; ^-O_2C–...–CO_2^-
6	Guanidinium-SDC salt, (Guan)$_2$(SDC)·4H$_2$O	H_2N–C($^+$NH$_2$)–NH$_2$; ^-O_2C–...–CO_2^-
7	4-Aminopyridinium-SDC salt, (4-APH)$_2$(SDC)·2H$_2$O	HN^+=pyridine–NH_2; ^-O_2C–...–CO_2^-
8	Piperizinium-SDC Salt, (Pip)(SDC)	
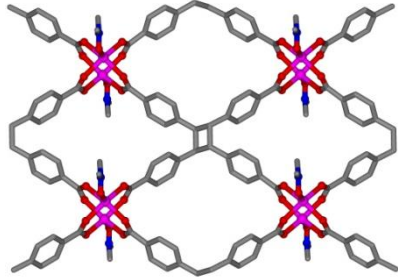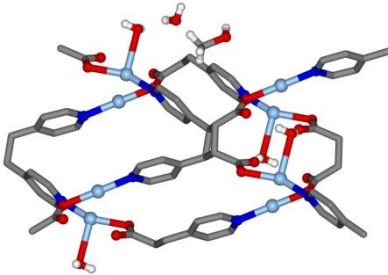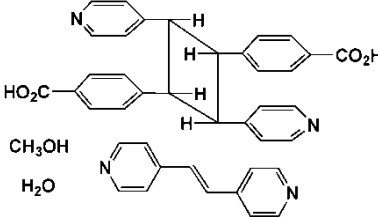
		O_2C—...—CO_2 (with $H_2N^{\oplus}$, $NH_2^{\oplus}$)
9	3,3′-dipropylaminoaminonium-SDC, $(DPA)_2(SDC)_3 \cdot 8H_2O$	$H_3N^{\oplus}$—...—$N^{\oplus}H_2$—...—$NH_3^{\oplus}$; O_2C—...—CO_2
10	Ammonium Salt of SDC, $(NH_4)(HSDC)$	O_2C—...—CO_2 ; $NH_4^{\oplus}$
11	Trifluoroacetate Salt of 4-PAH, $CF_3CO_2(4\text{-}PAH_2)$	$HN^{\oplus}$—pyridine—...—CO_2H ; $CF_3CO_2^{\ominus}$
12	$(rctt\text{-}HT\text{-}4,4\text{-}BPCDH_2)(CF_3CO_2)_2$	$HN^{\oplus}$-pyridine, $CF_2CO_2^{\ominus}$, HO_2C, CO_2H, $CF_2CO_2^{\ominus}$, $NH^{\oplus}$
13	$rctt\text{-}HT\text{-}4,4\text{-}BPCD$	pyridine-N, HO_2C, CO_2H, pyridine-N
14	Sulphate-bisulphate Salt of 3-PAH, $(4\text{-}PAH_2)_3(SO_4)(HSO_4)(H_2O)$	$HSO_4^{\ominus}$, $SO_4^{2\ominus}$, H_2O, $HN^{\oplus}$—pyridine—...—CO_2H
15	$rctt\text{-}HH\text{-}4,4\text{-}BPCD$	pyridine-N, CO_2H, pyridine-N, CO_2H
16	Chloride Salt of 4-PAH,	

	(4-PAH₂)Cl·H₂O	
17	Perchlorate Salt of 4-PAH, (4-PAH₂)ClO₄	
18	Hexafluorophosphate Salt of 4-PAH, (4-PAH₂)(4-PAH)PF₆	
19	Nitrate Salt of 4-PAH, (4-PAH₂)NO₃	
20	Tetrafluoroborate Salt of 4-PAH, (4-PAH₂)BF₄	
21	Biphosphate Salt of 4-PAH, (4-PAH₂)H₂PO₄	
22	(*rctt*-HT-3,3-BPCDH₂)(ClO₄)₂	
23	Trifluoroacetate Salt of HPVBA, (H₂PVBA)(CF₃CO₂)	
24	Perchlorate Salt of HPVBA, (H₂PVBA)ClO₄·MeOH	
25	Perchlorate Salt of HPVBA, (H₂PVBA)ClO₄	

26	Sulphate-bisulphate Salt of HPVBA, $(H_2PVBA)_4(HSO_4)_2(SO_4)\cdot H_2O$	
27	Sulphate-bisulphate Salt of HPVBA, $(H_2PVBA)_3(HSO_4)_3(H_2SO_4)(H_2O)_{6.5}$	
28	Nitrate Salt of HPVBA, $(H_2PVBA)NO_3$	
29	1,4-Diammoniumbutane-PVBA salt, (DABH)(PVBA) salt	
30	$[Ag(3\text{-}PAH)_2](BF_4)$	
31	$[Ag(3\text{-}PAH)_2](ClO_4)$	
32	$[Ag(4\text{-}PAH)_2](ClO_4)\cdot H_2O$	
33	$[Ag(3\text{-}PA)]_2\cdot(1.5H_2O)$	
34	$[Ag(4\text{-}PA)]$	
35	$[Ag_2(4\text{-}PA)_2(PPh_3)_2]\cdot$ $(Et_2O)(0.5CH_3CN)(2.5H_2O)$	

XX

36	[Ag$_2$(3-PA)(dppm)$_2$]BF$_4$·(2CH$_3$CN)	
37	[Ag$_2$(4-PA)$_2$(dppe)]·CH$_3$CN	
38	[Ag$_2$(4-PA)$_2$(dppp)]·(3H$_2$O)(0.5Et$_2$O)	
39	[Ag(3-PA)(dppp)$_{0.5}$]·H$_2$O	
40	[Ag$_4$(dppm)$_4$(PVBA)$_2$](TFA)$_2$	
41	[Ag$_2$(4-SP)$_2$(dppe)(TFA)$_2$]	

42	[Ag₂(dppm)(4-SP)₂][Ag₂(dppm)₂]₀.₅(BF₄)₃·(2THF)	
43	Co-crystal, (TCCB)(4,4'-bpy)₂·2DMF	
44	Co-crystal, (TCCB)(4,4'-bpe)·MeOH	
45	Co-crystal, (TCCB)(4,4'-bpethane)·2DMA·H₂O	
46	Co-crystal, (TCCB)(4,4'-bpdb)·MeOH	
47	[Zn₂(C₃₂H₂₀O₈)(C₂H₇NO)₂]·2DMF	

48	[Ag$_2$(HH-4,4-BPCD)(H$_2$O)]·(2H$_2$O)(0.5MeOH)	
49	Co-crystal, (HT-4,4-BPBCCB)(4,4'-bpe)(MeOH)$_{0.75}$(H$_2$O)$_2$	

List of Figures

Chapter 1

Chapter 2

Chapter 3

Chapter 4

Chapter 5

Chapter 6

Chapter 7

List of Schemes

Chapter 1

Chapter 2

Chapter 3

Chapter 4

Chapter 5

Chapter 6

List of Tables

Chapter 2

Chapter 3

Chapter 4

Chapter 5

Chapter 6

Chapter 7

Lists of Publications, Presentations and Awards

List of Publications

1. **G. K. Kole,** G. K. Tan, J. J. Vittal, "Anion-controlled stereoselective synthesis of cyclobutane derivatives by solid state [2 + 2] cycloaddition reaction of the salts of *trans*-3-(4-pyridyl) acrylic acid" *Org. Lett.*, **2010**, 12, 128-131.

2. **G. K. Kole**, L. L. Koh, S. Y. Lee, S. S. Lee, J. J. Vittal, "A new ligand for metal–organic framework and co-crystal synthesis: mechanochemical route to *rctt*-1,2,3,4-tetrakis-(4'-carboxyphenyl)- cyclobutane" *Chem. Commun.*, **2010**, 46, 3660-3662.

3. **G. K. Kole**, A. J. Cairns, M. Eddaoudi, J. J. Vittal, "Solvent-free porous framework resulted from 3D entanglement of 1D zigzag coordination polymer" *New J. Chem.*, **2010**, 34, 2392-2395.

4. **G. K. Kole**, G. K. Tan, J. J. Vittal, "Crystal engineering studies on the salts of *trans*-4,4'-stilbenedicarboxylic acid in the context of solid state [2 + 2] cycloaddition reaction" *CrystEngComm*, **2011**, 13, 3138-3145.

5. **G. K. Kole**, G. K. Tan, J. J. Vittal, "Role of Anions in the Synthesis of Cyclobutane Derivatives via [2 + 2] Cycloaddition Reaction in the Solid State and Their Isomerisation in Solution" *J. Org. Chem.*, **2011**, 76, 7860-7865.

6. R. Medishetty, L. L. Koh, **G. K. Kole**, J. J. Vittal, "Solid state structural transformation from 2D-interdigitated layer to 3D-interpenetrated structure" *Angew. Chem. Int. Ed.*, **2011**, 50, 10949–10952.

7. M. H. Mir, J. X. Ong, **G. K. Kole**, G. K. Tan, M. J. McGlinchey, Y. Wu and J. J. Vittal "Photoreactive gold(I) macrocycles with diphosphine and *trans, trans*- muconate ligands" *Chem. Commun.*, **2011**, *47*, 11633–11635.

8. **G. K. Kole**, G. K. Tan, J. J. Vittal, "Photoreactivity of Ag(I) Complexes and Coordination Polymers of Pyridyl Acryclic Acids" *Cryst. Growth Des.*, **2012**, *12*, 326–332.

List of Presentations (Poster and Oral)

1. XX International Conference on the Chemistry of Organic Solid State (ICCOSS XX), June 2011, Bangalore, India.

2. The 10th Conference of the Asian Crystallographic Association (AsCA2010), October 2010, Busan, South Korea. (**'The Rising Star' Award**)

3. 1st China-India-Singapore Symposium on Crystal Engineering, August 2010, NUS, Singapore. (**Best Poster Award**)

4. Summer School on Mathematical Crystallography, June 2010 Nancy, France.

5. Gordon Research Conference on Crystal Engineering, June 2010, NH, USA.

6. 2nd NUS-SNU Joint Symposium on March, 2010, NUS, Singapore.

7. 6th Singapore International Chemical Conference (SICC-6), December 2009, Singapore.

8. The Fifth Mathematics and Physical Sciences Graduate Congress (MPSGC-5), December 2009, Chulalongkorn University, Bangkok, Thailand.

List of Awards

1. **Kiang Ai Kim Scholar** Award for 2010-2011 from the Department of Chemistry, NUS, Singapore.

2. "**The Rising Star**" award in 'The 10th Conference of the Asian Crystallographic Association (AsCA2010)' October 2010, Busan, South Korea.

3. **Best Poster award** in '1st China-India-Singapore Symposium on Crystal Engineering' August 2010, NUS, Singapore.

4. Partial travel support was awarded for attending Summer School on Mathematical Crystallography, June 2010 Nancy, France.

5. Partial travel support was awarded for attending Gordon Research Conference on Crystal Engineering, June 2010, NH, USA.

Chapter 1

Introduction

....

The title of this doctoral dissertation is 'Crystal Engineering Studies on the Molecular Salts and Silver(I) Coordination Compounds for [2 + 2] Cycloaddition Reaction in the Solid State'. After discussing the definition of the subject 'crystal engineering' and its widely spread scope, the terms molecular salts, coordination compounds / polymers and [2 + 2] cycloaddition reaction or photodimerization reaction in the solid state will be discussed. Hence this chapter is meant to provide a succinct discussion of the background literature with the emphasis to cover the significance of the above topics. The results consolidated in the subsequent chapters can be appreciated in the right perspective of the background literature coverage in this chapter.

1.1 Crystal Engineering

The subject crystal engineering began its journey in the late 1960s from the fundamental research work by Schmidt[1] *et al.* while attempts were made to understand the solid state packing patterns of various organic compounds in their polymorphs and their photoreactivity in the solid state. The name 'crystal engineering' was first coined by Schmidt and its working definition was later provided by Desiraju in 1989 as *"the understanding of intermolecular interactions in the context of crystal packing and in the utilisation of such understanding in the design of new solids with desired physical and chemical properties"*.[2] The subject is therefore of wide scope and an ensemble of ideas and techniques from supramolecular chemistry, X-ray crystallography, materials science and solid-state chemistry. To taste the essence of crystal engineering, it is highly essential to understand the basics of supramolecular interactions which are briefly discussed below.

1.2 Hydrogen Bonding as a Supramolecular Interaction

Among all the directional supramolecular interactions, hydrogen bonding is the most important one and is ubiquitous. A large extent of this thesis work is also based

on various types of hydrogen bonding interactions. This weak bonding is responsible for many abnormalities known in chemistry including anomalous behaviour of water. When hydrogen is covalently bonded to a strongly electronegative element (X) the bond becomes dipolar and the fractional positive charge confers on it an extra potential to drag electron density from other negatively polarised end forming a weak bond known as hydrogen bonding.[3] The strength of hydrogen bonding depends on electronegativity of the X element in X-H···A. The group X-H is called proton donor or electron acceptor and A is called proton acceptor or electron donor. The X-H bonds with reverse polarity (such as in metal hydrides) can also form such directional interaction. The energies involved in hydrogen bonding have been computed to be in the range of 0.2 - 40 kcal/mol.[4]
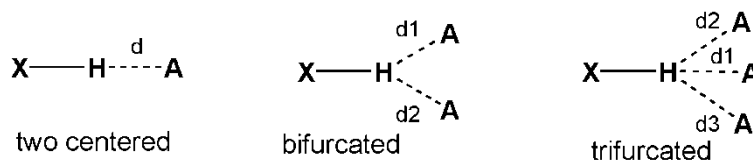
Scheme 1.1 Types of hydrogen bonding.

Although, each hydrogen atom can form only one covalent bond, it is capable of forming multiple H-bonding with multiple electronegative elements. In a simple hydrogen bond, the donor interacts with one acceptor and termed as two-centred hydrogen bond. The terms 'bifurcated' and trifurcated' are used when donor interacts with two and three acceptors respectively as described in Scheme 1.1.[4] The geometry of hydrogen bonding is very important for constructing functional molecular solids which often involve infinite chains or arrays and can be represented by graph set notation.

A set of molecules that are hydrogen bonded to one another by repetition of different types of H-bonding patterns, as provided by the nature of H-bond donors and acceptors present in the structure of interest, is known as a motif. Motifs that are involved in intermolecular H-bonding, are generally characterized by one of four

designators known that indicates whether the motif is finite or infinite and cyclic or not. These designators are named as: **C** stands for a chain, **R** stands for a ring, **D** stands for dimer or other finite set and **S** stands for an intramolecular hydrogen bond. The number of the H-bond donor and acceptors are represented as subscript and superscript respectively. The number specified in parentheses indicates the size or degree of the motif (the number of atoms in the repeating unit).[5] The examples of graph set notation of some common H-bonded motifs are illustrated in Scheme 1.2. Chemically different functional groups having the same graph set are called isographic.
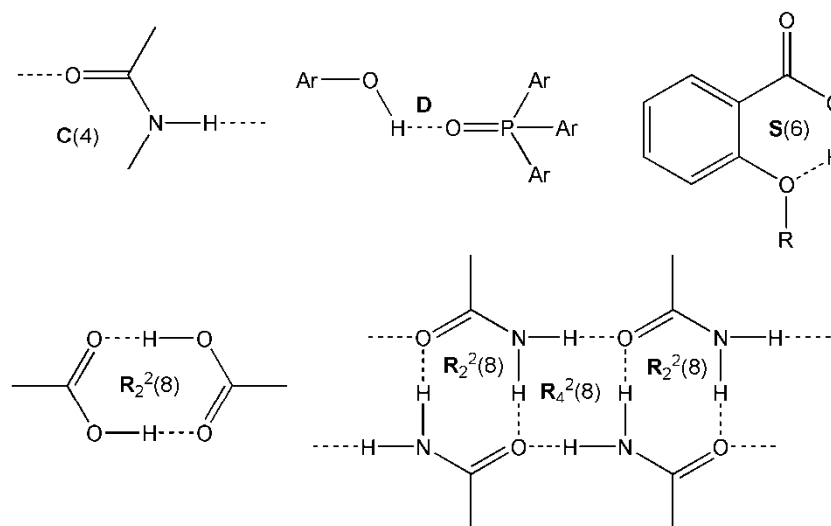
Scheme 1.2 Examples of graph set notation for hydrogen bonding

1.3 Supramolecular Synthons

Desiraju has brought the concept of 'supramolecular synthon' in the field by adopting the concept 'synthon' by Corey[6] in molecular synthesis. To synthesize a supramolecular entity with desired properties, the self assemblies of molecular fragments and their geometrical pattern into one or multidimensional network is very crucial. The strong or weak but directional supramolecular interactions can be utilized to achieve the designed arrangement of functional groups in the molecular skeleton i.e. supramolecular synthons. Therefore 'supramolecular synthons' was defined as "*...structural units within molecules which can be formed and or assembled by known*

or conceivable synthetic operations involving intermolecular interactions". Supramolecular synthons play the same role in supramolecular synthesis as synthons do in molecular synthesis and are illustrated in Scheme 1.3.[2b, 7] The concept of supramolecular synthon is, therefore, very helpful for the designed synthesis of co-crystals and molecular salts with desired properties.
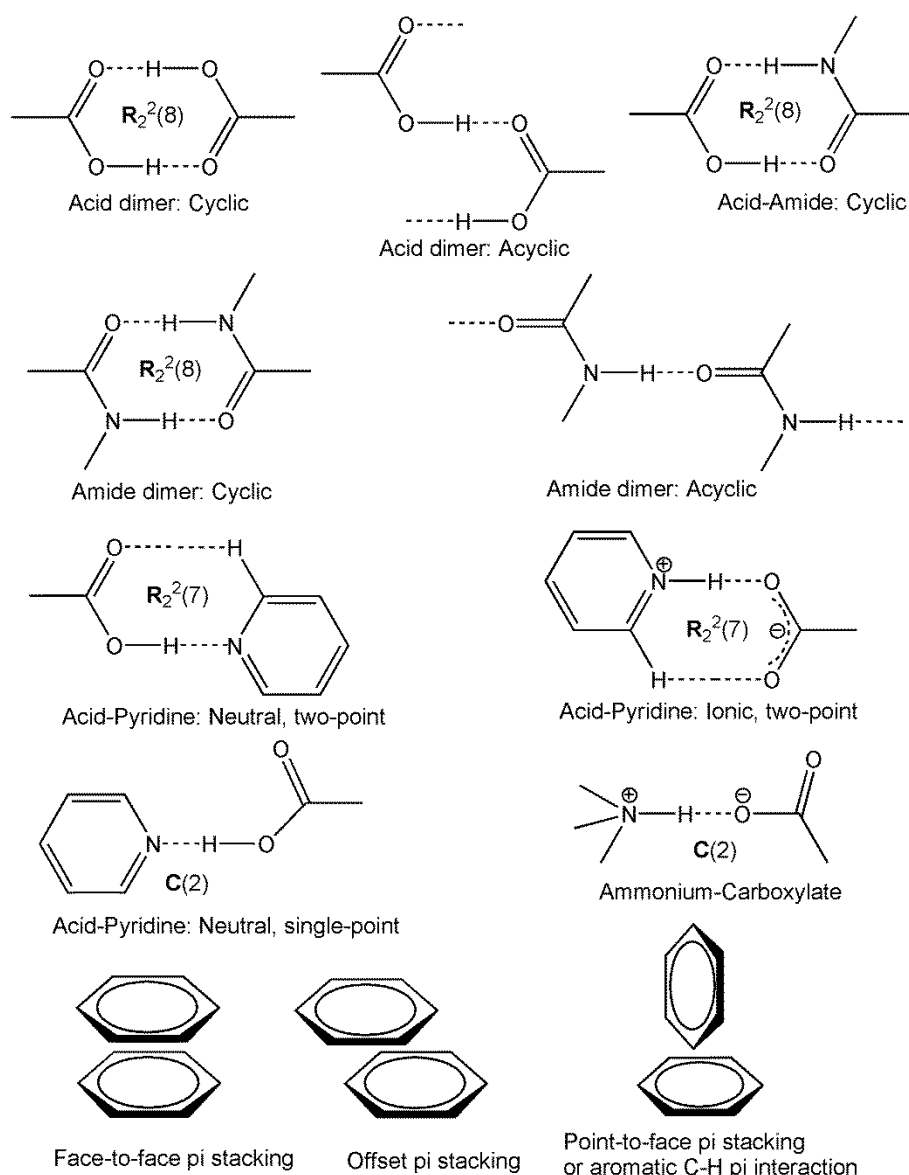
Scheme 1.3 Example of various types of supramolecular synthons

1.4 Co-crystal and Molecular Salts

The designed synthesis of a co-crystal or molecular salt with desired properties is the ultimate goal of a crystal engineer. A multi-component crystal in which the

....

components that are solid at ambient condition coexist through supramolecular interactions is known as co-crystal.[8] When different molecules with complementary functional groups construct hydrogen bonding that are energetically more favourable than those between like molecules of each component, then the formation of a co-crystal is favoured. Generally, supramolecular synthons like carboxylic acid-pyridine, carboxylic acid-amide, and alcohol-pyridine favour the formation co-crystals. Depending upon the acidity or basicity (pKa values) of the reacting molecules in the co-crystal, proton transfer often takes place that results in the formation of a molecular salt.[9] Generally, the reaction of a acid with a base is expected to form a salt when ΔpKa value [pKa(base) – pKa(acid)] is greater than 3. There are, of course, many exceptions to this assumption – the salt co-crystal continuum.[10] Steiner and co-workers have described the salt co-crystal continuum on 4-methylpyridine·pentachlorophenol complex (ΔpKa = 0.77) by variable temperature neutron diffraction study.[11] It was shown that this co-crystal (at room temperature) became a salt due to the migration of the proton from pentachlorophenol to pyridyl N by cooling at 20K, while it showed an equal O···H···N distances at 90K. The co-crystals or molecular salts have wide range of applications including in pharmaceutical science (pharmaceutical co-crystals)[12] and stereoselective synthesis in the solid state ([2 + 2] cycloaddition reactions which is discussed in section 1.6).

1.5 Coordination Polymers or Metal Organic Framework (MOF)

Coordination polymers (CPs) are the polymeric materials constructed by the self-assembly of metal ions or metal clusters as node, which are connected by organic ligands as linker via coordination bonds and other weaker secondary forces or supramolecular interactions. These rapidly emerging inorganic-organic hybrid materials have ever increasing scientific and industrial interest for their various potential applications in gas storage/separation, ion exchange, catalysis, drug delivery and optoelectronics etc.[13] This class of materials is alternatively known as metal

organic frameworks (MOFs) or porous coordination polymers (PCPs) when they exhibit permanent porosity accessible to guests. All these compounds collectively are also called as metal organic materials (MOMs).[14]

Transition metal ions are extensively used to synthesize CPs due to their versatile coordination geometries such as linear, T-shaped, trigonal planar, tetrahedral, square planar, octahedral, trigonal-prismatic, pentagonal-bipyramidal etc. By utilizing the versatile geometries around the metal centres and the judicial choice of organic ligands (linker) with varying size and shape, varieties of new CPs with fascinating architectures and topologies such as linear, zigzag, ladder, honeycomb, square grid, diamondoid etc have been obtained as shown in Figure 1.1.[15]

ribbon   zig-zag   ladder   helical   honeycomb

square grid   diamondoid   cubic, pcu
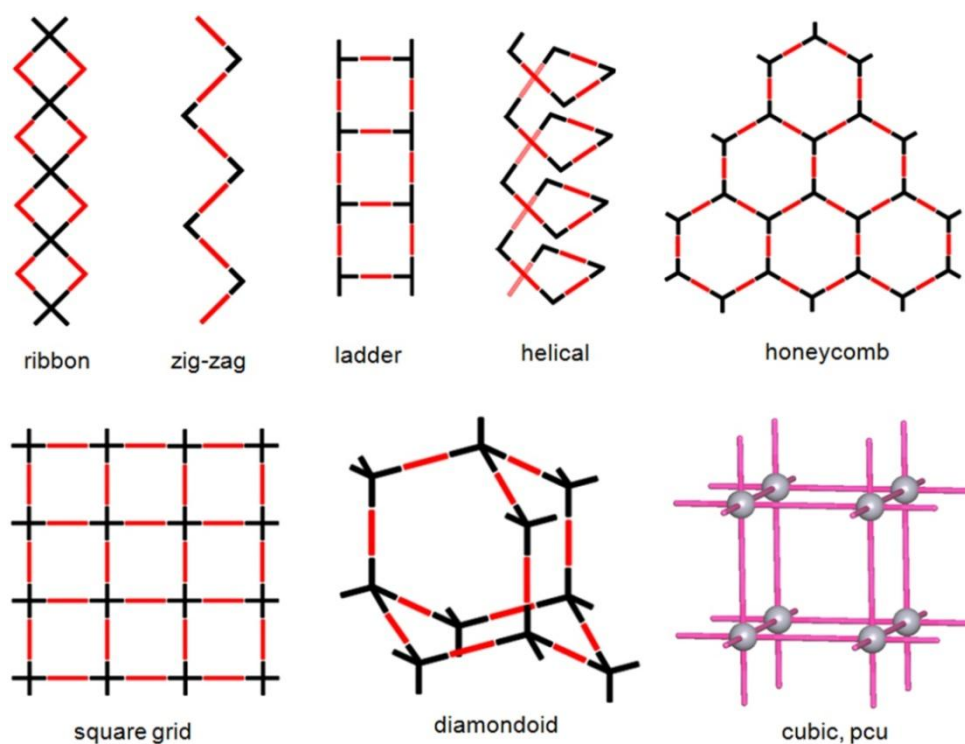
Figure 1.1 The schematic representation of various observed geometries of coordination polymers

The tremendous growth of these types of materials has started by the pioneering work by Robson *et al.* It is in the late 1990s, they established the way to design and synthesis of various types of polymeric networks on the basis of Wells[16] net-based approach that resulted in rapid growth of coordination polymers.[17] Later,

Yaghi and co-workers introduced special and unique type of coordination polymers composed of metal clusters such as Zn_4O^{6+} as nodes and linear and angular multi-carboxylates as linkers (Figure 1.2) which showed permanent microporosity suitable for gas storage.[18] The stronger metal-carboxylate coordination bond, which is as strong as covalent bond, led these materials to exhibit exceptional thermal stability and found to be better material than the conventional inorganic porous materials like zeolites. These types of materials were termed as 'metal organic frameworks' and since then the interest of researchers on these materials has been accelerated by many fold. MOFs can be designed and synthesized in a rational way from molecular building block, known as secondary building block (SBU) and this realisation opened a new paradigm called 'reticular chemistry'.[19]
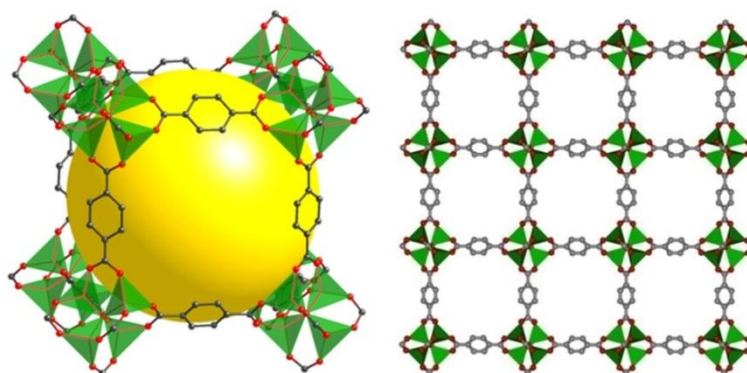
Figure 1.2 The structure of MOF-5

Kitagawa *et al.* introduced the concept of pillared-layer structured PCPs using two different types of ligands. Two dimensional layers, formed by the combination of metal ions and one type of ligands, are connected by neutral ditopic spacer ligands called as pillars coordinating to the open sites of the metal centres to result three dimensional frameworks.[20] The dynamic behaviours of these PCPs in response with various external stimuli, such as light, electric field, guest molecules etc, have been well explored.[20] Kitagawa *et al.* have classified PCPs into three different categories on the basis of their functions and responses to external stimuli (Figure 1.3). The first generation PCPs show guest dependent porosity and the framework structures

collapse when the guests are removed. The second generation PCPs are robust and stable; the framework structures are maintained even after the guest molecules are removed and in fact, guest removal and uptake occurs reversibly without destructing the framework. The third generation PCPs are very stable but dynamic and flexible. The collapsed framework upon guest removal can be recovered upon guest uptake, and they show various types reversible transformation in the framework in response to the external stimuli.[21] Such flexible and dynamic microporous CPs often exhibit contraction and expansion upon reversible uptake of guest molecules or super critical gases, which is known as breathing.[22]
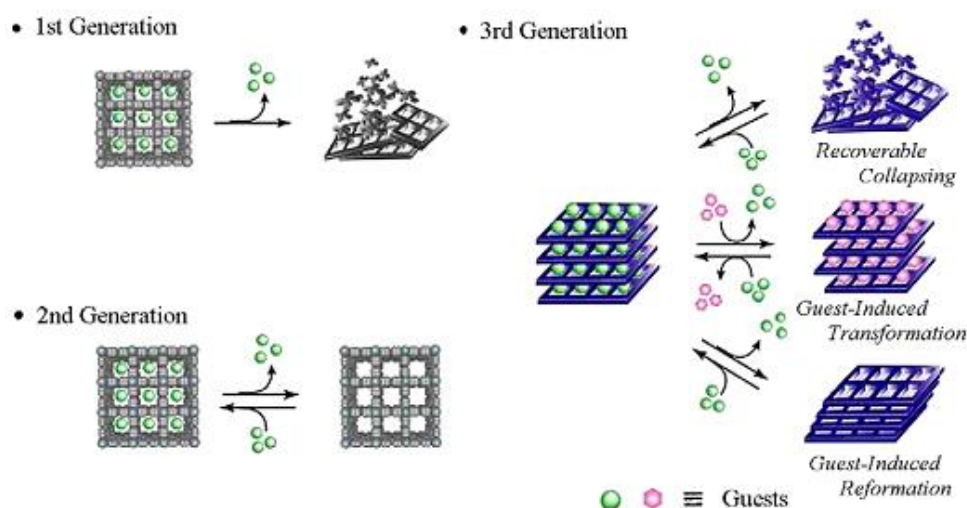
Figure 1.3 The schematic view of first, second and third generation microporous PCPs (reproduced from Kitagawa *et al. Coord. Chem. Rev*. **2007**, *251*, 2490-2509)

1.6 [2 + 2] Cycloaddition or Photodimerization Reaction in the Solid State

1.6.1 Reactions in the Solid State

Photodimerization reaction is a light driven addition reaction between two C=C bonds to form a cyclobutane product utilising two π-electrons from each reacting monomer. The reactivity of solid is essentially different from the reactivity of molecules in the liquid or gas phase. The formation of product in the solid state is driven by the ordered arrangement of the reacting molecules that lack long range molecular movement. The reactions in the solid state that occur with a minimum amount of atomic or molecular movement are called topochemical reactions. There

are many advantages of reactions in the solid state namely, stereoselectivity i.e. formation of one particular isomer of the product among its many possible isomers, high yield (usually quantitative) and it allows to access products which are inaccessible otherwise in solution. It is worth mentioning here the photoreactivity of *trans*-cinnamic acid and its analogues that were observed by Schmidt *et al.*[1a, 1c] *Trans*-cinnamic acid undergoes *trans-cis* isomerisation in solution. On the other hand, three different polymorphs show different photoreactivity in the solid state; namely α-form photodimerizes in *head-to-tail* fashion and convert to α-truxillic acid, β-truxinic acid can be obtained from β-form photodimerizing in *head-to-head* fashion, whereas, γ-form was found to be photostable (Figure 1.4).
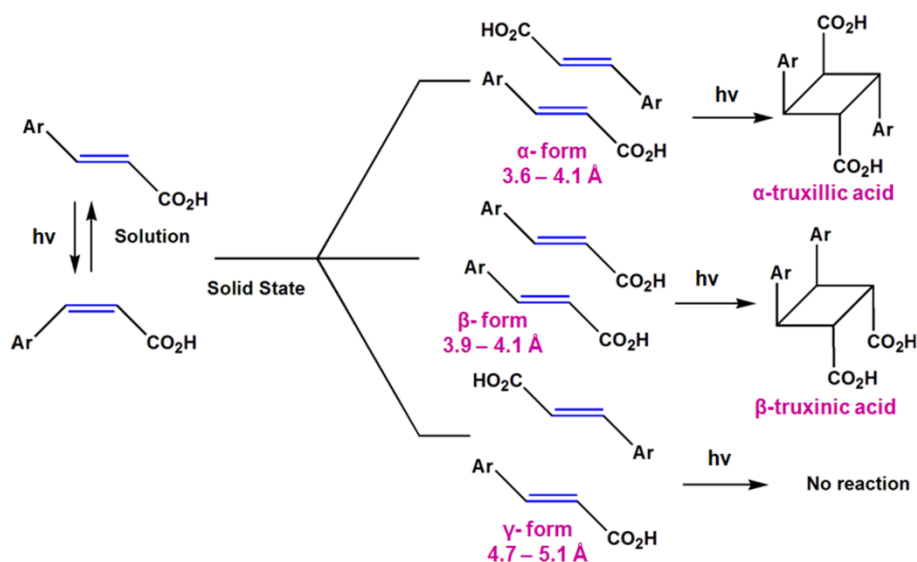
Figure 1.4 Schematic representation of solid state and solution phase photoreactivity of *trans*-cinnamic acid

1.6.2 Schmidt's Topochemical Postulates

The topochemical control on photodimerization was first recognised by Schmidt *et al.* in the context of solid state photoreactivity of cinnamic acid derivatives. Based on their observations on the photochemical studies and crystallographic analyses, Schmidt deduced the following conditions for this reaction which is known as Schmidt's topochemical postulate.[1a]

....

1. The photoreactive olefins must align parallel keeping a distance of 3.5 – 4.2 Å between two C=C bonds.

2. A minimum amount of atomic or molecular movement is necessary during reaction and the stereochemistry of the dimer depends on the contact geometry (antiparallel or parallel and *head-to-head* or *head-to-tail*) of the nearest-neighbour double bonds.

Therefore, the challenge in this type of reactions relies in designing and accomplishing the parallel alignment of photoreactive double bonds in solid state maintaining a proper distance between them. Since the pioneering work by Schmidt *et al.*, crystal engineering principles have been employed utilising directional nature of supramolecular interactions to control the self-assembly of olefins to design photoreactive solids. Among them hydrogen bonded co-crystals, organic salts, coordination compounds and polymers have been extensively studied to generate functional cyclobutane derivatives. The design strategy involves using a template either in the form of hydrogen bonding, ionic interaction or coordination bonding that can clip two olefins (hence two C=C bonds) parallel (Scheme 1.4).
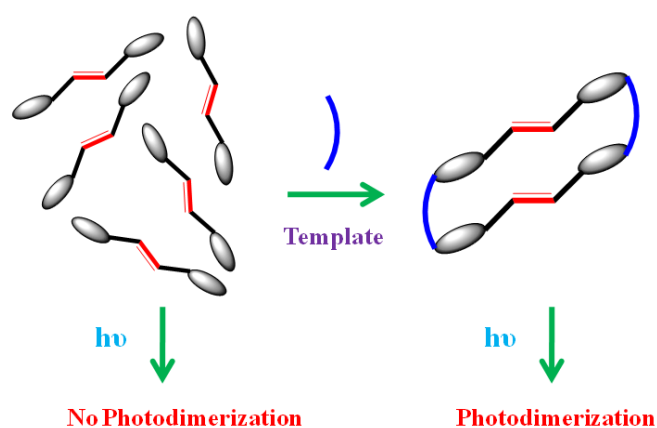
Scheme 1.4 The working principle for template driven preorganisation of C=C bonds

1.6.3 Template Controlled Photodimerization Reaction in Co-crystals

Photostable olefins are made photoreactive by aligning them parallel, also known as preorganisation, in the solid state by using another molecules known as

....

template. By exploiting the hydrogen bonding ability of the olefins, the templates are selected having functional groups complementary to the olefins. For example, *trans*-1,2-bis(4'-pyridyl)ethylene (4,4'-bpe) is a hydrogen bond acceptor and can be preorganised in the co-crystal with resorcinol having hydrogen bond donor phenolic functionality.[23] Extensive work has been reported by MacGillivary and others with analogous systems.[24,25] The synthesis of ladderane was successfully achieved in a single step (Figure 1.5).[26] The idea of template controlled solid state photoreactivity has also been extended to preorganise dicarboxylic acids (hydrogen bond donor) in
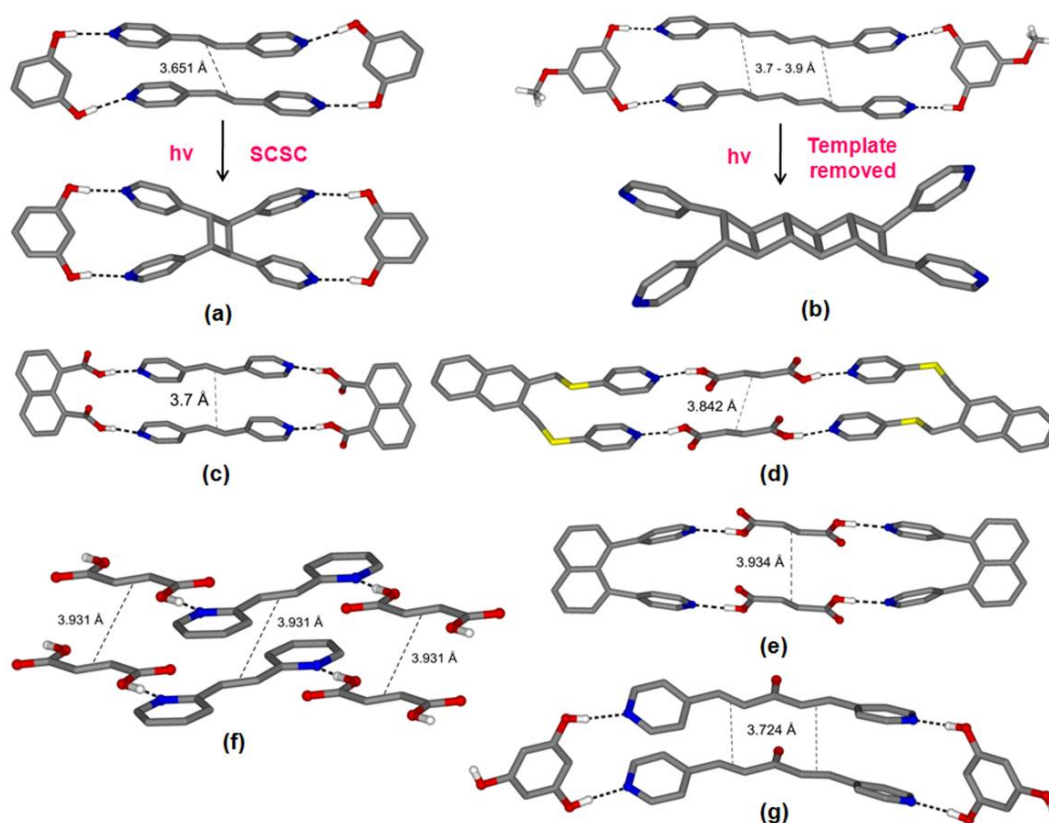
Figure 1.5 Template controlled alignments of C=C bonds in various types hydrogen bonded co-crystals

the co-crystals with various templates having functional groups as hydrogen bond acceptor.[27] Not only olefins could be aligned parallel using template, two photoreactive olefins like fumaric acid and *trans*-1,2-bis(2'-pyridyl)ethylene (2,2'-bpe) in a co-crystal were reported where both of them undergo concomitant

photodimerization. Therefore, each of them act as template to each other and vice-versa (Figure 1.5f).[28]

1.6.4 Photodimerization Reaction in Molecular Salts

A salt is the product of a reaction between an acid and a base, therefore composed of a cation and an anion. The parallel orientations of photoreactive ethylene double bonds and their photodimerization in organic molecular salts have been reported in the literature. Ito *et al.* used *trans-* and *cis*-1,2-diaminocyclohexane as salt former with *trans*-cinnamic acid whose photoirradiation resulted in ε-truxillic acid and β-truxinic acid respectively as major products.[29] They also introduced ethylenediamine as a salt former with derivatives of the same (including 2-chloro, 2-methoxy, 3-nitro) that resulted in β-truxinic acid in variable yields (Figure 1.6).[30] The authors did not realise the possible pedal-like motion that resulted in the formation of β-truxinic acid in a specific way from the crisscross alignment of the monomers. However, this was later investigated by Ramamurthy *et al.* with *trans*-1,2-diaminocyclohexane and *trans*-chlorocinnamic acids.[31] The pedal-like motion in the solid state is discussed in section 1.7.
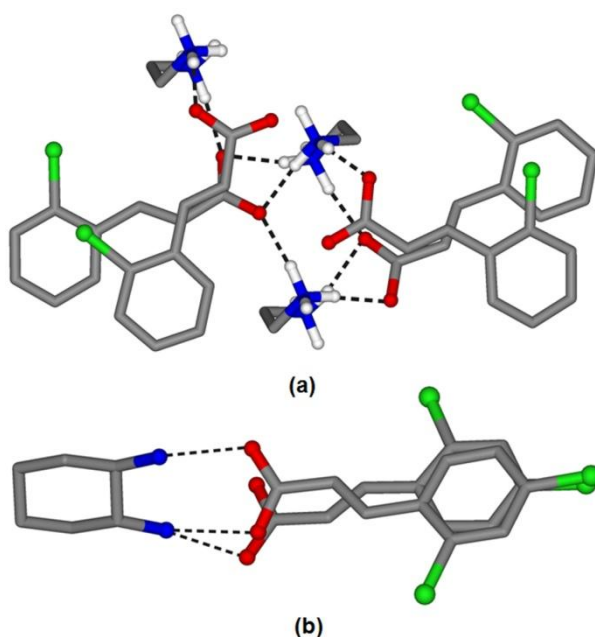
Figure 1.6 Crisscross orientation of of substituted *trans*-cinnamic acids in molecular salts with ethylenediamine (a) and *trans*-1,2-diaminocyclohexane (b)

....

Not only carboxylic acids that can be made salts with amines, olefins containing pyridyl functionality can also be aligned parallel for photodimerization via salt formation. Although 4-styrylpyridine (4-SP) is photostable, the photodimerization of its hydrochloride salt in HT-fashon (α-analogue) was known since 1977.[32] Later, Yamada *et al.* explained that the parallel alignment of 4-SPH$^+$ cations in HT-fashion as a consequence of cation-π interaction.[33] Phenyl ring is π-electron rich, where as the potonated pyridyl group is cationic. Therefore, the resulting cation-π interaction between two 4-SPH$^+$ cations help them to stack parallel in HT-fashion suitable for photodimerization reaction (Figure 1.7). Similarly 4-azachalcone, another olefin containing pyridyl functionality, was aligned parallel by salt formation with HCl. Unlike 4-SP, 4-azachalcone was photoreactive leading to the formation of a mixture of dimers and the *cis*-isomer. However, it underwent photodimerization and led to the formation of HT-dimer exclusively as its hydrochloride salt.[34]
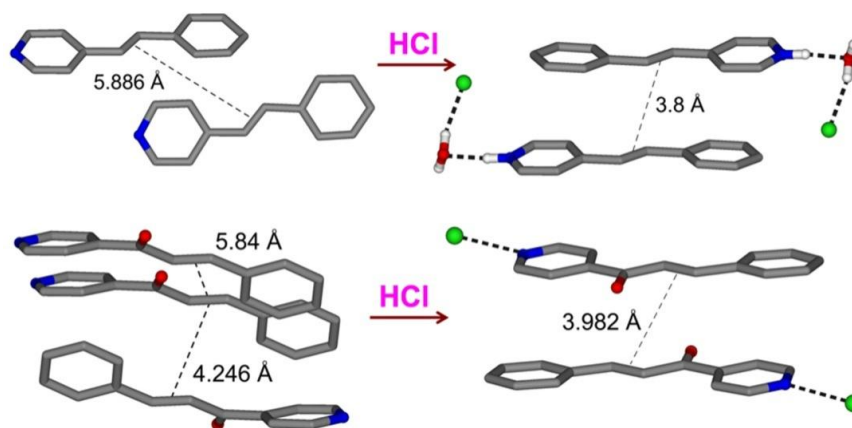
Figure 1.7 4-SP and 4-azachalcone were made photoreactive in HT-fashion by forming salt with HCl

All the salts discussed above are obtained by reacting olefins with either strong bases for carboxylic acid or with strong mineral acid for pyridines. It is also observed that the salt formation i.e. transfer of proton from acidic counterpart to basic counterpart takes place when ΔpKa is greater than 3. The serendipitous formation of salts containing carboxylic acid and pyridyl functionality are also reported during co-

....

crystalizations that undergo photodimerization. When 1,2,4,5-benzenetetracarboxylic acid (bta) was co-crystallized with 4,4'-bpe in 1:2 ratio, proton transfer from bta to one 'N' of 4,4'-bpe took place and the resulted salt underwent photodimerization quantitatively (Figure 1.8).[35] Similar salts were synthesized with bta and 4-styrylpyridine, 4-(4'-Chlorostyryl)pyridine etc in 1:2 ratio and were found to be photoreactive in HT-fashion.[36] Vittal *et al.* synthesized *rctt*-1,2,3,4-tetrakis-(4'-pyridyl)cyclobutane (*rctt*-4,4-tpcb) via salt formation of 4,4'-bpe with trifluoroacetic acid which undergo quantitative isomerisation to *rtct*-4,4-tpcb in acidic condition upon heating.[37] Therefore, the salt formation method is very important having additional advantage of accessing rare isomers of cyclobutanes containing pyridyl functionality. Several other photoreactive salts of benzo-annellated acridizinium derivatives containing quarternary nitrogen and halide anions were also reported that underwent [4+4] photocycloaddition reaction stereoselectively in the soild state.[38]
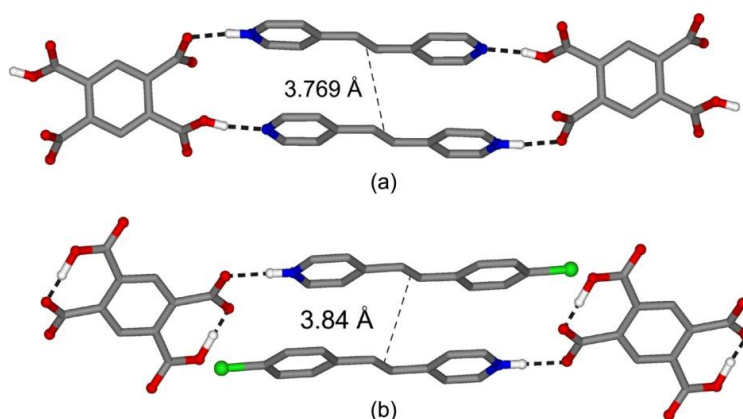
Figure 1.8 The parallel alignment of 4,4'-bpe and 4-(4'-chlorostyryl)pyridine in their salts with bta.

1.6.5 Photodimerization Reactions of Coordination Compounds and Polymers

Like hydrogen bond driven self assembly in co-crystals and salts, metal-ligand coordination bonds also have been extensively studied for aligning photoreactive olefinic ligand and their photodimerization. Coordination bond driven oligomerization and ploymerization are well known in the literature.[39] By exploiting the known coordination geometry around a metal centre, 4,4′-bpe was well aligned in

15

various types of coordination compounds and polymers. The metal-metal distance with open coordination site in the hydroxo bridged dinuclear zinc complex [$Zn_2(L)(OH)$] (where L = 2,6-bis[N-(2-pyridylethyl)formimidoyl]-4-methylphenol) has been used to template a pair of 4,4'-bpe molecules with distances of 3.64 Å between C=C bonds and this resulted its photodimerization in a SCSC manner (Figure 1.9a).[40]

Organometallic compounds have also been studied for photodimerization reaction. An organometallic complex [$Cp^*_2M_2(\mu-\eta^2,\eta^2-C_2O_4)Cl_2$] was used as template to achieve parallel orientation of 4,4'-bpe pairs in a complex [$Cp^*_4M_4(\mu-4,4'-bpe)_2(\mu-\eta^2,\eta^2-C_2O_4)$](OTf)$_4$ [where M = Ir, Rh] which also underwent photodimerization in a SCSC manner (Figure 1.9b).[41] The idea of bridging coordinative mode of oxalate in organometallic complexes (as organometallic clip) was extended for oxamidato bridging ligands[42] and fumaric acid[43] later in similar systems for the same purpose.
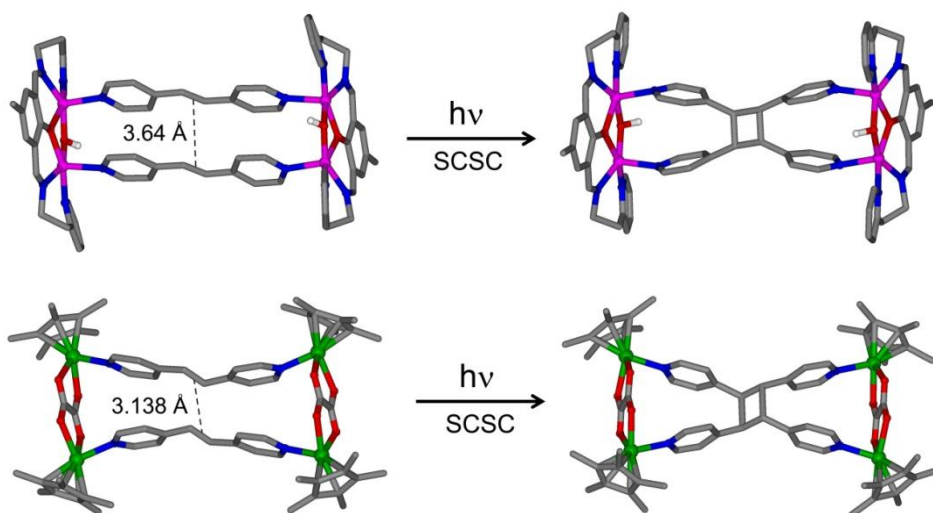
Figure 1.9 The photoreactivity of a dinuclear Zn(II) complex (a) and an organometallic compound of 4,4'-bpe (b)

Apart from discrete coordination complexes and organometallic compounds, polymeric coordination compounds have been extensively studied where metal-ligand coordination bond have been used to anchor the double bond of 4,4'-bpe. Vittal *et al.*

16

have utilized judicious combination of metal ions and bridging ligands to preorganise 4,4'-bpe in a 1D ladder like coordination polymer.[44] Pairs of 4,4'-bpe molecules in an infinte serial fashion have been aligned using zinc-carboxylate salt that resulted in two one dimensional coordination polymers with desired ladder structure $[\{(CH_3CO_2)(\mu\text{-}O_2CCH_3)Zn\}_2(\mu\text{-}4,4'\text{-bpe})_2]_n$ and $[\{(CF_3CO_2)(\mu\text{-}O_2CCH_3)Zn\}_2(\mu\text{-}4,4'\text{-bpe})_2]_n$.[44a] Although the quantitative conversion was observed for the former CP, the process in SCSC manner was found to occur for the second one only when 50% of the acetate anions were replaced by trifluoroacetate anions (Figure 1.10).[44a]

Several coordination complexes and hydrogen bonded coordination polymers have extensively been studied for aligning photoreactive C=C bonds suitable for photodimerization reactions,[45] however the same in higher dimensional coordination polymers was scarce. Vittal *et al.* have elegantly illustrated a series of interpenetrated pillared-layer coordination polymers of general formula [Zn(4,4'-bpe)L], (where L = *trans,trans*-muconic acid, 1,4-benzenedicarboxylic acid and fumeric acid; solvents are excluded), where the pillar 4,4'-bpe were found to stack parallel and underwent photodimerization (Figure 1.11) showing a photochemical method for 3D to 3D post synthetic modification of coordination polymers.[46]
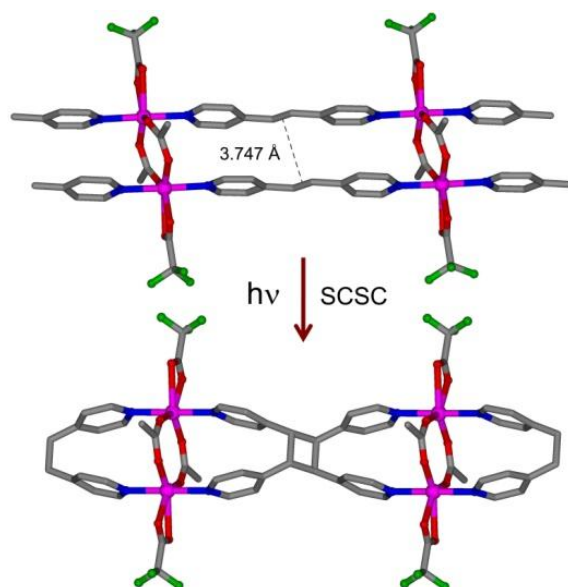
Figure 1.10 SCSC transformation of a 1D ladder-like coorination polymer.
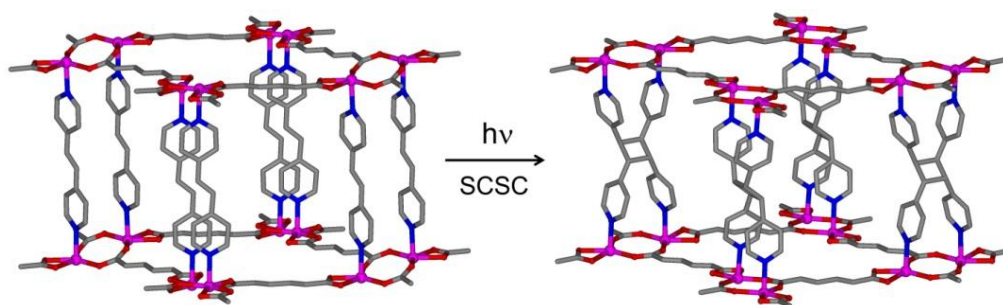
Figure 1.11 [2 + 2] photodimerization reaction in a pillared-layer structured 3D coordination polymer in SCSC manner

Although, the pyridyl based olefins have been extensively studied for cycloaddition reaction of coordination polymer in the solid state, carboxylic acid derived ligands have also been studied for this purpose. Eddaoudi and co-workers serendipitously discovered one dimensional metal-organic assembly of $[Cu(CDO)(py)_2(H_2O)]_n$, where H_2CDO = chelidonic acid, having proper orientation and positioning of CDO ligands (Figure 1.12). [2 + 2] photodimerization at both the C=C bonds of CDO resulted in the formation of higher dimensional heterocyclic carboxylic acid.[47]
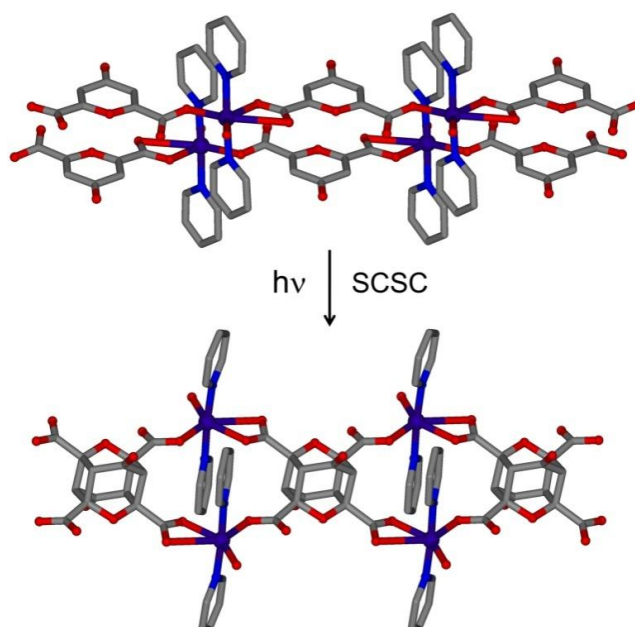
Figure 1.12 SCSC transformation to a higher dimensional cage molecules via metal-organic self-assembly

....

1.6.5.1 Photodimerization Reaction in Ag(I) Coordination Compounds and Polymers

A significant part of this thesis deals with the solid state photoreactivity of silver(I) coordination compounds and polymers. Therefore, the photodimerization of Ag(I) coordination compounds and polymers are discussed in this section separately from coordination polymers in general. Argentophilic interaction (Ag····Ag as well as aurophilic, Au···Au) is considered among the most important supramolecular interactions that have significant impact on the solid state packing. This interaction has been used to design photoreactive solids. Schröder *et al.* used Ag(I) complex of 4,4'-bpe which underwent photodimerization to a single dimer and resulted in a 3D coordination polymeric framework of the dimer.[48] The formation of a single photodimer in solution in presence of Ag(I) reflected a special role of argentophilic interaction in self-assembly. Several Ag(I) and Au(I) based metallo-macrocyclic compounds containing diphosphines and 4,4'-bpe ligands were synthesized by Puddephatt and co-workers, utilising metallophilic interactions (Figure 1.13).[49] The metal-metal distances in most of these macrocycles are less than the sum of van der Waal radii (3.44 Å for Ag and 3.32 Å for Au) showing that significant metallophilic interactions persist. Vittal *et al.* studied the photoreactivity of these metallomacrocycles undergoing 100% photochemical cycloaddition reaction both in solid state and in solution.[44c]
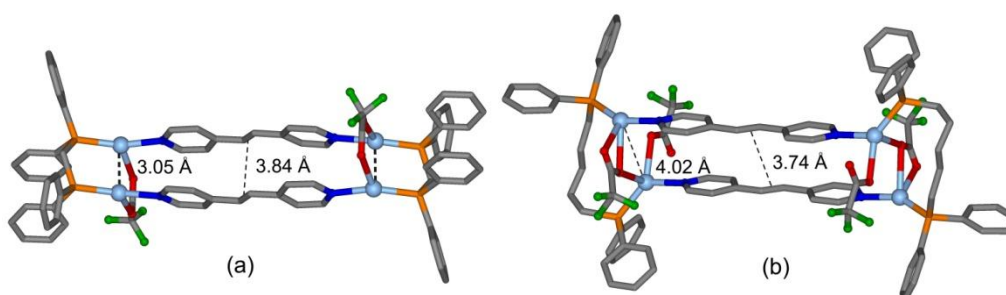
Figure 1.13 The parallel alignments of 4,4'-bpe in Ag(I) metallo-macrocycles suitable for photodimerization reaction; argentophilic interaction is present in (a).

....

MacGillivray *et al.* illustrated how argentophilic interaction can be used as template to preorganise C=C bonds of 4-styrylpyridines (or 4-stilbazole) by connecting at one side in its discrete complex. The C=C bonds have been found to orient in a crisscross fashion within the allowed distance undergoes 100% conversion to *rctt*-iosmer in SCSC manner (Figure 1.14).[50] The formation of *rctt*-isomer from pairs aligned in crisscross fashion suggested pedal-like motion (discussed in section 1.7) of the monomers prior to the cycloaddition reaction. The crystal structure determination of the photoirradiated complex showed bonding interaction between Ag(I) and phenyl ring carbon, indicating the conversion of a finite metal complex to a infinite coordination polymer.[50]
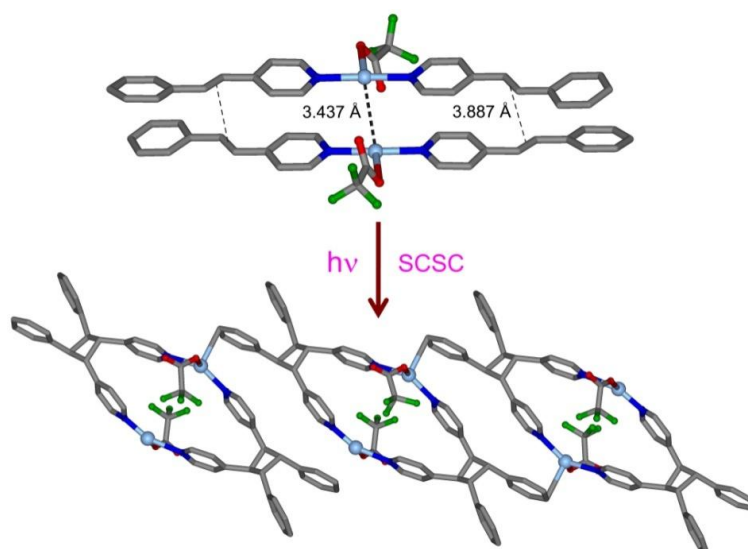
Figure 1.14 SCSC transformation of a discrete complex assembled by Ag···Ag interaction to 1D polymer

Vittal *et al.* investigated a silver coordination polymer [Ag(μ-4,4'-bpe)(H$_2$O)](CF$_3$CO$_2$)·CH$_3$CN (Figure 1.15), where the C=C bonds of 4,4'-bpe were neither found to stack within the required distance (5.15 Å) nor any aregentophilic interaction was detected (Ag···Ag distance is 5.17 Å). But the polymer underwent quantitative photodimerization reaction after desolvation. Desolvation led structural transformation where CF$_3$CO$_2^-$ anions coordinate two Ag(I) in bridging mode forming a ladder-like coordination polymer (refer to Figure 1.10) driven by

cooperative, anisotropic and long-range movements of polymeric chains, suitable for

photochemical cycloaddition reaction.[51] In the progress of designing photoreactive

silver coordination componds and polymers, various types of finite complexes[52] and

infinite polymers[53] have been documented with photoreactivity and their structural

insights. Recently, the photochemical cycloaddition reaction of the terminal olefin 4-

vinylpyridine was also achieved utilising argentophilic interaction.[54] The Ag···Ag

interactions in the presence of noncoordinating anions like BF_4^-, ClO_4^-, PF_6^- etc or in

the absence of any anion are termed as anion unsupported argentophilic interaction.[55]

On the other hand, in the presence of coordinating anions like acetate,

trifluoroacetate, nitrate etc which bridge two Ag(I) centres, the resulting Ag···Ag

interactions are termed as anion/ligand supported argentophilic interaction.[52-53]
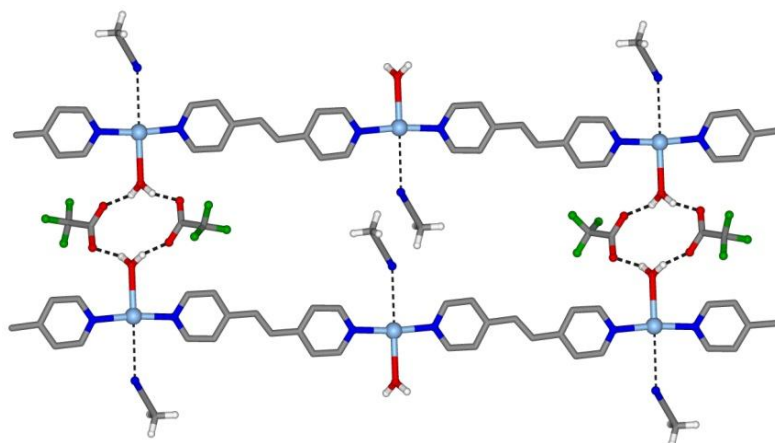
Figure 1.15 Long-range cooperative movement of coordination polymeric chain
upon desolvation led to photoreactivity

1.7 Pedal-like Motion in the Solid State: Conformational Change

In contrary to the minimum amount of molecular movement during

photodimerization, the deviation of the topochemical postulate and the formation of

unexpected products are known for many years.[56] Also, there are many systems

known, even after fulfilling the topochemical criteria, do not undergo

photodimerization.[36, 56] The photochemical reactions that require large amount

....

molecular movements are being gradually discovered.[31, 57] Ogawa *et al.* observed a

bicycle pedal-like motion of *trans*-stilbene and azobenzenes in the crystalline state by

X-ray diffraction at various temperatures which often result in crystallographic

disorder (Figure 1.16) and the authors highlighted that such a motion is common for

organic compounds having similar skeletons.[58] Pedal motion has been observed or

accounted to explain many anomalous observations during photodimerization,[31, 50, 57]

photoisomerization of butadienes,[59] photochromism of salicylideneaniline,[60] protein

photocycle[61] and so on.
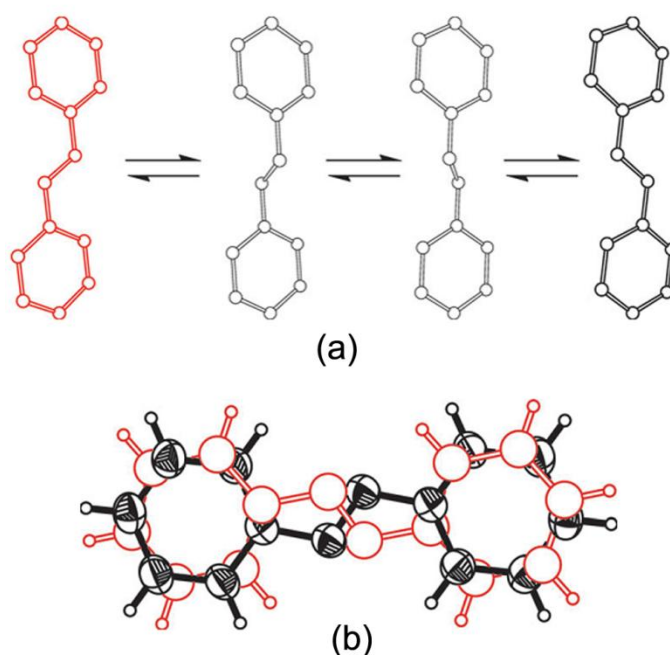
Figure 1.16 Pedal-like motion observed in *trans*-stilbene (a) and disordered crystal structure of azobenzene at room temperature (b) (reproduced from Harada and Ogawa, *Chem. Soc. Rev.*, **2009**, *38*, 2244–2252 with permission)

Pedal-like motion, which leads to the formation of unexpected products in

photodimerization reactions, is discussed in the Scheme 1.5 below. The product 'A'

and 'B' are the expected photodimers in absence of any pedal motion if the

cycloaddition proceed via 1 1' & 2 2' and 1 2' & 2 1' respectively. However, the

formation of 'C' is often observed as a major or the only photodimer from a pair of

C=C bonds aligned in crisscross fashion. A pedal motion of one olefin with respect to

other is necessary to anchor them in perfect parallel alignment prior to cycloaddition

reaction and then the formation of '**C**' can be justified. Pedal-like motion has also been accounted to explain the formation of photodimers in this thesis in Chapters 3 and 5.
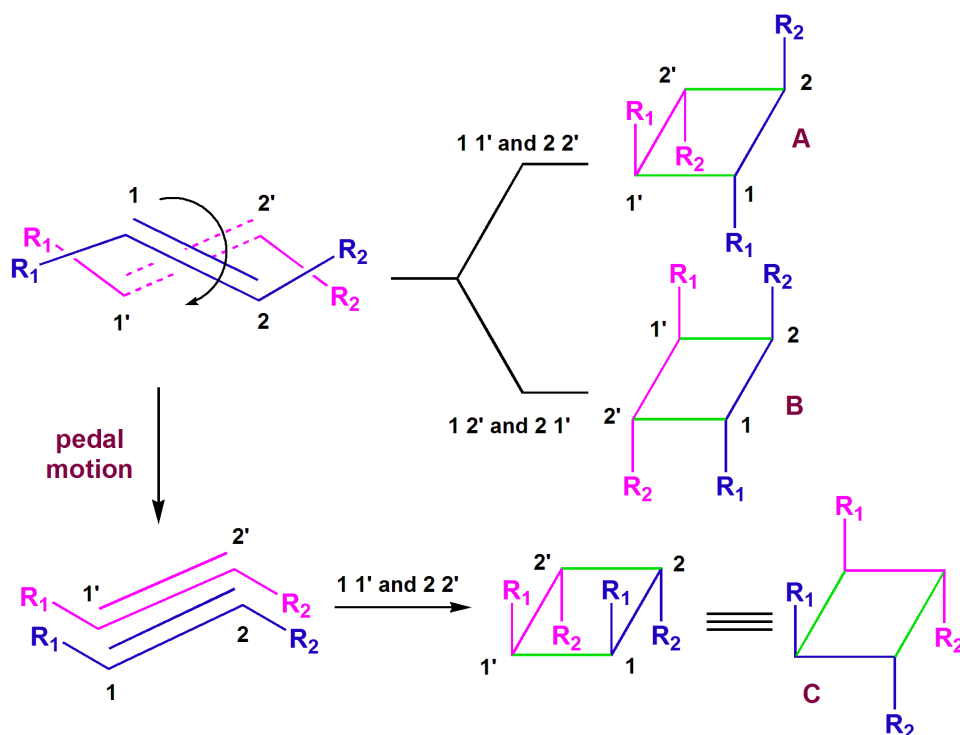
Scheme 1.5 Schematic representation of pedal-like motion involved in solid state that dictates the unusual product formation (newly formed bonds are shown in green).

1.8 Mechanochemical Reactions

Synthesis of complex molecules often requires multiple steps that consume gallons of hazardous solvents to purify the desired product from a mixture of by-products. Green synthetic route has become popular to synthetic chemists as it minimizes the use of hazardous solvents. When water becomes scarce, minimizing the usage of water as solvent in the synthesis is also considered as greener route. Recently, solvent-less or solvent-drop assisted (kneading) mechanochemical grinding route has become popular and drawn considerable attention of the researchers.[62] A wide range of materials including co-crystals, organometallic and coordination networks, host-guest adduct have been synthesized successfully by mechanochemical grinding approach.[63] Recently, mechanochemical grinding is gaining popularity for

....

aligning photoreactive double bonds in the solid state.[28, 52, 64] The structures of the mechanochemically ground samples are generally confirmed by matching the PXRD patterns of the bulk with the simulated patterns from the single crystal. The mechanochemical grinding method has also been exploited in this thesis when and wherever suitable.

1.9 Aim and Scope of This Dissertation

The research work presented in this thesis is concerned with organic solid state syntheses of several cyclobutane derived ligands via photochemical [2 + 2] cycloaddition reactions of various molecular salts and silver(I) coordination compounds. Molecular salts of both the dicarboxylic acid and pyridylcarboxylic acids will be synthesized by allowing them to react with various strong organic amines and mineral acids respectively. The photoreactivity of certain salts and photostability of certain salts of H_2SDC will be investigated to understand the correlation between the crystal packing and the chain length of organic amines. The identification of supramolecular synthons constructing the solid state structure of these salts may give useful insights on the design strategy of photoreactive organic molecular salts.

Although the molecular salts are well known for photodimerization reaction, the effects of counter ions were not studied before. The protonation to the pyridyl groups of the pyridylcarboxylic acids with strong mineral acids and hence the presence of counter anions has huge impact on the crystal packing. Also, the relative orientation between two asymmetric olefins aligned parallel, either *head-to-head* or *head-to-tail*, dictates the product formation in the photochemical cycloaddition reaction. The role of anions in controlling such arrangements of photoreactive cations and hence the stereoselective syntheses of functional cyclobutane compounds will be explored in this thesis. The photochemical cycloaddition reaction of olefins preorganised upon desolvation of lattice solvents are well established. The structural

transformation due to the absorption of moisture during mechanochemical grinding will be discussed in the context of quantitative formation of *rctt*-isomer. The acid catalysed isomerisation of pyridyl based cyclobutane ligands will be discussed in the context of organic synthesis of very rare isomers of cyclobutane.

Pyridylcarboxylic acids both as neutral and anionic ligands will be explored to synthesize silver(I) coordination compounds and polymers where C=C bonds will be aligned parallel not only by argentophilic interaction but along with the aid of other related supramolecular interaction collectively. Several mono- and diphosphine derived auxiliary ligands will also be employed along with pyridyl and pyridylcarboxylate ligands to synthesize finite and multidimensional silver(I) coordination polymers and will be discussed in the context of structural diversity and photoreactivity.

Finally, the utility of these cyclobutane derived compounds with pyridyl and carboxylate functionalities will be explored as potential ligands for making coordination polymers and co-crystals. The applicability of porous coordination polymer will also be addressed when and wherever applicable.

1.10   References

1.   (a) Schmidt, G. M. J., *Pure Appl. Chem.* **1971,** *27* (4), 647-678; (b) Cohen, M. D.; Schmidt, G. M. J., *J. Chem. Soc.* **1964**, 1996-2000; (c) Schmidt, G. M. J., *J. Chem. Soc.* **1964**, 2014-2021.

2.   (a) Desiraju, G. R., *Crystal engineering: the design of organic solids*. Elsevier: 1989; (b) Desiraju, G. R.; Vittal, J. J.; Ramanan, A., *Crystal Engineering: A Textbook*. World Scientific Pub. Co. Inc: 2011.

3.   Pauling, L., *The nature of the chemical bond and the structure of molecules and crystals: an introduction to modern structural chemistry*. Cornell University Press: 1960.

....

4.   Steiner, T., *Angew. Chem. Int. Ed.* **2002,** *41* (1), 48-76.

5.   Etter, M. C., *Acc. Chem. Res.* **1990,** *23* (4), 120-126.

6.   Corey, E. J., *Pure Appl. Chem.* **1967,** *14* (1), 19-38.

7.   Desiraju, G. R., *Angew. Chem. Int. Ed. Engl.* **1995,** *34* (21), 2311-2327.

8.   (a) Desiraju, G. R., *CrystEngComm* **2003,** *5* (82), 466-467; (b) Dunitz, J. D., *CrystEngComm* **2003,** *5* (91), 506-506; (c) Aakeroy, C. B.; Salmon, D. J., *CrystEngComm* **2005,** *7* (72), 439-448; (d) Bond, A. D., *CrystEngComm* **2007,** *9* (9), 833-834; (e) Zaworotko, M. J., *Cryst. Growth Des.* **2007,** *7* (1), 4-9.

9.   (a) Ballabh, A.; Trivedi, D. R.; Dastidar, P., *Cryst. Growth Des.* **2005,** *5* (4), 1545-1553; (b) Félix, O.; Hosseini, M. W.; De Cian, A.; Fischer, J., *Angew. Chem. Int. Ed. Engl.* **1997,** *36* (1-2), 102-104; (c) Sarma, B.; Nath, N. K.; Bhogala, B. R.; Nangia, A., *Cryst. Growth Des.* **2009,** *9* (3), 1546-1557.

10.   Childs, S. L.; Stahly, G. P.; Park, A., *Mol. Pharmaceutics* **2007,** *4* (3), 323-338.

11.   Steiner, T.; Majerz, I.; Wilson, C. C., *Angew. Chem. Int. Ed.* **2001,** *40* (14), 2651-2654.

12.   (a) Trask, A. V., *Mol. Pharmaceutics* **2007,** *4* (3), 301-309; (b) Bučar, D.-K.; Henry, R. F.; Lou, X.; Duerst, R. W.; Borchardt, T. B.; MacGillivray, L. R.; Zhang, G. G. Z., *Mol. Pharmaceutics* **2007,** *4* (3), 339-346; (c) Bis, J. A.; Vishweshwar, P.; Weyna, D.; Zaworotko, M. J., *Mol. Pharmaceutics* **2007,** *4* (3), 401-416; (d) Bhatt, P. M.; Azim, Y.; Thakur, T. S.; Desiraju, G. R., *Cryst. Growth Des.* **2008,** *9* (2), 951-957; (e) Aakeröy, C. B.; Fasulo, M. E.; Desper, J., *Mol. Pharmaceutics* **2007,** *4* (3), 317-322; (f) Shan, N.; Zaworotko, M. J., *Drug Discovery Today* **2008,** *13* (9-10), 440-446.

13.   (a) Yaghi, O. M., *Nat. Mater.* **2007,** *6* (2), 92-93; (b) Horcajada, P.; Serre, C.; Maurin, G.; Ramsahye, N. A.; Balas, F.; Vallet-Regí, M. a.; Sebban, M.; Taulelle, F.; Férey, G. r., *J. Am. Chem. Soc.* **2008,** *130* (21), 6774-6780; (c) Yang, J.; Sudik, A.; Wolverton, C.; Siegel, D. J., *Chem. Soc. Rev.* **2010,** *39* (2), 656-675; (d) Caskey, S.

R.; Wong-Foy, A. G.; Matzger, A. J., *J. Am. Chem. Soc.* **2008,** *130* (33), 10870-10871; (e) Seo, J. S.; Whang, D.; Lee, H.; Jun, S. I.; Oh, J.; Jeon, Y. J.; Kim, K., *Nature* **2000,** *404* (6781), 982-986; (f) Min, K. S.; Suh, M. P., *J. Am. Chem. Soc.* **2000,** *122* (29), 6834-6840; (g) Evans, O. R.; Lin, W., *Acc. Chem. Res.* **2002,** *35* (7), 511-522; (h) Hasegawa, S.; Horike, S.; Matsuda, R.; Furukawa, S.; Mochizuki, K.; Kinoshita, Y.; Kitagawa, S., *J. Am. Chem. Soc.* **2007,** *129* (9), 2607-2614.

14.   Zaworotko, M. J., *Nature* **2008,** *451* (7177), 410-411.

15.   (a) Moulton, B.; Zaworotko, M. J., *Chem. Rev.* **2001,** *101* (6), 1629-1658; (b) Zaworotko, M. J., *Chem. Commun.* **2001,** (1), 1-9; (c) Batten, S. R.; Neville, S. M.; Turner, D. R., *Coordination polymers: design, analysis and application*. Royal Society of Chemistry: 2009; (d) Hong, M. C.; Chen, L., *Design and construction of coordination polymers*. Wiley: 2009; (e) MacGillivray, L. R., *Metal-Organic Frameworks: Design and Application*. John Wiley & Sons: 2010.

16.   Wells, A. F., *Three dimensional nets and polyhedra*. Wiley: 1977.

17.   (a) Robson, R., *J. Chem. Soc., Dalton Trans.* **2000,** (21), 3735-3744; (b) Hoskins, B. F.; Robson, R., *J. Am. Chem. Soc.* **1990,** *112* (4), 1546-1554; (c) Gable, R. W.; Hoskins, B. F.; Robson, R., *J. Chem. Soc., Chem. Commun.* **1990,** (23), 1677-1678; (d) Abrahams, B. F.; Hoskins, B. F.; Liu, J.; Robson, R., *J. Am. Chem. Soc.* **1991,** *113* (8), 3045-3051; (e) Robson, R., *Dalton Trans.* **2008,** (38), 5113-5131.

18.   (a) Li, H.; Eddaoudi, M.; O'Keeffe, M.; Yaghi, O. M., *Nature* **1999,** *402* (6759), 276-279; (b) Rowsell, J. L. C.; Spencer, E. C.; Eckert, J.; Howard, J. A. K.; Yaghi, O. M., *Science* **2005,** *309* (5739), 1350-1354.

19.   Yaghi, O. M.; O'Keeffe, M.; Ockwig, N. W.; Chae, H. K.; Eddaoudi, M.; Kim, J., *Nature* **2003,** *423* (6941), 705-714.

20.   (a) Seo, J.; Matsuda, R.; Sakamoto, H.; Bonneau, C.; Kitagawa, S., *J. Am. Chem. Soc.* **2009,** *131* (35), 12792-12800; (b) Matsuda, R.; Kitaura, R.; Kitagawa, S.; Kubota, Y.; Kobayashi, T. C.; Horike, S.; Takata, M., *J. Am. Chem. Soc.* **2004,** *126* (43), 14063-14070; (c) Maji, T. K.; Uemura, K.; Chang, H.-C.; Matsuda, R.;

....

Kitagawa, S., *Angew. Chem. Int. Ed.* **2004,** *43* (25), 3269-3272; (d) Horike, S.;

Matsuda, R.; Kitaura, R.; Kitagawa, S.; Iijima, T.; Endo, K.; Kubota, Y.; Takata, M.,

Chem. Commun. **2004,** (19), 2152-2153; (e) Horike, S.; Matsuda, R.; Tanaka, D.;

Matsubara, S.; Mizuno, M.; Endo, K.; Kitagawa, S., *Angew. Chem. Int. Ed.* **2006,** *45*

(43), 7226-7230.

21.   (a) Kitagawa, S.; Kitaura, R.; Noro, S.-I., *Angew. Chem. Int. Ed.* **2004,** *43*

(18), 2334-2375; (b) Kitagawa, S.; Uemura, K., *Chem. Soc. Rev.* **2005,** *34* (2), 109-

119; (c) Kitagawa, S.; Matsuda, R., *Coord. Chem. Rev.* **2007,** *251* (21-24), 2490-

2509.

22.   (a) Halder, G. J.; Kepert, C. J.; Moubaraki, B.; Murray, K. S.; Cashion, J. D.,

Science **2002,** *298* (5599), 1762-1765; (b) Kitaura, R.; Seki, K.; Akiyama, G.;

Kitagawa, S., *Angew. Chem. Int. Ed.* **2003,** *42* (4), 428-431.

23.   MacGillivray, L. R.; Reid, J. L.; Ripmeester, J. A., *J. Am. Chem. Soc.* **2000,**

122 (32), 7817-7818.

24.   (a) Friščić, T.; Drab, D. M.; MacGillivray, L. R., *Org. Lett.* **2004,** *6* (25),

4647-4650; (b) Friščić, T.; MacGillivray, L. R., *Chem. Commun.* **2003,** (11), 1306-

1307; (c) Dutta, S.; Bučar, D.-K.; MacGillivray, L. R., *Org. Lett.* **2011,** *13* (9), 2260-

2262.

25.   (a) Santra, R.; Biradha, K., *CrystEngComm* **2011,** *13* (9), 3246-3257; (b)

Santra, R.; Biradha, K., *CrystEngComm* **2008,** *10*, 1524-1526; (c) Khan, M.;

Enkelmann, V.; Brunklaus, G., Cryst. Growth Des. **2009,** *9* (5), 2354-2362; (d) Khan,

M.; Enkelmann, V.; Brunklaus, G., *CrystEngComm* **2009,** *11*, 1001-1005.

26.   Gao, X.; Friščić, T.; MacGillivray, L. R., *Angew. Chem. Int. Ed.* **2004,** *43* (2),

232-236.

27.   (a) Friščić, T.; MacGillivray, L. R., *Chem. Commun.* **2005,** (46), 5748-5750;

(b) Mei, X.; Liu, S.; Wolf, C., *Org. Lett.* **2007,** *9* (14), 2729-2732.

28.   Avendano, C.; Briceño, A., *CrystEngComm* **2009,** *11* (3), 408-411.

29.   Ito, Y.; Borecka, B.; Trotter, J.; Scheffer, J. R., *Tetrahedron Lett.* **1995,** *36* (34), 6083-6086.

30.   Ito, Y.; Borecka, B.; Olovsson, G.; Trotter, J.; Scheffer, J. R., *Tetrahedron Lett.* **1995,** *36* (34), 6087-6090.

31.   Natarajan, A.; Mague, J. T.; Venkatesan, K.; Ramamurthy, V., *Org. Lett.* **2005,** *7* (10), 1895-1898.

32.   Horner, M.; Huenig, S., *J. Am. Chem. Soc.* **1977,** *99* (18), 6120-6122.

33.   Yamada, S.; Uematsu, N.; Yamashita, K., *J. Am. Chem. Soc.* **2007,** *129* (40), 12100-12101.

34.   Yamada, S.; Tokugawa, Y., *J. Am. Chem. Soc.* **2009,** *131* (6), 2098-2099.

35.   Shan, N.; Jones, W., *Tetrahedron Lett.* **2003,** *44* (18), 3687-3689.

36.   Linares, M.; Briceño, A., *New J. Chem.* **2010,** *34* (4), 587-590.

37.   Peedikakkal, A. M. P.; Peh, C. S. Y.; Koh, L. L.; Vittal, J. J., *Inorg. Chem.* **2010,** *49* (15), 6775-6777.

38.   (a) Ihmels, H.; Mohrschladt, Christian J.; Schmitt, A.; Bressanini, M.; Leusser, D.; Stalke, D., *Eur. J. Org. Chem.* **2002,** *2002* (15), 2624-2632; (b) Ihmels, H.; Leusser, D.; Pfeiffer, M.; Stalke, D., *Mol. Cryst. Liq. Cryst. Sect. A* **2001,** *356* (1), 433-441; (c) Ihmels, H.; Bosio, S.; Bressanini, M.; Schmitt, A.; Wissel, K.; Leusser, D.; Stalke, D., *Mol. Cryst. Liq. Cryst.* **2002,** *390* (1), 105-112.

39.   (a) Vela, M. J.; Snider, B. B.; Foxman, B. M., *Chem. Mater.* **1998,** *10* (10), 3167-3171; (b) Vela, M. J.; Buchholz, V.; Enkelmann, V.; Snider, B. B.; Foxman, B. M., *Chem. Commun.* **2000,** (22), 2225-2226.

40.   Papaefstathiou, G. S.; Zhong, Z.; Geng, L.; MacGillivray, L. R., *J. Am. Chem. Soc.* **2004,** *126* (30), 9158-9159.

41.   Han, Y.-F.; Lin, Y.-J.; Jia, W.-G.; Wang, G.-L.; Jin, G.-X., *Chem. Commun.* **2008,** (15), 1807-1809.

42.   Zhang, W.-Z.; Han, Y.-F.; Lin, Y.-J.; Jin, G.-X., *Organometallics* **2010,** *29* (13), 2842-2849.

....

43.   Yu, W.-B.; Han, Y.-F.; Lin, Y.-J.; Jin, G.-X., *Chem. Eur. J.* **2011,** *17* (6), 1863-1871.

44.   (a) Toh, N. L.; Nagarathinam, M.; Vittal, J. J., *Angew. Chem. Int. Ed.* **2005,** *44* (15), 2237-2241; (b) Vittal, J. J., *Coord. Chem. Rev.* **2007,** *251* (13-14), 1781-1795; (c) Nagarathinam, M.; Peedikakkal, A. M. P.; Vittal, J. J., *Chem. Commun.* **2008,** (42), 5277; (d) Nagarathinam, M.; Vittal, J. J., *Macromol. Rapid Commun.* **2006,** *27* (14), 1091-1099; (e) Nagarathinam, M.; Vittal, J. J., *Chem. Commun.* **2008,** (4), 438-440.

45.   (a) Briceño, A.; Hill, Y.; Gonzalez, T.; Diaz de Delgado, G., *Dalton Trans.* **2009,** (9), 1602-1610; (b) Peedikakkal, A. M. P.; Koh, L. L.; Vittal, J. J., *Chem. Commun.* **2008,** (4), 441-443; (c) Peedikakkal, A. M. P.; Vittal, J. J., *Inorg. Chem.* **2009,** *49* (1), 10-12.

46.   Mir, M. H.; Koh, L. L.; Tan, G. K.; Vittal, J. J., *Angew. Chem. Int. Ed.* **2010,** *49* (2), 390-393.

47.   Eubank, J. F.; Kravtsov, V. C.; Eddaoudi, M., *J. Am. Chem. Soc.* **2007,** *129* (18), 5820-5821.

48.   Blake, A. J.; Champness, N. R.; Chung, S. S. M.; Li, W.-S.; Schröder, M., *Chem. Commun.* **1997,** (17), 1675-1676.

49.   (a) Irwin, M. J.; Vittal, J. J.; Yap, G. P. A.; Puddephatt, R. J., *J. Am. Chem. Soc.* **1996,** *118* (51), 13101-13102; (b) Brandys, M.-C.; Puddephatt, R. J., *Chem. Commun.* **2001,** (16), 1508-1509; (c) Brandys, M.-C.; Jennings, M. C.; Puddephatt, R. J., *J. Chem. Soc., Dalton Trans.* **2000,** (24), 4601-4606.

50.   Chu, Q.; Swenson, D. C.; MacGillivray, L. R., *Angew. Chem. Int. Ed.* **2005,** *44* (23), 3569-3572.

51.   Nagarathinam, M.; Vittal, J. J., *Angew. Chem. Int. Ed.* **2006,** *45* (26), 4337-4341.

52.   Santra, R.; Biradha, K., *Cryst. Growth Des.* **2010,** *10* (8), 3315-3320.

....

53.   Liu, D.; Li, H.-X.; Ren, Z.-G.; Chen, Y.; Zhang, Y.; Lang, J.-P., *Cryst. Growth Des.* **2009,** *9* (10), 4562-4566.

54.   Georgiev, I. G.; Bucar, D.-K.; MacGillivray, L. R., *Chem. Commun.* **2010,** *46* (27), 4956-4958.

55.   Singh, K.; Long, J. R.; Stavropoulos, P., *J. Am. Chem. Soc.* **1997,** *119* (12), 2942-2943.

56.   Ramamurthy, V.; Venkatesan, K., *Chem. Rev.* **1987,** *87* (2), 433-481.

57.   (a) Peedikakkal, A. M. P.; Vittal, J. J., *Chem. Eur. J.* **2008,** *14* (17), 5329-5334; (b) Ohba, S.; Hosomi, H.; Ito, Y., *J. Am. Chem. Soc.* **2001,** *123* (26), 6349-6352.

58.   (a) Harada, J.; Ogawa, K., *J. Am. Chem. Soc.* **2001,** *123* (44), 10884-10888; (b) Harada, J.; Ogawa, K., *Chem. Soc. Rev.* **2009,** *38* (8), 2244.

59.   (a) Saltiel, J.; Krishna, T. S. R.; Turek, A. M.; Clark, R. J., *Chem. Commun.* **2006,** (14), 1506-1508; (b) Nishizawa, N.; Furukawa, D.; Kobatake, S.; Matsumoto, A., *Cryst. Growth Des.* **2010,** *10* (7), 3203-3210; (c) Furukawa, D.; Kobatake, S.; Matsumoto, A., *Chem. Commun.* **2008,** (1), 55-57.

60.   Harada, J.; Uekusa, H.; Ohashi, Y., *J. Am. Chem. Soc.* **1999,** *121* (24), 5809-5810.

61.   Liu, R. S. H.; Hammond, G. S., *Acc. Chem. Res.* **2005,** *38* (5), 396-403.

62.   (a) Trask, A. V.; Jones, W., *Top. Curr. Chem.* **2005,** *254*, 41-70; (b) Kaupp, G., *Top. Curr. Chem.* **2005,** *254*, 95-183; (c) Tanaka, K.; Toda, F., *Chem. Rev.* **2000,** *100* (3), 1025-1074; (d) Friščić, T.; Jones, W., *Cryst. Growth Des.* **2009,** *9* (3), 1621-1637.

63.   (a) Cinčić, D.; Friščić, T.; Jones, W., *J. Am. Chem. Soc.* **2008,** *130* (24), 7524-7525; (b) Braga, D.; Giaffreda, S. L.; Grepioni, F.; Pettersen, A.; Maini, L.; Curzi, M.; Polito, M., *Dalton Trans.* **2006,** (10), 1249-1263; (c) Orita, A.; Jiang, L.; Nakano, T.; Ma, N.; Otera, J., *Chem. Commun.* **2002,** (13), 1362-1363; (d) Braga, D.;

....

Curzi, M.; Johansson, A.; Polito, M.; Rubini, K.; Grepioni, F., *Angew. Chem. Int. Ed.* **2006,** *45* (1), 142-146.

64.   (a) Shan, N.; Jones, W., *Green Chem.* **2003,** *5* (6), 728-730; (b) Atkinson, M. B. J.; Bucar, D.-K.; Sokolov, A. N.; Friscic, T.; Robinson, C. N.; Bilal, M. Y.; Sinada, N. G.; Chevannes, A.; MacGillivray, L. R., *Chem. Commun.* **2008,**   (44), 5713-5715; (c) Sokolov, A. N.; Bučar, D.-K.; Baltrusaitis, J.; Gu, S. X.; MacGillivray, L. R., *Angew. Chem. Int. Ed.* **2010,** *49* (25), 4273-4277.

Chapter 2

Solid State Photodimerization of Molecular Salts of *Trans*-4,4'-stilbenedicarboxylic Acid (H$_2$SDC)[*]

2.1 Introduction

Solid state photodimerization reaction has been well studied in the past on co-crystals, metal complexes and coordination polymers, host-guest compounds and molecular salts. Among these classes of materials, molecular salts have drawn greater attention for their advantages over co-crystals in organic materials. Molecular salts differ from co-crystals by the position of the hydrogen while forming the hydrogen bond between acidic and basic counterparts. The advantages of molecular salts over co-crystals are: a) greater stability due to robust charge assisted hydrogen-bonded supramolecular ionic synthons over their neutral counterparts; b) better control of the stoichiometry; c) better solubility in water and d) easy separation of the dimeric product. Electrostatic interaction, being less directional compared to other supramolecular interactions, makes it a challenge to rationalize the orientations of ionic counterparts in solid molecular salts, compared to co-crystals, in synthesising functional molecular solids utilising the directionality of the H-bonding. Generally, the carboxylic acid and phenolic hydroxyl functionalities (H-bond donors) are being extensively used to direct the parallel alignment of olefins containing pyridyl groups (H-bond acceptors) in their co-crystals. The parallel alignments of carboxylic acids via the salt formation with organic amines were reported by Ito *et al.* and Ramamurthy *et al.* In some early contributions, Ito *et al.* have reported the photodimerization of fumaric acid and certain *trans*-cinnamic acid derivatives via the salt formation with some organic amines such as ethylenediamine, *trans*-1,2-diaminocyclohexane etc.[1] Ramamurty *et al.* also have studied the photodimerization reaction of diamine double salts of *trans*-cinnamic acid derivatives with *trans*-1,2-diaminocyclohexane where they reported the formation of β-truxinate as the major product due the pedal-like motion involved in the system.[2] Despites these reports, the challenge in aligning C=C bonds in molecular salts still persist and research has to be

continued to fully understand the design strategy involved in controlling charge assisted hydrogen bonding or electrostatic interactions.

Since the identification of the 'supramolecular synthons' and the patterns of the charge assisted hydrogen bonded motifs constructing the solid state architecture are significant to align C=C bonds in molecular salts, there is a need of systematic investigation. Hence this chapter is meant to describe molecular salt of *trans*-4,4′-stilbenedicarboxylic acid (H$_2$SDC) with various amines and their solid state photoreactivity.

The solid nature and the insolubility of H$_2$SDC in most of the common organic solvents forced to synthesize the molecular salts to explore the crystal engineering properties. Generally for salt formation, the difference in pKa values of base and acid should be greater than 3 (section 1.4). The pKa values of H$_2$SDC, calculated by SPARC program (http://ibmlc2.chem.uga.edu/sparc/), are shown in Scheme 2.1 below. A series of organic bases that are reasonably strong to abstract acidic proton from H$_2$SDC have been employed in order to make molecular salts. The pKa values of all the amines used in this study are listed below in Scheme 2.2.
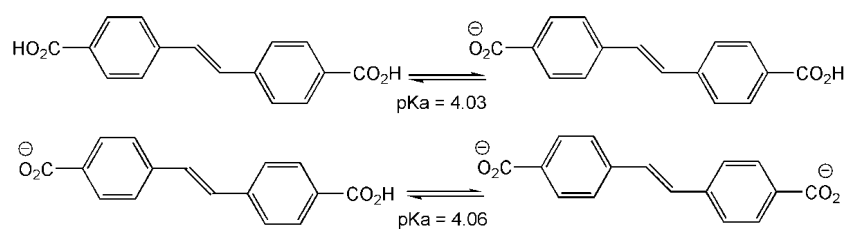
Scheme 2.1 The calculated pKa values of H$_2$SDC are shown

Therefore, this chapter describes the structural features of the molecular salts of H$_2$SDC that exhibit interesting patterns and packing. The identification of the 'supramolecular synthons' and the patterns of the charge assisted hydrogen bonded motifs constructing the solid state architecture of these molecular salts have been characterized crystallographically. A series of molecular salts obtained by reacting

H$_2$SDC with cyclohexylamine (**1**), ethylenediamine (**2**), 1,3-diaminopropane (**3**) 1,4-diaminobutane (**4**), dithiobisethanamine (**5**), guanidine (**6**), 4-aminopyridine (**7**) and piperizine (**8**) have been synthesized, characterized and the hydrogen bonded motifs constructing the solid state architectures have been identified to rationalize their solid state photoreactivity.
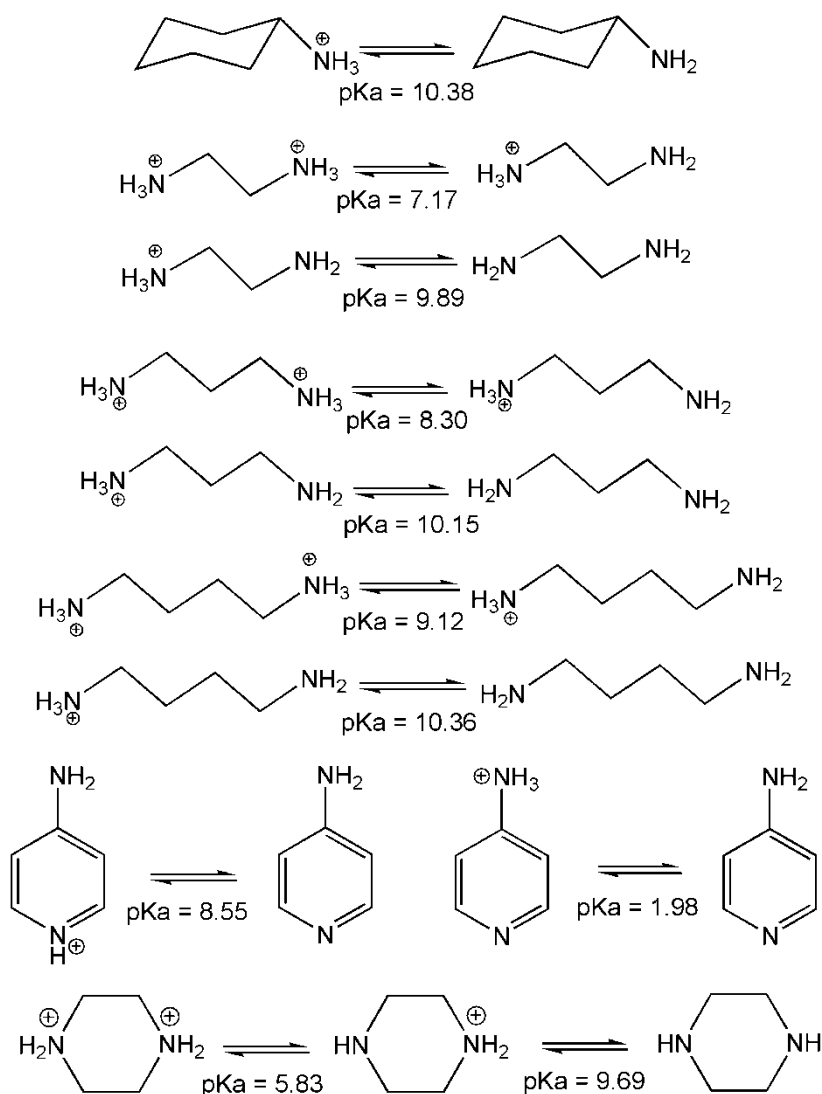
Scheme 2.2 The pKa values of the amines are listed

2.2 Results and Discussion

2.2.1 Description of the Crystal Structures

2.2.1.1 Crystal Structure of Cyclohexylammonium-Stilbenedicarboxylate salt, (cyclohexa)$_2$(SDC) (1)

The structure of the salt of composition $C_{42}H_{57}N_3O_6$ (**1**) crystallizes in the triclinic space group, $P\bar{1}$. The asymmetric unit contains one and a half anions $C_{16}H_{10}O_4$ (SDC) and three cations $C_6H_{14}N$ (cyclohexylammonium cation) where one of the cations is disordered. The crystal structure is stabilized by the charge assisted H-bonding interactions between NH_3^+ and CO_2^- units. The hydrogen bonding parameters are listed in Table 2.1. Each carboxylate unit interacts with three different NH_3^+ units where one of the carboxylate oxygen atoms interacts with two NH_3^+ proton donors (Figure 2.1a). On the other hand, each NH_3^+ unit of the cation donates H-bond to three carboxylate groups of three different SDC^{2-} anions (Figure 2.1b). The hydrogen bonding assembly found to be photo-stable. The overall packing structure of this salt propagates in all the directions which results in a complicated three dimensional network. Among the H-bonding patterns that exist in the packing, the rings are identified with graph set notations $R_4^4(12)$ and $R_4^2(8)$ and are described in Figure 2.1c. Another interesting feature of this salt is that the SDC^{2-} anions are in offset parallel alignment. NH_3^+ unit of cyclohexylammonium cation acts as clipping template towards SDC^{2-} anions and organises them with a separation of 4.665 Å between the centres of the olefinic double bonds (Figure 2.1d). The distance is beyond the Schmidt's criteria[3] for solid state [2 + 2] cycloaddition reaction, the salt was also found to be photo-stable. The overall packing structure is shown in Figure 2.2.

....

Table 2.1 The hydrogen bonding parameters for **1**

D-H⋯A	D(D-H) (Å)	D(H⋯A) (Å)	D(D⋯A) (Å)	<(DHA) (°)	Symmetry Operator
N(1)-H(1A)⋯O(1)	0.90	1.96	2.840(3)	167	-x+1, -y, -z+1
N(1)-H(1B)⋯O(2)	0.90	1.89	2.781(3)	170	x-1, y+1, z
N(1)-H(1C)⋯O(4)	0.90	1.86	2.757(3)	177	-x, -y+2, -z
N(2)-H(2A)⋯O(6)	0.90	1.91	2.798(3)	171	x, y, z+1
N(2)-H(2B)⋯O(3)	0.90	1.86	2.733(3)	162	-x, -y+2, -z
N(2)-H(2C)⋯O(1)	0.90	1.89	2.781(3)	173	x-1, y+1, z
N(3)-H(3A)⋯O(6)	0.90	1.87	2.745(3)	165	-x+1, -y+1, -z
N(3)-H(3B)⋯O(5)	0.90	1.85	2.729(3)	166	-x, -y+2, -z
N(3)-H(3C)⋯O(3)	0.90	1.89	2.770(3)	165	-x+1, -y+1, -z+1
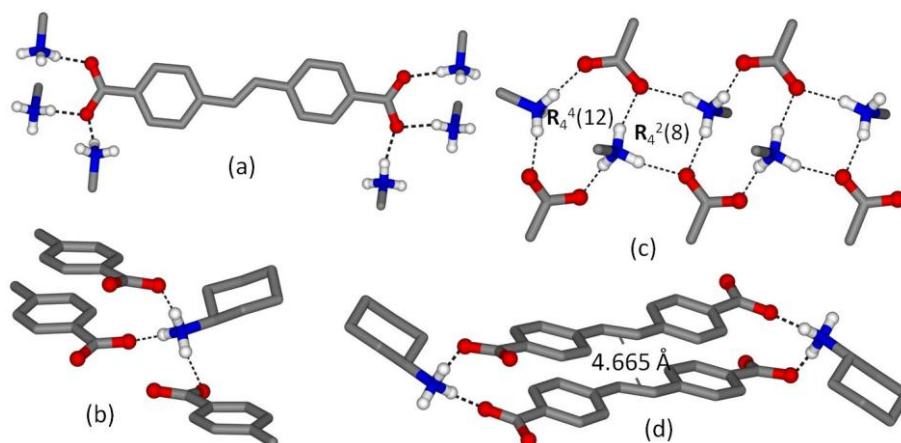
Figure 2.1 Various types of hydrogen bonding interactions, supramolecular synthons and orientation of SDC^{2-} anions in the crystal structure of **1**.
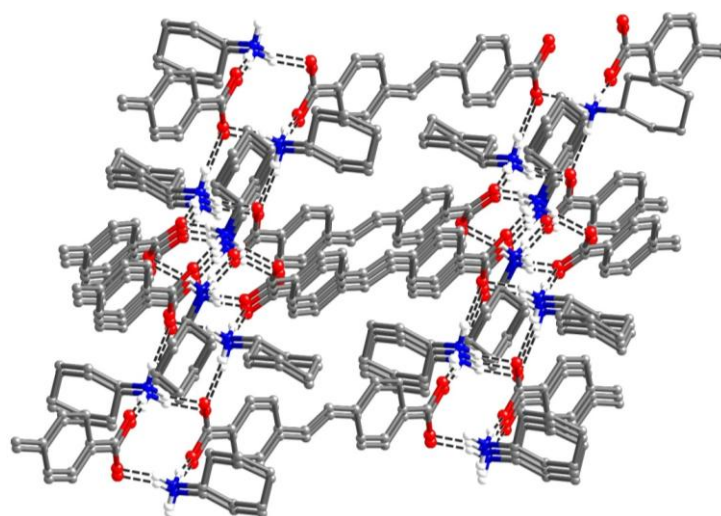
Figure 2.2 The packing of ionic counter parts of **1** approximately along *a*-direction.

....

2.2.1.2 Crystal Structure of Ethylenediammonium-SDC Salt, (EDA)(SDC) (2)

Single-crystal X-Ray diffraction analysis reveals that the asymmetric unit of the salt of composition $C_{18}H_{20}N_2O_4$ (**2**), contains one anion $C_{16}H_{10}O_4$ (SDC) and one cation $C_2H_{10}N_2$ (EDA). The structure crystallizes in the monoclinic space group, $P2_1/c$. The anions and cations are held together by various charge assisted N-H⋯O hydrogen bonds (see Table 2.2). Each NH_3^+ unit of the diammonium cation interacts with three carboxylate groups of three different SDC^{2-} anions (Figure 2.3a). Both the carboxylate units of each SDC^{2-} anion interact with three NH_3^+ units while two oxygen atoms in a carboxylate unit interact dissimilarly (Figure 2.3b). One of the carboxylate oxygen atoms accepts one H-bond from NH_3^+ unit whereas the other one accepts two H-bonds from two NH_3^+ units. Both the NH_3^+ end of one ethylenediammonium cation act as H-bond donor toward three carboxylates units that result in an undefined three dimensional hydrogen bonded network. A view on the *ac*- plane shows the organised arrangement of cations and anions where the dications are interspersed between the anionic layers. A closer look to the H-bonding pattern reveals that there is H-bonded ring with graph set $\mathbf{R}_4^4(12)$ formed by two NH_3^+ and two carboxylate units (Figure 2.3c). The distance between two nearest SDC moieties (two C=C bonds) is 6.274Å indicating no effective preorganisation for photoreactivity.

Table 2.2 The hydrogen bonding parameters for **2**

D-H⋯A	D(D-H) (Å)	D(H⋯A) (Å)	D(D⋯A) (Å)	<(DHA) (°)	Symmetry Operator
N(1)-H(3N)⋯O(1)	0.94	1.88	2.766(3)	157(3)	-x+1, -y+1, -z+2
N(1)-H(2N)⋯O(2)	1.01	1.73	2.729(3)	171(3)	x, -y+1/2, z-1/2
N(1)-H(1N)⋯O(2)	0.96	1.82	2.774(3)	173(3)	-x+2, -y+1, -z+1
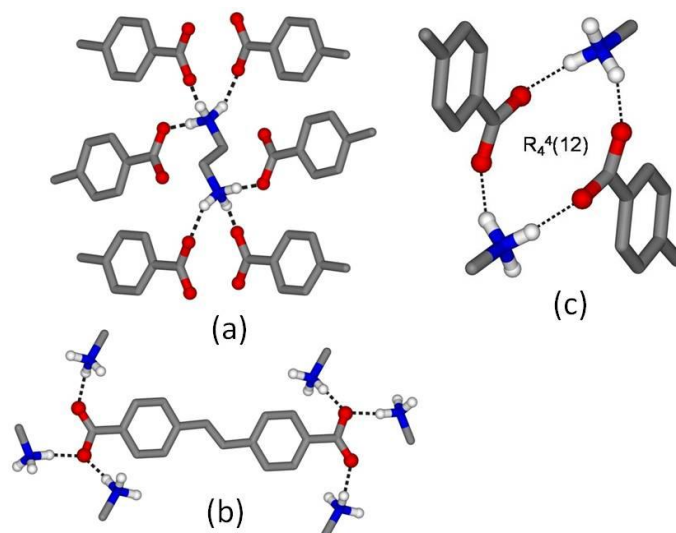
Figure 2.3 Various types of hydrogen bonding interactions and supramolecular synthons in the crystal structure of **2**.
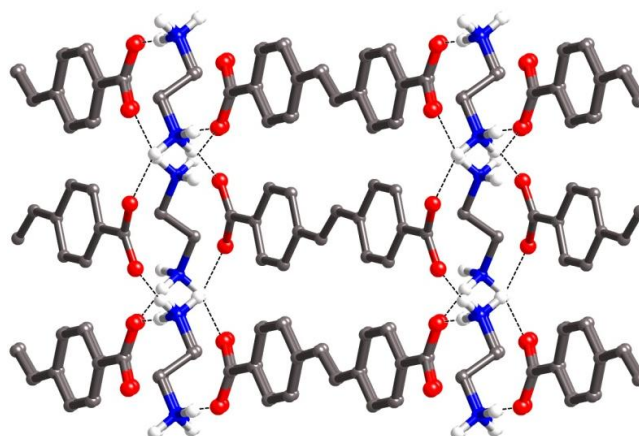
Figure 2.4 The packing of ionic counter parts of **2** approximately along *c*-direction.

2.2.1.3 Crystal Structure of 1,3-Diammoniumpropane-SDC Salt, (DAP)(SDC)·H₂O (3)

The asymmetric unit of the salt contains one SDC anion, one DAP cation and one water molecule. Each CO_2^- unit of SDC^{2-} anion is involved in charge assisted H-bonding interactions with NH_3^+ units of different DAP cations and H-bonding interaction with water molecules present in the crystal (Figure 2.5a). In terms of supramolecular interactions exhibited, two carboxylate ends of each SDC^{2-} anion,

....

like two NH_3^+ units of each DAP cations, are uneven. One carboxylate unit involves in charge assisted H-bonding interaction with three different NH_3^+ units of three different DAP cations. The other carboxylate unit interacts with two water molecules and two NH_3^+ units of two different DAP cations. Similarly, one end of DAP interacts with three carboxylate units of three SDC^{2-} where as the other end interacts with two carboxylate units of two SDC^{2-} unit and one water molecule (Figure 2.5b). Each water molecule plays the role of H-bond donor to two carboxylates end as well as acceptor to one NH_3^+ unit. The hydrogen bonded assembly of cation, anion and water molecules propagates in all the directions to result in a very complicated three dimensional network.
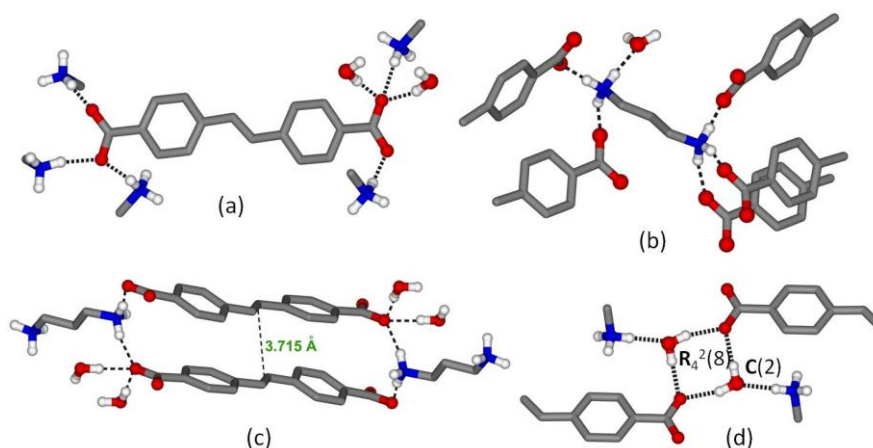
Figure 2.5 Various types of hydrogen bonding interactions, supramolecular synthons and orientation of SDC^{2-} anions in the crystal structure of **3**.

A thorough examination of the H-bonding patterns in the packing structure (Figure 2.6) reveals that there is a H-bonded ring with graph set $\mathbf{R}_4^2(8)$ as shown in Figure 2.5d. The most interesting property of this salt is the parallel orientation of the SDC^{2-} anions where the centre-to-centre distance between two parallel aligned SDC^{2-} anions is 3.715 Å that satisfies the Schmidt's criteria[3] for solid state photochemical reaction (Figure 2.5c). Here, NH_3^+ units of the diammoniumpropane act as clipping templates for aligning dicarboxylate units with the help of water molecules present in the crystal. Upon irradiation under UV light for 30 h the salt was observed to undergo

....

quantitative photodimerization to yield the salt of 1,2,3,4-tetrakis(4′-carboxyphenyl)cyclobutane (TCCB). The mechanochemical synthesis and the characterizations of this compound from this salt have been described later in this chapter and also it is shown to be a potential candidate for synthesizing co-crystals and MOFs in the Chapter 7.

Table 2.3 The hydrogen bonding parameters for **3**

D-H···A	D(D-H) (Å)	D(H···A) (Å)	D(D···A) (Å)	<(DHA) (°)	Symmetry Operator
N(1)-H(1A)···O(1)	0.89	1.90	2.774(1)	164	1-x, 1-y, -z
N(1)-H(1B)···O(1)	0.92	1.81	2.721(1)	167	1-x, 1/2+y, 1/2-z
N(1)-H(1C)···O(4)	0.90	1.98	2.853(1)	164	
N(2)-H(2A)···O(2)	0.92	1.87	2.774(1)	165	1+x, 3/2-y, -1/2+z
N(2)-H(2B)···O(3)	0.90	1.87	2.736(1)	160	2-x, 1-y, -z
N(2)-H(2C)···O(5)	0.90	1.93	2.829(1)	177	x, 3/2-y, 1/2+z
O(5)-H(5A)···O(4)	0.87	1.87	2.718(1)	164	
O(5)-H(5B)···O(4)	0.86	1.90	2.763(1)	178(2)	2-x, 1-y, -z
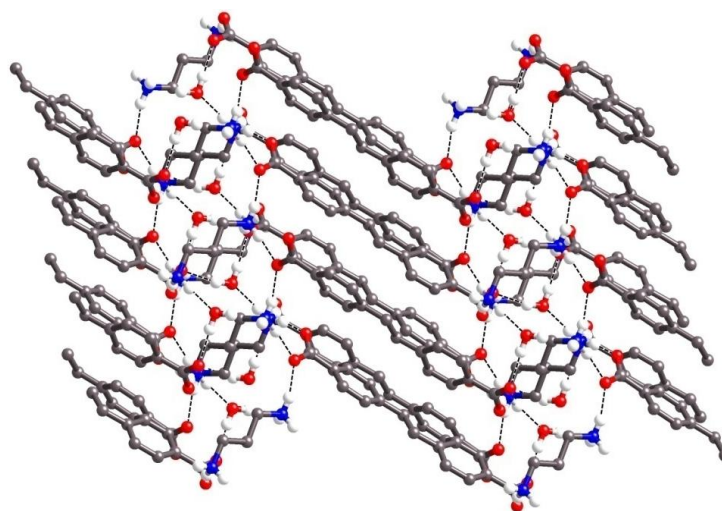
Figure 2.6 A view of packing along the *b*-axis shows that the components are packed in zigzag manner in **3**

2.2.1.4 Crystal Structure of 1,4-Diammoniumbutane-SDC salt, (DAB)(SDC)·2H₂O (4)

The structure of this salt of composition $C_{20}H_{28}N_2O_6$ (**4**) crystallizes in the triclinic space group, $P\bar{1}$. The asymmetric unit contains two halves of the anion SDC, one DAB cation and two water molecules. Each carboxylate oxygen atom of each SDC^{2-} is interacting with one water molecule and one NH_3^+ unit of a DAB (Figure 2.7a). Each water molecule acts as H-bond donor to two carboxylate oxygen atoms and H-bond acceptor to one NH_3^+ unit. Each NH_3^+ unit of DAB is connected to two carboxylate units of two different SDC^{2-} anions through charge assisted H-bonding and one water molecule (Figure 2.7b). The hydrogen bonding parameters are listed in Table 2.4 below.

A detailed scrutiny to the packing (Figure 2.8) of the crystal structure reveals the presence of two types of H-bonded rings with graph set $\mathbf{R}_3^3(8)$ and $\mathbf{R}_7^5(16)$ (Figure 2.7d). Another interesting feature of the salt is that the SDC^{2-} anions are involved in π–π stacking interactions. The distance between two planes of parallel aligned offset SDC^{2-} anions is 3.592 Å and between the centroids of two nearest aromatic rings is 3.867 Å (Figure 2.7c). However, the crystal is found to be

43

photostable as the olefinic double bonds of two parallel aligned SDC^{2-} anions are slipped away.

Table 2.4 The hydrogen bonding parameters for **4**

D-H···A	D(D-H) (Å)	D(H···A) (Å)	D(D···A) (Å)	<(DHA) (°)	Symmetry Operator
N(1)-H(1A)···O(1W)	0.90	2.20	2.794(2)	123	-x+1, -y+1, -z+1
N(1)-H(1B)···O(2)	0.90	1.79	2.691(2)	178	x+1, y, z
N(1)-H(1C)···O(4)	0.90	1.90	2.789(2)	167	-x+1, -y+2, -z+1
N(2)-H(2A)···O(1)	0.90	1.93	2.826(2)	174	-x, -y+1, -z+1
N(2)-H(2B)···O(3)	0.90	1.83	2.728(2)	177	x-1, y, z
N(2)-H(2C)···O(2W)	0.90	1.98	2.767(2)	145	-x, -y+2, -z+1
O(1W)-H(1WA)···O(1)	0.90	1.93	2.820(2)	172(3)	-x, -y+1, -z+1
O(1W)-H(1WB)···O(3)	0.97	1.83	2.789(2)	170(3)	
O(2W)-H(2WA)···O(4)	0.93	1.85	2.764(2)	168(3)	-x+1, -y+2, -z+1
O(2W)-H(2WB)···O(2)	0.88	1.95	2.819(2)	168(3)	
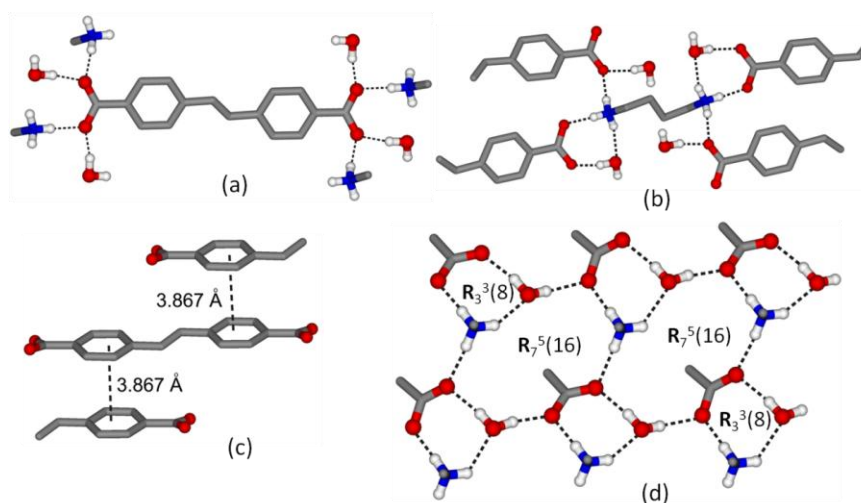
Figure 2.7 Various types of hydrogen bonding interactions, supramolecular synthons and orientation of SDC^{2-} anions in the crystal structure of **4**.

Chapter 2

....
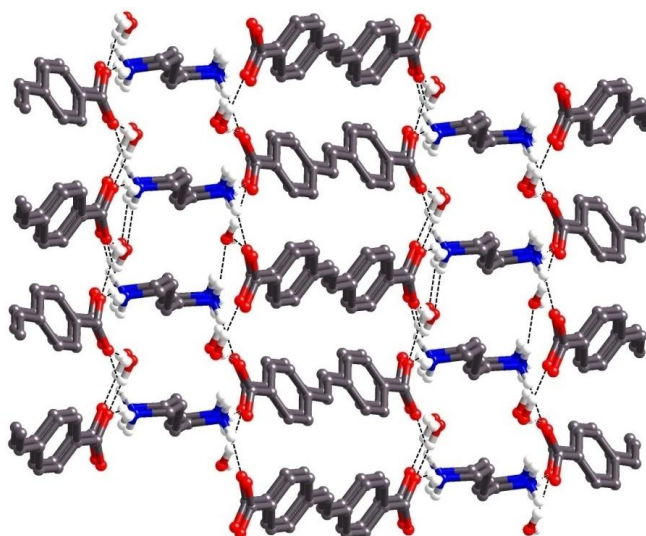
Figure 2.8 A perspective view of packing of the ionic counter parts of **4**.

2.2.1.5 Crystal Structure of 2,2′-Dithiobis(ethanammonium)–SDC salt, (DBEA)(SDC) (5)

Single crystal X-ray diffraction analysis shows that the asymmetric unit of the salt of composition $C_{20}H_{24}N_2O_4S_2$ (**5**), contains two halves of the anion SDC and one cation DBEA. Both the carboxylate units of SDC^{2-} anions interact via charge assisted hydrogen bonding with three NH_3^+ units of three DBEA cations. One of the carboxylate oxygen atoms accepts H-bonding from two NH_3^+ units and while the other one from only a single NH_3^+ unit (Figure 2.9a). On the other hand, each NH_3^+ unit of the cation is hydrogen bonded to three CO_2^- units (Figure 2.9b). In the crystal structure of the salt, we find two dimensional sheets where SDC^{2-} ions orient in such a way that they undergo aromatic C-H$\cdots\pi$ interactions with a distance of 3.908 Å (Figure 2.10) between carbon to centroid of the phenyl ring. Two dimensional sheets of such kind are stacked parallel also by aromatic C-H$\cdots\pi$ interaction between phenyl rings of the SDC^{2-} anions having a distance of 3.67 Å (C atom to centroid of phenyl ring, as shown in Figure 2.9c). The H-bonded motifs present in the structure can be represented by graph set notation as $\mathbf{R}_4^2(8)$ and $\mathbf{R}_4^4(12)$ as described in Figure 2.9e.

Table 2.5 The hydrogen bonding parameters for **5**

D-H⋯A	D(D-H) (Å)	D(H⋯A) (Å)	D(D⋯A) (Å)	<(DHA) (°)	Symmetry Operator
N(1)-H(1A)⋯O(1)	0.91	1.89	2.776(1)	165	x+1, y, z
N(1)-H(1B)⋯O(4)	0.91	1.75	2.656(1)	173	-x+2, -y, -z+2
N(1)-H(1C)⋯O(1)	0.91	1.94	2.849(1)	180	-x+1, -y, -z+2
N(2)-H(2A)⋯O(3)	0.91	1.90	2.779(1)	163	-x+1, -y+1, -z+2
N(2)-H(2B)⋯O(2)	0.91	1.84	2.742(1)	174	x, y+1, z
S(1)⋯N(1)-H(1A 1B 1C)	-	-	3.486	-	-x+2, -y, 2-z
S(2)⋯N(2)-H(2A 2B 2C)	-	-	3.283	-	-x+1, -y+1, -z+2

Another interesting feature of the packing is the conformation of the dication. DBEA dications present in both the M- and P-type helical conformation and this particular conformation is stabilised by the weak interactions between sulfur and NH_3^+ units of the two types of conformers (Figure 2.9d). The distances between sulphur and nitrogen of NH_3^+ are 3.283 Å and 3.487 Å that are in order of the sum of the van der Waal radii of nitrogen and sulphur (3.35 Å). Hence, the existing weak interaction between sulphur and nitrogen is responsible for the helical conformation as shown in Figure 2.10. The existence of helical conformation of this cation has been noted before in the literature.[4]
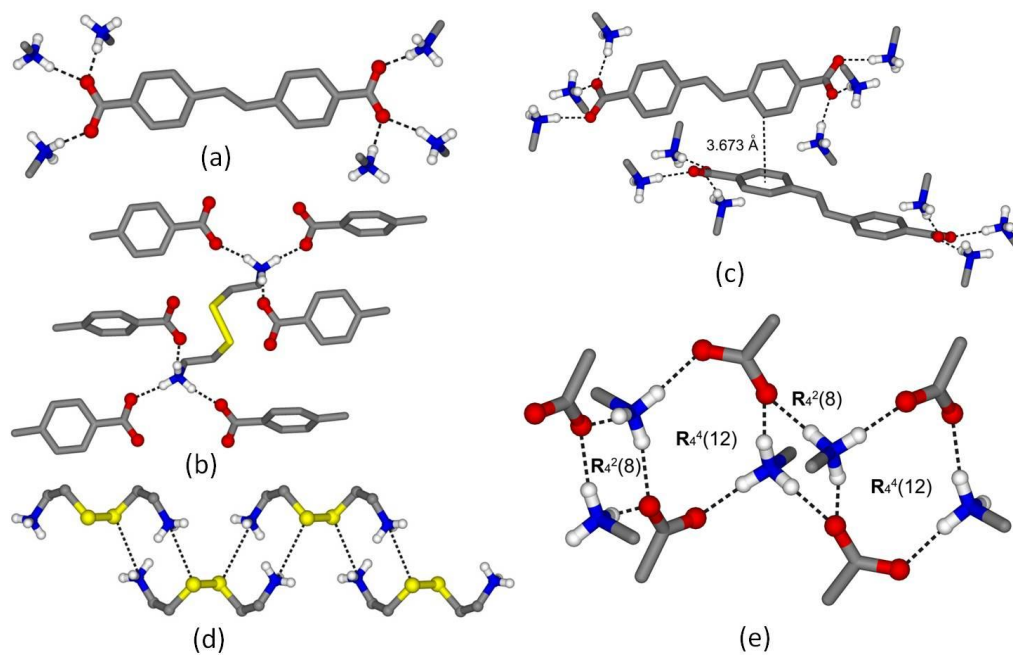
Figure 2.9 Various types of hydrogen bonding interactions and supramolecular synthons in the crystal structure of **5**.
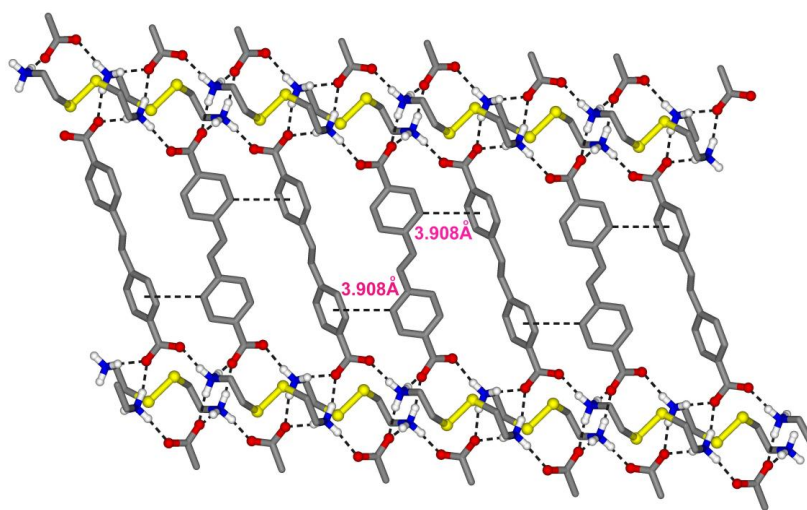
Figure 2.10 Two dimensional sheet-like structure and aromatic C-H···π interaction in **5**.

2.2.1.6 Crystal Structure of Guanidinium–SDC salt, (Guan)$_2$(SDC)·4H$_2$O (6)

The asymmetric unit of the salt of composition $C_9H_{15}N_3O_4$ (**6**) crystallized in the monoclinic space group, $P2_1/c$ and it contains half an anion SDC and one Guan cation and two water molecules. Each carboxylate unit interacts with two Guan cations and two water molecules where one carboxylate oxygen is bonded to two N-H

....

(Guan) and one O-H (water) and the other one with one N-H (Guan) and one O-H (water) (Figure 2.11a). The geometric parameters for hydrogen bonding are listed in the Table 2.6. Generally, the Guan cation due to its inherent 3-fold axial symmetry, is able to form three pairs of strong hydrogen bonds to various oxyanions to construct (6,3) connected Rosette like networks with C_3-symmetric oxoanion building blocks.[5] Again, guanidine hydrochloride was utilised by Ito *et al.* to make two different co-crystals of fumaric acid that undergo photodimerization partially under UV light.[1a]

However, in the present study, Guan cation has been used for synthesising molecular salts with SDC^{2-} where each Guan cation is bonded to two SDC^{2-} anions and two water molecules. The structure resembles neither the (6, 3) connected Rosette networks nor the SDC^{2-} anions are found parallel. The supramolecular interactions between neutral fumaric acids with Guan cations in the co-crystals (where Cl^- ions balances the charge)[1a] are different from that of between SDC^{2-} anions and the same cations in **6**. H-bonding centred around each Guan cation can be represented by graph set notation as $\mathbf{R}_2^2(8)$ and $\mathbf{R}_3^2(8)$ (Figure 2.11b). A thorough perusal of the H-bonding patterns in the packing of this salt reveals that there is 1D zigzag water chain passing along *c*-direction. Various H-bonds stabilise the water
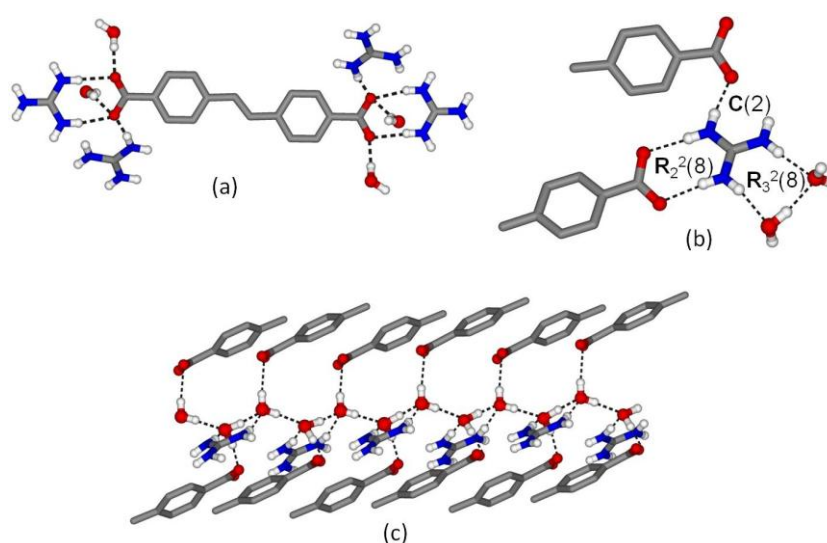
Figure 2.11 Various types of hydrogen bonding interactions, supramolecular synthons and existence of 1D water chain in the crystal structure of **6**.

Table 2.6 The hydrogen bonding parameters for **6**

D-H⋯A	D(D-H) (Å)	D(H⋯A) (Å)	D(D⋯A) (Å)	<(DHA) (°)	Symmetry Operator
N(1)-H(1A)⋯O(2W)	0.87	2.16	3.029(2)	175	-x, y-1/2, -z+3/2
N(2)-H(2A)⋯O(1)	0.87	1.97	2.831(2)	171	x, -y+1/2, z-1/2
N(2)-H(2B)⋯O(1W)	0.87	2.07	2.921(2)	167	x, y-1, z
N(3)-H(3A)⋯O(2)	0.87	2.05	2.895(2)	164	x, -y+1/2, z-1/2
N(3)-H(3B)⋯O(2)	0.87	1.98	2.845(2)	172	
O(1W)-H(1WA)⋯O(2W)	0.91	1.86	2.761(2)	169(2)	-x, y+1/2, -z+3/2
O(2W)-H(2WA)⋯O(1W)	0.83	1.94	2.758(2)	171(2)	-x, -y+1, -z+1
O(1W)-H(1WB)⋯O(1)	0.90	1.82	2.723(2)	175(2)	
O(2W)-H(2WB)⋯O(2)	0.85	2.08	2.906(2)	163(2)	

chain in the crystal. Each water molecule acts as H-bond donor to one carboxylate oxygen and one water molecule; whereas it accepts two H-bond from another water molecule and one N-H from Guan ion (Figure 2.11c). Interestingly, a discrete $(H_2O)_{32}$ cluster, encapsulated in an organic salt of Guan cations, has been reported in literature.[6]
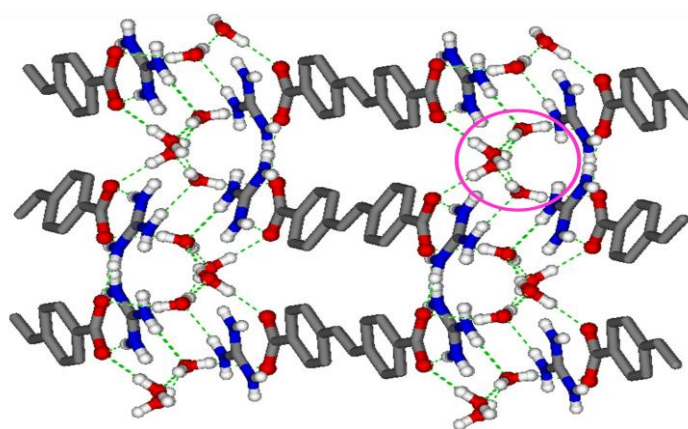
Figure 2.12 A perspective view of packing diagram along *c*-direction in **6**. Water cluster is shown in pink circle

2.2.1.7 Crystal Structure of 4-Aminopyridinium–SDC salt, (4-APH)₂(SDC)·2H₂O (7)

Single-crystal X-ray diffraction analysis reveals that the asymmetric unit of the title salt of composition $C_{26}H_{28}N_4O_6$ (**7**), contains half of the SDC^{2-} anion, one 4-AP cation and a water molecule. Two-point ionic synthon PyNH$^+\cdots^-O_2C$ plays the key role in the building of hydrogen-bonded network in the solid state structure. The protonation to Py-N rather than NH₂ group can be rationalized from all possible pK_a values of 4-AP (Scheme 2.2). Both the carboxylate groups are bonded to pyridinium cation via charge assisted two-point (cyclic) PyNH$^+\cdots^-O_2C$ synthon and also bonded to two water molecules via H-bonding. The parameters for hydrogen bonding are listed in Table 2.7. The NH₂ groups of the cations are pointed towards each other and are bridged by two water molecules via H-bonding (Figure 2.13a,b). From the packing of the crystal structure (Figure 2.14), it can be observed that the cations and anions are involved in the $\pi\cdots\pi$ stacking interaction and cations are interspersed between two SDC^{2-} anions. A closer look at the H-bonding pattern reveals that there are three types of H-bonded motifs and can be represented by graph set notation as $\mathbf{R}_2^2(7)$, $\mathbf{R}_4^2(8)$, $\mathbf{R}_4^4(12)$ (Figure 2.13d). The closest distance between C=C bonds of SDC is 10.61 Å which explains the reason of photostability of this salt.

Table 2.7 The hydrogen bonding parameters for **7**

D-H···A	D(D-H) (Å)	D(H···A) (Å)	D(D···A) (Å)	<(DHA) (°)	Symmetry Operator
N(1)-H(1N)···O(2)	1.01	1.62	2.626(1)	173	
N(1)-H(1N)···O(1)	1.01	2.50	3.201(2)	126	
N(2)-H(21)···O(1W)	0.91	2.03	2.928(2)	168	-x+1/2, y+1/2, -z+3/2
N(2)-H(22)···O(1W)	0.88	2.08	2.940(2)	163	x-1/2, -y+1/2, z+1/2
O(1W)-H(1WA)···O(2)	0.88	1.96	2.804(1)	161	-x+1, -y+1, -z+1
O(1W)-H(1WB)···O(1)	0.92	1.81	2.722(1)	171	
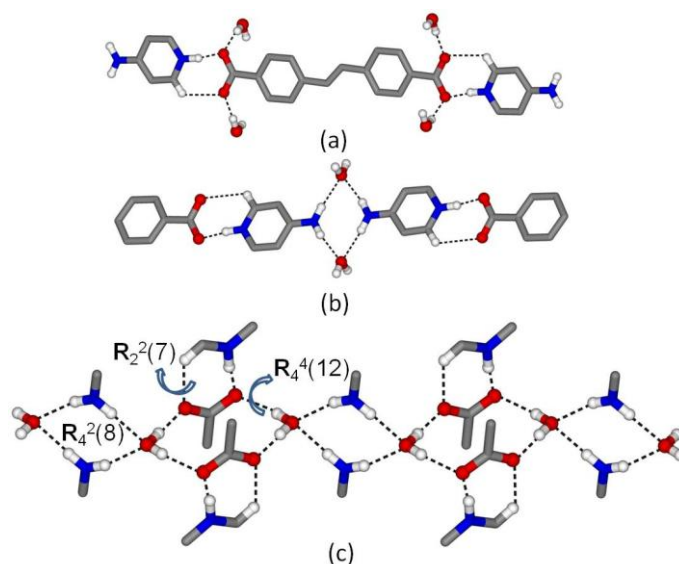
Figure 2.13 Various types of hydrogen bonding interactions, supramolecular synthons and existence of 1D water chain in the crystal structure of **7**.
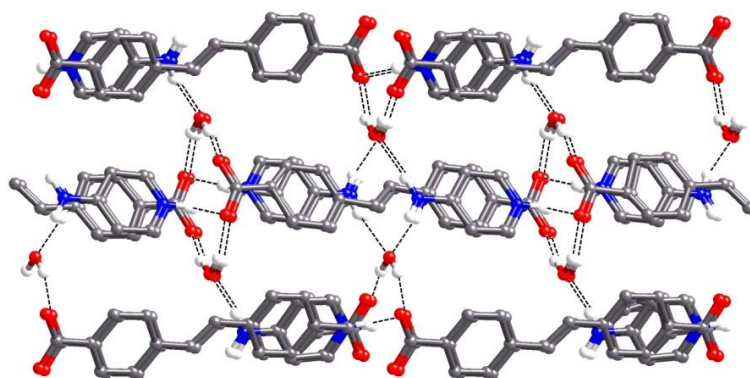
Figure 2.14 A perspective view of packing of the ionic counter parts approximately along *b*-axis in **7**.

2.2.1.8 Crystal Structure of Piperizinium–SDC Salt, (Pip)(SDC) (8)

The asymmetric unit of this salt of composition $C_{20}H_{22}N_2O_4$ (**8**) contains half an anion SDC and half a Pip cation. The ionic synthon, $NH_2^+\cdots{}^-O_2C$ plays principal role in the formation of the solid state architecture. Each carboxylate unit is bonded to four NH_2^+ units of four cations and each Pip cation is bonded to four carboxylate units of four SDC^{2-} anions in **C**(2) fashion (Figure 2.15). The geometric parameters for hydrogen bonding are listed in the Table 2.8 below.
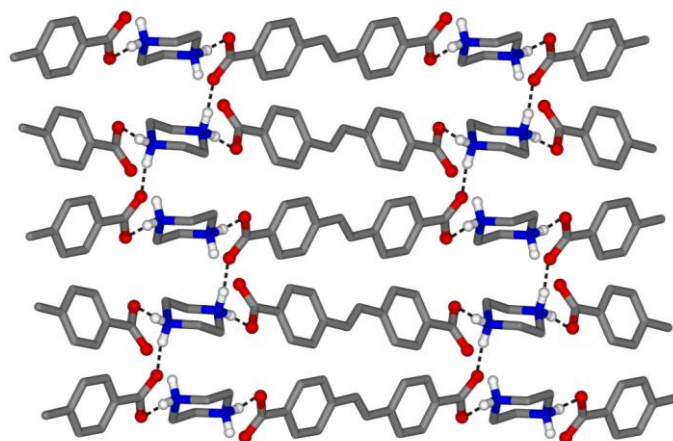
Figure 2.15 The packing of the ionic counter parts in **8** along *c*-direction.

Table 2.8 The hydrogen bonding parameters for **8**

D–H⋯A	D(D-H) (Å)	D(H⋯A) (Å)	D(D⋯A) (Å)	<(DHA) (°)	Symmetry Operator
N(1)-H(1A)⋯O(1)	0.92	1.70	2.617(2)	175	
N(1)-H(1A)⋯O(2)	0.92	2.65	3.265(2)	125	
N(1)-H(1B)⋯O(2)	0.92	1.82	2.727(2)	167	x, -y+3/2, z+1/2

2.2.2 Photoreactivity under UV light

All the compounds were irradiated under UV light to check their photo-reactivities irrespective of their alignment. The observed photoreactivity of these salts were then explained with the solid sate structures analysed by X-ray crystallography. Among the above compounds, we have found that only **3** undergoes quantitative photodimerization after 30 h irradiation.

2.2.2.1 Mechanochemical Synthesis of *rctt*-1,2,3,4-tetrakis(4′-Carboxyphenyl)cyclobutane from (DAP)(SDC)·H₂O (3)

The 1:1 mixture of H₂SDC, DAP and few drops of water were ground well for 20 min on an agate mortar (Scheme 2.3). The powder X-ray diffraction pattern (PXRD) of the mechanically ground powder matches well with the simulated pattern

for the compound **3** (Figure 2.16) which indicates that the parallel alignment of SDC^{2-}, which is essential for the solid-state photochemical cycloaddition reaction, has been achieved by the mechanochemical grinding of the reactants. The ground powder was packed in between two glass slides and then irradiated under UV light for 30 h. The quantitative photodimerization was confirmed by ^1H NMR spectroscopy by the disappearance and appearance of the peaks for ethylenic (δ 7.32 ppm) and cyclobutane protons (δ 5.56 ppm) respectively and m/z 535.4 in ESI-MS. The diamine abstracts acidic protons from H_2SDC during grinding to form conjugate acid-base pairs and resulted in ionic interactions between NH_3^+ and COO^- units. Here NH_3^+ units of the diamine act as clipping templates for aligning dicarboxylate units with the aid of water molecules present in the crystal (Figure 2.5c). Each carboxylate end of SDC^{2-} is involved in ionic interaction with two NH_3^+ units of two different DAP and H-bonding interaction with water molecule present in the crystal.
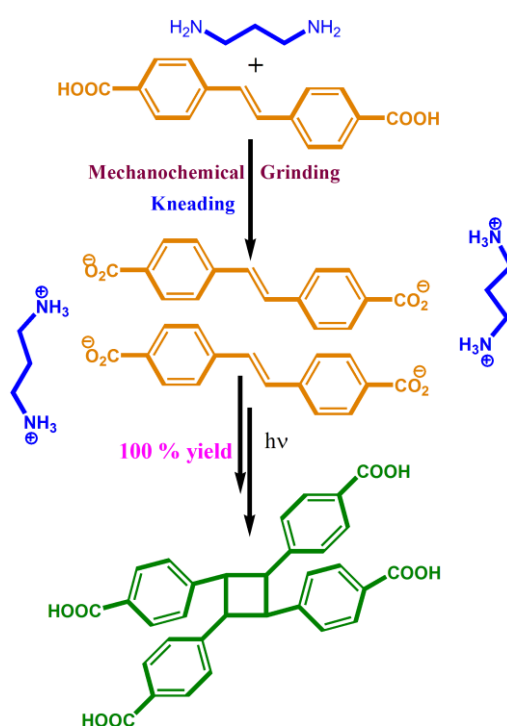
Scheme 2.3 Synthetic route for TCCB
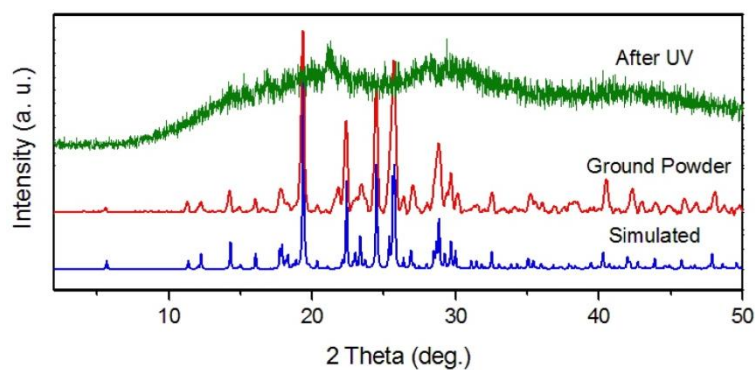
Figure 2.16 PXRD patterns: simulated pattern from single crystals data, before and after UV irradiation of the ground powder of **3**.
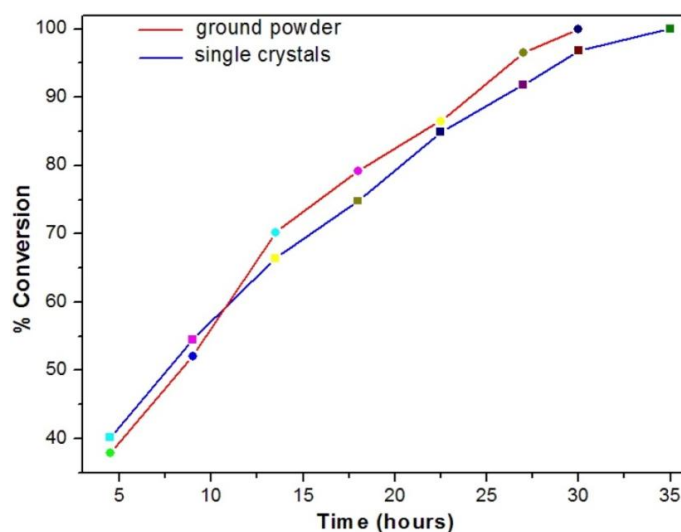
Figure 2.17 Percentage conversion *vs.* time plots for single crystals and ground powder of **3**.

PXRD pattern of the sample after UV irradiation reveals that there is considerable loss of crystallinity (Figure 2.16). Quantitative photodimerization of both the ground powder and single crystals was monitored by ^{1}H NMR spectroscopy to confirm their similar reactivity towards UV light by plotting the percentage of conversion *vs.* time (Figure 2.17). Slight increase in the reactivity kinetics for the ground powder compared to the single crystalline sample might be due to the smaller particle size and hence larger surface area.

....

The dimer product, *rctt*-1,2,3,4-tetrakis(4′-carboxyphenyl)cyclobutane (TCCB) was separated by acid work up, re-crystallized from methanol and was confirmed by ^{1}H and ^{13}C-NMR spectroscopy, mass spectroscopy and elemental analysis (see characterization section). Although the compound TCCB was known to form by the photo-irradiation of stilbamidine[7] and via the duplex formation of 4,4′-stilbenedicarboxamide with oligonucleotides,[8] selective or direct formation from H_2SDC in the solid state was not demonstrated before. The detailed crystal engineering studies on this new ligand for making co-crystals and metal organic frameworks (MOFs) are discussed in Chapter 7.

2.2.3 Discussion

In accordance with the plan to synthesize 1,2,3,4-tetrakis(4′-carboxyphenyl)cyclobutane via [2 + 2] cycloaddition reaction of H_2SDC, we have investigated a series of molecular salts. The photostable nature of H_2SDC in the solid state demands crystal engineering and the limited solubility of H_2SDC in common organic solvents prompted us to employ the salt formation route over co-crystals strategy. In the crystal structures of all these molecular salts, we have identified the supramolecular synthons that are exploited in the robust three dimensional ionic architectures in the solid state. The complex nature of these synthons are due to the less directional charge-assisted hydrogen bonding generated by the interactions between NH_3^+ and CO_2^- units of two ionic counterparts. The formation of molecular salts in aqueous media is in good agreement with the differences in the pK_a values of H_2SDC and the amines used for this study. The orientation of ionic counterparts in crystalline solids built on electrostatic interaction is less directional and hence imposes designing challenge as opposed to hydrogen bonds in co-crystals. In the salt with cyclohexylamine, SDC^{2-} anions are aligned parallel with a distance of 4.665 Å, which is over the Schmidt's distance limit and thus found to be photostable under UV light. Whereas in the case of DAP, the centre-to-centre distance of two SDC^{2-} anions

aligned parallel is 3.715 Å and undergoes quantitative dimerization under UV light obeying Schmidt's topochemical postulates. Although, in case of DAB the SDC^{2-} anions are parallel, the crystal was found to be photostable as the olefinic double bonds of two parallel aligned SDC^{2-} anions are slip-stacked. In the series of linear primary diamines, only DAP was found to result in the parallel alignment of SDC^{2-} anion that suggest the possibility of some correlation between the chain length of the diamine and the parallel orientation of the ionic counterparts in the solid state. One can rationalize our findings to the $n = 3$ rule for the intramolecular excimer formation in bichromophoric molecules linked by a short flexible chain.[9] Also, our result can be correlated with the enhancement of photocyclization of trimethylene dicinnamates.[10] In **5**, DBEA cations are identified to adopt a rare finite helical shape (called 'helicate') which is stabilised by the weak interactions between sulfur and NH_3^+ units.

These results observed for **3** motivated us to find out another salt of H_2SDC with 3,3′-dipropylaminoamine [$H_2NCH_2CH_2CH_2N(H)CH_2CH_2CH_2NH_2$, DPA], where NH and NH_2 groups are separated by trimethylene chain. The salt of composition, $(DPAH_3)_2(SDC)_3 \cdot 8H_2O$ or $C_{60}H_{86}N_6O_{20}$ (**9**) undergoes 62% photodimarization upon irradiation under UV light for 40 h. Although we were unable to grow data collection quality single crystals, the result helps us to understand the relation between the chain length of the diamine and the parallel stacking of SDC^{2-} anion. An infinite arrangement of the SDC^{2-} anions or partial antiparallel stacking of C=C bonds is proposed to account for the partial solid-state photochemical activity. In the series of these salts we have studied the ammonium salt (by reacting H_2SDC with NH_4OH) of the same carboxylate. To our disappointment we were unable to grow suitable single crystals for data collection. However, the salt of composition $(NH_4)(HSDC)$ (**10**) was found to undergo 80% photodimerization after 50 h of irradiation under UV light. Although we do not have the solid state structure of this salt, the orientation of the SDC^{2-} anions can be predicted to be partially in parallel.

For the purpose of aligning SDC^{2-} anions in parallel orientation we basically need two hydrogen atoms in the protonated amines. We see three hydrogen atoms available in the protonated form of the primary amines to form charge assisted hydrogen bonding. We therefore, have chosen piperizine as a secondary amine which can thus serve the purpose. Yet it is observed that C=C bonds in the SDC^{2-} anions are not in parallel alignment in the solid state structure of **8**. At this stage, it is thus a very formidable task to design or predict the solid state structure of organic salts where the robust and non-directional charge assisted hydrogen bonding predominant in the solid state architecture. More work should be carried out in order to understand whether these types of non-covalent interactions can be reliably employed to rationally design the molecular packing in the solid state.

2.3 Summary

In this chapter, the solid state structure of several molecular salts are discussed with the identification of more complex supramolecular synthons that are involved in the construction of solid state architecture. The solid state structure and the orientations of SDC^{2-} anion are rationalised from this series of molecular salts. We anticipate that the parallel orientation of SDC^{2-} has some correlation with the chain lengths of the diamines used. We have introduced a synthetic method of TCCB, a new tetracarboxylic acid as a ligand for making co-crystals and MOFs. We have reported for the first time on the solid state photodimerization of H$_2$SDC.

2.4 Syntheses and Characterizations

Trans-4,4′-stilbenedicarboxylic acid (H$_2$SDC) was synthesized via dehydrodimerization reaction as reported in literature.[11] All the amines used in this study are all moderately strong to snatch the acidic protons from H$_2$SDC to form molecular salts in aqueous medium (pK_a values are listed in Scheme 2.2). Single crystals of all the molecular salts were grown from the aqueous solutions. Solid

....

H$_2$SDC was dissolved in water by adding equivalent amount of amines with sonication. The resultant clear solutions were allowed to evaporate slowly to obtain suitable single crystals of **1 – 4** and **7 – 8**. For the molecular salts **5** and **6**, triethylammonium salts of H$_2$SDC were mixed with corresponding hydrochloride salts of the amines in aqueous media. The yields for such crystallizations are in the range of 85 – 95%. All the compounds were characterized by NMR spectroscopy and elemental analysis in addition to X-ray crystallographic characterization. Thermogravimetric analysis (TGA) was carried out for the hydrated salts and other characterization techniques were used when and where ever were necessary.

(cyclohexa)$_2$(SDC) (1)

^{1}H NMR (300 MHz, D$_2$O, 298K): δ_H = 7.82 (d, 4H, Ar-H), 7.62 (d, 4H, Ar-H), 7.33 (s, 2H, CH=CH), 3.07 (q, 2H, CH-CH), 1.89 (m, 4H, CH-CH), 1.72 (m, 4H, CH-CH), 1.57 (d, 2H, CH-CH), 1.26 (q, 8H, CH-CH), 1.11 (q, 2H, CH-CH). FT-IR (KBr, cm^{-1}): 2936, 2857, 2576, 2192, 1631, 1597, 1544, 1448, 1366, 1173, 1095, 1044, 959, 851, 788, 706, 629, 530, 458. Analysis found (%): C 72.05, H 7.92, N 5.94; C$_{42}$H$_{57}$N$_3$O$_6$ requires: C 72.07, H 8.21, N 6.00.

(EDA)(SDC) (2)

^{1}H NMR (300 MHz, D$_2$O, 298K): δ_H = 7.84 (d, 4H, Ar-H), 7.65 (d, 4H, Ar-H), 7.35 (s, 2H, CH=CH), 3.0 (s, 4H, CH-CH). FT-IR (KBr, cm^{-1}): 2901, 2492, 2360, 2137, 1605, 1576, 1530, 1376, 1348, 1175, 1083, 1009, 982, 960, 859, 787, 705, 628, 544, 519. Analysis found (%): C 65.52, H 6.22, N 8.66; C$_{18}$H$_{20}$N$_2$O$_4$ requires: C 65.84, H 6.14, N 8.53.

(DAP)(SDC)·H$_2$O (3)

^{1}H NMR (300 MHz, D$_2$O, 298K): δ_H = 7.83 (d, 4H, Ar-H), 7.62 (d, 4H, Ar-H), 7.32 (s, 2H, CH=CH), 3.01 (t, 4H, CH-CH), 1.97 ppm. (q, 2H, CH-CH). FT-IR (KBr,

....

cm^{-1}): 3602, 2821, 2746, 2610, 2537, 2171, 1640, 1580, 1537, 1383, 1221, 1177, 1095, 990, 950, 856, 786, 706, 629, 517, 457. Analysis found (%): C 63.24, H 6.60, N 7.81; $C_{19}H_{24}N_2O_5$ requires: C 63.32, H 6.71, N 7.77.
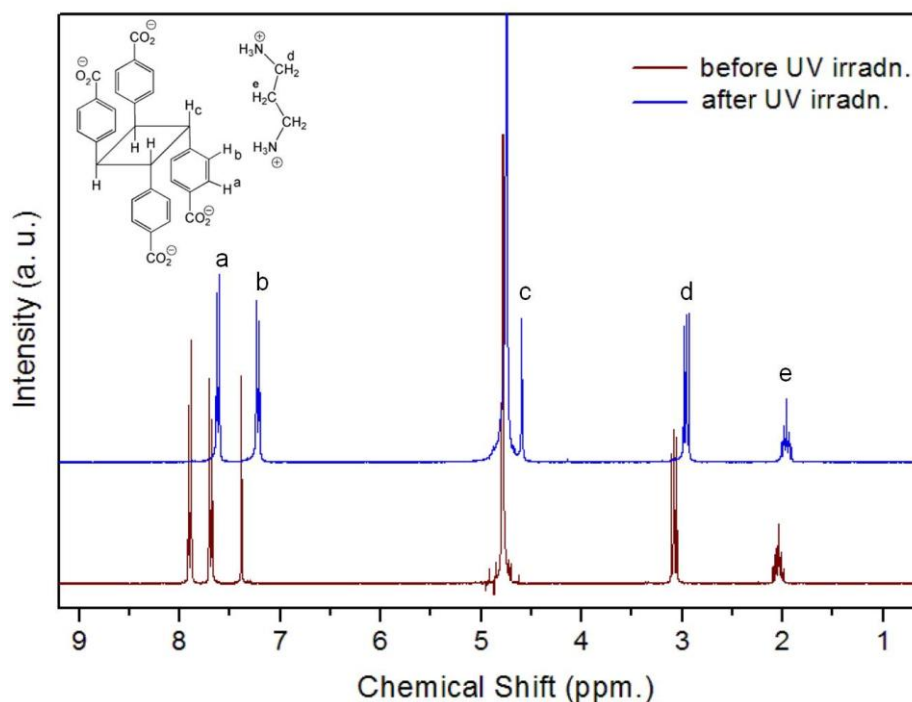
Figure 2.18 ^{1}H NMR spectra of **3** before and after UV irradiation show quantitative conversion

The compound underwent quantitative dimerization upon irradiation under UV light for 30 h. ^{1}H NMR (300 MHz, D_2O, 298K): δ_H = 7.59 (d, 8H, Ar-H), 7.19 (d, 8H, Ar-H), 5.56 (s, 4H, CH-CH), 2.93 (t, 8H, CH-CH), 1.93 ppm. (q, 4H, CH-CH). 5.2% water loss (calculated value 5%) in the thermogravimetric analysis (TGA) above 100 °C shows strong hydrogen bonding interactions present in the lattice.

TCCB: After irradiation, the product was dissolved in water and acidified while hot, with dilute HCl to precipitate the dimer. The crude product was dried under reduced pressure and recrystallized from methanol. ^{1}H NMR (300 MHz, d_6-DMSO, 298K): δ_H = 7.70 (d, 8H, Ar-H), 7.33 (d, 8H, Ar-H), 4.71 ppm. (s, 4H, CH-CH). ^{13}C-NMR (75MHz, d_6-DMSO, 298K): δ_C = 167.12, 145.27, 128.96, 128.5,

....

128.21, 46.25. m/z 535.4 represents (M-1) peak in ESI-MS. FT-IR (KBr, cm^{-1}): 3428, 3056, 3012, 2657, 2542, 1688, 1609, 1572, 1511, 1419, 1317, 1286, 1181, 1114, 1017, 945, 854, 798, 775, 729, 707, 598, 528. Analysis found for TCCB (%): C 66.99, H 4.88; $C_{32}H_{24}O_8 \cdot 2H_2O$ requires C 67.12, H 4.93. TGA of TCCB shows the presence water molecule with dimerized product. 6.7% water loss below 100 °C (calculated water loss 6.3%) proved the co-existence of two water molecules with each dimer molecule and hence it supported for the correct elemental analysis.

(DAB)(SDC)·2H$_2$O (4)

^{1}H NMR (300 MHz, D$_2$O, 298K): δ_H = 7.93 (d, 4H, Ar-H), 7.73 (d, 4H, Ar-H), 7.43 (s, 2H, CH=CH), 3.06 (m, 4H, CH-CH), 1.97 ppm. (m, 4H, CH-CH). FT-IR (KBr, cm^{-1}): 3419, 3052, 2502, 2136, 1655, 1582, 1527, 1506, 1451, 1381, 1264, 1172, 1109, 1088, 1037, 1010, 972, 960, 923, 892, 852, 789, 709, 626, 592, 548, 519, 449. Analysis found (%): C 61.27, H 7.40, N 7.24; $C_{20}H_{28}N_2O_6$ requires: C 61.21, H 7.19, N 7.14. The observed 9.3% water loss in TGA experiment was matched with the calculated value 9.2%.

(DBEA)(SDC) (5)

^{1}H NMR (300 MHz, D$_2$O, 298K): δ_H = 7.80 (d, 4H, Ar-H), 7.61 (d, 4H, Ar-H), 7.32 (s, 2H, CH=CH), 3.29 (t, 4H, CH-CH), 2.91ppm. (t, 4H, CH-CH). FT-IR (KBr, cm^{-1}): 3444, 2922, 2856, 2736, 2628, 2362, 2139, 1626, 1575, 1533, 1389, 1366, 1453, 1322, 1258, 1177, 1120, 1044, 1010, 974, 908, 866, 847, 809, 788, 708, 625, 554, 490, 461. Analysis found (%): C 57.25, H 5.45, N 6.55; $C_{20}H_{24}N_2O_4S_2$ requires: C 57.12, H 5.75, N 6.66.

(Guan)$_2$(SDC)·4H$_2$O (6)

^{1}H NMR (300 MHz, D$_2$O, 298K): δ_H = 7.82 (d, 4H, Ar-H), 7.62 (d, 4H, Ar-H), 7.33 (s, 2H, CH=CH), FT-IR (KBr, cm^{-1}): 3487, 3082, 2834, 1686, 1656, 1602, 1583,

....

1517, 1382, 1301, 1222, 1177, 1148, 1007, 973, 955, 874, 850, 797, 757, 709, 629, 564, 517, 466. Analysis found (%): C 47.22, H 6.41, N 18.05; $C_9H_{15}N_3O_4$ requires: C 47.16, H 6.60, N 18.33. Both the calculated and observed water losses in TGA were 15.7% for this compound.

(4-APH)$_2$(SDC)·2H$_2$O (7)

^{1}H NMR (300 MHz, D$_2$O, 298K): δ_H = 7.84 (d, 4H, Ar-H), 7.79 (d, 4H, Ar-H), 7.57 (d, 4H, Ar-H), 7.25 (s, 2H, CH=CH), 6.70 (d, 4H, Ar-H). FT-IR (KBr, cm^{-1}): 3348, 3299, 3177, 1714, 1627, 1566, 1516, 1414, 1376, 1334, 1287, 1225, 1196, 1180, 1137, 1107, 1008, 955, 857, 829, 783, 701, 571, 516, 454. Analysis found (%): C 62.96, H 5.60, N 11.25; $C_{26}H_{28}N_4O_6$ requires: C 63.40, H 5.73, N 11.38. 7.2% water loss was found in TGA experiment which matched with the calculated value 7.3%.

(Pip)(SDC) (8)

^{1}H NMR (300 MHz, D$_2$O, 298K): δ_H = 7.81 (d, 4H, Ar-H), 7.61 (d, 4H, Ar-H), 7.32 (s, 2H, CH=CH), 3.03 (s, 8H, CH-CH). FT-IR (KBr, cm^{-1}): 3441, 3246, 3003, 2711, 2599, 1637, 1603, 1545, 1477, 1444, 1384, 1367, 1293, 1224, 1175, 1095, 1007, 987, 884, 785, 707, 629, 596, 543, 518, 456. Analysis found (%): C 67.88, H 6.12, N 7.94; $C_{20}H_{22}N_2O_4$ requires: C 67.78, H 6.26, N 7.90.

(DPAH$_3$)$_2$(SDC)$_3$·8H$_2$O (9)

^{1}H NMR (300 MHz, D$_2$O, 298K): δ_H = 7.83 (d, 12H, Ar-H), 7.61 (d, 12H, Ar-H), 7.31 (s, 6H, CH=CH), 2.90 (t, 8H, CH-CH), 2.80 (t, 8H, CH-CH), 1.87 (q, 8H, CH-CH). FT-IR (KBr, cm^{-1}): 3413, 3022, 1714, 1604, 1588, 1543, 1412, 1380, 1332, 1305, 1223, 1179, 1107, 1007, 956, 857, 784, 701, 630, 521, 454. Analysis found (%): C 59.33, H 7.11, N 6.83; $C_{60}H_{86}N_6O_{20}$ requires: C 59.49, H 7.16, N 6.94. The observed 12.1% weight loss in TGA experiment matched with the calculated value

....

(11.9%) for the composition $(DPA)_2(SDC)_3 \cdot 8H_2O$. Hence it supported the elemental analysis to determine the correct composition. After irradiation under UV light for 40 h, the compound underwent 62% dimerization. ^1H NMR spectrum showed the peaks for the presence of both monomer and dimer; (300 MHz, D_2O, 298K): δ_H = 7.83 (d, 4.8H, Ar-H), 7.61 (d, 4.8H, Ar-H), 7.58 (d, 7.2H, Ar-H), 7.31 (s, 2.4 H, CH=CH), 7.16 (d, 7.2H, Ar-H), 4.53 (s, 3.6 H, CH-CH), 2.90 (t, 8H, CH-CH), 2.80 (t, 8H, CH-CH), 1.87 (q, 8H, CH-CH).

$(NH_4)(HSDC)$ (10)

^1H NMR (300 MHz, D_2O, 298K): δ_H = 7.89 (d, 4H, Ar-H), 7.64 (d, 4H, Ar-H), 7.38 (s, 2H, CH=CH). FT-IR (KBr, cm^{-1}): 3170, 3022, 1698, 1605, 1563, 1509, 1417, 1372, 1332, 1178, 1134, 1109, 1005, 958, 856, 780, 701, 636, 523, 457. Analysis found (%): C 67.04, H 5.17, N 4.67; $C_{16}H_{15}NO_4$ requires: C 67.36, H 5.30, N 4.91. TGA of this compound showed that the anhydrous nature and supported for the correct composition. After irradiation under UV light for 50 h, the compound underwent 80% dimerization. ^1H NMR spectrum showed the peaks for the presence of both monomer and dimer; (300 MHz, D_2O, 298K): δ_H = 7.89 (d, 4H, Ar-H), 7.64 (d, 4H, Ar-H), 7.38 (s, 2H, CH=CH) and δ_H = 7.66 (d, 8H, Ar-H), 7.26 (d, 8H, Ar-H), 4.64 (s, 4H, CH-CH).
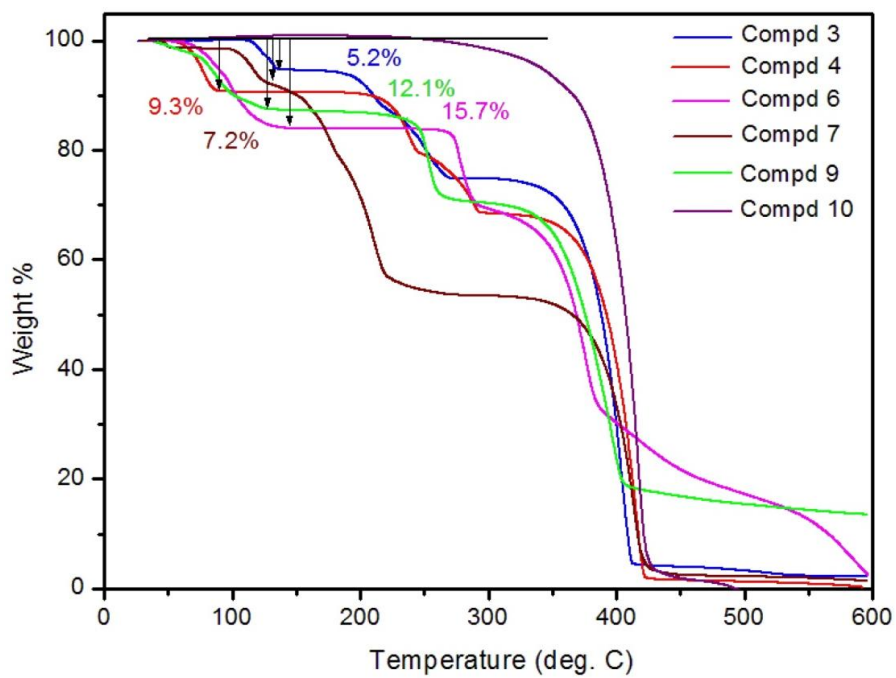
Figure 2.19 TGAs for various salts show the respective water losses.

Table 2.9 Crystallographic data of compound **1 – 4**

Compounds	1	2	3	4
Formula	$C_{42}H_{57}N_3O_6$	$C_{18}H_{20}N_2O_4$	$C_{19}H_{24}N_2O_5$	$C_{20}H_{28}N_2O_6$
M	699.91	328.36	360.40	392.44
T (K)	223(2)	100(2)	223(2)	223(2)
λ (Å)	0.71073	0.71073	0.71073	0.71073
Cryst syst / Space group	Triclinic / $P\bar{1}$	Monoclinic / $P2_1/c$	Monoclinic / $P2_1/c$	Triclinic / $P\bar{1}$
a (Å)	12.1042(10)	10.156(2)	16.0565(8)	7.4542(13)
b (Å)	12.6256(10)	9.334(2)	11.7861(6)	9.7070(16)
c (Å)	15.2007(11)	8.385(2)	9.6935(5)	13.610(2)
α (°)	110.722(2)	90	90	100.688(2)
β (°)	111.880(2)	94.400(5)	104.5700(10)	96.117(3)
γ (°)	95.796(2)	90	90	90.070(3)
Volume (Å^3) / Z	1942.3(3) / 2	792.5(3) / 2	1775.44(16) / 4	962.0(3) / 2
D_{calcd} (g/cm^3) / μ (mm^{-1})	1.197 / 0.080	1.376 / 0.098	1.348 / 0.098	1.355 / 0.100
Reflns col. / Ind. Reflns.	13954 / 8874	4309 / 1812	14488 / 5163	12348 / 4407
R_{int} / Goof on F^2	0.0361 / 1.034	0.0701 / 1.100	0.0211 / 1.044	0.0377 / 1.097
Final R[I>2σ]^a R$_1$ / wR2	0.0793 / 0.1976	0.0795 / 0.1516	0.0495 / 0.1343	0.0629 / 0.1722

^{a} R1 = $\Sigma||F_o| - |F_c||/ \Sigma|F_o|$, ^{b} wR2 = $[\Sigma w(F_o^2 - F_c^2)^2/\Sigma w(F_o^2)^2]^{1/2}$

Table 2.10 Crystallographic data of compound **5** – **8**

Compounds	5	6	7	8
Formula	$C_{20}H_{24}N_2O_4S_2$	$C_9H_{15}N_3O_4$	$C_{26}H_{28}N_4O_6$	$C_{20}H_{22}N_2O_4$
M	420.53	229.24	492.52	354.40
T (K)	100(2)	223(2)	223(2)	100(2)
λ (Å)	0.71073	0.71073	0.71073	0.71073
Cryst syst / Space group	Triclinic / $P\bar{1}$	Monoclinic / $P2_1/c$	Monoclinic / $P2_1/n$	Monoclinic / $P2_1/c$
a (Å)	8.9392(4)	11.6939(8)	8.5009(6)	12.5672(16)
b (Å)	10.5683(5)	10.6964(7)	10.6106(7)	8.3029(10)
c (Å)	12.3610(6)	8.8496(6)	13.7800(9)	8.2837(11)
α (°)	71.1670(10)	90	90	90
β (°)	75.9040(10)	93.170(2)	101.6510(10)	94.708(3)
γ (°)	67.6480(10)	90	90	90
Volume (Å^3) / Z	1012.43(8) / 2	1105.24(13) / 4	1217.34(14) / 2	861.44(19) / 2
D_{calcd} (g/cm^3) / μ (mm^{-1})	1.379 / 0.292	1.378 / 0.109	1.344 / 0.097	1.366 / 0.096
Reflns col. / Ind. Reflns.	13335 / 4634	7613 / 2529	8398 / 2783	5803 / 1956
R_{int} / Goof on F^2	0.0228 / 1.035	0.0240 / 1.056	0.0221 / 1.042	0.0286 / 1.130
Final R[I>2σ] R_1/ wR2	0.0320 / 0.0866	0.0482 / 0.1260	0.0460 / 0.1292	0.0491 / 0.1222

^{a} R1 = Σ||F_o| − |F_c||/ Σ|F_o|, ^{b} wR2 = [Σ$w(F_o^2 − F_c^2)^2$/Σ$w(F_o^2)^2$]$^{1/2}$

Chapter 2

....

2.5 References

1.   (a) Ito, Y., *Tetrahedron* **2003,** *59* (37), 7323-7329; (b) Ito, Y.; Borecka, B.; Trotter, J.; Scheffer, J. R., *Tetrahedron Lett.* **1995,** *36* (34), 6083-6086.

2.   Natarajan, A.; Mague, J. T.; Venkatesan, K.; Ramamurthy, V., *Org. Lett.* **2005,** *7* (10), 1895-1898.

3.   Schmidt, G. M. J., *Pure Appl. Chem.* **1971,** *27* (4), 647-678.

4.   (a) Louvain, N.; Mercier, N.; Luc, J.; Sahraoui, B., *Eur. J. Inorg. Chem.* **2008,** *2008* (23), 3592-3596; (b) Bi, W.; Louvain, N.; Mercier, N.; Luc, J.; Rau, I.; Kajzar, F.; Sahraoui, B., *Adv. Mater.* **2008,** *20* (5), 1013-1017; (c) Mercier, N.; Barres, A.-L.; Giffard, M.; Rau, I.; Kajzar, F.; Sahraoui, B., *Angew. Chem. Int. Ed.* **2006,** *45* (13), 2100-2103.

5.   (a) Abrahams, B. F.; Haywood, M. G.; Robson, R., *J. Am. Chem. Soc.* **2004,** *127* (3), 816-817; (b) Lam, C.-K.; Xue, F.; Zhang, J.-P.; Chen, X.-M.; Mak, T. C. W., *J. Am. Chem. Soc.* **2005,** *127* (33), 11536-11537; (c) Mak, T. C. W.; Xue, F., *J. Am. Chem. Soc.* **2000,** *122* (40), 9860-9861; (d) Russell, V. A.; Evans, C. C.; Li, W.; Ward, M. D., *Science* **1997,** *276* (5312), 575-579.

6.   Xu, W.-Z.; Sun, J.; Huang, Z.-T.; Zheng, Q.-Y., *Chem. Commun.* **2009,** (2), 171-173.

7.   Fulton, J. D., *Brit. J. Pharmacol.* **1948,** *3*, 75-79.

8.   Lewis, F. D.; Wu, T.; Burch, E. L.; Bassani, D. M.; Yang, J.-S.; Schneider, S.; Jaeger, W.; Letsinger, R. L., *J. Am. Chem. Soc.* **1995,** *117* (34), 8785-8792.

9.   De Schryver, F. C.; Collart, P.; Vandendriessche, J.; Goedeweeck, R.; Swinnen, A. M.; Van der Auweraer, M., *Acc. Chem. Res.* **1987,** *20* (5), 159-166.

10.   Kuzuya, M.; Tanaka, M.; Okuda, T., *Tetrahedron Lett.* **1983,** *24* (39), 4237-4240.

11.   (a) Khalaf, A. I.; Pitt, A. R.; Scobie, M.; Suckling, C. J.; Urwin, J.; Waigh, R. D.; Fishleigh, R. V.; Young, S. C.; Wylie, W. A., *Tetrahedron* **2000,** *56* (29), 5225-

5239; (b) Toland, W. G.; Wilkes, J. B., *J. Am. Chem. Soc.* **1954,** *76* (1), 307-308; (c)

Toland, W. G.; Wilkes, J. B.; Brutschy, F. J., *J. Am. Chem. Soc.* **1953,** *75* (9), 2263-

2264.

Chapter 3

Anion Controlled Stereo-selective [2 + 2] Cycloaddition Reaction of *Trans*-3-(4'-pyridyl) Acrylic Acid in the Solid State and Isomerisation of Cyclobutane Derivatives in Solution[*]
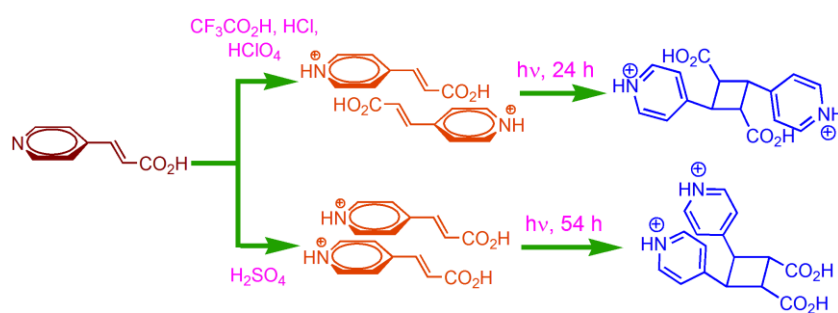
*The research work described in this chapter has been published / presented in the following journals / conferences

1. *Org. Lett.*, **2010**, *12*, 128-13

2. *J. Org. Chem.*, **2011**, manuscript accepted

3. XX International Conference on the Chemistry of Organic Solid State (ICCOSS XX), June 2011, Bangalore, India.

4. The 10th Conference of the Asian Crystallographic Association (AsCA2010), October 2010, Busan, South Korea. **'The Rising Star' Award!**

5. 1st China-India-Singapore Symposium on Crystal Engineering, August 2010, NUS, Singapore. **Best Poster Award!**

6. Gordon Research Conference (GRC) on Crystal Engineering, June 2010, NH, USA.

7. 2nd NUS-SNU Joint Symposium on March, 2010, NUS, Singapore.

3.1 Introduction

In Chapter 2, we have discussed the importance of the synthesis of organic salts for [2 + 2] cycloaddition reaction in the solid state. We also have introduced methods to synthesize *rctt*-1,2,3,4-tetrakis(4′-carboxyphenyl)cyclobutane, a new ligand for co-crystals and MOFs syntheses. In this chapter, we shall discuss the syntheses of molecular salts of *trans*-3-(4'-pyridyl)acrylic acid (4-PAH), *trans*-3-(3'-pyridyl)acrylic acid (3-PAH) for solid state photodimerization reactions and selective syntheses of two possible dimers of 4-PAH *viz.* HH- and HT-4,4-BPCD by tuning the anion of the salts. Moreover, we shall extend our synthetic procedure to obtain the HT-dimer of *trans*-3-(3'-pyridyl)acrylic acid (3-PAH) whose HH-dimer has been reported.[1,2]

Unlike H_2SDC, 3-PAH and 4-PAH have a pyridyl group at one end and a carboxylic acid group at the other end, making the molecule unsymmetrical. Both the functional groups can be employed for making organic salts. Although the name suggests them to be acid, they can act as base if we exploit the pyridyl groups. We have exploited the basic nature of these molecules and allowed to react with some strong acids to make a series of molecular salts that have been used to synthesize the above mentioned two cyclobutane derivatives.

Extensive work has been reported in the past for making various types of coordination polymers (CPs) containing 4-PA with varieties of structures and functions.[3] However, the crystal engineering studies on this molecule in organic perspective is relatively unexplored. Nishikiori *et al.* reported a hydrogen bonded coordination inclusion compound host $[Ni(SCN)_2(4\text{-}PAH)_2]_n$ where the distance between the C═C double bonds of *head-to-head* (HH) oriented 4-PAHs (centroid-to-centroid) is 3.807 Å (Figure 3.1).[4] However, the authors have not addressed the photoreactivity of that compound. Again, Lang *et al.* also reported a 3D lead CP

....

[Pb(4-PA)$_2$]$_n$ where 4-PA ligands were found parallel in HH-fashion with a distance of 4.258 Å.[5] Although the distance is on the border line of Schmidt's distance criteria, the photoreactivity of this CP was not investigated. 4-PAH has never been reported for its solid state photodimerization reaction and in addition this molecule was found to be photostable. These observations challenge the crystal engineers to use their tool box organise pair of these molecules in parallel fashion to force it to be photoreactive.
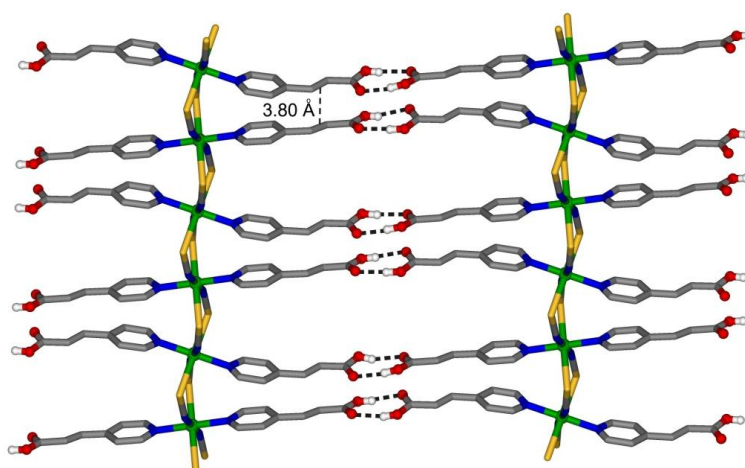
Figure 3.1 Crystal structure of [Ni(SCN)$_2$(4-PAH)$_2$]$_n$, as reported in literature,[4a] shows parallel alignment of 4-PAH.

The solid state photoreactivity of three well known polymorphs of *trans*-cinnamic acid is described in Chapter 1. Here the phenyl group is replaced by 4-pyridyl group in 4-PAH. Yamada *et al.* introduced the importance of cation-π interaction towards the parallel orientation of photoreactive pyridyl molecules.[6] However, this supramolecular interaction always resulted in *head-to-tail* (HT) parallel orientation and the role of the anions in such interactions is relatively unexplored. In our present study, we undertake to understand the influence of different anions in combination with pyridyl cations and their solid state packing. We have achieved both the HH- and HT-parallel orientations of [4-PAH$_2$$^+$] cations in salts hence the selective syntheses of two hetero-functional cyclobutane derivatives just by

Chapter 3

....

tuning the anions of the salts were possible and the concept has been extrapolated to achieve HT-photodimer of 3-PAH.

3.2 Results and Discussion

3.2.1 General Synthetic Procedure

All the molecular salts were synthesized from aqueous media. Solid 4-PAH was dissolved in water by adding equivalent amount of strong acids in water. Then diffraction quality single crystals were obtained by slow evaporation technique. The yields of these crystallization processes vary in the ranges of 90-95%.

3.2.2 Description of the Crystal Structures of Salts Containing 4-PAH

3.2.2.1 Molecular Salt of 4-PAH with CF_3CO_2H (11) and Its Photoreactivity

The 1:1 salt of composition $C_{10}H_8F_3NO_4$ (**11**) crystallizes in the orthorhombic space group, $Pca2_1$. The protonated 4-PAH$_2^+$ cations and $CF_3CO_2^-$ anions are found to exert various kinds of C-H$\cdots$O, N-H$\cdots$O and C-H$\cdots$F hydrogen bonding interactions to furnish two dimensional sheets in the ab-plane. One of the oxygen atoms of the $CF_3CO_2^-$ anion accepts two H-bonding from H-N of py-H$^+$ and carboxylic acid protons of another 4-PAH$_2^+$ cation. The other oxygen atom accepts a H-bonding from C-H (α) of py-H$^+$. The keto-oxygen of the carboxylic acid group of 4-PAH$^+$ forms H-bonding with C-H (α) of another py-H$^+$. The F atoms of $CF_3CO_2^-$ are also involved in C-H$\cdots$F interactions with C-H (α and β) of py-H$^+$ (Figure 3.2). The parameters for hydrogen bondings are shown in Table 3.1. These two dimensional sheets are found parallel where 4-PAH$_2^+$ cations lie one above another in infinite parallel orientation in HT-fashion with a distance of separation 3.766 Å (Figure 3.3).

Figure 3.2 The two dimensional sheet structure of **11** shows various kinds supramolecular interactions

Table 3.1 The hydrogen bonding parameters for **11**

D-H···A	D(D-H) (Å)	D(H···A) (Å)	D(D···A) (Å)	<(DHA) (°)	Symmetry Operator
O(1)-H(1)···O(3)	0.83	1.83	2.653(2)	169	-1/2+x, 2-y, z
N(1)-H(1N)···O(3)	0.91	1.76	2.669(3)	173(4)	
C(8)-H(3)···O(4)	0.94	2.49	3.196(3)	131	
C(4)-H(10)···F(2A)	0.94	2.38	3.090(6)	132	x, 1+y, z
C(4)-H(10)···O(2)	0.94	2.31	3.099(3)	141	1/2+x, 2-y, z

Figure 3.3 The infinite *head-to-tail* parallel arrangement of 4-PAH$_2^+$ cations in **11** satisfying Schmidt criteria

UV irradiation of a powdered crystalline sample of **11** placed between two glass plates produced a quantitative photodimerization to yield the CF$_3$CO$_2^-$ salt of 2,4-bis(4'-pyridyl)cyclobutane-1,3-dicarboxylic acid (HT-4,4-BPCD) after a period of 24 h, as determined by ^{1}H NMR spectroscopy by the disappearance of olefinic

protons at δ 7.65 and 6.94 ppm and the appearance of cyclobutane protons at δ 4.52 and 4.1 ppm, as well as a 297.3 *m/z* peak in the ESI-MS [M]⁻. There is no significant difference noted between the reactivity of the single crystals and powdered samples which furnished 100% HT-4,4-BPCD in 30 and 24 h respectively under similar experimental conditions. This was confirmed by measuring ¹H NMR spectra at various time intervals during the course of reaction and then by plotting % conversion *vs* time (see appendix I).

3.2.2.1.1 Crystal Structure of $CF_3CO_2^-$ Salt of HT-BPCD (12)

The stereochemistry of HT-4,4-BPCD as its $CF_3CO_2^-$ salt was confirmed by X-ray crystallography. After complete photodimerization, the powdered sample of **11** was dissolved in water and the single crystals were grown for X-ray diffraction experiment. The salt of composition $C_{20}H_{16}F_6N_2O_8$ (**12**) was found to crystallize in the monoclinic space group, $P2_1/c$. Various types of hydrogen bonding like O-H···O, N-H···O, C(α)-H···O (Table 3.2) play crucial role to construct the solid state architecture. The asymmetric unit contains a $CF_3CO_2^-$ anion and half of the protonated HT-4,4-BPCD cation. $CF_3CO_2^-$ anions accept H-bonding from both the protonated pyridyl and carboxylic acid groups. The geometry of the cyclobutane ring is *rctt* as shown in Figure 3.4.

Table 3.2 The hydrogen bonding parameters for **12**

D-H···A	D(D-H) (Å)	D(H···A) (Å)	D(D···A) (Å)	<(DHA) (°)	Symmetry Operator
O(1)-H(1)···O(4)	0.83	1.78	2.603(2)	173	x, -1+y, z
N(1)-H(1N)···O(3)	0.93	1.77	2.696(2)	172(2)	
C(1)-H(1A)···O(2)	0.99	2.46	3.267(2)	138	-x, -1/2+y, 3/2-z
C(5)-H(5)···O(3)	0.94	2.35	3.288(2)	173	1-x, 1-y, 1-z
C(7)-H(7)···O(4)	0.94	2.56	3.232(2)	129	
C(7)-H(7)···O(2)	0.94	2.47	3.193(2)	134	-x, 1/2+y, 3/2-z

Figure 3.4 The crystal structure of HT-4,4-BPCD as its $CF_3CO_2^-$ salt confirms its stereochemistry as *rctt*

3.2.2.1.2 Crystal Structure of *rctt*-HT-4,4-BPCD (13)

Neutral form of *rctt*-HT-4,4-BPCD, $C_{16}H_{14}N_2O_4$ (**13**) was obtained by neutralising the aqueous solution of the above salt by NaOH (aq). Neutral *rctt*-HT-4,4-BPCD was separated out in the form of single crystals upon keeping the neutralised solution for a few hours. The compound crystallizes in $P2_1/c$ space group and it reveals that the solid state structure is stabilised by O-H···N hydrogen bonding (Table 3.3) between the carboxylic acid and pyridyl groups as shown in Figure 3.5. The compound forms 4-connected uninodal planar net considering the centroids of cyclobutane as the nodes. These planar nets are parallel and the distance of separation is 5.901 Å. The length of each side of the nets is 9.748 Å. The topology of this net is sql/Shubnikov tetragonal plane net ($4^4.6^2$) (Figure 3.6).

Table 3.3 The hydrogen bonding parameters for **13**

D-H···A	D(D-H) (Å)	D(H···A) (Å)	D(D···A) (Å)	<(DHA) (°)	Symmetry Operator
O(1)-H(1)···N(1)	0.84	1.88	2.652(2)	153	1-x, 1/2+y, 1/2-z
C(1)-H(1A)···O(2)	1.0	2.58	3.416(2)	141	-1+x, y, z
C(6)-H(6)···O(2)	0.95	2.34	3.290(2)	177	1-x, 1-y, -z

Figure 3.5 H-bonded structure of *rctt*-HT-4,4-BPCD

Figure 3.6 The topology of *rctt*-HT-4,4-BPCD was analysed to be sql/Shubnikov tetragonal plane net

3.2.2.2 Molecular Salt of 4-PAH with H_2SO_4 (14) and Its Photoreactivity

4-PA was reacted with H_2SO_4 in water and the salt $C_{24}H_{27}N_3O_{15}S_2$ or, $(C_8H_8NO_2)_3(SO_4)(HSO_4)(H_2O)$ (**14**) was resulted. This salt crystallizes in space group, $P2_1/n$. All the 4-PAHs are found protonated and the presence of both the sulphate and bisulphate anions makes the salt interesting to investigate its structural insights. Various kinds of H-bonding like O-H···O and N-H···O play fundamental role to stabilise the solid as shown in Figure 3.7 below and the parameters for these hydrogen bonding are shown in Table 3.4. The 4-PAH$_2^+$ cations are found to arrange in infinite parallel orientation in HH-fashion with unequal distances between them. There are three 4-PAH$_2^+$ cations **A**, **B** and **C** in the asymmetric unit of the salt. The possible cation-cation repulsion in *head-to-head* orientation is balanced and stabilized by cation-anion interactions of bisulphate and sulphate anions. Among the three 4-PAH$_2^+$ cations in the asymmetric unit, the two 4-PAH$_2^+$ cations **A** and **C** shown in

Figure 3.7 are parallel to the other counterparts keeping a center-to-center distance of 3.68 Å; while the middle one (**B**), which is directly connected to a water molecule, is crisscross with both **A** and **C**, but keeping center-to-center distances between the adjacent C=C bonds of 3.672 Å and 3.754 Å.

Figure 3.7 Infinite *head-to-head* arrangement of 4-PAH$_2^+$ cations in **14**, where **B** is crisscrossed to both **A** and **C**.

Although these two distances are well within the Schmidt criteria and further the [2 + 2] cycloaddition reaction of C=C bonds aligned in crisscross positions are known to take place as a result of pedal-like motion (discussed in section 1.7).[7] In this regard, the cationic monomer **B** has been found not to furnish 100% dimerized product. Upon irradiation of single crystals of this salt under UV light, only 66% dimerization was observed as monitored by ^{1}H NMR spectroscopy, which indicated that only the cations **A** and **C** underwent dimerization. It is anticipated that during dimerization process neither **A** nor **C** reacted with **B** which has crisscross orientation with the both.

Table 3.4 The hydrogen bonding parameters for **14**

D-H⋯A	D(D-H) (Å)	D(H⋯A) (Å)	D(D⋯A) (Å)	<(DHA) (°)	Symmetry Operator
O1W-H1WA⋯O13	0.88	1.85	2.729(2)	174(3)	
N1-H1N⋯O12	0.91	1.94	2.812(2)	159	1/2+x, 3/2-y, 1/2+z
O1-H1O⋯O14	0.85	1.81	2.655(2)	177(3)	
O11-H1S⋯O7	0.88	1.63	2.489(2)	165(3)	1+x, y, z
O1W-H1WB⋯O9	0.86	1.86	2.719(2)	172(3)	
N2-H2N⋯O9	0.95	1.75	2.673(2)	163(2)	1/2+x, 3/2-y, 1/2+z
N3-H3N⋯O8	0.91	1.82	2.716(2)	170	1/2+x, 3/2-y, 1/2+z
O3-H3O⋯O10	0.87	1.76	2.631(2)	179	
O5-H5O⋯O1W	0.92	1.65	2.568(2)	172(3)	
C1-H1A⋯O14	0.94	2.48	3.279(2)	143	3/2-x, -1/2+y, 1/2-z
C2-H2⋯O2	0.94	2.59	3.253(2)	127	3/2-x, -1/2+y, 1/2-z
C2-H2⋯O4	0.94	2.57	3.326(2)	137	1/2-x, -1/2+y, 1/2-z
C5-H5⋯O11	0.94	2.43	3.086(2)	127	3/2-x, 1/2+y, 1/2-z
C5-H5⋯O13	0.94	2.47	3.167(2)	131	1/2+x, 3/2-y, 1/2+z
C7-H7⋯O4	0.94	2.57	3.195(2)	124	1/2-x, -1/2+y, 1/2-z
C9-H9⋯O8	0.94	2.49	3.383(2)	160	1/2-x, -1/2+y, 1/2-z
C10-H10⋯O4	0.94	2.57	3.336(2)	138	1/2-x, -1/2+y, 1/2-z
C13-H13⋯O9	0.94	2.46	3.346(2)	156	1/2-x, 1/2+y, 1/2-z
C15-H15⋯O6	0.94	2.49	3.395(2)	162	1/2-x, 1/2+y, 1/2-z
C21-H21⋯O13	0.94	2.39	3.178(2)	141	1/2-x, 1/2+y, 1/2-z
C23-H23⋯O2	0.94	2.43	3.177(2)	136	1/2-x, -1/2+y, 1/2-z

Figure 3.8 Percentage conversion versus time plots show different reactivity for single crystals and ground powder of **14**

Surprisingly, when the single crystals were ground into powder, the crystalline powder sample was found to undergo 100% dimerization in 54 h. The formation of *syn-head-to-head*-dimer, namely, 3,4-bis(4'-pyridyl)cyclobutane-1,2-dicarboxylic acid (*rctt*-HH-4,4-BPCD), was confirmed by the disappearance of the peaks for ethylenic protons at δ 7.86 and 6.98 ppm and the appearance of two doublet peaks at δ 4.51 and 4.04 ppm for the cyclobutane protons in the ^{1}H NMR spectrum (see characterization section) and the percentage conversion versus time plot is shown in Figure 3.8. The crystallographic characterization of *rctt*-HH-4,4-BPCD is also presented below. This observed difference in photoreactivity of the single crystals and ground powder lead us to investigate the solid state structure of the salt in detail. The PXRD pattern of the ground powder does not match with the simulated pattern from single crystal data (Figure 3.9), confirming that this is a different crystalline material with a different packing arrangement. From the 100% photochemical product indicated by the ^{1}H NMR spectrum, it is expected that in the powdered sample, the 4-PAH_2^+ cations are likely to be oriented as parallel pairs in *head-to-head* fashion. Further, the TGA of the powdered sample of the salt is shown in Figure 3.10, which indicates that the sample has absorbed an extra water molecule in the crystal

78

lattice after grinding. The water loss for single crystals was found as 2.8%, where as the calculated water loss for one H_2O is 2.7% for the composition $(C_8H_8NO_2)_3(SO_4)(HSO_4)(H_2O)$. On the other hand, the water loss for the ground powder was found as 5.4%, which compares well with the calculated loss of $2H_2O$ (5.3%) for the composition $(C_8H_8NO_2)_3(SO_4)(HSO_4)(H_2O)_2$. Thus the difference in the reactivity of single crystals and the powder sample is attributed to a different composition and hence a different molecular packing.

Figure 3.9 The disagreement of PXRD patterns of the single crystals and ground powder confirms different molecular packing

Figure 3.10 TGA plots for single crystals and ground powder of **14** show that the ground powder contained more water

....

It has been observed previously that the removal of solvents from crystal lattices triggers structural transformations.[8] Further, pedal-like motion of double bonds has also been found to take place during grinding.[7d] In this case, the grinding of single crystals into powder in the lab environment incorporates an additional water molecule, which in turn influences the molecular packing. From the observed photoreactivity, it can be assumed that all of the 4-PAH$_2^+$ cations in the powdered sample of **14** are packed in *head-to-head* fashion with perfectly aligned C=C bond pairs satisfying the Schmidt criteria for photoreactivity. Here the single crystal does not represent the bulk due to compositional disparity.

3.2.2.2.1 Crystal Structure of *rctt*-HH-BPCD (15)

The recrystallization of the ground sample of **14** after complete photodimerization failed to produce single crystals. Therefore, we have neutralized the UV irradiated powdered sample with NaOH (aq.) in water. Diffraction quality single crystals were obtained after 2-3 days upon evaporating the solution slowly. The compound of composition $C_{16}H_{14}N_2O_4$ (**15**) crystallizes in monoclinic space group, *Cc* and the stereochemistry has been confirmed. The asymmetric unit contains one molecule of *rctt*-HH-BPCD. The solid state structure is stabilised by O-H⋯N hydrogen bonding between the carboxylic acid and pyridyl groups to form one dimensional chain like structure as shown in Figure 3.11. These 1D linear chains are parallel to each other and propagate along *b*-direction. They interact very weakly with each other via C(α)-H⋯O (keto) interaction. The hydrogen bonding parameters are are shown in Table 3.5.

Figure 3.11 Crystal structure of *rctt*-HH-4,4-BPCD and its H-bonding are shown

Table 3.5 The hydrogen bonding parameters for **15**

D-H⋯A	D(D-H) (Å)	D(H⋯A) (Å)	D(D⋯A) (Å)	<(DHA) (°)	Symmetry Operator
O(2)-H(2)⋯N(1)	0.83	1.91	2.712(8)	162	x, y+1, z
O(3)-H(3)⋯N(2)	0.83	1.98	2.773(8)	160	x, y+1, z
C(12)-H(12)⋯O(3)	0.94	2.59	3.484(1)	158	x, 1-y, -1/2+z

3.2.2.3 Molecular Salt of 4-PAH with HCl (16) and Its photoreactivity

4-PAH was reacted with HCl and the single crystals of the salt of composition (4-PAH$_2$)Cl·H$_2$O, C$_8$H$_{10}$ClNO$_3$ (**16**) was grown from water. The hydrated salt crystallizes in the triclinic space group, $P\bar{1}$. Various types of hydrogen bonding such as O-H⋯Cl and N-H⋯O play constructive roles to stabilise the solid state architecture. The hydrogen bonding parameters are listed in Table 3.6. In this salt also 4-PAH$_2$$^+$ cations are found parallel in HT-fashion with a distance between C=C bonds of 3.80 Å. As in **14**, water molecules play important role to align 4-PAH$_2$$^+$ cations parallel and to minimize repulsive interactions between the Cl$^-$ ions as shown in Figure 3.12. [(Cl$^-$)$_2$(H$_2$O)$_2$] aggregates nicely align the pairs of 4-PAH$_2$$^+$ cations to form hydrogen bonded tape-like structure propagating along x-axis. Such [(Cl$^-$)$_2$(H$_2$O)$_2$] aggregates are common to occur in the crystals structures of various inorganic coordination complexes[9, 10] and organic materials[6c, 11, 12] where they were found to aggregate both in planar[9, 11] and nonplanar forms.[10,12] Unlike in **11** and **14**, the 4-PAH$_2$$^+$ cations are aligned parallel as discrete pairs in a serial fashion with a distance between C=C bond pair of 3.80 Å and this leads to the arrangement of linear polymeric H-bonded chains which run parallel to each other approximately on the bc-plane. Both the ground powder and single crystals of this salt undergo 100% photodimerization upon irradiation under UV light for 50 h, as was observed in ^{1}H NMR spectroscopy.

Figure 3.12 Ladder-like arrangement of discrete parallel pairs of 4-PAH$_2^+$ cations aligned in HT-fashion by [(Cl$^-$)$_2$(H$_2$O)$_2$] aggregates in **16**.

Table 3.6 The hydrogen bonding parameters for **16**

D-H···A	D(D-H) (Å)	D(H···A) (Å)	D(D···A) (Å)	<(DHA) (°)	Symmetry Operator
N(1)-H(1N)···O(1W)	0.88	1.88	2.687(1)	152(2)	
N(1)-H(1N)···O(2)	0.88	2.67	3.195(3)	120(1)	x, y+1, z-1
O(1)-H(1)···Cl(1)	0.86	2.19	3.053(1)	173(2)	
O(1W)-H(2W)···Cl(1)	0.86	2.26	3.105(1)	167(2)	-x, -y+1, -z+1
O(1W)-H(1W)···Cl(1)	0.82	2.47	3.235(1)	155(2)	x, y+2, z-1
C(5)-H(5)···O(2)	0.94	2.37	3.055(2)	130	x, 1+y, -1+z

3.2.2.4 Molecular Salt of 4-PAH with HClO$_4$ (17) and Its Photoreactivity

4-PAH was reacted with HClO$_4$ in water and allowed to evaporate slowly to grow another salt of composition (4-PAH$_2$)ClO$_4$, C$_8$H$_8$ClNO$_6$ (**17**) that crystallizes in $P\bar{1}$ space group. The charge assisted hydrogen bonding of type N-H···O-Cl and O-H···O-Cl play constructive role in stabilising the solid state structure of the salt. Each ClO$_4^-$ anion is involved in H-bonding with one N-H groups (charge assisted H-bonding) of pyridyl moieties and one O-H from carboxylic acid group. It further involves in electrostatic interaction with two N-H groups. Each pyridyl N-H moiety donates H-bonding to one ClO$_4^-$ anion and further exerts electrostatic interaction with two ClO$_4^-$ anions. All these interactions result the overall structure of this salt three dimensional (see Table 3.7 for hydrogen bonding parameters). The alignment of the 4-PAH$_2^+$ cations are again found to be parallel in HT-fashion and the distance of

separation between the isolated C=C bond pairs is 3.91 Å (Figure 3.13). Both the

ground powder and single crystals undergo 100% photodimerization under UV light

for 30 h as was observed in ^{1}H NMR spectroscopy.

Figure 3.13 Discrete parallel pairs of 4-PAH$_2$$^+$ cations in HT-fashion in **17**.
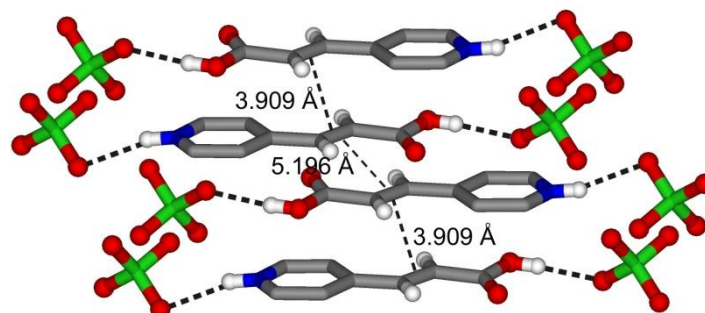
Table 3.7 The hydrogen bonding parameters for **17**

D-H⋯A	D(D-H) (Å)	D(H⋯A) (Å)	D(D⋯A) (Å)	<(DHA) (°)	Symmetry Operator
O(1)-H(1)⋯O(4)	0.83	1.95	2.748(2)	161	x-2, y-1, z-1
N(1)-H(1N)⋯O(6)	0.84	2.18	2.984(2)	162(2)	
N(1)-H(1N)⋯O(5)	0.84	2.54	3.210(2)	137(2)	
C(4)-H(4)⋯O(5)	0.94	2.52	3.436(2)	165	3-x, 1-y, 2-z
C(7)-H(7)⋯O(2)	0.94	2.37	3.266(2)	159	-x, 1-y, 1-z
C(8)-H(8)⋯O(6)	0.94	2.37	3.254(2)	157	2-x, 2-y, 2-z

3.2.2.5 Molecular Salt of 4-PAH with HPF$_6$ (18)

When 4-PAH was reacted with HPF$_6$ in water, the anhydrous salt of

composition C$_{16}$H$_{15}$F$_6$N$_2$O$_4$P (**18**) was crystallized out which was refined in

monoclinic space group, $P2_1/n$. The composition implies that there are one neutral 4-

PAH molecule and one 4-PAH$_2$$^+$ cation for one PF$_6$$^-$ anion where the 4-PAH is a

zwitter ion. Unlike the other salts, it is a 2:1 salt, comprising one 4-PAH$_2$$^+$, one 4-

PAH zwitter ion and one PF$_6$$^-$ anion. Each 4-PAH molecule has a cationic part *viz.*

the protonated pyridyl group but the proton is disordered between 4-PAH$_2$$^+$ and 4-

PAH and difficult to distinguish CO_2^- from CO_2H. Therefore, they have been treated as quasi-zwitterions here. Various types of weak and strong H-bonding, as shown in Figure 3.14, play important role to construct the solid state architecture. The quasi-zwitterionic 4-PAHs are arranged on two dimensional plane forming strong intermolecular N-H···O hydrogen bonding and the PF_6^- anions sit at the middle forming weaker C-H···F bonds as shown in Figure 3. The other F atoms of PF_6^- anions, above and below the plane, have similar weaker C-H···F interaction with 4-PAHs of nearby layers. The parameters for these hydrogen bonding interactions are listed in Table 3.8.
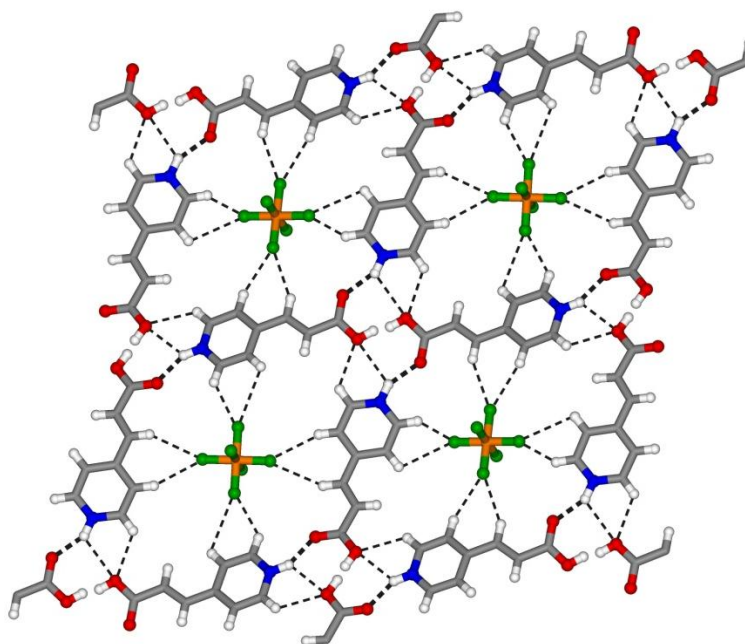
Figure 3.14 A quasi-zwitterionic arrangement of 4-PAHs in **18**.

A detailed scrutiny to the solid state structure of this salt reveals that the quasi-zwitterionic 4-PAHs are oriented in slipped stacked infinite parallel arrangement in HH-fashion. The distance of separation is 5.10 Å (Figure 3.15) which is same as the length of the *a*-axis. The salt was found photostable when irradiated under UV light for 60 h, the distance was found to be too long to undergo photodimerization. This long distance and slipped stacked arrangement can be rationalized from the cation-

....

cation repulsion which is not properly balanced by monovalent PF_6^- anion; unlike in

14 where the cation-cation repulsion was partially stabilised by the bivalent sulphate

anion.

Table 3.8 The hydrogen bonding parameters for **18**

D-H···A	D(D-H) (Å)	D(H···A) (Å)	D(D···A) (Å)	<(DHA) (°)	Symmetry Operator
O(1)-H(1O)···O(1)	0.83	1.63	2.453(3)	173(8)	-x+2, -y+1, -z+2
N(1)-H(1N)···O(2)	0.93	1.82	2.656(2)	149(3)	x-3/2, -y+1/2, z-1/2
N(1)-H(1N)···O(1)	0.93	2.62	3.205(2)	122(2)	-x+1/2, y-1/2, -z+3/2
C(1)-H(1)···F(3)	0.94	2.39	3.110(3)	133	-x, 1-y, 1-z
C(2)-H(2)···F(1)	0.94	2.37	3.300(2)	168	
C(4)-H(4)···F(1)	0.94	2.59	3.110	115(6)	1/2-x,-1/2+y,3/2-z
C(4)-H(4)···F(2)	0.94	2.59	3.481	158(1)	1/2+x,1/2-y,1/2+z
C(5)-H(5)···O(1)	0.94	2.52	3.162(2)	126	1/2-x, -1/2+y, 3/2-z
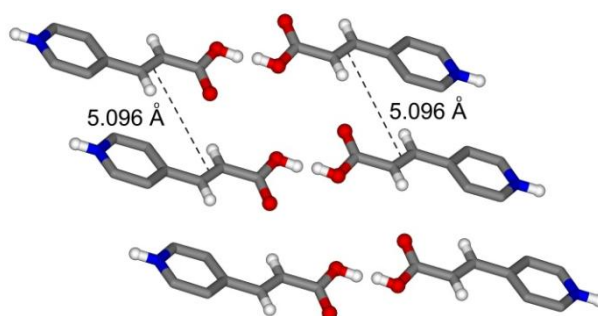
Figure 3.15 The quasi-zwitterionic 4-PAHs are oriented in slipped stacked infinite parallel arrangement in HH-fashion

3.2.3 Description of the Molecular Salts of 4-PAH with HNO$_3$ and HBF$_4$ and H$_3$PO$_4$ (19 - 21)

4-PAH was also reacted with these three acids and the resulting compounds were characterized and tested for their photoreactivity. The composition of nitrate, tetrafluoroborate and biphosphate salts were determined from elemental analysis and thermogravimetric analysis as (4-PAH$_2$)NO$_3$ or C$_8$H$_8$N$_2$O$_5$ (**19**), (4-PAH$_2$)BF$_4$ or C$_8$H$_8$NO$_2$BF$_4$ (**20**), (4-PAH$_2$)H$_2$PO$_4$ or C$_8$H$_{10}$NO$_6$P (**21**) respectively in the absence of suitable single crystals. Upon irradiation under UV light, **20** underwent quantitative photodimerization in the solid sate in HT-fashion, whereas **19** and **21** were found not to furnish any photodimerization. From this observation, we rationalize that in **20**, 4-PAH$_2^+$ cations are stacked parallel in HT-fashion in the solid state where the distance of separation is 3.5 – 4.2 Å. The parallel orientation can either be infinite parallel or discrete pairs. The orientation of 4-PAH$_2^+$ cations in **19** and **21** can be expected to be nonparallel or the distance is beyond the Schmidt's distance limit.[13]
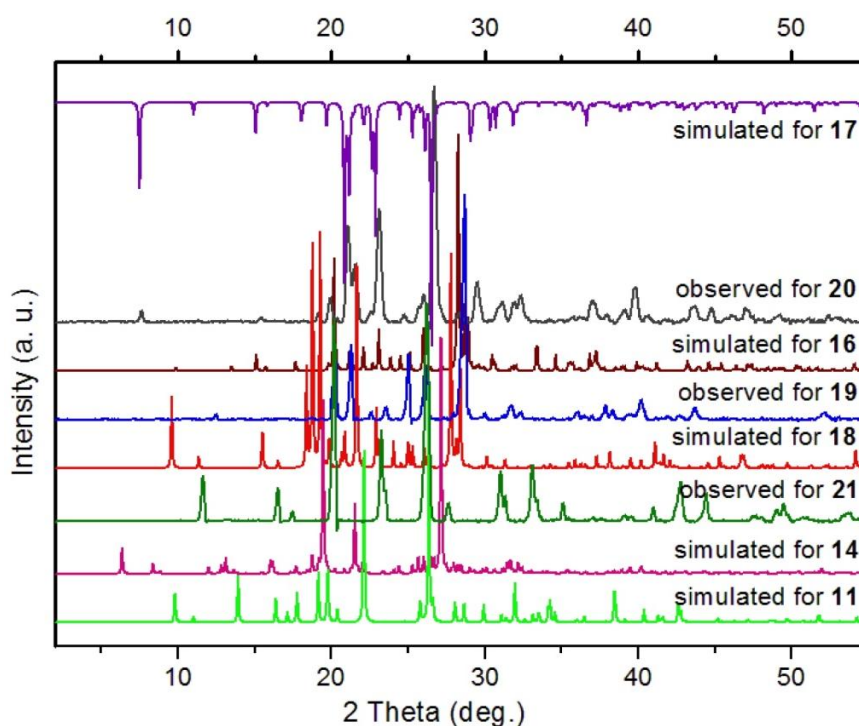
Figure 3.16 The PXRD patterns of **19** – **21** are compared with the simulated patterns of the known salts

To determine the structure of the salt **19**, **20** and **21** in absence of single crystals, their PXRD patterns were compared with simulated patterns from the known structures. From Figure 3.16, it can be concluded that the structures of **19** and **21** are not matching with any known structure. However, the pattern for **20** is matching with simulated pattern of **17**. Therefore, the structure of **20** resembles with the structure of **17** which is reminiscent and can be expected from the sizes and shapes of ClO_4^- and BF_4^- anions. It also can be observed that the patterns of the other salts are not matching although having 4-PAH$_2^+$ cation in common. Therefore, it can be understood that a huge difference in the soild state packing and hence in photoreactivity are observed while the anions are tuned.

3.2.4 Comparative Study of the Molecular Salts of 4-PAH

Having discussed the solid state structure and photoreactivity of the series of salts of 4-PAH, now they would be compared in terms of structural diversity and photoreactivity. The HT-parallel orientations of 4-PAH$_2^+$ cations have been observed in **11**, **16**, **17**, and **20** and HH-parallel orientation in **14** which underwent quantitative photodimerization (Table 3.9). Among them, the discrete parallel pairs are found in **16** and **17**; whereas in **11** the arrangement is infinite. Again, in **16** the discrete pairs arrange along ladder-like one-dimensional chains aligned by $[(Cl^-)_2(H_2O)_2]$ clusters; on the contrary, in **17** it occur randomly. The differences in mode of packing in **16** and **17** can be rationalized from the sizes and shapes of a single point charge Cl^- anion with the tetrahedral ClO_4^- anion. In **18**, the 4-PAH$_2^+$ cations are found to stack parallel in HH-fashion but with a longer distance of 5.096 Å. On the other hand in **14**, the 4-PAH$_2^+$ cations stack in infinitely parallel with partial crisscross orientation in HH-fashion with distances permeable for photodimerization. Single crystals of this salt underwent 66% photodimerization; the same salt showed quantitative conversion upon grinding on a mortar which was witnessed to absorb an extra molecule of water during grinding that triggered structural rearrangement. The presence of bivalent

sulphate anions in **14** can stabilize the possible cation-cation repulsion but the monovalent PF_6^- anion is inadequate to balance the cation-cation repulsion in **18**; therefore the distance (5.096 Å) is longer. It is also observed that water molecules present in the crystals play crucial role in the arrangements of 4-PAH_2^+ cations in both **14** and **16** but in a different way, which can be attributed by the charge and sizes of the Cl^- and SO_4^{2-} anions. H_3PO_4 was chosen to achieve HH-orientation of 4-PAH_2^+ by the presence of bivalent HPO_4^{2-} anion, but it has resulted in 1:1 salt with monovalent $H_2PO_4^-$; therefore the HH-orientation parallel orientation have not been obtained.

Table 3.9 The list of all the salts and their photoreactivity

Acid used to form salts	Photoreactivity	Nature of alignment	Details of alignment	% of Conversion
CF_3CO_2H (**11**)	Photo-reactive	Infinitely parallel	Head-to-tail 3.766 Å	100
H_2SO_4 (**14**)	Photo-reactive	Infinitely Parallel	Head-to-head 3.672 – 3.754 Å	100 upon grinding
HCl (**16**)	Photo-reactive	Parallel; discrete pairs	Head-to-tail 3.80 Å	100
$HClO_4$ (**17**)	Photo-reactive	Parallel; discrete pairs	Head-to-tail 3.909 Å	100
HPF_6 (**18**)	Photo-stable	Infinitely parallel	Head-to-head 5.096 Å	0
HNO_3 (**19**)	Photo-stable	Predicted to be non-parallel	-	0
HBF_4 (**20**)	Photo-reactive	Predicted to be parallel	Head-to-tail < 4.2 Å	100
H_3PO_4 (**21**)	Photo-stable	Predicted to be non-parallel	-	0

In the context of stereoselective synthesis, the two isomers of the cyclobutane compounds *viz. rctt*-HH- and HT-BPCD were synthesized in quantitative yield. The corresponding selective preorganisation of 4-PAH_2^+ cations before UV irradiation were achieved just by changing the acid for salt formation; namely by tuning the anion present in the salts. Now, one question may arise whether these alignments are predictable. From the above table, we can see that only the sulphate-bisulphate salt

produced HH-dimer and all the other monovalent anions produced either HT-dimer or photostable salts. Hence, one can assume that HT-parallel orientation is quite common and thermodynamically more stable because of the cation-π interaction.[6, 14] On the other hand, HH-parallel orientation is quite unstable because of the cation-cation repulsion which is needed to be stabilized by some bi- or trivalent anions. The observed longer distance between 4-PAH$_2^+$ cations in **18** shows some evidence of the cation-cation repulsion where PF$_6^-$ anion is inadequate to balance the repulsive force.

3.3 Synthesis of *head-to-tail* Photodimer of 3-PAH

Unlike 4-PAH, 3-PAH is photoreactive and was first reported by Schmidt *et al.*[1] Crystallographic characterization of 3-PAH was later presented by Briceño *et al.*[2] It was found to stack parallel on its own, in *head-to-head* fashion with a distance of separation 3.82 Å, like β-cinnamic acid (Figure 3.17). Therefore, the synthesis of a tetratopic cyclobutane ligand 3,4-bis(3'-pyridyl)cyclobutane-1,2-dicarboxylic acid (HH-3,3-BPCD) was possible without any modification in the solid state. The polymorph where 3-PAH can be aligned parallel in *head-to-tail* fashion (α-analouge of *trans*-cinnamic acid) has not yet been discovered. Therefore, the synthesis of 2,4-bis(3'-pyridyl)cyclobutane-1,3-dicarboxylic acid (HT-3,3-BPCD) is still a challenge and crystal engineering principle can be applied to target HT-parallel orientation of 3-PAH. We, therefore, have extrapolated our idea of salt formation with strong acid and have successfully achieved the parallel orientation of 3-PAH$_2^+$ with ClO$_4^-$ anion.

3-PAH was reacted with HClO$_4$ in water and the resultant poly-crystalline salt was irradiated under UV light for 16 h to attain quantitative photodimerization in HT-fashion. Although we could not grow any diffraction quality single crystals, we are able to crystallize the dimer-salt after photodimerization reaction to characterize the formation of HT-dimer by X-ray crystallography. The anhydrous salt of composition [HT-3,3-BPCD](ClO$_4$)$_2$ or C$_{16}$H$_{16}$Cl$_2$N$_2$O$_{12}$ (**22**) crystallizes in the triclinic

spacegroup, *P*ī. The pyridyl groups are found protonated and involve in charge assisted H-bonding and electrostatic interaction with two 'O' from ClO_4^- anions. The carboxylic acid proton also donates H-bonding to perchlorate oxygen. The geometry of the dimer compound is confirmed as *rctt*, as shown in the Figure 3.18 below and the geometric parameters for hydrogen bonding are listed in Table 3.10.
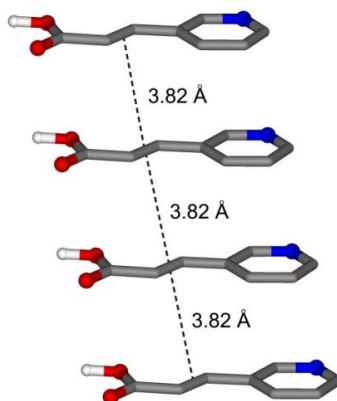
Figure 3.17 Infinitely parallel stacking of 3-PAH in the solid state makes it photoreactive
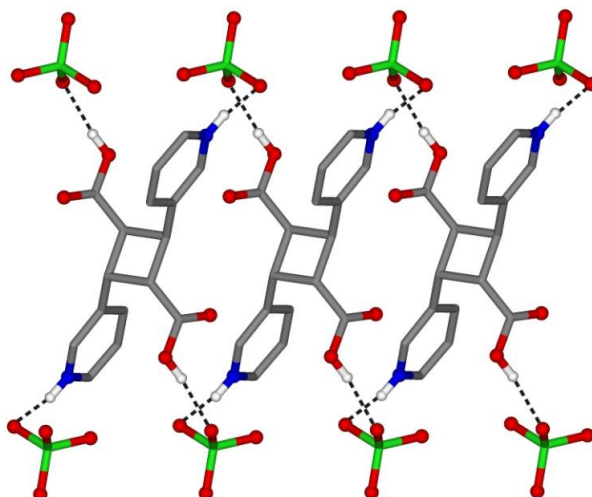
Figure 3.18 Crystal structure of *rctt*-HT-3,3-BPCD as its ClO_4^- salt

Table 3.10 The hydrogen bonding parameters for **22**

D-H···A	D(D-H) (Å)	D(H···A) (Å)	D(D···A) (Å)	<(DHA) (°)	Symmetry Operator
N(1)-H(1N)···O(3)	0.85	2.32	3.029(2)	140	x, -1+y, z
N(1)-H(1N)···O(3)	0.85	2.45	3.115(2)	135	-x, 1-y, 1-z
C(3)-H(3)···O(2)	1.0	2.35	3.166(2)	138	-x, 1-y, -z
C(4)-H(4)···O(2)	0.95	2.39	3.245(2)	150	-x, 1-y, -z
C(7)-H(7)···O(5)	0.95	2.56	3.372(2)	144	1+x, y, z
C(7)-H(7) ···O(5)	0.95	2.51	3.345(2)	147	1-x, 1-y, 1-z
C(8)-H(8)···O(4)	0.95	2.47	3.343(2)	152	1-x, 1-y, 1-z

3.4 Isomerisation of Cyclobutane Derivatives

Isomerisation of cyclobutane derivatives containing pyridyl groups was reported in the past by Horner and Hünig.[15] Recently, we also studied the acid catalyzed isomerisation of *rctt*-4,4-tpcb [4,4-tpcb = 1,2,3,4-tetrakis(4'-pyridyl)cyclobutane] to *rtct*-4,4-tpcb quantitatively via *rcct*-4,4-tpcb where *rtct* isomer is the most stable.[16] 1,2,3,4-tetrakis(4'-carboxyphenyl)cyclobutane, another cyclobutane derivative described in Chapter 2, was not observed to show any such isomerisation, neither in acidic nor in alkaline pH. These observations indicate that free pyridyl bases are responsible for such isomerisation. The coordination polymer of 4,4-tpcb, $[Zn_2(CF_3CO_2)_2(\mu\text{-}CH_3CO_2)_2(rctt\text{-}4,4\text{-}tpcb)]^{17}$ was also observed not to undergo any such isomerisation in presence of CF_3CO_2H reflecting the mechanism of such isomerisation involves protonation of the uncoordinated pyridyl groups in acidic pH. Both the *rctt*-HT- and HH-4,4-BPCD were interestingly found to undergo isomerisation in acidic solution which is observed to be faster upon heating. On the contrary, both *rctt*-HT- and HH-3,3-BPCD were found not to furnish such isomerisation under similar condition. These observations gave us an opportunity to study the mechanistic aspect of such isomerisation in details.
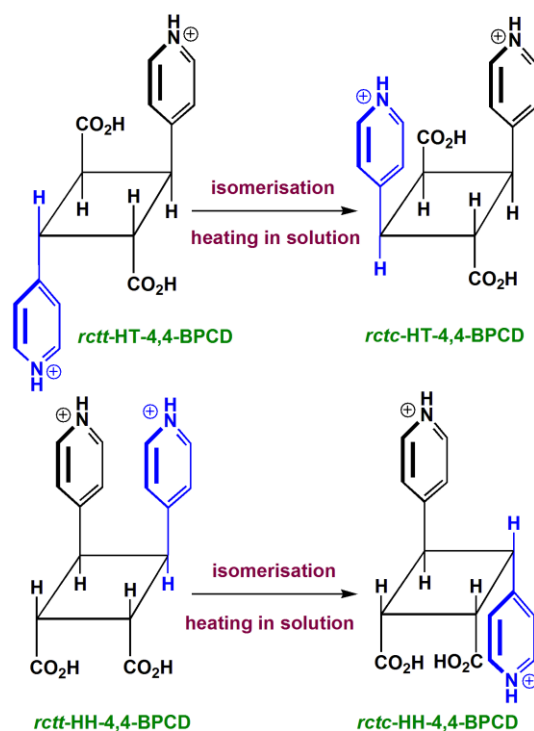
Scheme 3.1 The structures of the *rctc-* isomers of HT and HH-4,4-BPCD after isomerisation

If we consider the geometries of *rctt*-HT- and HH-4,4-BPCD molecules, flipping of either pyridyl group can result in isomerisation. If both the pyridyl groups flip to the other side of the cyclobutane ring for HH-4,4-BPCD, the resulting isomer would be *rccc* which is not stable. Therefore, the structures of the resulting isomers are expected be *rctc-* as shown in the Scheme 3.1. We can see from the structures that the product *rctc*-isomer is less stable than *rctt*-isomers as three substituents are on the same side of the cyclobutane ring resulting steric hindrance. Further, this isomerisation was not quantitative and about 90% conversion was observed in ^{1}H NMR spectra. Although, to our disappointment, we could not grow bigger single crystals for X-ray diffraction data collection, the isolation of *rctc*-HT-4,4-BPCD was confirmed by ^{1}H NMR spectrum of the recrystallized salt with $CF_3CO_2^-$ (Figure 3.19). Two doublet of doublet peaks *rctt*-cyclobutane have converted to three triplet (1:2:1) peaks for *rctc*-cyclobutane.
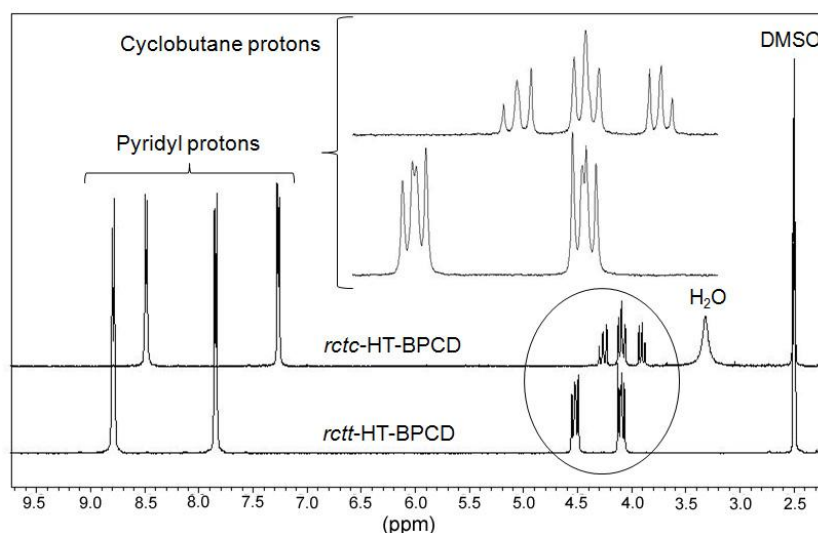
Figure 3.19 ^{1}H NMR spectra show the isomerisation of *rctt*-HT-4,4-BPCD to *rctc*-HT-4,4-BPCD; two doublet of doublet (dd) peaks for cyclobutane protons converted to three triplet peaks (1:2:1).

From these findings and our previous observations, we propose a mechanism for such isomerisation involving protonation and deprotonation of the pyridyl groups, as shown in Scheme 3.2 below. The proposed mechanism can successfully explain the observed isomerisation of both the 4-pyridyl substituted cyclobutane derivatives namely, *rctt*-HT-4,4-BPCD and *rctt*-HH-4,4-BPCD to their corresponding *rctc*-forms. It is also able to explain the inertness of both the 3-pyridyl substituted cyclobutane derivatives namely, *rctt*-HT-3,3-BPCD and *rctt*-HH-3,3-BPCD to such isomerisation under similar condition (Scheme 3.3). Following this mechanism it can also be predicted that the 2-pyridyl substituted cyclobutane derivatives (both HH- and HT-) can undergo such isomerisation under similar condition. Therefore, this idea can further be extended to investigate the isomerisation of various types pyridyl based cyclobutane derivative with varying positions of N in the ring.

3.5 Summary

In this chapter, the solid state structure of various molecular salts of 4-PAH have been discussed with complete characterizations. The solid state photoreactivity of these salts are addressed and hence the anion controlled stereoselective
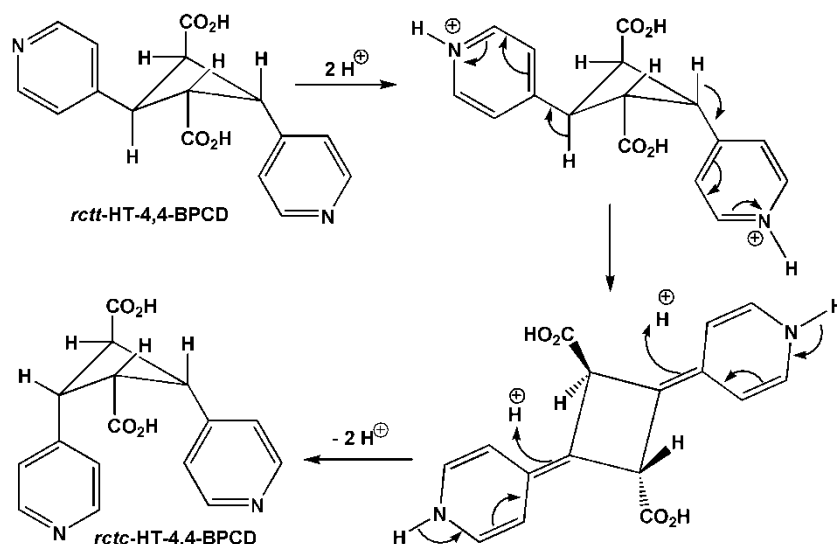
Scheme 3.2 The mechanism of isomerisation of *rctt*-HT-4,4-BPCD to *rctc*-HT-4,4-BPCD and similar applies for HH-4,4-BPCD which is not shown here.
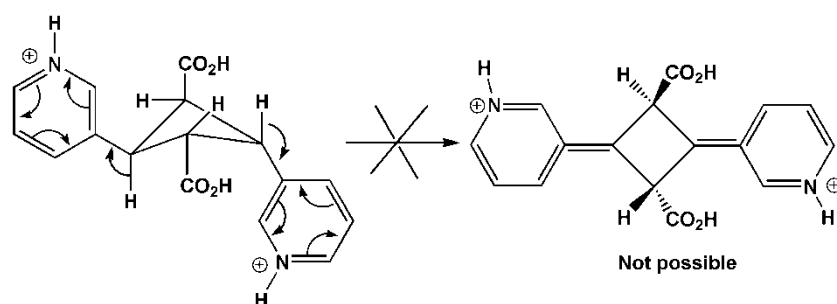
Scheme 3.3 The inertness of both the HH- and HT-3,3-BPCD (dimers of 3-PAH) to such isomerisation can be explained by this mechanism

dimerization of 4-PAH to *rctt*-HT- and HH-BPCD are discussed. From the series of these salts we anticipate that bivalent anion like sulphate has crucial role to stabilise the cation-cation repulsion in HH-orientation. On the other hand, HT-orientation is stable due to possible cation-π interaction between two olefins forming the pair. Our work is the first report on the solid state photodimerization of 4-PAH. We have extrapolated our idea of salt formation to achieve HT-parallel orientation of 3-PAH. All these pyridyl based cyclobutane derivatives were tested for acid catalysed isomerisation and it was found that 4-pyridyl substituted cyclobutane derivatives undergo isomerisation from *rctt*- to *rctc*- forms under acidic condition; whereas, 3-

....

pyridyl analogues are inert. The proposed mechanism for such isomerisation is able to explain the divergent behaviour of such compounds. All these functional cyclobutane derivatives are potentials ligands for making co-crystals and CPs/MOFs which are discussed in Chapter 7.

3.6 Syntheses and Characterizations

All the compounds were characterized by ^{1}H and ^{13}C-NMR spectroscopy, elemental analysis in addition to X-ray crystallographic characterization. Thermogravimetric analysis (TGA) was carried out for the hydrated salts and other characterization techniques were used when and wherever were necessary.

CF_3CO_2(4-PAH$_2$) (11)

^{1}H NMR (300 MHz, DMSO-d_6, 298K): δ_H = 8.78 (d, 2H, Ar-H), 7.95 (d, 2H, Ar-H), 7.63 (d, 1H, CH=CH), 6.93 (d, 1H, CH=CH). ^{13}C-NMR (75 MHz, DMSO-d_6, 298K): δ_C = 166.64, 158.7, 148.89, 145.78, 138.52, 127.38, 123.88, 118.07, 114.18. Analysis found (%): C 45.58, H 3.19, N 5.36; $C_{10}H_8F_3NO_4$ requires C 45.64, H 3.06, N 5.32. No solvent loss was observed in TGA experiment.

(*rctt*-HT-4,4-BPCDH$_2$)(CF$_3$CO$_2$)$_2$ (12)

^{1}H NMR (300 MHz, DMSO-d_6, 298K): δ_H = 8.79 (d, 4H, Ar-H), 7.84 (d, 4H, Ar-H), 4.52 (dd, 2H, CH-CH), 4.09 (dd, 2H, CH-CH). ^{13}C-NMR (75 MHz, DMSO-d_6, 298K): δ_C = 171.78, 158.88, 158.43, 155.55, 144.22, 125.02, 118.19, 114.39, 44.88, 40.78. FT-IR (KBr, cm^{-1}): 3097, 2609, 2162, 2060, 1944, 1737, 1649, 1536, 1508, 1405, 1341, 1295, 1198, 1153, 1104, 1003, 918, 846, 797, 724, 636, 582, 510, 444, 416. Analysis found (%): C 45.43, H 3.03, N 5.36; $C_{20}H_{16}F_6N_2O_8$ requires C 45.64, H 3.06, N 5.32. No solvent loss was observed in TGA experiment.

rctt-HT-4,4-BPCD (13)

^{1}H NMR (300 MHz, DMSO-d_6, 298K): δ_H = 12.39 (s, 2H, CO$_2$H), 8.52 (d, 4H, Ar-H), 7.38 (d, 4H, Ar-H), 4.30 (dd, 2H, CH-CH), 3.90 (dd, 2H, CH-CH). ^{13}C-NMR (75 MHz, DMSO-d_6, 298K): δ_C = 172.27, 149.33, 147.98, 122.89, 44.89, 40.29. FT-IR (KBr, cm^{-1}): 3059, 3040, 1707, 1607, 1556, 1503, 1426, 1377, 1337, 1287, 1244, 1198, 1132, 1071, 1012, 987, 950, 931, 844, 794, 741, 666, 636, 587, 522, 391. m/z 297.3 represents (M-1) peak in ESI-MS. Analysis found (%): C 64.40, H 4.77, N 9.28; $C_{16}H_{14}N_2O_4$ requires 64.42; H, 4.73; N, 9.39.

(4-PAH$_2$)$_3$(SO$_4$)(HSO$_4$)(H$_2$O) (14)

^{1}H NMR (300 MHz, DMSO-d_6, 298K): δ_H = 8.82 (d, 2H, Ar-H), 8.08 (d, 2H, Ar-H), 7.86 (d, 1H, CH=CH), 6.98 (d, 1H, CH=CH). ^{13}C-NMR (75 MHz, DMSO-d_6, 298K): δ_C = 166.51, 148.08, 144.77, 139.15, 128.13, 124.41. FT-IR (KBr, cm^{-1}): 3175, 3116, 3076, 2773, 2664, 2559, 2469, 1706, 1633, 1584, 1495, 1396, 1319, 1290, 1233, 1204, 1187, 1120, 1015, 995, 871, 852, 809, 741, 684, 619, 580, 529, 497. Analysis found: C 43.36, H 4.50, N 6.32%; $C_{24}H_{27}N_3O_{15}S_2$ requires: C 43.57, H 4.11, N 6.35%. 2.8 % water loss was observed in TGA experiment, where as the calculated value is 2.7%.

rctt-HH-4,4-BPCD (15)

^{1}H NMR (300 MHz, DMSO-d_6, 298K): δ_H = 12.84 (s, 2H), 8.28 (d, 4H), 7.09 (d, 4H), 4.28 (d, 2H), 3.90 (d, 2H). ^{13}C-NMR (75 MHz, DMSO-d_6, 298K): δ_C = 173.45, 149.02, 147.55, 123.13, 43.48, 41.51. FT-IR (KBr, cm^{-1}): 3055, 2918, 2483, 1730, 1609, 1556, 1422, 1368, 1330, 1275, 1195, 1122, 1069, 1012, 964, 923, 903, 852, 838, 817, 752, 707, 650, 625, 555, 522, 442. Analysis found (%): C, 64.40; H, 4.77; N, 9.28. $C_{16}H_{14}N_2O_4$ requires C, 64.42; H, 4.73; N, 9.39.
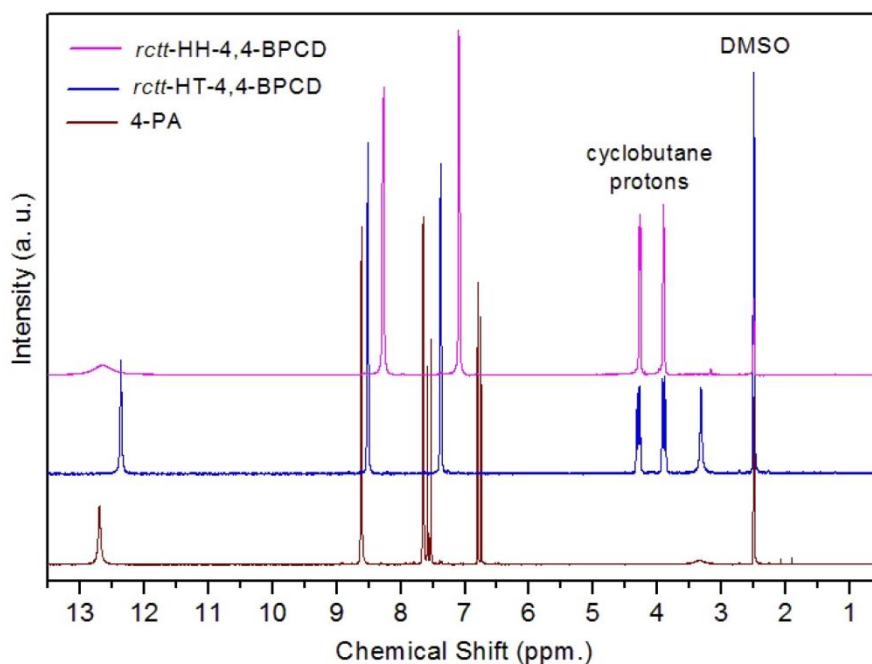
Figure 3.20 ^{1}H NMR spectra of 4-PAH, *rctt*-HT-4,4-BPCD and *rctt*-HH-4,4-BPCD
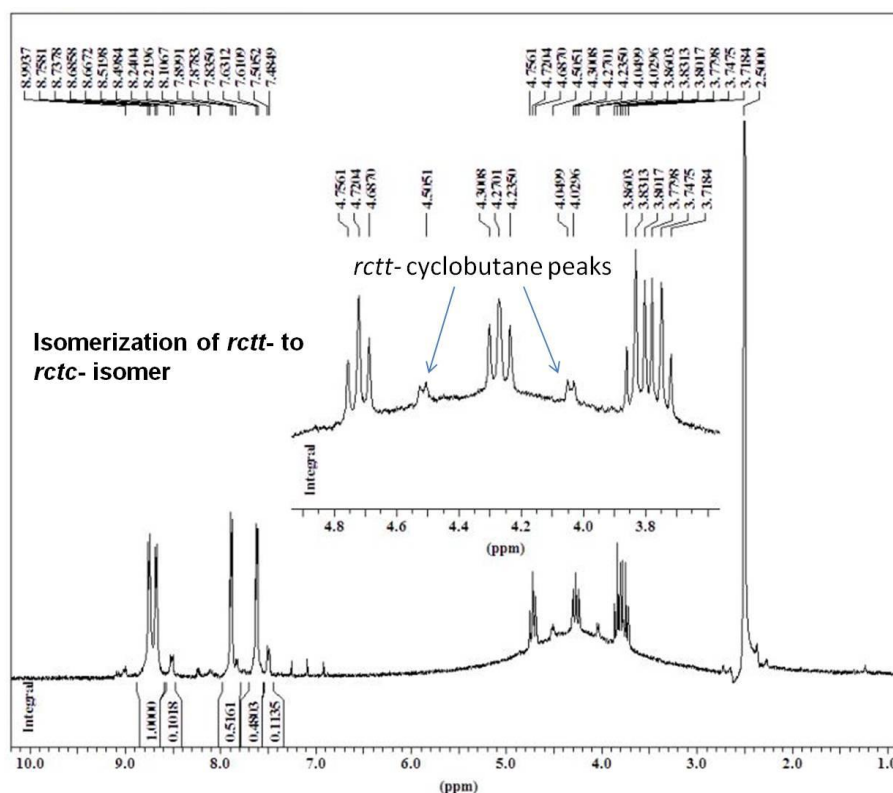
Figure 3.21 ^{1}H NMR spectrum shows the isomerisation of *rctt*-HH-BPCD to *rctc*-HH-BPCD. There are four different types of cyclobutane protons instead of two for *rctt*-form. This isomerisation is not quantitative as *rctc*-form is less stable than *rctt*-form.

(4-PAH$_2$)Cl·H$_2$O (16)

^{1}H NMR (300 MHz, DMSO-d_6, 298K): δ_H = 8.90 (d, 2H), 8.24 (d, 2H), 7.73 (d, 1H), 7.07(d, 1H). ^{13}C-NMR (75 MHz, DMSO-d_6, 298K): δ_C = 166.33, 150.09, 142.51, 138.45, 129.38, 125.14. FT-IR (KBr, cm^{-1}): 3174, 3114, 2773, 2557, 1704, 1632, 1584, 1494, 1396, 1290, 1233, 1187, 1064, 994, 941,852, 808, 740, 682, 528, 497. After UV irradiation, ^{1}H NMR (300 MHz, DMSO-d_6, 298K): δ_H = 8.90 (d, 4H), 8.05 (d, 4H), 4.64 (dd, 2H), 4.19 (dd, 2H). Analysis found (%): C, 47.28; H, 4.64; N, 6.76. C$_8$H$_{10}$ClNO$_3$ requires: C, 47.19; H, 4.95; N, 6.88. The calculated and observed water losses in TGA experiment are 8.8% and 8.7%.

(4-PAH$_2$)ClO$_4$ (17)

^{1}H NMR (300 MHz, DMSO-d_6, 298K): δ_H = 8.90 (d, 2H), 8.25 (d, 2H), 7.73 (d, 1H), 7.07(d, 1H). ^{13}C-NMR (75 MHz, DMSO-d_6, 298K): δ_C = 166.37, 150.46, 142.81, 138.42, 129.59, 125.12. FT-IR (KBr, cm^{-1}): 3114, 2774, 1704, 1632, 1585, 1496, 1395, 1290, 1233, 1187, 1142, 1086, 993, 940, 851, 808, 740, 682, 627, 578, 528, 497. After UV irradiation, ^{1}H NMR (300 MHz, DMSO-d_6, 298K): δ_H = 8.91 (d, 4H), 8.07 (d, 4H), 4.65 (dd, 2H), 4.19 (dd, 2H). Analysis found (%): C, 38.09; H, 3.32; N, 5.53. C$_8$H$_8$ClNO$_6$ requires: C, 38.50; H, 3.23; N, 5.61.

(4-PAH$_2$)(4-PAH)PF$_6$ (18)

^{1}H NMR (300 MHz, DMSO-d_6, 298K): δ_H = 8.73 (d, 4H), 7.90 (d, 4H), 7.62 (d, 2H), 6.89 (d, 2H). ^{13}C-NMR (75 MHz, DMSO-d_6, 298K): δ_C = 166.74, 147.53, 144.75, 140.18, 126.02, 123.19. FT-IR (KBr, cm^{-1}): 3112, 2787, 1705, 1633, 1607, 1496, 1395, 1348, 1312, 1244, 1214, 1091, 991, 961, 826, 745, 686, 558, 524. Analysis found (%): C, 43.54; H, 3.40; N, 6.50. C$_{16}$H$_{15}$F$_6$N$_2$O$_4$P requires: C, 43.26; H, 3.40; N, 6.31. No solvent loss was observed in TGA experiment.

....

(4-PAH$_2$)NO$_3$ (19)

^{1}H NMR (300 MHz, D$_2$O, 298K): δ_H = 8.72 (d, 2H), 8.14 (d, 2H), 7.70 (d, 1H), 6.92 (d, 1H). ^{13}C-NMR (75 MHz, DMSO-d_6, 298K): δ_C = 166.46, 150.59, 142.91, 138.51, 129.7, 125.3. FT-IR (KBr, cm^{-1}): 3112, 2773, 2557, 1704, 1632, 1585, 1496, 1381, 1289, 1232, 1186, 1091, 994, 960, 852, 809, 740, 681, 579, 528, 498. Analysis found (%): C, 45.10; H, 3.89; N, 13.21. C$_8$H$_8$N$_2$O$_5$ requires C, 45.29; H, 3.80; N, 13.20. No solvent loss was observed in TGA experiment.

(4-PAH$_2$)BF$_4$ (20)

^{1}H NMR (300 MHz, D$_2$O, 298K): δ_H = 8.70 (d, 2H), 8.13 (d, 2H), 7.62 (d, 1H), 6.93 (d, 1H). ^{13}C-NMR (75 MHz, DMSO-d_6, 298K): δ_C = 166.62, 150.74, 142.89, 138.61, 129.79, 125.37. FT-IR (KBr, cm^{-1}): 3174, 3114, 2774, 2558, 1704, 1632, 1585, 1496, 1395, 1290, 1233, 1187, 1142, 1086, 993, 940, 851, 808, 740, 682, 627, 578, 528, 497. Analysis found (%): C, 40.06; H, 3.34; N, 5.73. C$_8$H$_8$NO$_2$BF$_4$ requires C, 40.55; H, 3.40; N, 5.91. No solvent loss was observed in TGA experiment.

(4-PAH$_2$)H$_2$PO$_4$ (21)

^{1}H NMR (300 MHz, D$_2$O, 298K): δ_H = 8.72 (d, 2H), 8.15 (d, 2H), 7.69 (d, 1H), 6.93 (d, 1H). ^{13}C-NMR (75 MHz, DMSO-d_6, 298K): δ_C = 167.12, 149.02, 143.42, 140.89, 125.32, 122.98. FT-IR (KBr, cm^{-1}): 3112, 2787, 2114, 1706, 1634, 1607, 1497, 1396, 1348, 1312, 1245, 1215, 1092, 991, 962, 827, 745, 687, 558, 524. Analysis found (%): C, 38.46; H, 3.89; N, 6.02. C$_8$H$_{10}$NO$_6$P requires C, 38.88; H, 4.08; N, 5.67. No solvent loss was observed in TGA experiment.

(*rctt*-HT-3,3-BPCDH$_2$)(ClO$_4$)$_2$ (22)

^{1}H NMR (300 MHz, DMSO-d_6, 298K): δ_H = 8.87 (s, 2H, Ar-H), 8.73 (d, 2H, Ar-H), 8.38 (d, 2H, Ar-H), 7.86 (dd, 2H, Ar-H), 4.55 (dd, 2H, CH-CH), 4.07 (dd, 2H, CH-CH). ^{13}C-NMR (75 MHz, DMSO-d_6, 298K): δ_C = 172.09, 144.11, 143.41,

141.47, 137.49, 125.52, 45.03, 38.43. Analysis found: C 38.10, H 3.17, N 6.12%; $C_{16}H_{16}Cl_2N_2O_{12}$ requires C 38.50, H 3.23, N 5.61%. No solvent loss was observed in TGA experiment. m/z 297.1 represents (M-1) peak in ESI-MS.

Table 3.11 Crystallographic data for compounds **11 - 14**

Compounds	11	12	13	14
Formula	$C_{10}H_8F_3NO_4$	$C_{20}H_{16}F_6N_2O_8$	$C_{16}H_{14}N_2O_4$	$C_{24}H_{27}N_3O_{15}S_2$
M	263.17	526.35	298.29	661.61
T (K)	223(2)	223(2)	100(2)	223(2)
λ (Å)	0.71073	0.71073	0.71073	0.71073
Cryst syst / Space group	Orthorhombic / $Pca2_1$	Monoclinic / $P2_1/c$	Monoclinic / $P2_1/c$	Monoclinic / $P2_1/n$
a (Å)	18.015(2)	12.3692(7)	5.9012(7)	11.0902(8)
b (Å)	8.9617(10)	8.2108(5)	6.9480(8)	9.1024(7)
c (Å)	6.7552(8)	10.8302(6)	16.0585(19)	27.822(2)
α (°)	90	90	90	90
β (°)	90	94.9560(10)	99.931(2)	94.3890(10)
γ (°)	90	90	90	90
Volume ($Å^3$) / Z	1090.6(2) / 4	1095.81(11) / 1.595	648.56(13) / 2	2800.4(4) / 4
D_{calcd} (g/cm^3) / μ (mm^{-1})	1.603 / 0.156	1.595 / 0.155	1.527 / 0.112	1.569 / 0.272
Reflns col. / Ind. Reflns.	7168 / 2398	7498 / 2506	4332 / 1466	18729 / 6427
R_{int} / Goof on F^2	0.0301 / 1.060	0.0232 / 1.041	0.0229 / 1.131	0.0256 / 1.055
Final R[I>2σ]^a R$_1$ / wR2	0.0595, wR2 = 0.1616	0.0451 / 0.1203	0.0493 / 0.1510	0.0386 / 0.1015

^{a} R1 = Σ||F_o| − |F_c||/ Σ|F_o|, ^{b} wR2 = [Σ$w(F_o^2 − F_c^2)^2$/Σ$w(F_o^2)^2$]$^{1/2}$

Table 3.12 Crystallographic data for compounds **15 – 18** and **22**

Compounds	15	16	17	18	22
Formula	$C_{16}H_{14}N_2O_4$	$C_8H_{10}ClNO_3$	$C_8H_8ClNO_6$	$C_{16}H_{15}F_6N_2O_4P$	$C_{16}H_{16}Cl_2NO_{12}$
M	298.29	203.62	249.60	444.27	499.21
T (K)	223(2)	223(2)	223(2)	223(2)	100(2)
λ (Å)	0.71073	0.71073	0.71073	0.71073	0.71073
Cryst syst / Space group	Monoclinic / Cc	Triclinic / $P\bar{1}$	Triclinic / $P\bar{1}$	Monoclinic / $P2_1/n$	Triclinic / $P\bar{1}$
a (Å)	14.723(2)	6.8763(4)	5.0430(3)	5.0962(3)	5.6256(11)
b (Å)	9.6367(14)	8.0599(5)	8.4238(6)	15.5577(10)	7.3895(14)
c (Å)	10.5485(16)	9.6919(5)	12.5243(9)	11.4752(8)	11.519(2)
α (°)	90	69.9810(10)	105.6250(10)	90	81.854(4)
β (°)	118.305(3)	73.3820(10)	100.4850(10)	95.9440(10)	83.101(4)
γ (°)	90	68.9960(10)	95.5600(10)	90	80.622(4)
Volume (Å^3) / Z	1317.7(3) / 4	462.92(5) / 2	497.81(6) / 2	904.92(10) / 2	465.35(15) / 1
D_{calcd} (g/cm^3) / μ (mm^{-1})	1.504 / 0.110	1.461 / 0.386	1.665 / 0.398	1.630 / 0.239	1.781 / 0.425
Reflns col. / Ind. Reflns.	3927 / 1997	5927 / 2120	6455 / 2283	6198 / 2069	6189 / 2132
R_{int} / Goof on F^2	0.0445 / 1.666	0.0223 / 1.145	0.0209 / 1.065	0.0221 / 1.047	0.0235 / 1.095
Final R[I>2σ]^a R$_1$ / wR2	0.1405 / 0.3440	0.0330 / 0.0928	0.0339 / 0.0936	0.0464 / 0.1221	0.0315 / 0.0867

^{a} R1 = Σ||F_o| − |F_c||/ Σ|F_o|, ^{b} wR2 = [Σw($F_o^2 − F_c^2$)^2/Σw(F_o^2)^2]$^{1/2}$

3.7 References

1.   Lahav, M.; Schmidt, G. M. J., *J. Chem. Soc. B: Phy. Org.* **1967**, 239-243.

2.   Briceño, A.; Atencio, R.; Gil, R.; Nobrega, A., *Acta Crystallogr. Sect. C* **2007,** *63* (8), o441-o444.

3.   (a) Wang, X.-S.; Zhao, H.; Qu, Z.-R.; Ye, Q.; Zhang, J.; Xiong, R.-G.; You, X.-Z.; Fun, H.-K., *Inorg. Chem.* **2003,** *42* (19), 5786-5788; (b) Evans, O. R.; Lin, W., *Chem. Mater.* **2001,** *13* (8), 2705-2712; (c) Evans, O. R.; Xiong, R.-G.; Wang, Z.; Wong, G. K.; Lin, W., *Angew. Chem. Int. Ed.* **1999,** *38* (4), 536-538; (d) Zhu, Y.-J.; Chen, J.-X.; Zhang, W.-H.; Ren, Z.-G.; Zhang, Y.; Lang, J.-P.; Ng, S.-W., *J. Organomet. Chem.* **2005,** *690* (14), 3479-3487.

4.   (a) Sekiya, R.; Nishikiori, S.-i., *Chem. Commun.* **2001,** (24), 2612-2613; (b) Sekiya, R.; Nishikiori, S.-i., *Chem. Eur. J.* **2002,** *8* (20), 4803-4810.

5.   Zhu, Y.-J.; Ren, Z.-G.; Zhang, W.-H.; Chen, Y.; Li, H.-X.; Zhang, Y.; Lang, J.-P., *Inorg. Chem. Commun.* **2007,** *10* (4), 485-488.

6.   (a) Yamada, S.; Nojiri, Y.; Sugawara, M., *Tetrahedron Lett.* **2010,** *51* (18), 2533-2535; (b) Yamada, S.; Tokugawa, Y., *J. Am. Chem. Soc.* **2009,** *131* (6), 2098-2099; (c) Yamada, S.; Uematsu, N.; Yamashita, K., *J. Am. Chem. Soc.* **2007,** *129* (40), 12100-12101.

7.   (a) Natarajan, A.; Mague, J. T.; Venkatesan, K.; Ramamurthy, V., *Org. Lett.* **2005,** *7* (10), 1895-1898; (b) Harada, J.; Ogawa, K., *J. Am. Chem. Soc.* **2001,** *123* (44), 10884-10888; (c) Harada, J.; Ogawa, K., *Chem. Soc. Rev.* **2009,** *38* (8), 2244; (d) Peedikakkal, A. M. P.; Vittal, J. J., *Chem. Eur. J.* **2008,** *14* (17), 5329-5334; (e) Ohba, S.; Hosomi, H.; Ito, Y., *J. Am. Chem. Soc.* **2001,** *123* (26), 6349-6352.

8.   Nagarathinam, M.; Vittal, J. J., *Angew. Chem. Int. Ed.* **2006,** *45* (26), 4337-4341.

9.   (a) Hewitt, I. J.; Tang, J.; Madhu, N. T.; Anson, C. E.; Lan, Y.; Luzon, J.; Etienne, M.; Sessoli, R.; Powell, A. K., *Angew. Chem. Int. Ed.* **2010,** *49* (36), 6352-

Chapter 3

....

6356; (b) Tong, Y.-Z.; Wang, Q.-L.; Yang, G.; Yang, G.-M.; Yan, S.-P.; Liao, D.-Z.; Cheng, P., *CrystEngComm* **2010,** *12* (2), 543-548; (c) Zucchi, G.; Thuery, P.; Riviere, E.; Ephritikhine, M., *Chem. Commun.* **2010,** *46* (48), 9143-9145; (d) Aronica, C.; Chastanet, G.; Pilet, G.; Le Guennic, B.; Robert, V.; Wernsdorfer, W.; Luneau, D., *Inorg. Chem.* **2007,** *46* (15), 6108-6119.

10.   (a) Hines, C. C.; Cordes, D. B.; Griffin, S. T.; Watts, S. I.; Cocalia, V. A.; Rogers, R. D., *New J. Chem.* **2008,** *32* (5), 872-877; (b) Li, C.-Y.; Liu, C.-S.; Li, J.-R.; Bu, X.-H., *Cryst. Growth Des.* **2006,** *7* (2), 286-295; (c) Wei, M.; Willett, R. D., *Inorg. Chem.* **1996,** *35* (22), 6381-6385.

11.   (a) Bonnot, C. M.; Chambron, J.-C.; Espinosa, E.; Bernauer, K.; Scholten, U.; Graff, R., *J. Org. Chem.* **2008,** *73* (20), 7871-7881; (b) Kamiński, D. M.; Hoser, A. A.; Gagoś, M.; Matwijczuk, A.; Arczewska, M.; Niewiadomy, A.; Woźniak, K., *Cryst. Growth Des.* **2010,** *10* (8), 3480-3488; (c) Ostermeier, M.; Limberg, C.; Ziemer, B.; Karunakaran, V., *Angew. Chem. Int. Ed.* **2007,** *46* (28), 5329-5331; (d) Verdan, S.; Melich, X.; Bernardinelli, G.; Williams, A. F., *CrystEngComm* **2009,** *11* (7), 1416-1426.

12.   (a) Au-Yeung, H. Y.; Pengo, P.; Pantos, G. D.; Otto, S.; Sanders, J. K. M., *Chem. Commun.* **2009,**   (4), 419-421; (b) Delval, F.; Spyratou, A.; Verdan, S.; Bernardinelli, G.; Williams, A. F., *New J. Chem.* **2008,** *32* (8), 1394-1402; (c) Köhler, T.; Seidel, D.; Lynch, V.; Arp, F. O.; Ou, Z.; Kadish, K. M.; Sessler, J. L., *J. Am. Chem. Soc.* **2003,** *125* (23), 6872-6873.

13.   Schmidt, G. M. J., *Pure Appl. Chem.* **1971,** *27* (4), 647-678.

14.   Yamada, S., *Org. Biomol. Chem.* **2007,** *5* (18), 2903-2912.

15.   Horner, M.; Hünig, S., *J. Am. Chem. Soc.* **1977,** *99* (18), 6122-6124.

16.   (a) Peedikakkal, A. M. P.; Koh, L. L.; Vittal, J. J., *Chem. Commun.* **2008,** (4), 441-443; (b) Peedikakkal, A. M. P.; Peh, C. S. Y.; Koh, L. L.; Vittal, J. J., *Inorg. Chem.* **2010,** *49* (15), 6775-6777.

17.   Toh, N. L.; Nagarathinam, M.; Vittal, J. J., *Angew. Chem. Int. Ed.* **2005,** *44* (15), 2237-2241.

Chapter 4

Solid State Photodimerization of Molecular Salts of 4-trans-2-(pyrid-4-yl-vynyl) benzoic acid (HPVBA)[*]
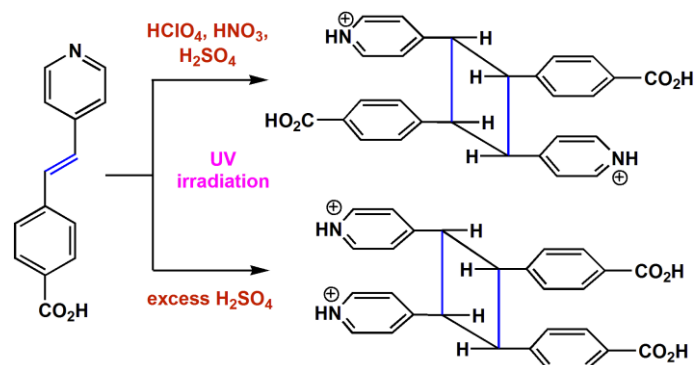
4.1 Introduction

In Chapter 2 and 3, a series of molecular salts of H_2SDC, 3-PAH and 4-PAH and their solid-state photodimerization reactions have been discussed. We have seen that the anions play crucial roles in the packing of 3-PAH_2^+ and 4-PAH_2^+ and which dictated the structures of the photo-dimers. This chapter is meant to extend a similar study on the influence of anions in the packing of HPVBA cations in various types of salts. HPVBA molecules were extensively studied in the past for the chiral recognition on various surfaces like Ag(111), Pd(111) etc.[1] There are only a few reports for coordination polymers using this ligand[2] and there is no report on the crystal engineering studies for photodimerization reaction in the solid state. Only diamondoid coordination polymers with 8-fold interpenetrated nets exhibiting NLO properties[2a, 2b] and guest exchangeable 7-fold interpenetrated nets[2c] have been reported with HPVBA.

This ligand has been chosen for photodimerization study to allocate hetero-functionality to the cyclobutane ring and to understand the anion effect on the packing of H_2PVBA^+ ions in the solid state. In this chapter, various molecular salts of HPVBA will be synthesized and discussed in the context of their solid state packing and photoreactivity. The cyclobutane derived ligands will be synthesized by controlling the packing of H_2PVBA^+ in the soild state with desired functionality and will be used for making various co-crystal and coordination polymers, which is the content of Chapter 7.

4.2 Results and Discussion

4.2.1 General Synthetic Procedure

HPVBA was allowed to react with various strong acids and amines. All the molecular salts were synthesized from aqueous media and the diffraction quality

....

single crystals were grown by slowly evaporating their alcoholic solutions. The yields

of these crystallization processes vary in the ranges of 90 – 95%.

4.2.2 Crystal Structure and Photoreactivity of Molecular Salts Containing HPVBA

4.2.2.1 Trifluoroacetate Salt of HPVBA (23)

Like 4-PAH, HPVBA was also reacted with CF_3CO_2H and the resulting salt

was characterized and tested for its photoreactivity. The single crystals of anhydrous

salt of composition $(H_2PVBA)(CF_3CO_2)$ or $C_{16}H_{12}F_3NO_4$ (**23**) were grown by

evaporating methanolic solution slowly and the structure was refined in triclinic space

group, $P\bar{1}$. As expected, the pyridyl group of HPVBA was found protonated. Various

kinds of charge assisted hydrogen bonding like N-H$\cdots$O, O-H$\cdots$O, C-H$\cdots$O play an

important role to construct the solid-state structure as shown in Figure 4.1. The

hydrogen bonding parameters are listed in Table 4.1. One oxygen atoms of the TFA

anions form N-H$\cdots$O hydrogen bonds to a PVBAH$^+$ cation and another oxygen form

O-H$\cdots$O hydrogen bonds to another H_2PVBA^+ cation and therefore, clipping them in

parallel orientation in *head-to-tail* fashion. The distance between the C=C bonds is

found to be 4.235 Å (Figure 4.2) and the salt was found photostable under UV light

although the distance is almost at the borderline of Schmidt's distance criteria.
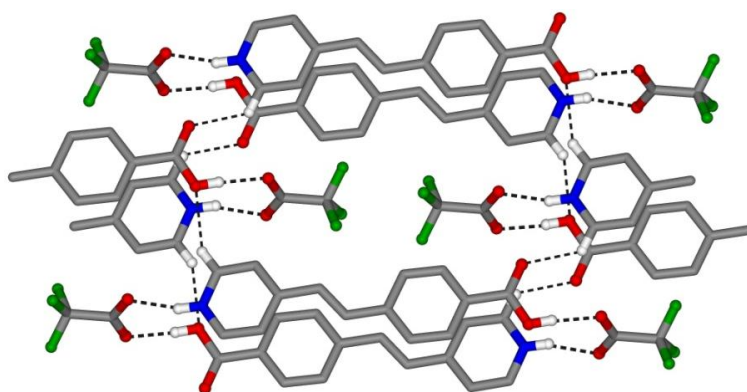
Figure 4.1 Various kinds of supramolecular interactions in **23**.
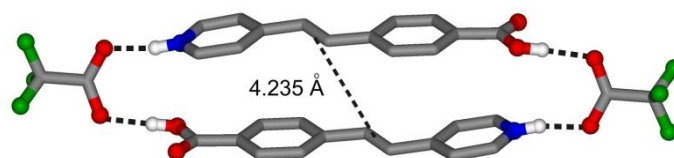
Figure 4.2 The *head-to-tail* parallel orientation of H_2PVBA^+ clipped by TFA anions.

Table 4.1 The hydrogen bonding parameters for **23**

D-H⋯A	D(D-H) (Å)	D(H⋯A) (Å)	D(D⋯A) (Å)	<(DHA) (°)	Symmetry Operator
O(1)-H(1O)⋯O(4)	0.84	1.79	2.633(2)	175(3)	x, y, z-1
N(1)-H(1N)⋯O(3)	0.87	1.86	2.701(2)	163(3)	-x, -y+1, -z+1
C(10)-H(10)⋯O(1)	0.95	2.39	3.245(3)	148	-1+x, y, 1+z
C(14)-H(14)⋯O(2)	0.95	2.28	3.000(3)	132	x, -1+y, 1+z
C(13)-H(13)⋯F(1)	0.95	2.42	3.307(3)	155	x, -1+y, z
C(14)-H(14)⋯O(4)	0.95	2.57	3.339(3)	138	x,-1+y, z

4.2.2.2 Perchlorate Salt of HPVBA (24)

HPVBA was reacted with $HClO_4$ and the resulting molecular salt was studied for its photoreactivity. Single crystal X-ray analysis revealed that the salt of composition $(H_2PVBA)ClO_4 \cdot MeOH$ or $C_{15}H_{15}ClNO_7$ (**24**) crystallizes in the triclinic space group, $P\bar{1}$. Various types of hydrogen bonding interactions including O-H⋯O, N-H⋯O, C-H⋯O play crucial role to construct the solid state structure. The geometric parameters for these hydrogen bondings are listed in Table 4.2. The pyridinium cations form charge assisted hydrogen bonding with one ClO_4^- anion in $\mathbf{R}_2^2(7)$ fashion and interact with another ClO_4^- ion in $\mathbf{C}(2)$ fashion via weak C(α)-H bonds. The carboxylic acid groups involve in hydrogen bonding with methanol molecules present in the crystal in $\mathbf{R}_4^4(12)$ fashion to form carboxylic acid dimer synthon (via methanol). A thorough perusal of the crystal structure reveals that the H_2PVBA^+ cations are aligned parallel in *head-to-tail* fashion with a distance of 3.837 Å between two C=C bonds (Figure 4.3). Upon irradiation under UV light for 40 h,

....

this salt was found to furnish only 80% photodimerization as monitored by ^{1}H NMR spectroscopy from the appearance of a singlet for cyclobutane protons at δ 5.01 ppm. The incomplete conversion might be due to the loss of MeOH solvent molecules during the process of dimerization. When the salt of the dimer compound was neutralised with aqueous NaOH, the peak for cyclobutane protons shifts at δ 4.69 (m) ppm but two quartet (doublet of doublet) peaks were not observed as they have been generally observed for *rctt*-HT-3,3-BPCD and *rctt*-HT-4,4-BPCD. This may be due to the fact that the cyclobutane protons with 4-pyridyl and 4-carboxyphenyl substituent are almost degenerate (Figure 4.4). The photoreactivity of this salt can be employed to synthesize a new cyclobutane derived ligand *viz. rctt*-1,3-Bis(4'-carboxyphenyl)-2,4-bis(4"-pyridyl)cyclobutane or *rctt*-HT-4,4-BCBPCB.
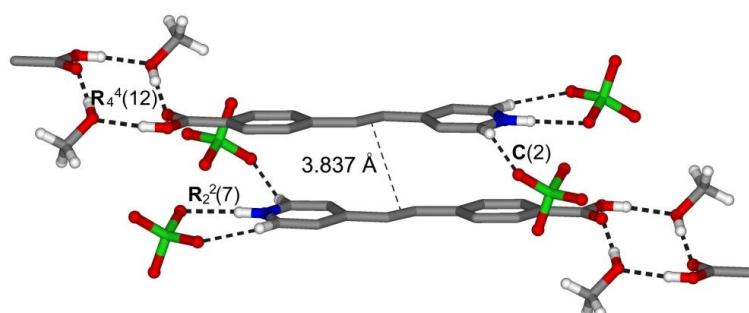
Figure 4.3 The *head-to-tail* parallel arrangement of H_2PVBA^+ cations in **24**.

Table 4.2 The hydrogen bonding parameters for **24**

D-H···A	D(D-H) (Å)	D(H···A) (Å)	D(D···A) (Å)	<(DHA) (°)	Symmetry Operator
N(1)-H(1A)···O(3)	0.87	2.16	2.935(7)	149	x, y-1, z
N(1A)-H(1AB)···Cl(1)	0.87	2.88	3.70(2)	159	x, y-1, z
O(1)-H(1)···O(1S)	0.83	1.75	2.574(4)	172	-x+1, -y+2, -z+1
O(1S)-H(1S)···O(2)	0.80	1.98	2.771(4)	173(5)	x+1, y, z-1
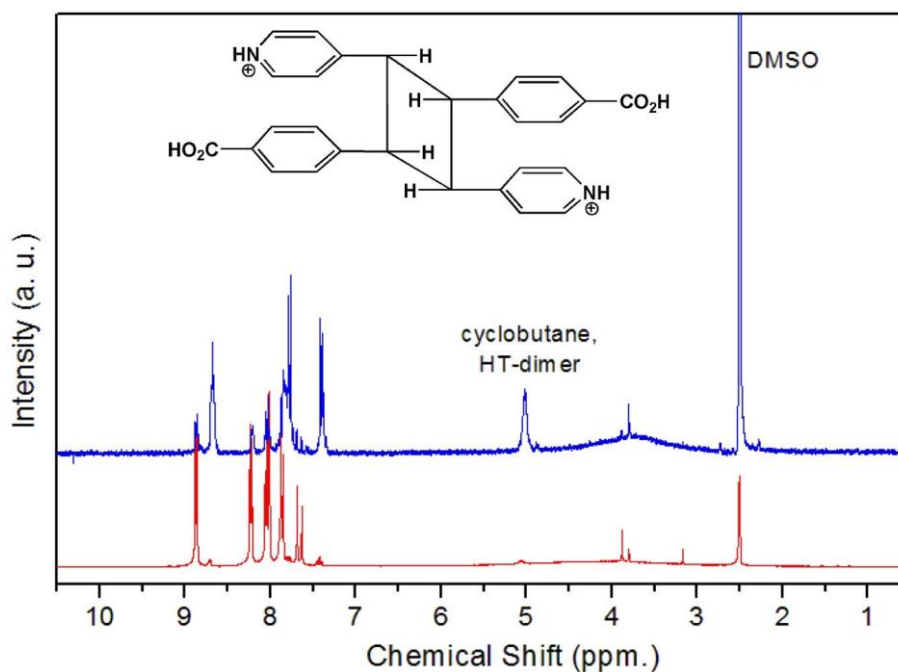
Figure 4.4 ^{1}H NMR spectra of **24** before and after UV irradiation

Another interesting point to note is that methanol molecules present in the structure have significant role on the packing of H_2PVBA^+ cations. The same salt when crystallized from ethanol and 1,4-dioxane separately, both were found not to undergo any photodimerization. The single crystal obtained from ethanol was too small for X-ray data collection. Due to the rapid loss of 1,4-dioxane from single crystals when taken out of the mother liquor also prevented us from determining its structure. However, both of their compositions were determined by elemental analysis and TGA to be $C_{14}H_{12}ClNO_6$ (**25**) (as 1,4-dioxane is lost from the system). The photostability of this anhydrous salt (obtained from ethanol) and the photoreactivity of the solvated salt (containing methanol) clearly indicate the role of methanol in the parallel arrangement of H_2PVBA^+ cations. Therefore, the partial conversion (80%) can be accounted to the loss of MeOH solvent from the single crystals during the process of photodimerization.

4.2.2.3 Sulphate-bisulphate Salt of HPVBA (26)

HPVBA was also reacted with H_2SO_4 in methanol and the single crystals obtained were tested for their photoreactivity. The hydrated salt of composition $(H_2PVBA)_4(HSO_4)_2(SO_4) \cdot H_2O$ or $C_{56}H_{52}N_4O_{21}S_3$ (26) crystallizes in the triclinic space group, $P\bar{1}$. The asymmetric unit contains one formula unit namely, four H_2PVBA^+ cations, two bisulphate anion, one sulphate bianion and one water molecule. As expected, various types of normal and charge assisted hydrogen bonding (see Table 4.3) like N-H⋯⋯O, O-H⋯O are present in the solid-state structure as shown in Figure 4.5. The carboxylic acid groups of H_2PVBA^+ cations form carboxylic acid dimer homosynthon ($\mathbf{R}_2^2(8)$). The water molecule present in this salt also donates hydrogen bonding to sulphate, bisulphate anions and accepts from the protonated pyridyl group (H-N) of H_2PVBA^+ cation and form a H-bonded ring with graph set $\mathbf{R}_6^4(16)$. The C(α)-H of H_2PVBA^+ cations also interact with the neighbouring sulphate / bisulphate anions which is not shown in the Figure 4.5 for clarity.
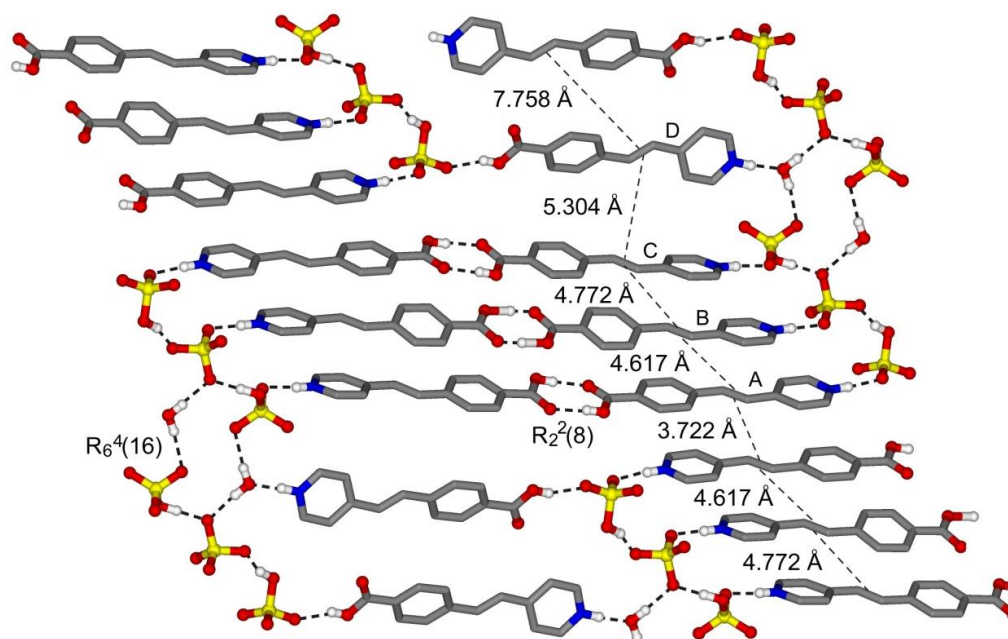
Figure 4.5 The crystal structure of sulphate-bisulphate salt of HPVBA, **26**

Now if we look into the relative orientations of H_2PVBA^+ cations, the combination of both the *head-to-head* and *head-to-tail* manner are observed. All the four H_2PVBA^+ cations in the asymmetric unit, labelled as **A - D** in the Figure 4.5, are oriented in HH-fashion with distances between C=C bonds of 4.617, 4.772 and 5.304 Å. All these distances are not favourable for photodimerization reaction. However, when we analyze the relative orientations of H_2PVBA^+ units which are related by a centre of inversion, we see that they are (labelled as **A**) orientated parallel in HT-fashion. The distance between C=C bonds is 3.772 Å which is well within the range of Schmidt criteria. Therefore, among the four H_2PVBA^+ cations in the asymmetric unit one is photoreactive and the compound is supposed to show 25% photodimerization reaction in HT-fashion. When this compound was irradiated under UV light for 50 h, we observed only about 25% photodimerization in ^1H NMR spectroscopy leading to the formation of HT-BCBPCB (Figure 4.6).
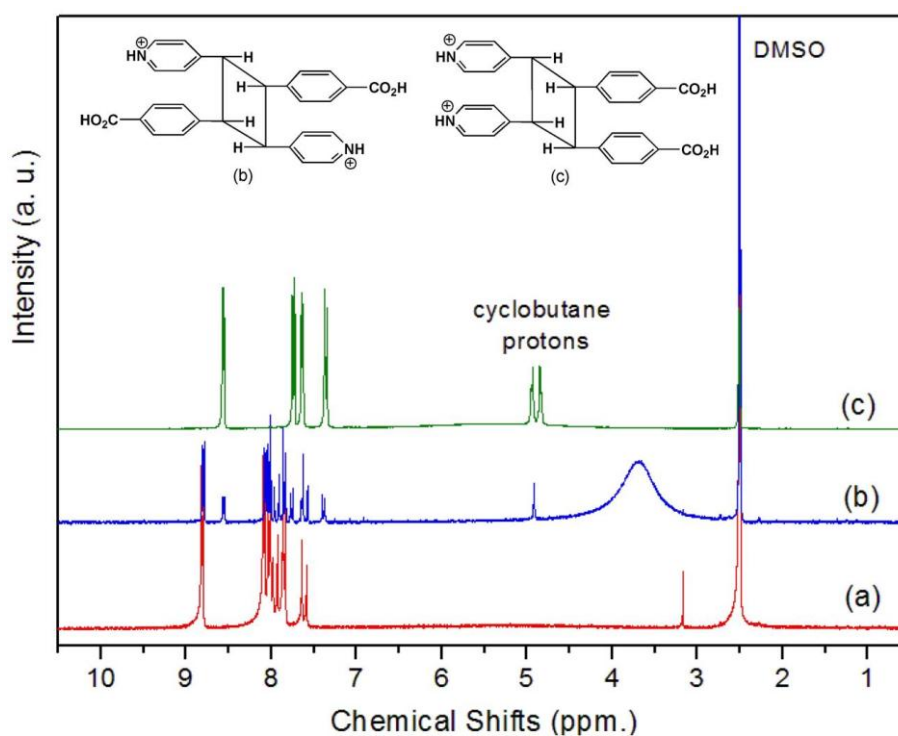
Figure 4.6 ^1H NMR spectra of **26** before (a) and after UV irradiation (b); (c) for **27** after UV irradiation and recrystallization

....

Table 4.3 The hydrogen bonding parameters for **26**

D-H···A	D(D-H) (Å)	D(H···A) (Å)	D(D···A) (Å)	<(DHA) (°)	Symmetry Operator
O1W-H1WB···O18	0.84	1.87	2.715(3)	173(4)	-x+1, -y+1, -z+1
O1W-H1WA···O12	0.85	1.95	2.783(3)	167(3)	x-1, y-1, z
O14-H14O···O20	0.87	1.69	2.524(3)	159(4)	
O9-H9O···O18	0.94	1.57	2.507(3)	176(4)	x, y, z+1
N4-H4N···O15	0.90	1.81	2.705(3)	175(3)	-x+1, -y+1, -z
N3-H3N···O19	0.90	1.75	2.658(3)	176(3)	-x+1, -y+1, -z
N2-H2N···O1W	0.91	1.72	2.631(3)	175(3)	x, y+1, z
N1-H1N···O11	0.90	1.81	2.709(3)	179(3)	-x+2, -y+1, -z+1
O7-H7···O2	0.83	1.81	2.642(3)	176	-x+1, -y+2, -z+1
O6-H6O···O5	1.26	1.35	2.613(3)	176(5)	-x, -y+2, -z+1
O3-H3···O16	0.83	1.82	2.595(3)	155	
O1-H1···O8	0.83	1.82	2.647(3)	176	-x+1, -y+2, -z+1
C11-H11···O3	0.94	2.57	3.448(4)	154	1+x, y, z
C12-H12···O15	0.94	2.42	3.279(4)	151	1+x, y, z
C13-H13···O17	0.94	2.39	3.083(4)	131	
C14-H14···O13	0.94	2.54	3.365(4)	147	
C18-H18···O16	0.94	2.40	3.325(4)	167	1-x, 1-y, 1-z
C26-H26···O10	0.94	2.30	3.161(4)	151	-1+x, y, z
C27-H27···O20	0.94	2.30	3.204(4)	161	1-x, 2-y, 1-z
C28-H28···O4	0.94	2.53	3.401(4)	154	1-x, 2-y, 1-z
C40-H40···O19	0.94	2.42	3.308(4)	158	
C40-H40···O20	0.94	2.59	3.345(4)	138	
C53-H53···O1W	0.94	2.38	3.296(4)	165	1-x, 1-y, 1-z
C54-H54···O11	0.94	2.31	3.205(4)	160	x, y, -1+z
C56-H56···O10	0.94	2.28	3.192(4)	163	-1+x, y, -1+z

When HPVBA was reacted with excess of H_2SO_4 in water, an intense yellow coloured solid was obtained (**27**). Surprisingly, this yellow solid furnished 80% photodimerization in *head-to-head* fashion upon irradiation under UV light for 50 h which was confirmed by ^{1}H NMR spectroscopy (Figure 4.6). The formation of HH-

dimer 1,2-bis(4'-carboxyphenyl)-3,4-bis(4''-pyridyl)cyclobutane or *rctt*-HH-4,4-BCBPCB was confirmed by the presence of two doublet peaks at δ 4.93 and 4.83 ppm which can be correlated with the ^{1}H NMR spectrum of *rctt*-HH-4,4-BPCD discussed in Chapter 3. When this UV irradiated product was neutralised with NaOH (aq.), these two doublet peaks coalesce to a single doublet peak at δ 4.68 ppm. The composition of this precipitated yellow powder was determined by TGA and elemental analysis as $(H_2PVBA)_3(HSO_4)_3(H_2SO_4)(H_2O)_{6.5}$ or $C_{42}H_{54}N_3O_{28.5}S_4$ (see section 4.8 for details). Therefore, the amount of H_2SO_4 added during salt formation is very crucial and that lead to a different packing of H_2PVBA^+ cations and entirely opposite photoreactivity. The role of extra H_2SO_4 in the packing of H_2PVBA^+ cations is not clearly understood due to the lack of single crystal structure. To the best of my knowledge, this type of inverse photoreactivity just by changing the concentration of salt former was not known before.

4.2.3 Photoreactivity of salts of HPVBA with HNO$_3$ and HCl

HPVBA was also reacted with HNO$_3$ and HCl and the resulting yellow crystalline samples were studied for their photoreactivity. We could not grow diffraction quality single crystals for both but the composition of these salts were determined by elemental analysis and TGA. An anhydrous salt of composition $(H_2PVBA)NO_3$ or $C_{14}H_{12}N_2O_5$ (**28**) was synthesized with HNO$_3$ which underwent quantitative photodimerization upon irradiation under UV light for 30 h. The absence of peaks for ethylenic protons and the presence of a singlet peak for cyclobutane protons at δ 5.04 ppm in ^{1}H NMR spectrum confirm the formation of HT-dimer in quantitative yield (Figure 4.7). On the other hand, the anhydrous salt obtained by reacting with HPVBA and HCl in methanol was found to be photostable.
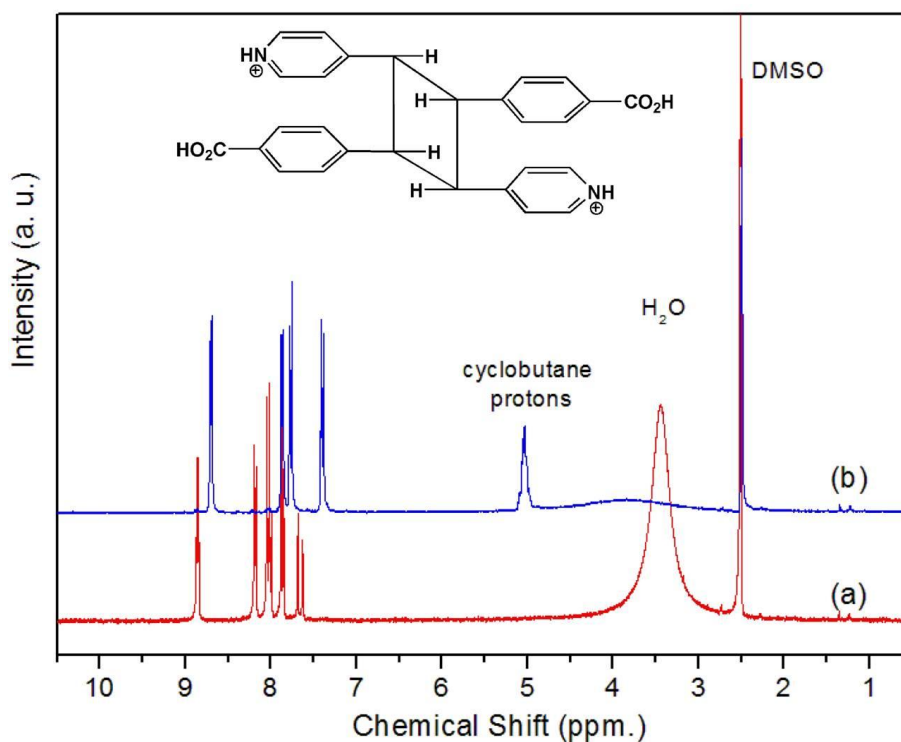
Figure 4.7 ^{1}H NMR spectra of **28** before (a) and after (b) UV irradiation show quantitative conversion

4.2.4 Photoreactivity of Salts of HPVBA with 1,4-Diaminobutane

In Chapter 2, the photoreactivity of H_2SDC have been discussed as its salts with various diamines like ethylenediamine, 1,3-diaminopropane, 1,4-diaminobutane (DAB) etc. The utilisation of $-CO_2H$ groups in various photoreactive olefins for making molecular salts and their photoreactivity is also reported in literature.[3] Here, we attempted to exploit the carboxylic acid functionality of HPVBA by deprotonating the acidic proton by ethylenediamine, 1,3-diaminopropane, 1,4-diaminobutane. The flaky crystals obtained from these three diamines were studied for their photoreactivity and we found only the salt with 1,4-diaminobutane (**29**) underwent about 75% photodimerization in HT-fashion after UV irradiation for 40 h.

Ethylenediamine is known to template *trans*-cinnamic acid analogues that undergo photodimerization.[3b] We also have discussed in Chapter 2 that 1,3-diaminopropane can template H_2SDC for the same purpose but not ethylenediamine

116

....

or 1,4-diaminobutane. Here, we observe that for HPVBA, 1,4-diaminobutane exhibit templating effect and not the other two amines in the series. These observations clearly indicate that there is definitely some correlation of crystal packing with the chain length of diamines and olefinic spacers. To our disappointment, all the crystals isolated were flaky and not suitable for X-ray diffraction.

4.3 Isomerisation of HH-BCBPCB and HT-BCBPCB

The acid catalysed isomerisation of *rctt*-HH-4,4-BPCD, *rctt*-HT-4,4-BPCD to their corresponding *rctc*-isomers have been discussed in Chapter 3. The isomerisation of *rctt*-4,4-tpcb was also reported from our laboratory before.[4] The above two cyclobutane compounds were also observed to undergo similar isomerisation from *rctt*- to *rctc*- isomers under acidic pH, which was observed to be faster upon heating. The ^{1}H NMR spectra confirming the isomerisation for HH-dimer is shown in Figure 4.8 and the structures of the corresponding *rctc*-isomers are shown in Scheme 4.1. Two doublet peaks for cyclobutane protons for *rctt*-HH-4,4-BCBPCB converts to four triplet peaks upon heating which indicate that the degeneracy of the cyclobutane protons is lifted due to isomerisation to *rctc*-isomer (symmetry reduced). We also observed that the isomerisation is not quantitative because the product *rctc*-isomer is less stable than *rctt*-isomers as three substituents are on the same side of the cyclobutane ring resulting steric hindrance. The *rctt*-HT-4,4-BCBPCB also undergoes similar isomerisation under similar condition and the mechanistic details of such isomerisation is discussed in Chapter 3.
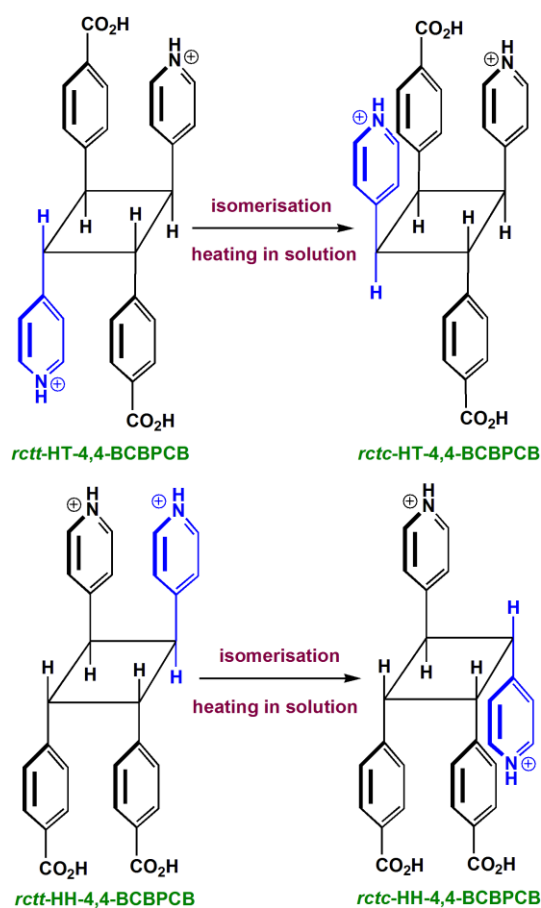
Scheme 4.1 The structures of the *rctc-* isomers of HT and HH-4,4-BCBPCB after isomerisation
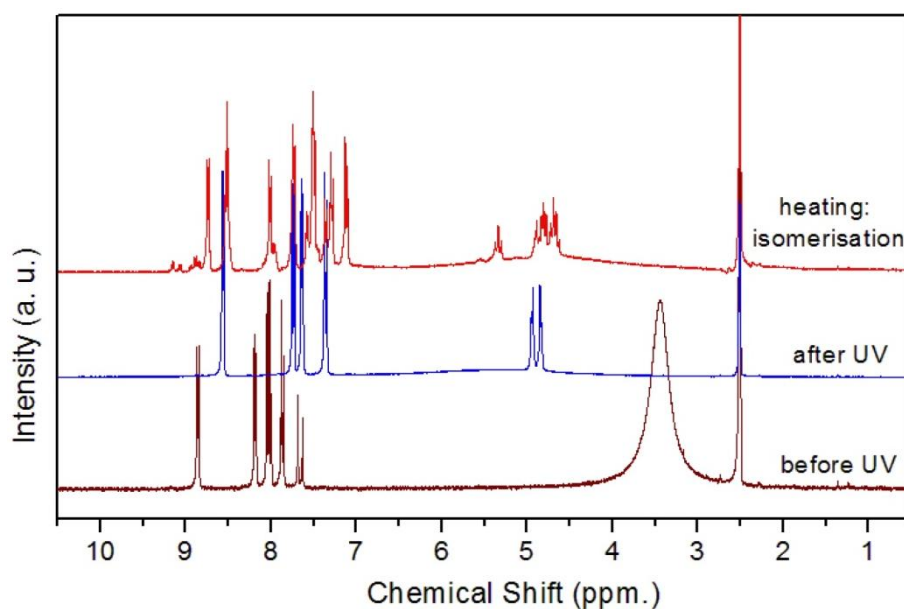
Figure 4.8 ^{1}H NMR spectra show the isomerisation of *rctt*-HH-4,4-BCBPCB (a) to corresponding *rctc*-isomer (b). Refer to the above scheme for structures.

4.4 Comparative Discussion of Salts of 4-PAH and HPVBA

Now, if we consider two olefins 4-PAH and HPVBA, it is evident that both are very similar in terms of their shapes and functionalities. The only diference arises from their lengths, HPVBA being a longer olefin having an extra phenyl ring in between C=C double bond and the carboxylic acid group. As the dimensions of molecules are very important in the crystal packing, we also can observe some differences in crystal packing of their salts. For example, the anhydrous $CF_3CO_2^-$ salt of 4-PAH crystallizes in orthorhombic space group, $Pca2_1$, where both the cation and anion form two dimenstional sheet like structure and 4-PAH$_2$+ cations from neighbouring sheets are stacked infinitely parallel in HT-fashion. On the other hand, in the case of HPVBA-salt which crystallizes in triclinic space group, $P\bar{1}$, the H_2PVBA^+ cations are clipped by $CF_3CO_2^-$ anions at both sides. The two carboxylate 'O's of $CF_3CO_2^-$ anions form hydrogen bonding to protonated pyridyl group of one H_2PVBA^+ cation and carboxylic acid group of another H_2PVBA^+ cation and in this way, it clips them in HT-fashion and as discrete pairs; unfortunately it was found to be photostable.

Again, if we compare their ClO_4^- salts, we find an anhydrous salt was obtained from 4-PAH; where as, a solvated (MeOH) salt was obtained for HPVBA. In both the salts, discrete parallel pairs of olefinic cations were found in HT-fashion. Although, hydrated salts contained sulphate and bisulphate anions were found for both, their alignments maintaining proper distances were different. The HH-dimer was obtained from sulphate-bisulphate salt of 4-PAH in 66% yield; where as in the case of HPVBA-salt, the HT-dimer was obtained in 25 % yield. The structures of the nitrate salts of both were not determined in absence of suitable single crystals. However, the diference in their photoreactivity, hence in structure, is noteworthy. The nitrate salt of 4-PAH was found photostable but the analogous salt of HPVBA was found to undergo quantitative photodimerization in HT-fashion. Therefore, it can be

assumed that H_2PVBA^+ cations in nitrate salts are aligned parallel in HT-fashion, however, the 4-PAH_2^+ cations are not. All these observations clearly indicate that the solid state packing always depends on dimensions (*e.g.* length) of molecular fragments, as was concluded in chapter 2.

4.5 Summary

In this chapter, we have discussed various salts of HPVBA that undergo photodimerization in the solid state. Although HPVBA was aligned parallel in the salt with CF_3CO_2H, it was found photostable. The anhydrous salt obtained with HNO_3 and the solvated (with methanol) salt obtained with $HClO_4$ were observed to furnish HT-photodimer in moderate yield. The presence of methanol solvents in perchlorate salt has been shown to have very crucial role for this salt to be photoreactive. The presence of excess H_2SO_4 during salt formation (or crystallization) has tremendous effect on the photoreactivity, as we have observed the inverse photoreaction due to the presence of extra H_2SO_4 molecule in the solid salt that altered the packing H_2PVBA^+ cations in **27**. It is also important to note that only the salt with excess H_2SO_4 led to the formation of HH-photodimer. The photoreactivity of PVBA-DABH salt and the photostability of ethylenediamine and DAP analogues indicate some correlation of crystal packing with the chain length of diamines, which was also discussed in Chapter 2. By extending the idea developed in the previous chapter, it is shown that the strategy of salt formation works well and might be a preferred method for making functional cyclobutane derived ligands with desired functionality.

4.5 Syntheses and Characterization

HPVBA was synthesized by modifying the literature reported method.[5] HPVBA was allowed to react with the strong acids and amines to form molecular salts. The diffraction quality single crystals were obtained by slowly evaporating the alcoholic solutions. The yields of these crystallization processes vary in the range of

Chapter 4

....

90 – 95 %. The single crystals or the powder samples were irradiated under UV light and their photoreactivity have been confirmed by ^{1}H NMR spectroscopy. All the salts were characterized by NMR, FT-IR spectroscopy, elemental analysis and thermogravimetric analysis.

$(H_2PVBA)(CF_3CO_2)$ (23)

^{1}H NMR (300 MHz, d_6-DMSO, 298K): δ_H 8.78 (d, 2H, Py-H), 8.05 (d, 2H, Ar-H), 8.01 (d, 2H, Py-H), 7.91 (d, 1H, CH=CH), 7.84 (d, 2H, Ar-H), 7.58 (d, 1H, CH=CH). FT-IR (KBr, cm^{-1}): 3340, 3091, 1686, 1624, 1499, 1385, 1292, 1182, 1142, 973, 852, 818, 717, 578, 534, 443. Analysis found (%): C 56.84, H 3.42, N 4.09; $C_{16}H_{12}F_3NO_4$ requires C 56.64, H 3.56, N 4.13. No solvent loss was observed in TGA experiment.

$(H_2PVBA)ClO_4 \cdot MeOH$ (24)

^{1}H NMR (300 MHz, d_6-DMSO, 298K): δ_H 8.86 (d, 2H, Py-H), 8.21 (d, 2H, Ar-H), 8.06 – 8.0 (m, 3H, CH=CH and Py-H), 7.84 (d, 2H, Ar-H), 7.65 (d, 1H, CH=CH). FT-IR (KBr, cm^{-1}): 3408, 3215, 2780, 2623, 1709, 1621, 1501, 1419, 1379, 1286, 1113, 963, 844, 803, 720, 690, 625, 533, 460. Analysis found (%): C 51.95, H 3.84, N 4.08; $C_{14}H_{11}ClNO_6$ (excluding MeOH from formula unit) requires C 51.79, H 3.41, N 4.31. A little discrepancy in H and N may be due to incomplete loss of MeOH.

After UV irradiation for 40 h, ^{1}H NMR (300 MHz, d_6-DMSO, 298K): δ_H 8.68 (d, 4H, Py-H), 7.91 (d, 4H, Ar-H), 7.80 (d, 4-H, Py-H), 7.39 (d, 4H, Ar-H), 5.01 (m, 4H, CH-CH). ^{1}H NMR (300 MHz, d_6-DMSO, 298K) of HT-4,4-BCBPCB (after neutralisation): δ_H 12.82 (s, 2H, CO$_2$H), 8.32 (d, 4H, Py-H), 7.78 (d, 4H, Ar-H), 7.35 (d, 4H, Ar-H), 7.21 (d, 4H, Py-H), 4.69 (m, 4H, CH-CH). ^{13}C-NMR (75 MHz, d_6-DMSO, 298K) of $rctt$-HT-4,4-BCBPCB: δ_C 167.19, 149.11, 148.78, 144.63, 129.11, 128.8, 128.2, 123.44, 45.43, 45.25.

....

(H$_2$PVBA)$_4$(HSO$_4$)(SO$_4$)·H$_2$O (26)

^{1}H NMR (300 MHz, d_6-DMSO, 298K): δ_H 7.79 (d, 2H, Py-H), 8.07 (d, 2H, Ar-H), 8.01 (d, 2H, Ar-H), 7.94 (d, 1H, CH=CH), 7.79 (d, 2H, Py-H), 7.60 9d, 1H, CH=CH). FT-IR (KBr, cm^{-1}): 3340, 3126, 2919, 1705, 1622, 1502, 1415, 1383, 1341, 1223, 1190, 1150, 1107, 968, 845, 896, 718, 592, 530, 454. Analysis found (%): C 54.97, H 4.60, N 4.47; C$_{56}$H$_{52}$N$_4$O$_{21}$S$_3$ requires C 55.44, H 4.32, N 4.62.

The representative peaks for photodimerization after UV irradiation for 50 h, ^{1}H NMR (300 MHz, d_6-DMSO, 298K): δ_H 8.56 (d, 4H, Py-H), 7.76 (d, 4H, Ar-H), 7.63 (d, 4H, Py-H), 7.39 (d, 4H, Ar-H), 4.91 (s, 4H, CH-CH).

(H$_2$PVBA)$_3$(HSO$_4$)$_3$(H$_2$SO$_4$)(H$_2$O)$_{6.5}$ (27)

FT-IR (KBr, cm^{-1}): 3340, 3180, 3126, 2919, 2590, 2461, 1933, 1705, 1622, 1502, 1415, 1383, 1341, 1223, 1190, 1150, 1107, 968, 845, 796, 718, 598, 530, 454. Analysis found (%): C 42.67, H 4.13, N 3.41; C$_{42}$H$_{54}$N$_3$O$_{28.5}$S$_4$ requires C 42.56, H 4.59, N 3.55. This composition is supported by the observed water loss in TGA experiment. The observed water loss 9.7% is well agreement with the calculated value 9.8% for the proposed formula.

After irradiation under UV light 50 h, it was dissolved in water (monomer salt is weakly soluble in water) and then was dried. ^{1}H NMR (300 MHz, d_6-DMSO, 298K): δ_H 8.55 (d, 4H, Py-H), 8.06 (d, 4H, Ar-H), 7.73 (d, 4H, Py-H), 7.35 (d, 4H, Ar-H), 4.93 (d, 2H, CH-CH), 4.83 (d, 2H, CH-CH). Two doublet peaks for cyclobutane protons indicate the formation of HH-photodimer. After neutralization, ^{1}H NMR (300 MHz, d_6-DMSO, 298K): δ_H 12.78 (s, CO$_2$H), 8.33 (d, 4H, Py-H), 7.71 (d, 4H, Ar-H), 7.32 (d, 4H, Py-H), 7.23 (d, 4H, Ar-H), 4.68 (d, 4H, CH-CH). ^{13}C-NMR (75 MHz, d_6-DMSO, 298K): δ_C 167.2, 149.2, 148.2, 144.83, 129.04, 128.72, 128.22, 123.44, 45.47, 45.24.

Chapter 4

....

(H₂PVBA)NO₃ (28)

^{1}H NMR (300 MHz, d_6-DMSO, 298K): δ_H 8.86 (d, 2H, Py-H), 8.20 (d, 2H, Ar-H), 8.06 – 8.01 (m, 1H, CH=CH and 2H, Py-H), 7.86 (d, 2H, Ar-H), 7.66 (d, 1H, CH=CH). After UV irradiation for 30 h, ^{1}H NMR (300 MHz, d_6-DMSO, 298K): δ_H 8.70 (d, 4H, Py-H), 7.87 (d, 4H, Ar-H), 7.76 (d, 4H, py-H), 7.40 (d, 4H, Ar-H), 5.04 (m, 4-H, CH-CH). Analysis found (%): C 58.01, H 4.14, N 9.36; $C_{14}H_{12}N_2O_5$ requires C 58.33, H 4.20, N 9.72. There was no solvent loss in TGA experiment.

(DABH)(PVBA) salt (29)

^{1}H NMR (300 MHz, d_6-DMSO, 298K): δ_H 8.54 (d, 2H, Py-H), 7.86 (d, 2H, Ar-H), 7.58 – 7.52 (m, 5H, Ar-H, Py-H, CH-CH), 7.25 (d, 1H, CH-CH), 2.62 and 1.42 (m, CH₂, DAB). The representative peaks for HT-dimer after irradiation under UV light for 40 h, ^{1}H NMR (300 MHz, d_6-DMSO, 298K): δ_H 8.33 – 8.28 (m, 8H, Py-H, Ar-H), 7.22 – 7.12 (m, 8H, Py-H, Ar-H), 4.60 (s, 4H, CH-CH).

....

Table 4.4 Crystallographic data for compounds **23**, **24** and **26**

Compounds	23	24	26
Formula	$C_{16}H_{12}F_3NO_4$	$C_{15}H_{15}ClNO_7$	$C_{56}H_{52}N_4O_{21}S_3$
M	339.27	356.73	1213.20
T (K)	100(2)	223(2)	223(2)
λ (Å)	0.71073	0.71073	0.71073 Å
Cryst syst / Space group	Triclinic / $P\bar{1}$	Triclinic / $P\bar{1}$	Triclinic / $P\bar{1}$
a (Å)	7.2580(9)	8.6037(11)	11.1151(9)
b (Å)	8.4271(10)	9.5432(12)	11.8964(9)
c (Å)	12.6094(15)	10.2702(13)	22.1546(18)
α (°)	77.860(2)	93.248(2)	91.414(2)
β (°)	75.529(2)	101.615(2)	98.911(2)
γ (°)	72.829(3)	107.129(2)	110.246(2)
Volume (Å^3) / Z	705.67(15) / 2	783.27(17) / 2	2705.6(4) / 2
D_{calcd} (g/cm^3) / μ (mm^{-1})	1.597 / 0.140	1.513 / 0.283	1.489 / 0.224
Reflns col. / Ind. Reflns.	9191 / 3233	10107 / 3589	35723 / 12429
R_{int} / Goof on F^2	0.0299 / 1.091	0.0357 / 1.096	0.0613 / 1.035
Final R[I>2σ]^a R$_1$ / wR2	0.0578 / 0.1395	0.0718 / 0.2017	0.0652 / 0.1352

^{a} R1 = $\Sigma||F_o| - |F_c||/ \Sigma|F_o|$, ^{b} wR2 = $[\Sigma w(F_o^2 - F_c^2)^2/\Sigma w(F_o^2)^2]^{1/2}$

4.6 References

1.   (a) Cai, C.; Bösch, M. M.; Müller, B.; Tao, Y.; Kündig, A.; Bosshard, C.; Gan, Z.; Biaggio, I.; Liakatas, I.; Jäger, M.; Schwer, H.; Günter, P., *Adv. Mater.* **1999,** *11* (9), 745-749; (b) Kim, B.-I.; Cai, C.; Deng, X.; Perry, S. S., *Surf. Sci.* **2003,** *538* (1-2), 45-52; (c) Barth, J. V.; Weckesser, J.; Trimarchi, G.; Vladimirova, M.; De Vita, A.; Cai, C.; Brune, H.; Günter, P.; Kern, K., *J. Am. Chem. Soc.* **2002,** *124* (27), 7991-8000; (d) Kim, B. I., *Langmuir* **2006,** *22* (22), 9272-9280.

2.   (a) Xiong, R.-G.; Zuo, J.-L.; You, X.-Z.; Abrahams, B. F.; Bai, Z.-P.; Che, C.-M.; Fun, H.-K., *Chem. Commun.* **2000,** (20), 2061-2062; (b) Lin, W.; Ma, L.; Evans, O. R., *Chem. Commun.* **2000,** (22), 2263-2264; (c) Sharma, M. K.; Lama, P.; Bharadwaj, P. K., *Cryst. Growth Des.* **2011,** *11* (4), 1411-1416; (d) Lin, W.; Wang, Z.; Ma, L., *J. Am. Chem. Soc.* **1999,** *121* (48), 11249-11250.

3.   (a) Ito, Y., *Tetrahedron* **2003,** *59* (37), 7323-7329; (b) Ito, Y.; Borecka, B.; Trotter, J.; Scheffer, J. R., *Tetrahedron Lett.* **1995,** *36* (34), 6083-6086; (c) Natarajan, A.; Mague, J. T.; Venkatesan, K.; Ramamurthy, V., *Org. Lett.* **2005,** *7* (10), 1895-1898.

4.   (a) Peedikakkal, A. M. P.; Peh, C. S. Y.; Koh, L. L.; Vittal, J. J., *Inorg. Chem.* **2010,** *49* (15), 6775-6777; (b) Peedikakkal, A. M. P.; Koh, L. L.; Vittal, J. J., *Chem. Commun.* **2008,** (4), 441-443.

5.   Gimeno, N.; Ros, M. B.; Serrano, J. L.; de la Fuente, M. R., *Angew. Chem. Int. Ed.* **2004,** *43* (39), 5235-5238.

Chapter 5

Photoreactivity of Ag(I) Complexes and Coordination Polymers of Pyridyl Acryclic Acids[*]
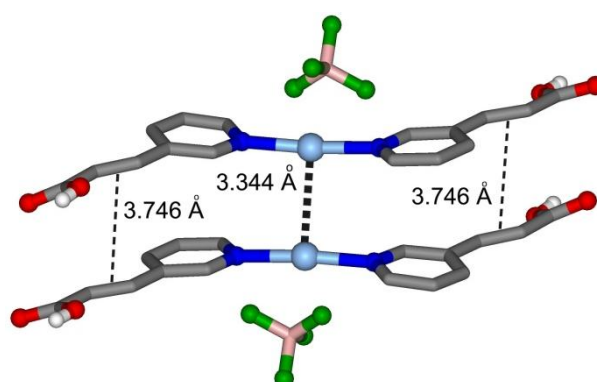
---

[*]The research work described in this chapter has been published / presented in the following journals / conferences

1. XX International Conference on the Chemistry of Organic Solid State (ICCOSS XX), June 2011, Bangalore, India.

2. Manuscript is under preparation.

5.1 Introduction

In the previous Chapters 2 – 4, various molecular salts of H_2SDC, 3-PAH, 4-PAH and HPVBA have been discussed and highlighted for their importance in the selective synthesis of cyclobutane derivatives in the solid state. In Chapter 1, the usefulness of metallophilic interaction, a supramolcular interaction, for the purpose of aligning photoreactive C=C bonds in the solid state was discussed. The aurophilic and argentophilic interactions became popular after Puddephatt and coworkers designed several diphosphine bridged gold(I) and silver(I) based macrocycles where linear olefin ligands, aligned parallel via aurophilic[1] and argentophilic[2] interactions, suitable for photodimerization reaction. MacGillivray *et al.* reported argentophilic interaction as a tool to preorganise photoreactive olefins with pyridyl functionality at only one side (Chapter 1) which upon photochemical cycloaddition reaction, transform to one dimensional polymer from a finite complex.[3] A silver coordination polymer [Ag(μ-4,4'-bpe)(H_2O)](CF_3CO_2)·CH_3CN, was investigated in our laboratory which underwent quantitative photodimerization reaction after desolvation.[4] Argentophilic interaction was later exploited to 4-vinylpyridine, a liquid and terminal olefin, for its solid state photoreactivity in Ag(I) complexes by MacGillivray *et al.*[5] In many cases argentophilic interactions occur with the aid of bridging ligands or anions bonded to Ag(I) atoms and this geometry is suitable for bringing a pair Ag(I) atoms closer within a distance less than the sum of their van der Waals radii resulting argentophilic interaction. This is known as anion or ligand supported argentophilic interaction.[4, 6] When an argentophilic interaction results without any support from ligands or anions, is termed as ligand or anion unsupported argentophilic interaction.[7] Biradha *et al.* have reported silver coordination compounds of *trans*-3-(4'-pyridyl)acrylic acid (4-PAH) and analogues that undergo photodimerization in *head-to-head* fashion via nitrate anion supported argentophilic interaction.[6b]
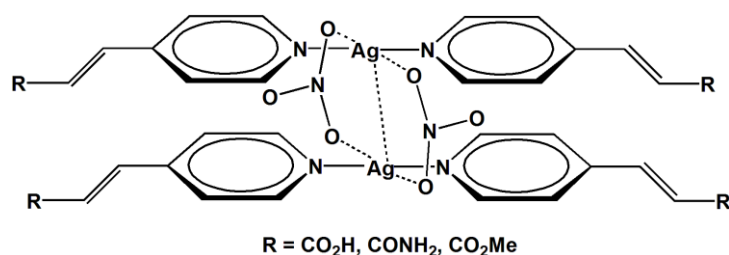
Scheme 5.1 Nitrate anion supported argentophilic interaction and preorganisation of 4-PAH analogues

The coordination chemistry of 3-PAH and 4-PAH ligands is well explored in the past[8] but the silver (I) coordination compounds using these ligands are relatively unexplored.[6b] The synthesis and structures of Ag(I) complexes and coordination polymers of neutral and deprotonated 3-PAH and 4-PAH and their photoreactivity are discussed in this chapter. The silver(I) coordination compounds using non-coordinating anions that have hardly any influence on argentophilic interaction, have been undertaken to understand how argentophilic interaction cooperate with the other supramolecular interaction in aligning C=C bonds.

5.2 Results and Discussion

When neutral 3-PAH or 4-PAH was reacted with $AgBF_4$ or $AgClO_4$ in 1:2 molar ratio, the hydrogen-bonded coordination complexes $[Ag(3\text{-PAH})_2](BF_4)$ (**30**), $[Ag(3\text{-PAH})_2](ClO_4)$ (**31**) and $[Ag(4\text{-PAH})_2](ClO_4)\cdot H_2O$ (**32**) have been obtained in almost quantitative yield. When deprotonated ligands were used, neutral coordination polymers $[Ag(3\text{-PA})]_2\cdot(1.5H_2O)$ (**33**) and $[Ag(4\text{-PA})]$ (**34**) have been isolated. The crystal structures of **30 – 34** were analyzed to understand the influence of various supramolecular forces on the packing of the olefin bonds. The detailed synthetic procedure for all these compounds is described in section 5.5.

5.2.1 Crystal Structure and Photoreactivity of Complex [Ag(3-PAH)$_2$](BF$_4$) (30)

Single crystal X-ray diffraction experiment reveals that the pyridyl N atoms of the two 3-PAH ligands coordinate to Ag(I) in almost a linear fashion (with N-Ag-N angle 173.7°) to result in a cationic complex [Ag(3-PAH)$_2$](BF$_4$) (**30**). The role of BF$_4^-$ anions appears to balance the charge and no significant interaction with Ag (I) has been found as seen from the shortest Ag···F distance of 3.089 Å. The carboxylic acid groups are involved in H-bonding to form the classical carboxylic acid dimer and resulted in a H-bonded zigzag polymeric structure propagating approximately along [0 1 1] direction (Figure 5.1). The parameters for other weaker hydrogen bonding interactions are listed in Table 5.1. Two such [Ag(3-PAH)$_2$]$^+$ cations stack in parallel orientation which may be attributed to the weak argentophilic interaction, as shown in Figure 5.2. The Ag···Ag distance of 3.344 Å is close to the sum of van der Waals radii of two Ag(I), 3.44 Å.[9] The 3-PAH ligands are aligned in *head-to-head* fashion and the distance between the C=C bond pairs, 3.746 Å is close enough to be photoreactive. Indeed **30** was found to undergo quantitative photodimerization under UV light for 15 h as was followed by ^{1}H NMR spectroscopy by the disappearance of two peaks for ethylenic protons at δ 7.63 and 6.69 ppm and appearance of two peaks for cyclobutane protons at δ 4.31 and 3.93 ppm (Figure 5.3).
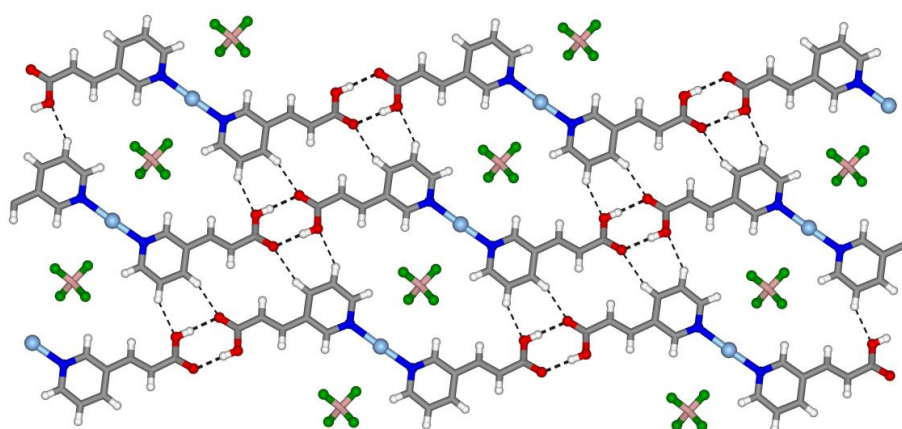
Figure 5.1 Hydrogen bonded 1-D zigzag chain and various weaker supramolecular interactions in **30** are shown.

129

....
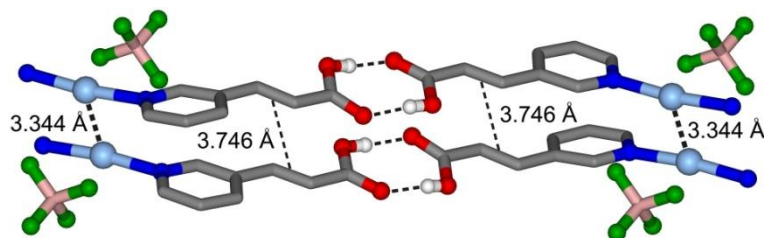
Figure 5.2 Cationic complexes are stacked parallel in **30** by 'anion unsupported' argentophilic interaction

Table 5.1 The hydrogen bonding parameters for **30**.

D-H···A	D(D-H) (Å)	D(H···A) (Å)	D(D···A) (Å)	<(DHA) (°)	Symmetry Operator
O(1)-H(1A)···O(4)	0.84	1.80	2.641(2)	176	x+2, y-1, z-1
O(3)-H(3A)···O(2)	0.84	1.81	2.646(2)	176	x-2, y+1, z+1
C(3)-H(3)···O(4)	0.95	2.35	3.250(3)	159	1+x, -1+y, -1+z
C(4)-H(4A)···O(1)	0.95	2.53	3.306(3)	139	-1+x, y, z
C(5)-H(5)···F(3)	0.95	2.48	3.168(3)	129	-x, 1-y, 1-z
C(11)-H(11)···F(3)	0.95	2.53	3.273(3)	135	
C(13)-H(13)···F(1)	0.95	2.45	3.273(3)	145	1-x, 1-y, 1-z
C(13)-H(13)···F(2)	0.95	2.35	3.246(3)	157	1-x, 1-y, 1-z
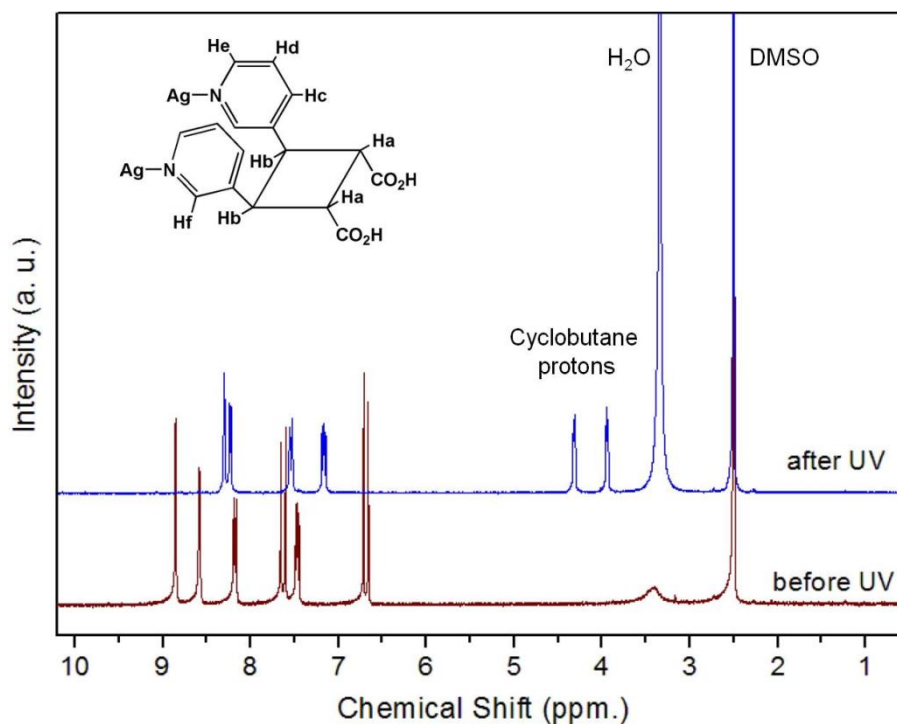
Figure 5.3 ^{1}H NMR spectra of **30** before and after UV irradiation

5.2.2 Crystal Structure and Photoreactivity of Complex [Ag(3-PAH)$_2$](ClO$_4$) (**31**)

Single crystal X-ray diffraction study reveals that **31** is isomorphous and isostructural to **30** and the two pyridyl N coordinate to Ag(I) with an angle of 173.5° in the coordination complex cation and the charge is balanced by the presence of ClO$_4^-$ anion which interacts very weakly with Ag(I) centres as indicated by the closest Ag···OClO$_3$ distance, 2.973 Å. The carboxylic acid groups are involved in H-bonding to form the classical carboxylic acid dimer and the parameters for several other weaker hydrogen bonding interactions are listed in Table 5.2. The [Ag(3-PAH)$_2$]$^+$ cationic pairs are again stacked by anion unsupported argentophilic interaction with Ag···Ag distance of 3.443 Å (Figure 5.4) which is equal to the sum of the van der Waals radii of two Ag atoms (3.44 Å).[9] The distance between the well-aligned C=C bond pairs of 3-PAH molecules in a '*head-to-head*' manner is 3.74 Å. As expected, **31** was also found to undergo quantitative photodimerization upon

irradiation under UV light for 16 h and was witnessed by the disappearance of two peaks for ethylenic protons at δ 7.63 and 6.69 ppm and appearance of two peaks for the cyclobutane protons at δ 4.32 and 3.94 ppm in ^{1}H NMR spectroscopy.
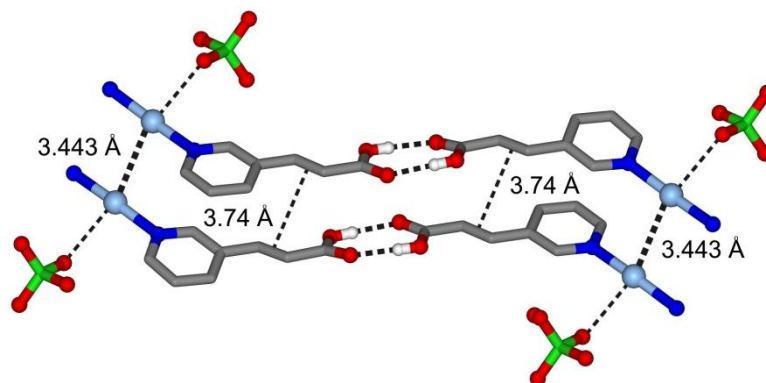
Figure 5.4 The cationic complexes are stacked parallel in **31** by anion unsupported argentophilic interaction

Table 5.2 The hydrogen bonding parameters for **31**.

D-H···A	D(D-H) (Å)	D(H···A) (Å)	D(D···A) (Å)	<(DHA) (°)	Symmetry Operator
O(1)-H(1A)···O(4)	0.84	1.80	2.641(2)	176	x+2, y-1, z-1
O(3)-H(3A)···O(2)	0.84	1.81	2.646(2)	176	x-2, y+1, z+1
C(1)-H(1A)···O(6)	0.93	2.34	3.238(6)	162	1-x, 1-y, 1-z
C(3)-H(3A)···O(4)	0.93	2.37	3.246(3)	156	-1+x, 1+y, 1+z
C(4)-H(4)···O(1)	0.93	2.52	3.306(3)	143	1+x, y, z
C(11)-H(11)···O(7)	0.93	2.57	3.204(7)	126	
C(13)-H(13)···O(5)	0.93	2.49	3.311(3)	146	1-x, 1-y, 1-z
C(13)-H(13)···O(8)	0.93	2.54	3.380(7)	150	1-x, 1-y, 1-z

5.2.3 Crystal Structure and Photoreactivity of Complex [Ag(4-PAH)$_2$](ClO$_4$)·H$_2$O (**32**)

X-ray diffraction study reveals that there are two independent formula units in the asymmetric unit in the monoclinic space group, $P2_1/m$ for Z = 4. Of the four 4-

PAH ligands in the asymmetric unit, the 'acrylic acid' fragments in two bearing oxygen atoms O1, O2, O7 & O8 were found to be disordered. It is interesting to note that all the atoms in the two $[Ag(4\text{-}PAH)_2]^+$ cations, the chlorine atoms of the two ClO_4^- anions and oxygen atoms of the two water molecules occupy the crystallographic ac-mirror plane. This imposes crystallographic disorder on the two perchlorate anions. In the cation, the two crystallographically independent Ag(I) are bonded to the N atoms of the two 4-PAH ligands almost linearly with an N-Ag-N angles of 169.4° and 172.1°. The ClO_4^- anions interact with Ag(I) weakly in bridging fashion to bring the two Ag(I) centres closer (Figure 5.5). This influence is clearly noted from the shorter Ag···Ag distances of 3.315 and 3.429 Å as compared to the distances found in **30** and **31**. The $[Ag(4\text{-}PAH)_2]^+$ complex cations further involve in hydrogen-bonding with water molecules in one side and with carboxylic acid group of another complex unit in another side forming dicarboxylic acid dimer synthon. The hydrogen bonding interactions result in a finite oligomeric chain consisting of two complex units and two water molecules terminating the propagation into infinite chain (Figure 5.6). The hydrogen atoms of water molecules are not in favourable position (smaller angles of 110.6° and 118.8°) for hydrogen bonding interaction with the nearest oxygen atoms (3.21 Å) of the carboxylic acid groups (see Table 5.3 for hydrogen bonding parameters). The 4-PAH ligands are found to stack infinitely in *head-to-head* fashion with a distance of 3.716 and 3.810 Å (Figure 5.6a) along the *b*-axis with alternative crisscross pairs.
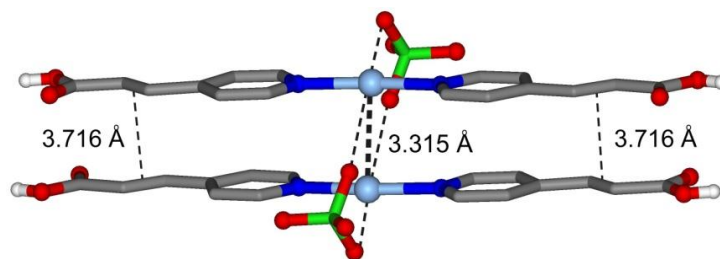
Figure 5.5 Discrete cationic complexes are stacked crisscross in **32** by anion supported argentophilic interaction. One set of distances are shown.

Table 5.3 The hydrogen bonding parameters for **32**.

D-H⋯A	D(D-H) (Å)	D(H⋯A) (Å)	D(D⋯A) (Å)	<(DHA) (°)	Symmetry Operator
O(3)-H(3)⋯O(2W)	0.84	1.77	2.61(2)	180	x-2, y, z
O(5)-H(5X)⋯O(2X)	0.84	1.99	2.83(6)	176	
O(6)-H(6O)...O(1)	0.84	1.90	2.74(3)	176	
O(8)-H(8)⋯O(1W)	0.84	1.97	2.80(2)	173	x+1, y, z-1
O(2)-H(2O)⋯O(5)	0.84	1.75	2.59(2)	172	
O(1X)-H(1X)⋯O(6)	0.84	1.64	2.44(5)	159	
C(2)-H(2)⋯O(4)	0.95	2.37	3.32(2)	172	1+x, y, z
C(7)-H(7)⋯O(4)	0.95	2.44	3.39(2)	179	1+x, y, z
C(17)-H(17)⋯O(12)	0.95	2.51	3.26(3)	135	x, y, -1+z
C(18)-H(18)⋯O(7)	0.95	2.40	3.35(3)	178	-1+x, y, z
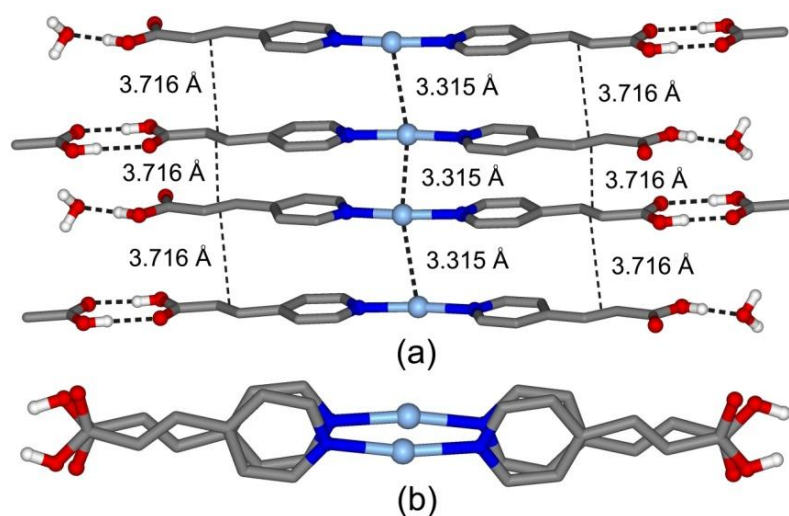
Figure 5.6 The infinite arrangement of cationic complex units of **32** with equal distance of separation (a) and a close look at the crisscrossed arrangement of 4-PAHs (b). ClO_4^- anions are not shown for clarity and one set of distances are shown.

134
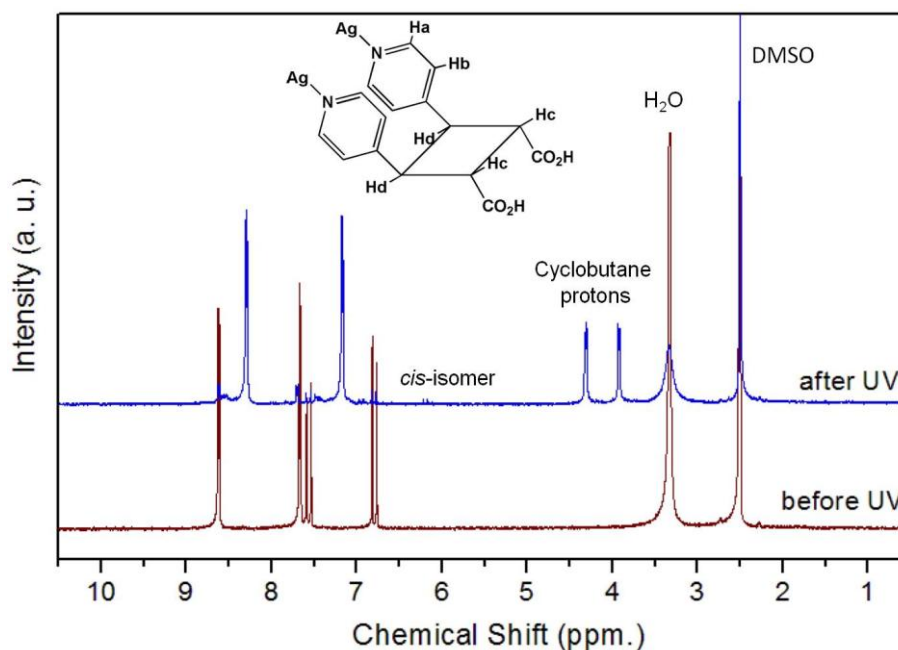
Figure 5.7 ^{1}H NMR spectra of **32** before and after UV irradiation

This compound was found to undergo photodimerization (~ 90%) to *rctt*-HH-4,4-BPCD as was observed by the disappearance of two peaks for ethylenic protons at δ 7.57 and 6.80 ppm and appearance of two peaks for cyclobutane protons at δ 4.30 and 3.92 ppm in ^{1}H NMR spectroscopy (Figure 5.7). This compound also underwent about 3% *trans-cis* isomerisation. The formation of only *rctt*-isomer of the product can be observed from the above ^{1}H NMR spectrum after UV irradiation. The formation of only *rctt*-isomer of the product from crisscross aligned pairs is the result of pedal-like motion of monomeric units with respect to each other, as was discussed in section 1.7 in Chapter 1.[3, 10]

A thorough perusal in the crystal structure reveals that one side of C=C-CO_2H unit in each independent $[Ag(4\text{-}PAH)_2]^+$ is disordered in two positions by 31 : 19. In both $[Ag(4\text{-}PAH)_2]^+$ in the asymmetric unit, the disorder fragment is paired with the normal 4-PAH. If we consider only the major component, it is crisscrossed by 62% and for the minor component it is 38% normal packing. Therefore, a pedal-like motion of at least 62% of the 4-PAH can be accounted for the formation *rctt*-

....

isomer of the product from the pairs aligned crisscross (Figure 5.6b) during photodimerization.

5.2.4 Crystal Structure and Photoreactivity of Coordination Polymer [Ag(3-PA)]·(1.5H$_2$O) (33)

3-PAH can coordinate metal ions as neutral ligand through pyridyl N donor, also as an anionic ligand via both the pyridyl N and carboxylate O when deprotonated. Indeed when the Na-salt of 3-PA was allowed to react with AgBF$_4$, a neutral coordination polymer **33** was isolated. Single crystal X-ray diffraction study revealed that all the donor sites are coordinated to Ag(I). The coordination number around each Ag(I) ion is three and with T-shaped geometry. The carboxylate groups bridge two Ag(I) ions in $\mu_{1,3}$ fashion and the distance is 2.883 Å reflecting very strong ligand supported argentophilic interaction. For Z = 1 in the space group $P\bar{1}$, there is a crystallographic inversion centre present in the middle of the 8-membered Ag$_2$(O$_2$C)$_2$ ring. The pyridyl N atoms are bonded to the neighbouring [Ag(3-PA)] repeating units to form a 1D ribbon like polymer which extends approximately along [0 1 1] direction as shown in Figure 5.8. These 1D ribbons are further slip-stacked in parallel arrangement (with Ag···Ag···Ag angle of 34°) via ligand unsupported argentophilic interactions. In this process the photoreactive C=C bonds are aligned infinitely in parallel and in *head-to-head* fashion. The distance between two C=C bonds is 3.608 Å, whereas between two diagonally Ag(I) ions it is 3.112 Å (Figure 5.9) which is smaller than the sum of their van der Waals radii (3.44 Å)[9] reflecting that significant argentophilic interaction prevails. Moreover, there is another Ag···Ag distance of 3.608 Å along the edge as shown in Figure 5.9, which is slightly higher than the sum of their van der Waals radii. Upon irradiation under UV light for 36 h, the powdered sample of **33** underwent quantitative photodimerization. To our disappointment, it was not an SCSC process. But we reckon that the dimerization process occurs

randomly, which is more probable, the resulting structure would probably be two dimensional. There are three molecules of disordered water also in the crystal structure with 50% occupancy, whose hydrogen atoms were not located.
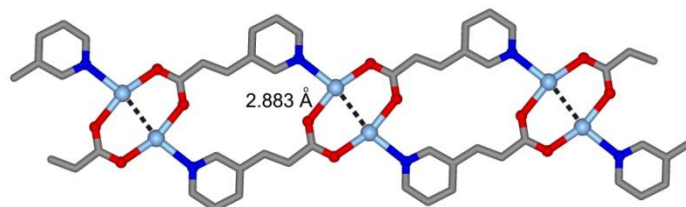
Figure 5.8 1D ribbon like structure of **33** shows stronger argentophilic interaction inside the ribbon
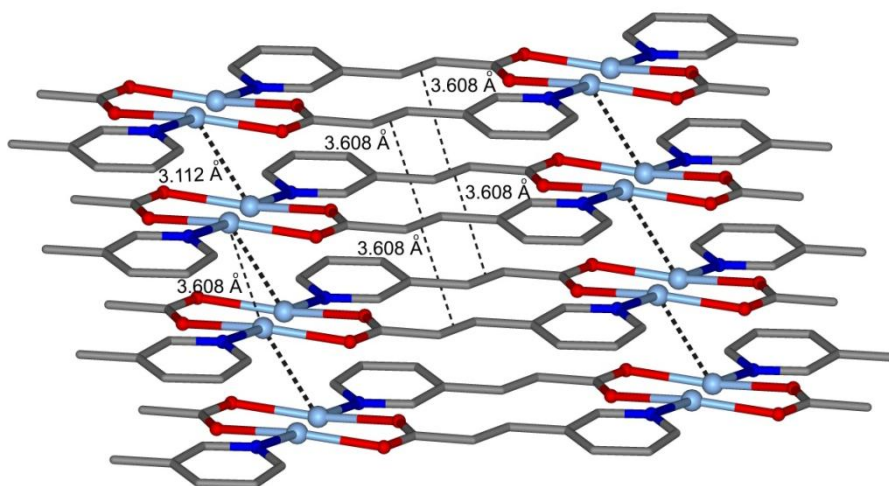
Figure 5.9 The infinitely slip-stacked arrangement of 3-PA as ribbon in **33** approximately along *a*-axis. The argentophilic interaction is between two diagonal Ag(I) centres.

5.2.5 Crystal Structure of Coordination Polymer [Ag(4-PA)] (34)

Single crystal X-ray diffraction study revealed that all the donor sites are coordinated to Ag(I). The coordination number around each Ag(I) ion is 3 and with the 'Y'-shaped geometry (Figure 5.10). The carboxylate groups are chelating to Ag(I) and the pyridyl N from the neighbouring repeating unit is bonded to provide a linear 1D coordination polymer which propagates along *b*-direction. In fact, all the 1D chains are aligned parallel to *b*-axis but not with perfect alignment of similar atoms

from the neighbouring chains. The distance between two nearest Ag(I) ions is 3.878 Å indicating there is no significant argentophilic interaction. The relative orientation of 4-PAs is crisscross and *head-to-tail* with center-to-centre distance between the C=C bonds of 5.202 Å. This polymer was found to be photostable. The structure is stabilized by the weak inter-chain Ag(I)···O interaction (3.02 Å) as shown in Figure 5.10.
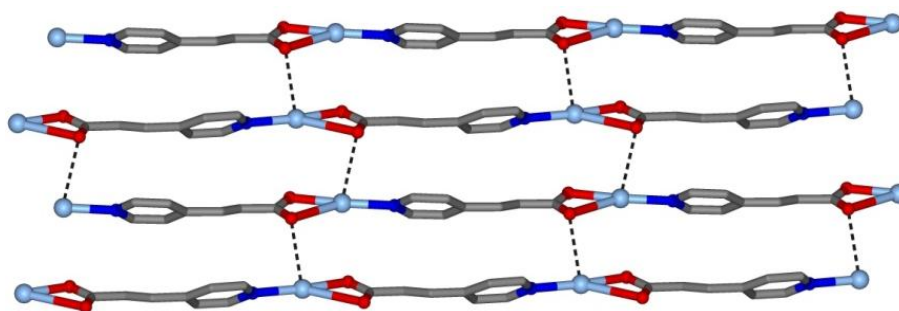
Figure 5.10 1D chains of **34** propagate along *b*-axis. There is hardly any argentophilic interaction between the chains.

5.3 Comparative Study on Structures and Photoreactivity

Among the above five compounds investigated, four were found to be photoreactive; the photoreactive C=C bonds were preorganized by argentophilic interaction along with other supramolecular interactions. In isostructural **30** and **31**, BF_4^- and ClO_4^- anions have little contribution in assisting the argentophilic interaction. But in **32**, ClO_4^- anions are found to bridge the Ag(I) atoms and therefore, have some role in assisting the argentophilic interaction. **30** and **31** form hydrogen-bonded infinite 1D zigzag chains through the classical carboxylic acid dimer synthon. On the other hand, **32** forms a hydrogen-bonded dimer in which the two molecules are interacting through carboxylic acid dimer with two terminal water molecules. In **30** and **31**, the observed N-Ag-N angles along with the shorter Ag···Ag distances compared to the distances between C=C bonds indicate that two Ag(I) centres are leaning towards each other reflecting the presence of argentophilic

Chapter 5

....

interactions. In **33**, there is no anion present, and thus the argentophilic interaction is absolutely free of any anion effect. Between **33** and **34**, the difference in the molecular packing and the photoreactivity arises from the position of the 'N' atoms in the pyridyl groups that make 3-PA an angular spacer and 4-PA a linear spacer ligand. Being an angular spacer, 3-PA can form 16 member ring structure comprising $\mu_{1,3}$-bridging mode of carboxylate and monodentate pyridyl groups. These ring structures extend to form 1D polymer and parallel orientation is resulted exclusively due to argentophilic interaction. On the other hand, the 1D polymer resulted from the chelating carboxylate and monodentate pyridyl groups has no scope of exerting argentophilic interaction and thus no alignment of C=C bonds in the solid state structure of **34**.

The above compounds were irradiated under UV light in d_6-dmso solution for 12 h and ^{1}H NMR spectra were acquired to study their photoreactivity in solution 3-PAH and 4-PAH were observed to isomerise in solutions of compounds **30 – 32** in the same condition indicating the absence of any argentophilic interaction in the solution phase. Coordination polymer **33** underwent incomplete photodimerization along with *trans–cis* isomerization which reflects that the parallel arrangement of 1D ribbons still partially exist in the solution. In addition, the compound still maintains the stereoselectivity during the solution phase dimerization as it results only in *rctt*-HH-dimer among all possible dimers of 3-PAH. The observed isomerization is the result of the dissociation and scrambling of 3-PAH in solution. Coordination polymer **34** underwent only *trans–cis* isomerization and no dimerization, which indicates that the 1D chains, although are in random motion in solution, cannot come closer within distance limit to be reactive. Generally, the compounds which are photostable in the solid state are observed to furnish a mixture of products in solution phase due to the Brownian motion. We also observed some molecular salts of 4-PAH which underwent quantitative photodimerization in the solid state but were observed not to

Chapter 5

....

furnish any dimerization in solution phase despite of higher freedom of molecular movents (chapter 3). Here we observed a similar phenomenon for **30** – **32**. The compounds **30** – **33** undergo quantitative dimerization in the solid state. It is surprising to observe that 3-PAH molecule alone does not undergo photodimerization in solution phase but dimerizes in the solid state. Therefore it can be concluded that the hydrogen bonded coordination complexes **30** – **32** behave like free ligand in the solution phase.

The synthesis of 3,4-bis(4'-pyridyl)cyclobutane-1,2-dicarboxylic acid (HH-4,4-BPCD) has been discussed in Chapter 3. Although, the synthesis of 3,4-bis(3'-pyridyl)cyclobutane-1,2-dicarboxylic acid (HH-3,3-BPCD, HH-dimer of 3-PAH) was discussed by Schmidt *et al.*,[11] the photoreactivity of these compounds can be used as an alternative route to synthesize them. These functional cyclobutane derivatives can be used as potential ligands for coordination polymers which are discussed in Chapter 7.

5.4 Summary

Several hydrogen bonded cationic silver(I) complexes and coordination polymers have been discussed in the context of their structures and photoreactivity. The preorganisation of photoreactive olefin ligands in cationic complexes were achieved not only by utilising argentophilic interaction alone but also with the aid from other supramolecular interactions. Relatively stronger argentophilic interaction (Ag⋯Ag distance of 3.112 Å) was observed between the neutral ribbons of [Ag(3-PA)] that are stacked parallel. The presence of anions in the cationic complexes has hardly any influence on the argentophilic interaction. All among these photoreactive compounds underwent photodimerization in HH-fashion. The observed *trans–cis* isomerisation instead of any photodimerization in solution phase for the cationic

silver(I) complexes implies that the effect of argentophilic interaction and other supramolecular interactions work well in the solid state.

5.5 Syntheses and Characterizations

[Ag(3-PAH)$_2$](BF$_4$) (30)

3-PAH (15 mg, 0.1 mmol) was dissolved 3 mL methanol, then AgBF$_4$ (19 mg, 0.1 mmol) in 2 mL CH$_3$CN were added. The resulting white ppt. was dissolved by adding 2 mL water. Single crystalline products were obtained by slow evaporation. Yield: 92%.

^{1}H NMR (300 MHz, DMSO-d_6, 298K): δ_H 12.56 (s, 1H, CO$_2$H), 8.85 (s, 1H, Py-H), 8.59 (d, 1H, Py-H), 8.18 (d, 1H, Py-H), 7.63 (d, 1H, CH=CH), 7.45 (dd, 1H, Py-H), 6.69 (d, 1H, CH=CH). Analysis found (%): C 38.58, H 2.93, N 5.64; C$_{16}$H$_{14}$AgBF$_4$N$_2$O$_4$ requires C 38.98, H 2.86, N 5.68. No solvent loss was observed in TGA experiment.

After UV irradiation for 15 h, ^{1}H NMR (300 MHz, DMSO-d_6, 298K): δ_H 12.58 (s, 2H, CO$_2$H), 8.30 (s, 2H, Py-H), 8.26 (d, 2H, Py-H), 7.54 (d, 2H, Py-H), 7.16 (dd, 2H, Py-H), 4.31 (d, 2H, CH-CH), 3.93 (d, 2H, CH-CH).

[Ag(3-PAH)$_2$](ClO$_4$) (31)

3-PAH (15 mg, 0.1 mmol) was dissolved 3 mL methanol, then AgClO$_4$ (21 mg, 0.1 mmol) in 2 mL CH$_3$CN were added. The resulting white ppt. was dissolved by adding 2 mL water. Single crystalline products were obtained by slow evaporation. Yield: 94%.

^{1}H NMR (300 MHz, DMSO-d_6, 298K): δ_H 12.59 (s, 1H, CO$_2$H), 8.86 (s, 1H, Py-H), 8.58 (d, 1H, Py-H), 8.18 (d, 1H, Py-H), 7.63 (d, 1H, CH=CH), 7.46 (dd, 1H,

....

Py-H), 6.69 (d, 1H, CH=CH). Analysis found (%): C 38.21, H 2.78, N 5.85; $C_{16}H_{14}AgClN_2O_8$ requires C 38.01, H 2.79, N 5.54.

After UV irradiation for 16 h, ^{1}H NMR (300 MHz, DMSO-d_6, 298K): δ_H 12.6 (s, 2H, CO_2H), 8.30 (s, 2H, Py-H), 8.23 (d, 2H, Py-H), 7.54 (d, 2H, Py-H), 7.18 (dd, 2H, Py-H), 4.32 (d, 2H, CH-CH), 3.94 (d, 2H, CH-CH).

[Ag(4-PAH)$_2$](ClO$_4$)·H$_2$O (32)

4-PAH (15 mg, 0.1 mmol) was dissolved 4 mL hot water, then AgClO$_4$ (21 mg, 0.1 mmol) in 2 mL CH$_3$CN was added. Single crystalline products were obtained by slow evaporation. Yield: 85%.

^{1}H NMR (300 MHz, DMSO-d_6, 298K): δ 12.59 (s, 1H, CO_2H), 8.57 (d, 2H, Py-H), 7.81 9d, 2H, Py-H), 7.57 (d, 1H, CH=CH), 6.80 (d, 1H, CH=CH). Analysis found (%): C 36.71, H 2.94, N 5.48; $C_{16}H_{16}AgClN_2O_9$ requires C 36.70, H 3.08, N 5.35. The observed water loss in TGA experiment 3.3% matches well with the calculated value 3.4%.

After UV irradiation for 30 h, ^{1}H NMR (300 MHz, DMSO-d_6, 298K): δ_H 8.29 (d, 4H, Py-H), 7.15 (d, 4H, Py-H), 4.30 (d, 2H, CH-CH), 3.92 (d, 2H, CH-CH). In addition there is small minute amount impurity of monomer and *cis*-isomer of 4-PAH at δ 6.95 and 6.19 ppm for ethylenic protons.

[Ag(3-PA)]·(1.5H$_2$O) (33)

AgBF$_4$ (19 mg, 0.1 mmol) in 2 mL methanol was carefully layered over Na-salt of 3-PA (15 mg 3-PAH was neutralized by NaOH (aq.)) in 3 mL water keeping 3 mL CH$_3$CN as buffer layer in the middle in a test tube. The product was crystallized out after a few days. Yield: 78%.

....

^{1}H NMR (300 MHz, DMSO-d_6, 298K): δ_H 8.81 (s, 1H, Py-H), 8.57 (d, 1H, Py-H), 8.15 (d, 1H, Py-H), 7.61 (d, 1H, CH=CH), 7.43 (dd, 1H, Py-H), 6.68 (d, 1H, CH=CH). Analysis found (%): C 34.50, H 2.29, N 5.09; Ag$_2$C$_{16}$H$_{12}$N$_2$O$_7$ requires C 34.23, H 2.16, N 5.00. The observed 8.7 % water loss in TGA experiment is in agreement with the calculated value 8.6%.

After irradiation under UV light for 36 h, ^{1}H NMR (300 MHz, DMSO-d_6, 298K): δ_H 8.25 (s, 2H, Py-H), 8.18 (d, 2H, Py-H), 7.49 (d, 2H, Py-H), 7.09 (dd, 2H, Py-H), 4.14 (d, 2H, CH-CH), 3.71 (d, 2H, CH-CH).

[Ag(4-PA)] (34)

AgBF$_4$ (19 mg, 0.1 mmol) in 2 mL methanol was carefully layered over Na-salt of 4-PA (15 mg 4-PAH was neutralized by NaOH (aq.)) in 3 mL water, keeping 3 mL CH$_3$CN as buffer layer in the middle in a test tube. The product was crystallized out after a few days. Yield: 75%.

^{1}H NMR (300 MHz, DMSO-d_6, 298K): δ_H 8.60 (d, 2H, Py-H), 7.63 (d, 2H, Py-H), 7.51 (d, 1H, CH=CH), 6.76 (d, 1H, CH=CH). Analysis found (%): C 37.05, H 2.08, N 5.35; C$_8$H$_6$AgNO$_2$ requires C 37.53, H 2.36, N 5.47. No solvent loss was observed in TGA experiment.

Table 5.4 Crystallographic data for **30** – **34**

Compounds	30	31	32	33	34
Formula	$C_{16}H_{14}AgBF_4N_2O_4$	$C_{16}H_{14}AgClN_2O_8$	$C_{16}H_{16}AgClN_2O_9$	$C_{16}H_{12}Ag_2N_2O_7$	$C_8H_6AgNO_2$
M	492.97	505.61	523.63	560.02	256.01
T (K)	100(2)	100(2)	100(2)	100(2)	223(2)
λ (Å)	0.71073	0.71073	0.71073	0.71073	0.71073
Cryst syst / Space group	Triclinic / $P\bar{1}$	Triclinic / $P\bar{1}$	Monoclinic / $P2_1/m$	Triclinic / $P\bar{1}$	Monoclinic / $P2_1/c$
a (Å)	8.075(2)	8.1979(6)	16.3714(18)	3.6084(7)	9.8546(9)
b (Å)	10.153(3)	10.1452(8)	6.4132(7)	9.9374(17)	11.4723(10)
c (Å)	11.524(3)	11.5751(9)	18.820(2)	12.728(2)	6.9163(6)
α (°)	74.675(5)	74.888(2)	90	73.315(3)	90
β (°)	77.784(5)	77.195(2)	109.452(3)	87.944(3)	109.346(2)
γ (°)	70.735(5)	70.615(2)	90	84.004(3)	90
Volume ($Å^3$) / Z	852.1(4) / 2	867.01(12) / 2	1863.2(4) / 4	434.78(14) / 1	737.77(11) / 4
D_{calcd} (g/cm^3) / μ (mm^{-1})	1.921 / 1.252	1.937 / 1.368	1.867 / 1.280	2.139 / 2.295	2.305 / 2.679
Reflns col. / Ind. Reflns.	10986 / 3899	11584 / 3964	11159 / 3603	5455 / 1987	5099 / 1689
R_{int} / Goof on F^2	0.0257 / 1.131	0.0254 / 1.092	0.0385 / 1.054	0.0302 / 1.151	0.0394 / 1.042
Final R[I>2σ][a] R_1 / wR2	0.0253 / 0.0675	0.0264 / 0.0657	0.0654 / 0.1534	0.0337 / 0.0916	0.0425 / 0.1027

[a] R1 = $\Sigma||F_o| - |F_c||/ \Sigma|F_o|$, [b] wR2 = $[\Sigma w(F_o^2 - F_c^2)^2/\Sigma w(F_o^2)^2]^{1/2}$

....

5.6 References

1. (a) Irwin, M. J.; Vittal, J. J.; Yap, G. P. A.; Puddephatt, R. J., *J. Am. Chem. Soc.* **1996,** *118* (51), 13101-13102; (b) J. Puddephatt, R., *Chem. Commun.* **1998,** (10), 1055-1062.

2. Brandys, M.-C.; Puddephatt, R. J., *Chem. Commun.* **2001,** (16), 1508-1509.

3. Chu, Q.; Swenson, D. C.; MacGillivray, L. R., *Angew. Chem. Int. Ed.* **2005,** *44* (23), 3569-3572.

4. Nagarathinam, M.; Vittal, J. J., *Angew. Chem. Int. Ed.* **2006,** *45* (26), 4337-4341.

5. Georgiev, I. G.; Bučar, D.-K.; MacGillivray, L. R., *Chem. Commun.* **2010,** *46* (27), 4956.

6. (a) Jung, O.-S.; Kim, Y. J.; Lee, Y.-A.; Kang, S. W.; Choi, S. N., *Cryst. Growth Des.* **2004,** *4* (1), 23-24; (b) Santra, R.; Biradha, K., *Cryst. Growth Des.* **2010,** *10* (8), 3315-3320.

7. (a) Chen, C. Y.; Zeng, J. Y.; Lee, H. M., *Inorg. Chim. Acta* **2007,** *360* (1), 21-30; (b) Liu, D.; Li, H.-X.; Ren, Z.-G.; Chen, Y.; Zhang, Y.; Lang, J.-P., *Cryst. Growth Des.* **2009,** *9* (10), 4562-4566; (c) Singh, K.; Long, J. R.; Stavropoulos, P., *J. Am. Chem. Soc.* **1997,** *119* (12), 2942-2943.

8. (a) Evans, O. R.; Xiong, R.-G.; Wang, Z.; Wong, G. K.; Lin, W., *Angew. Chem. Int. Ed.* **1999,** *38* (4), 536-538; (b) Wang, X.-S.; Zhao, H.; Qu, Z.-R.; Ye, Q.; Zhang, J.; Xiong, R.-G.; You, X.-Z.; Fun, H.-K., *Inorg. Chem.* **2003,** *42* (19), 5786-5788; (c) Mondal, K. C.; Sengupta, O.; Nethaji, M.; Mukherjee, P. S., *Dalton Trans.* **2008,** (6), 767-775; (d) Zhang, J.; Xiong, R.-G.; Zuo, J.-L.; Che, C.-M.; You, X.-Z., *J. Chem. Soc., Dalton Trans.* **2000,** (17), 2898-2900; (e) Kurmoo, M.; Estournès, C.; Oka, Y.; Kumagai, H.; Inoue, K., *Inorg. Chem.* **2004,** *44* (2), 217-224; (f) Tong, M.-L.; Chen, X.-M.; Batten, S. R., *J. Am. Chem. Soc.* **2003,** *125* (52), 16170-16171; (g) Gunning, N. S.; Cahill, C. L., *Dalton Trans.* **2005,** (16), 2788-2792.

....

9.   Bondi, A., *J. Phy. Chem.*, **1964,** *68*(3), 441-451.

10.   (a) Natarajan, A.; Mague, J. T.; Venkatesan, K.; Ramamurthy, V., *Org. Lett.* **2005,** *7* (10), 1895-1898; (b) Ohba, S.; Hosomi, H.; Ito, Y., *J. Am. Chem. Soc.* **2001,** *123* (26), 6349-6352; (c) Peedikakkal, A. M. P.; Vittal, J. J., *Chem. Eur. J.* **2008,** *14* (17), 5329-5334; (d) Harada, J.; Ogawa, K., *Chem. Soc. Rev.* **2009,** *38* (8), 2244.

11.   Lahav, M.; Schmidt, G. M. J., *J. Chem. Soc. B: Phy. Org.* **1967**, 239-243.

Chapter 6

Silver(I) Macrocycles and Coordination Polymers

Containing Pyridyl Carboxylate with Phosphine

Derived Ligands and Their Photoreactivity
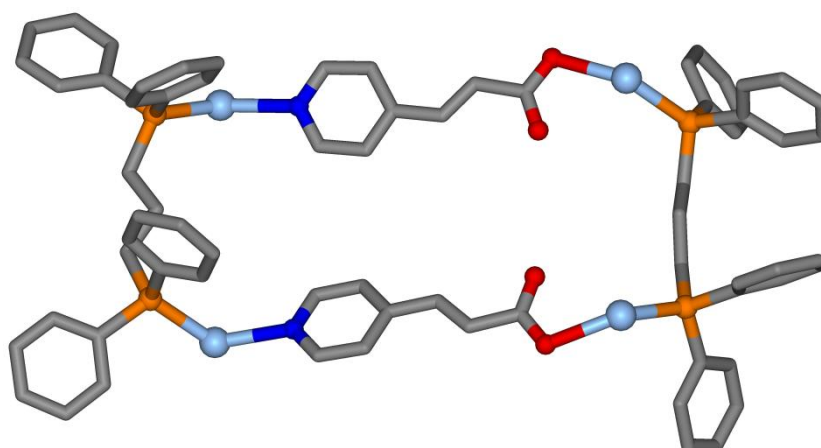
6.1 Introduction

In the previous chapter we have discussed the syntheses, characterizations and photoreactivity of several silver(I) coordination complexes and polymers where the preorganisation of the olefinic spacers were obtained either solely by argentophilic interaction or by other supramolecular interactions collectively. We also have discussed the roles of anions in such preorganisation wherever applicable. In Chapter 5, we also have referred the work of Puddephatt *et al.* on the designed syntheses of gold(I) and silver(I) macrocycles composed of 4,4'-bpe and linear diphosphine ligands of general formula $Ph_2P(CH_2)_nPPh_2$; where 4,4'-bpe were found to stack parallel and underwent [2 + 2] cycloaddition reaction.[1,2] The preferred *cissoid* conformations of the diphosphine ligands often are dictated by the aurophilic and argentophilic interactions or vice versa. However, the formation of such macrocyclic structures is limited and only dipyridyl spacers like 4,4'-bipyridyl, 4,4'-bpe etc have been explored for this purpose.[3] We intend to explore this chemistry with various pyridyl carboxylate ligands and to study the coordinative modes of carboxylate group towards Ag(I). In order to form such macrocyclic ring, carboxylate group has to coordinate to Ag(I) in monodentate fashion just like pyridyl 'N' donor.
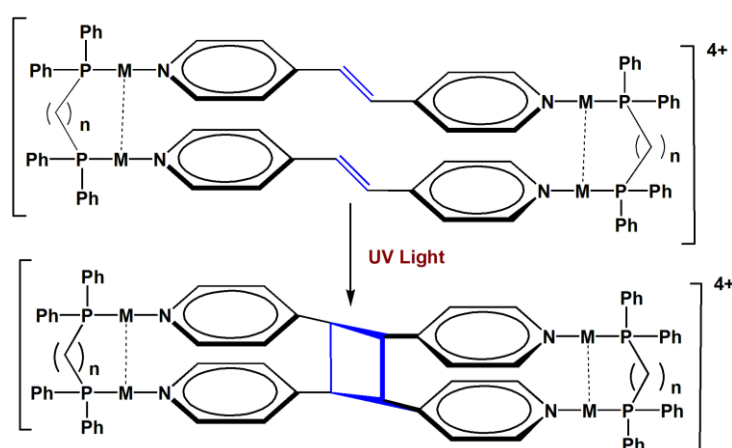
Scheme 6.1 Photoreactive macrocycles synthesized in Puddephatt's laboratory; for M = Au(I), n = 2 and for Ag(I), n = 1.

We know that silver(I) possesses high affinity towards N, P and O donors of the ligands. Recently there have been extensive studies on the framework with diverse structural motifs (also known as secondary building unit or SBU) by using mixed ligands and tuning reaction conditions.[4] The carboxylate group can coordinate to Ag(I) in various ways like monodentate, $\mu_{1,1}$ and $\mu_{1,3}$ bridging which result in structural diversity. In addition, varying coordination number and flexible coordination geometries around Ag(I) including linear, trigonal, pyramidal, square planar, tetrahedral, octahedral etc, have made it a distinct metal node to synthesize macrocycles, polymetallic clusters and higher periodic coordination polymers.[5] Therefore, designing discrete, macrocyclic and polymeric silver(I) based coordination compounds with ligands containing N, O and P donor sites, has always been a challenge to control its coordination number and geometry. Various mono- and diphosphine derived ligands have been explored in the past for their coordination behaviour with silver and other coinage metal ions.[1,3,6] This chapter discusses the details of the syntheses and structural characterizations of several 0D, 1D, 2D and 3D silver coordination complexes and polymers containing pyridyl carboxylate (3-PA, 4-PA and PVBA) or 4-styrylpyridine (4-SP) and phosphine-derived ligands like monodentate terminal ligand PPh_3 and bidentate bridging diphosphine ligands of general formula $Ph_2P(CH_2)_nPPh_2$. Various coordinative modes of carboxylate group toward Ag(I) and the coordination numbers and geometries around Ag(I) that led to the formation of polymers over macrocycles will be discussed. The relative orientations of these olefinic ligands and their photoreactivity will be addressed whenever applicable.

6.2 Results and Discussion

The silver(I) coordination compounds and polymers containing Ag(I) and the above mentioned ligands along with auxiliary ligands like PPh_3, bis(diphenylphosphino)methane (dppm), 1,2-bis(diphenylphosphino)ethane (dppe)

and 1,3-dis(diphenylphosphino)propane (dppp) were synthesized and characterized. The crystal structures of $[Ag_2(4\text{-}PA)_2(PPh_3)_2]\cdot(Et_2O)(0.5CH_3CN)(2.5H_2O)$ (**35**), $[Ag_2(3\text{-}PA)(dppm)_2]BF_4\cdot(2CH_3CN)$ (**36**), $[Ag_2(4\text{-}PA)_2(dppe)]\cdot CH_3CN$ (**37**), $[Ag_2(4\text{-}PA)_2(dppp)]\cdot(3H_2O)(0.5Et_2O)$ (**38**), $[Ag(3\text{-}PA)(dppp)_{0.5}]\cdot H_2O$ (**39**), $[Ag_4(dppm)_4(PVBA)_2](TFA)_2$ (**40**), $[Ag_2(4\text{-}SP)_2(dppe)(TFA)_2]$ (**41**), $[Ag_2(dppm)(4\text{-}SP)_2][Ag_2(dppm)_2]_{0.5}(BF_4)_3\cdot(2THF)$ (**42**) were analyzed to understand the solid state packing and structural diversity in various silver(I) coordination compounds and polymers. The affinity of the N, O and P donor sites of various pyridyl carboxylate and phosphine-derived ligands toward Ag(I) will be exploited to understand the coordination chemistry and solid state properties of these multi dimensional silver(I) coordination compounds. Generally, all these compounds were synthesized from aqueous THF and then the precipitates obtained were dissolved in aqueous acetonitrile (1:1). The single crystals were grown by diffusing either Et_2O or hexane. The detailed syntheses and characterizations for each of these compounds are discussed in section 6.5.

6.2.1 Structural Description of $[Ag_2(4\text{-}PA)_2(PPh_3)_2]\cdot(Et_2O)(0.5CH_3CN)(2.5H_2O)$ (35)

The compound $[Ag_2(4\text{-}PA)_2(PPh_3)_2]\cdot(Et_2O)(0.5CH_3CN)(2.5H_2O)$ (**35**) was refined in monoclinic space group, $P2_1/c$ where all the solvents molecules in the lattice were found disordered and the hydrogen atoms of all the water molecules were not located. There are two types of Ag(I) ions in the structure; both of them have distorted tetrahedral geometry stemming from one N from a pyridyl group, one P from PPh_3 and two oxygen atoms from two different carboxylate groups from the neighbouring ligands. The carboxylate oxygen atom in turn bridges two Ag(I) in $\mu_{1,1}$ fashion to generate a four membered Ag_2O_2 core with Ag···Ag distance of 3.764 Å as shown in Figure 6.1. An analysis of the structure reveals that these four-membered rings are further bridged by four 4-PA ligands (Figure 6.2) to form another 36-

....

membered metallo-macrocyclic ring. The opposite sides of the ring are formed by *head-to-tail* oriented 4-PA ligands. The overall structure of this compound is two dimensional 4-connected uninodal net whose topology was calculated to be sql/Shubnikov tetragonal plane net using TOPOS.[7] The nets are stacked parallel in ABAB fashion and the lengths of the sides of rectangular windows are 10.709 and 10.871 Å. This compound was found not to furnish any photodimerization, as evidenced from the ^{1}H NMR data, upon irradiation under UV light for 30 h.
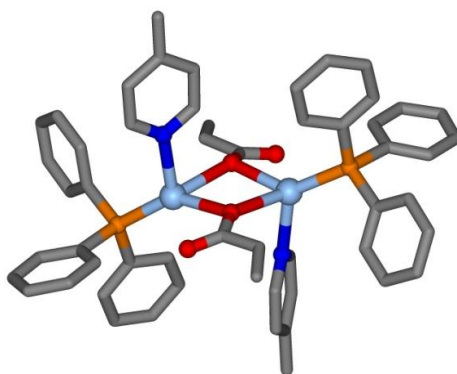
Figure 6.1 A part of the connectivity showing the coordination environment of Ag(I) in **35**.
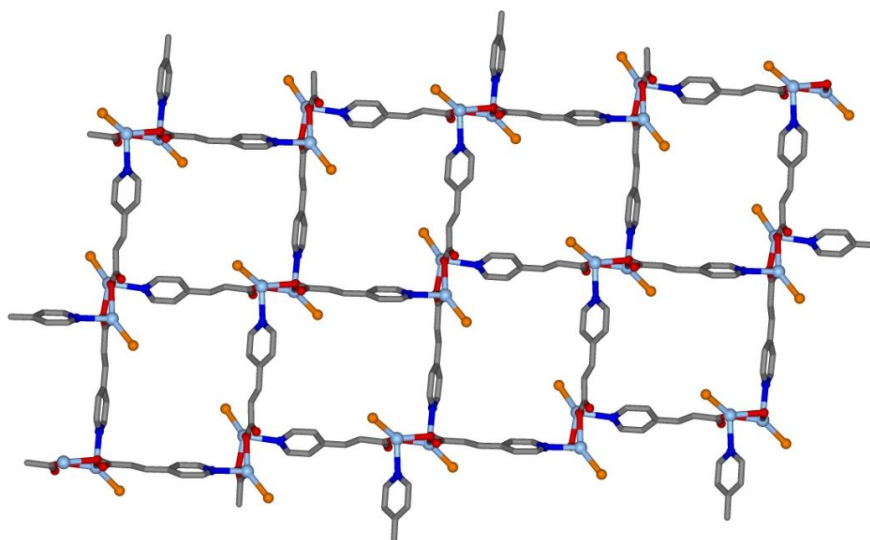
Figure 6.2 (4,4) connected tetragonal plane network in **35**. Phenyl rings of PPh$_3$ and solvent molecules are omitted for clarity.

6.2.2 Structural Description of [Ag$_2$(3-PA)(dppm)$_2$]BF$_4$·(2CH$_3$CN) (36)

The macrocyclic compound of composition [Ag$_2$(3-PA)(dppm)$_2$]BF$_4$·(2CH$_3$CN) (36) was refined in the monoclinic space group, $C2/c$ where 7 phenyl groups of dppm were found to be disordered. The extra BF$_4^-$ anion are present to balance the excess positive charge on Ag(I) which are not compensated by 3-PA. There are two distinct Ag(I) ions having coordination numbers 3 and 4 respectively. Two dppm ligands bridge two Ag(I) and adopt 'U' shaped conformation. In addition to dppm, carboxylate group of 3-PA further bridges two Ag(I) in µ$_{1,3}$ fashion that results the distance between them to be 2.897 Å which reflects stronger ligand supported argentophilic (Ag···Ag) interaction. Two P donor sites from two dppm and one carboxylate O from 3-PA are coordinated to Ag1. The angles between the coordinating atoms centring Ag1 are 111.2°, 112.8°, 134.6° and it occupies a position 0.167 Å above the plane composed of the coordinating O and two P atoms. On the other hand for Ag2, the additional coordination is offered by the pyridyl N of 3-PA that result the coordination geometry to be distorted tetrahedral. Now, the 3-PAs being angular spacer ligand, are able to form 16-membered macrocyclic ring while bridging Ag1 and Ag2, where they are found in *head*-to-*tail* orientation on the same plane with a distance of 5.629Å between two C=C bonds (Figure 6.3). These macrocycles stack along *b*-axis and the distance between the centres of such macrocycles is 12.76 Å, whereas the same for two neighbouring macrocycles on the *ac*-plane is 15.02 Å. Due to presence of bulky phenyl rings around the macrocycles, there is no scope for C=C bonds of 3-PA to stack closely between two macrocyclic moieties.
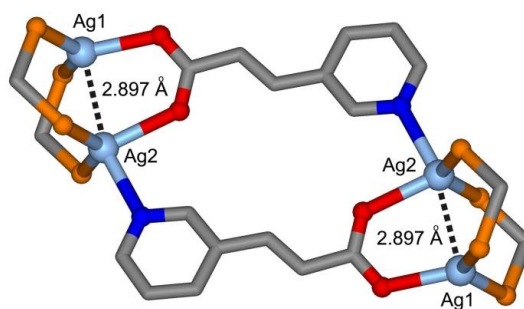
Figure 6.3 16-membered macrocyclic ring structure of **36**. The phenyl rings of dppm, BF_4^- anions and solvent molecules are omitted for clarity.

6.2.3 Structural Description of [Ag$_2$(4-PA)$_2$(dppe)]·CH$_3$CN (37)

The coordination polymer of composition [Ag$_2$(4-PA)$_2$(dppe)]·CH$_3$CN (**37**) crystallizes in the triclinic space group, $P\bar{1}$. In this structure one phenyl ring of dppe and one 4-PA ligand were found disordered. There are two crystallographically distinct Ag(I) atoms in the structure and both Ag(I) have distorted tetrahedral geometries (Figure 6.4). The coordination geometries are completed by one P from dppe, one N from 4-PA and two O from two bridging 4-PA ($\mu_{1,1}$) from opposite side and in this way Ag$_2$O$_2$ four-membered core is formed. Ag1 and Ag2 form two different Ag$_2$O$_2$ cores with Ag···Ag distance of 3.849 and 3.698 Å, as shown in Figure 6.5 and a dihedral angle of 83.6°. A detailed scrutiny to the structure revealed the formation of 28-membered macrocyclic ring as both the 4-PA and dppe ligands bridge Ag1 and Ag2. The 4-PA ligands at the opposite sides of the macrocycles are oriented in *head-to-tail* fashion and are away from each other by 6.54 Å. The topological analysis of this three periodic net resulted in 6-connected, uninodal, α-Po primitive cubic (pcu) net (Figure 6.6).
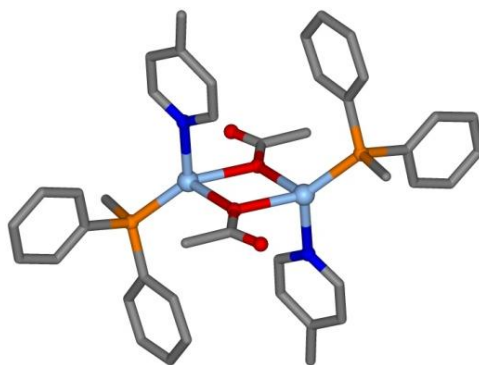
Figure 6.4 A part of the connectivity showing the formation of Ag$_2$O$_2$ ring in **37**.
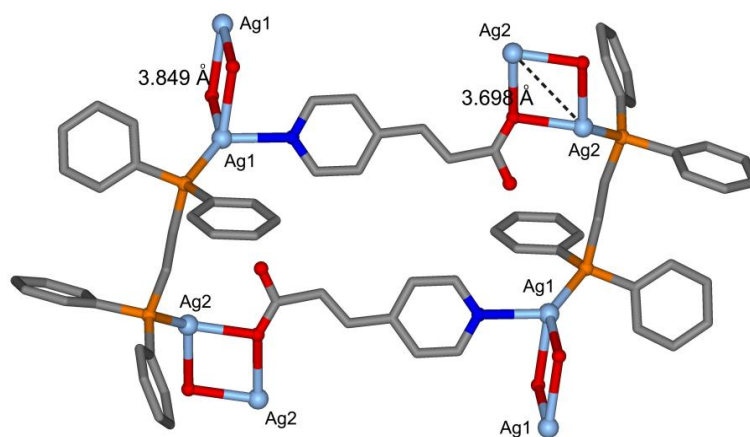
Figure 6.5 28-Membered macrocyclic ring as a part of the three dimensional network in **37**.
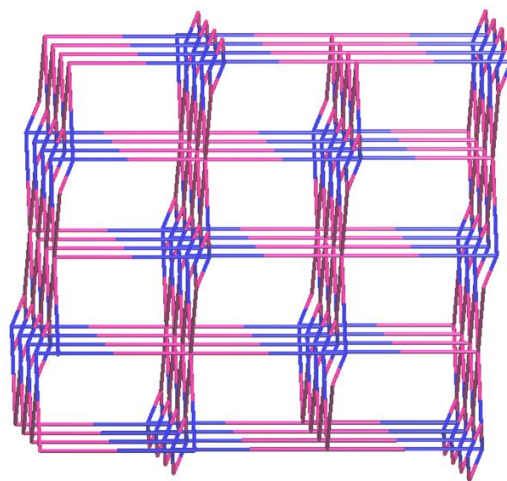
Figure 6.6 6-connected, uninodal, α-Po primitive cubic (pcu) net in **37**.

6.2.4 Structural Description of [Ag$_2$(4-PA)$_2$(dppp)]·(3H$_2$O)(0.5Et$_2$O) (38)

The coordination polymer of composition [Ag$_2$(4-PA)$_2$(dppp)]·(3H$_2$O) (0.5Et$_2$O) (38) crystallizes in the orthorhombic space group, *Pnma*. The cluster of solvents molecules sit on the mirror plane and the hydrogen atoms of the water molecules are not located. All the Ag(I) are equivalent and adopt distorted tetrahedral coordination geometry – one P from dppp, one N from 4-PA, and two bridging O from two 4-PA ($\mu_{1,1}$) at the opposite side to form Ag$_2$O$_2$ core with Ag···Ag distance of 3.95 Å as shown in Figure 6.7. Only one O of the carboxylate group participates in coordination. The coordination environment around Ag(I) and the formation of Ag$_2$O$_2$ core resemble 35, apart from the polymeric connectivity arising from dppp ligand as opposed to the terminating ligand PPh$_3$ in 35. Both 4-PA and dppp ligands bridge Ag(I) to form 30-membered and 36-membered metallo-macrocyclic rings as shown in Figure 6.8a, b. The 4-PA ligands at the opposite sides of the 30-membered macrocycle are oriented in *head*-to-*head* fashion with a distance of 6.61 Å between C=C bonds. On the other hand, the 4-PA ligands at the opposite sides of the 36-membered macrocycle are oriented in *head*-to-*tail* fashion with the distances of 10.56 Å and 13.14 Å between C=C bonds. The topological analysis of this three periodic net also resulted in 6-connected, uninodal, α-Po pcu net (Figure 6.8c).[7]
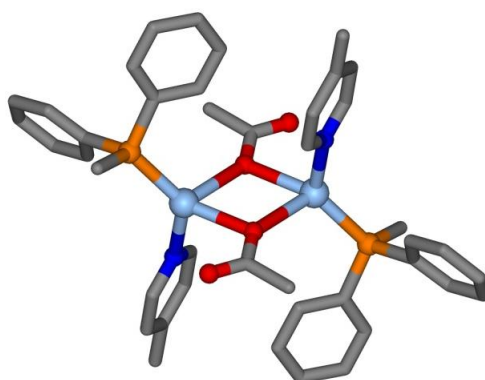
Figure 6.7 A part of the connectivity showing the formation of Ag$_2$O$_2$ ring in 38.
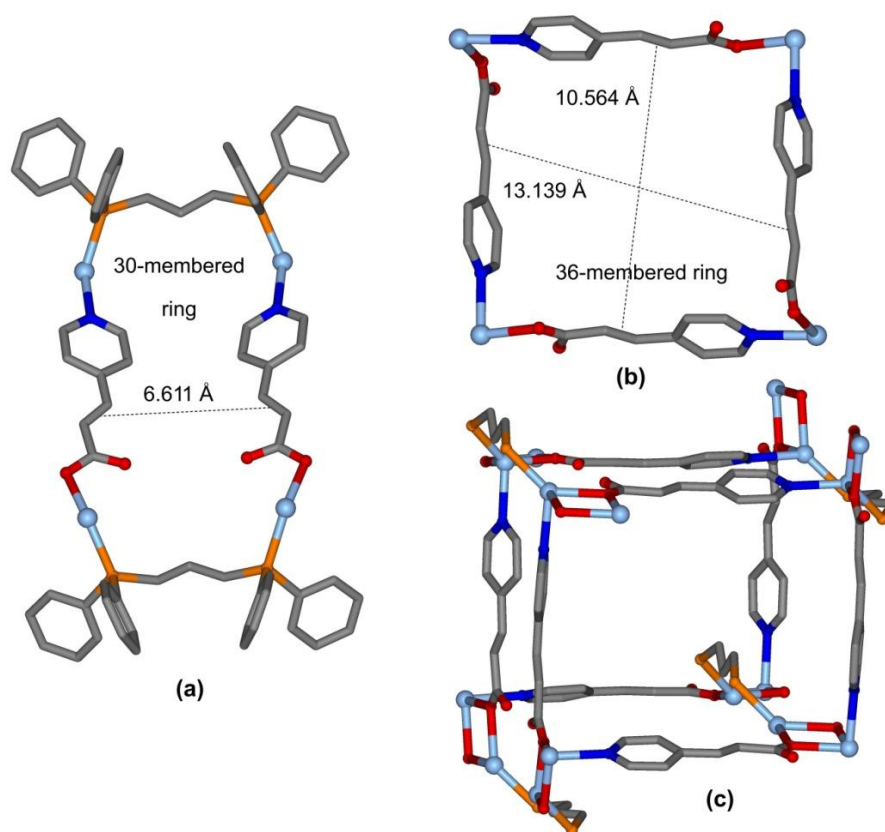
Figure 6.8 30-membered macrocyclic ring (a), 36-membered macrocyclic ring (b) and the cubic moiety (c) as a portion of the three dimensional 'pcu' network in **38**

6.2.5 Structural Description of [Ag(3-PA)(dppp)$_{0.5}$]·H$_2$O (39)

The coordination polymer of composition [Ag(3-PA)(dppp)$_{0.5}$]·H$_2$O (**39**) crystallizes in the monoclinic space group, *C*2/*c*. The coordination number of the symmetrically equivalent Ag(I) is 3; one P from dppp, one N from 3-PA and one monodentate carboxylate O from 3-PA. The angles at the Ag(I) center are 87.0°, 132.6° and 135.3° and Ag(I) is 0.29 Å above the NOP plane. The coordination geometry can better be represented as distorted and flattened pyramidal. The 3-PAs being angular spacer ligand, are able to form 16-membered metallo-macrocycle while bridging two Ag(I) where they are oriented in *head*-to-*tail* fashion with a distance of 5.45 Å between two C=C bonds (Figure 6.9). The Ag(I) ions are bridged by both the 3-PA and dppp ligand and the coordination network grows to form 1D wave-like polymer propagating along *c*-direction (Figure 6.10). The water molecule present in

the structure involves in H-bonding with the non-coordinating carbonyl-O of 3-PA. The 1D zigzag chains further interact via H-bonding and van der Waals interaction between carbonyl-O atoms (2.710 Å).
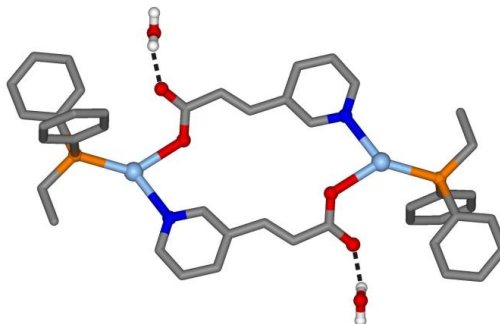
Figure 6.9 The 16-membered metallo-macrocycle observed in **39**.
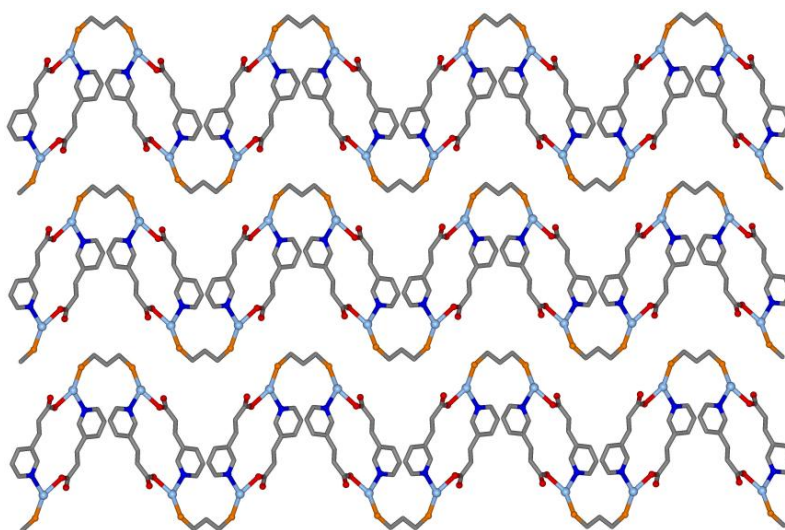
Figure 6.10 One-dimensional zigzag chains in **39** propagate along the *c*-direction. The phenyl rings of dppp and water molecules are omitted for clarity.

6.2.6 Structural Description of [Ag$_4$(dppm)$_4$(PVBA)$_2$](TFA)$_2$ (40)

The coordination polymer of composition [Ag$_4$(dppm)$_4$(PVBA)$_2$](TFA)$_2$ (**40**) crystallizes in the monoclinic space group, *P*2$_1$/*c*. There are four crystallographic independent Ag(I) atoms in the asymmetric unit with coordination numbers of 3 and 4 (Figure 6.11). The TFA anions are present to balance the charge on Ag(I) which are not compensated by insufficient PVBA anions. Each carboxylate of PVBA ligand is

bridging two Ag(I) in $\mu_{1,3}$ fashion with distances of 2.96 Å (between Ag1 and Ag2) and 2.97 Å (between Ag3 and Ag4) reflecting strong ligand supported argentophilic interactions. The dppm ligands coordinate two Ag(I) in bridging fashion. Ag1 and Ag4 have coordination number 3 from two P and one O with almost planar geometry. The angles at the Ag1 are 111.0, 117.6 and 130.4° and Ag1 is shifted from the POP plane by 0.137 Å. Ag4 has similar highly distorted and flattened pyramidal geometry with angles 115.6, 119.4 and 124.0° and Ag4 is deviated from the POP plane by 0.14 Å. On the other hand, the coordination geometry at Ag2 and Ag3 is distorted tetrahedral. The overall structure of this compound is one-dimensional polymeric zigzag chain which propagates along *a*-axis (Figure 6.12). The shortest distance between C=C bonds (interchain) in the lattice is 8.74 Å.
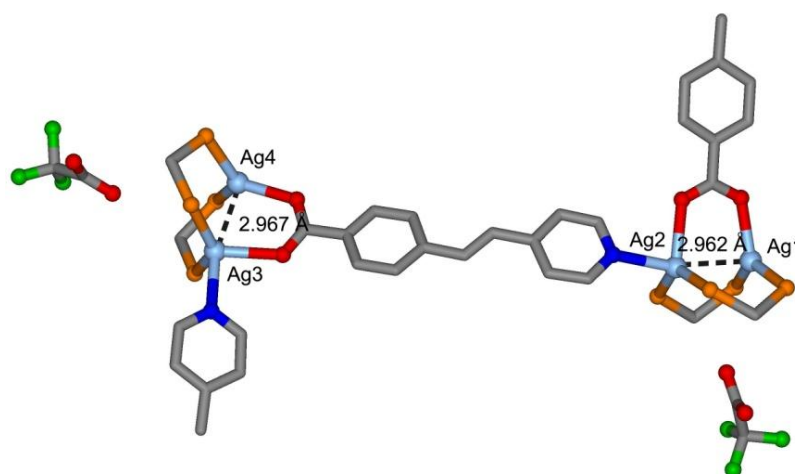
Figure 6.11 A part of the connectivity in **40**, phenyl rings are omitted for clarity.

Another interesting aspect of this structure is the shape of PVBA. It adopts a bow like shape instead of being planar. The centre of the C=C bond lies 0.58 Å away (either below or above) from the plane of N, and two O. In other way, the midpoint of two O atoms lays 1.50 Å away from the plane of the pyridyl ring. Another peculiar point is to note that the pyridyl N coordinates to Ag(I) in a nonlinear way; Ag2 and Ag3 sit 0.78 and 0.64 Å away from the plane of the pyridyl group (Figure 6.13).

These observations reflect that unlike 3-PA and 4-PA, PVBA is present in a very strained environment.
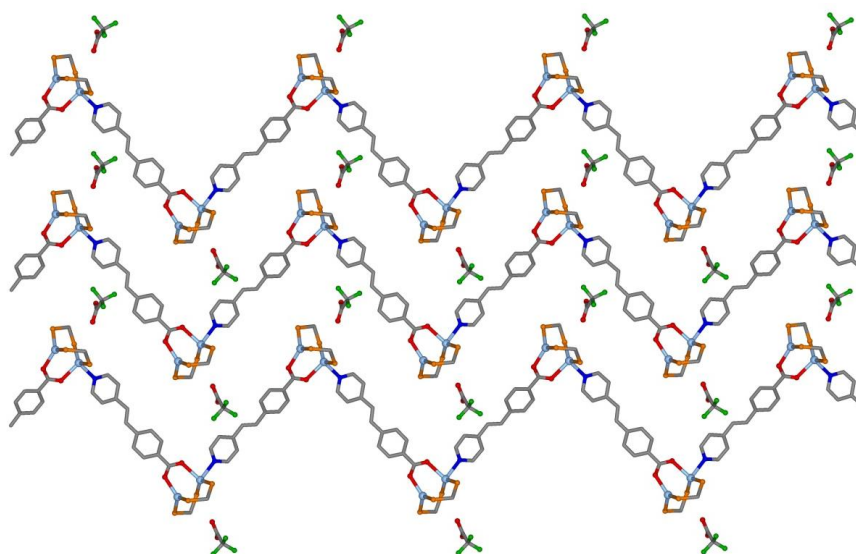
Figure 6.12 The zigzag 1D coordination polymeric structures of **40**, phenyl rings of dppm are omitted for clarity.
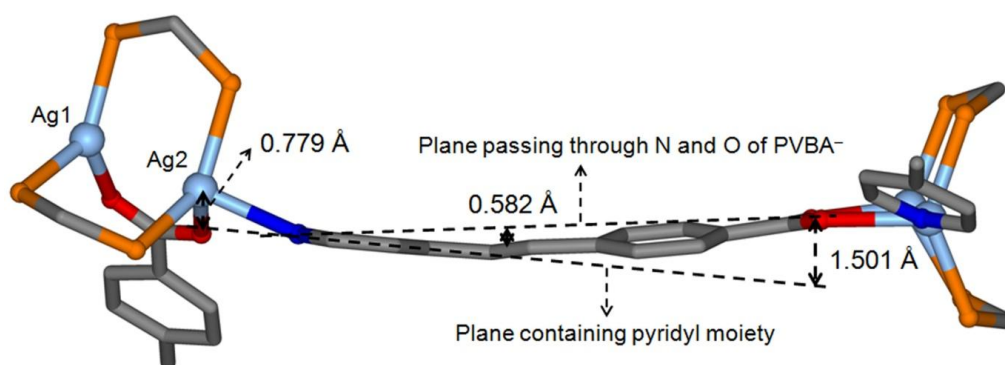
Figure 6.13 The strained conformation of PVBA in **40**, showing different aspects of deviation.

6.27 Structural Description of [Ag$_2$(4-SP)$_2$(dppe)(TFA)$_2$] (41)

The dinuclear, discrete and neutral coordination complex of composition [Ag$_2$(4-SP)$_2$(dppe)(TFA)$_2$] (**41**) crystallizes in the monoclinic space group, $P2_1/n$. The TFA anions were found to coordinate Ag(I) in addition to balancing the charge. One 4-SP coordinate to each Ag(I). The dppe ligand bridges two Ag(I) in *transoid* fashion and thus the silver ions are far away and unable to exert any argentophilic interaction

159

....

(Figure 6.14a). The coordination geometry at Ag(I) is triangular with the angles at the

AgNOP core are 103.4, 114.1 and 134.8°, where Ag(I) occupies 0.364 Å above the

NOP plane. As there is no argentophilic interaction, 4-SP ligands are also found not

to orient parallel and the shortest distance between the centres of two C=C bonds was

found to be 7.31 Å. The solid state structure is stabilised by various π-π stacking

interactions as shown in Figure 6.14b. The pyridyl moieties of 4-SP are found to

stack parallel but in opposite direction with a distance of 3.54 Å indicating significant

π-π stacking interactions. On the other hand, the phenyl ring of 4-SP has partial

interaction with the phenyl ring of dppe.
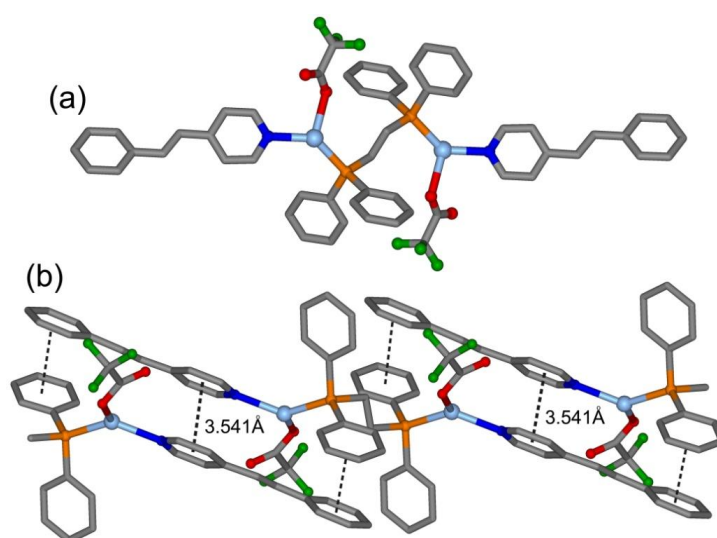
Figure 6.14 The structure of the discrete complex (a) and various kinds of π-π
stacking interactions (b) in **41**.

6.2.8 Structural Description of [Ag$_2$(dppm)(4-SP)$_2$][Ag$_2$(dppm)$_2$]$_{0.5}$(BF$_4$)$_3$·2(THF) (**42**)

The mixed coordination compound of composition [Ag$_2$(dppm)(4-SP)$_2$][Ag$_2$(dppm)$_2$]$_{0.5}$(BF$_4$)$_3$·2(THF) (**42**) contains two discrete cationic moieties [Ag$_2$(dppm)(4-SP)$_2$]$^{2+}$ and [Ag$_2$(dppm)$_2$]$^{2+}$. The asymmetric unit contains one [Ag$_2$(dppm)(4-SP)$_2$]$^{2+}$, half of the cation [Ag$_2$(dppm)$_2$]$^{2+}$, three BF$_4^-$ anions and two THF solvent molecules. The BF$_4^-$ anions balance the charge of Ag(I) and THF fill up

the void space in the lattice. The $[Ag_2(dppm)_2]^{2+}$ cation is more stable due to its ring structure as compared to $[Ag_2(dppm)_2(4\text{-}SP)_2]^{2+}$ and it is likely to be present in the solution along with other species and crystallized along with $[Ag_2(dppm)_2(4\text{-}SP)_2]^{2+}$. In both the cationic fragments, the dppm bridges two Ag(I) in *cissoid* conformation to bring them closer (Figure 6.15). In the cation $[Ag_2(dppm)_2]^{2+}$, both the Ag(I) have coordination number of 2 and adopt almost linear geometry with P-Ag-P angle of 173.3°. The distance of 3.04 Å between two Ag(I) indicate the presence of significant argentophilic interaction between them.
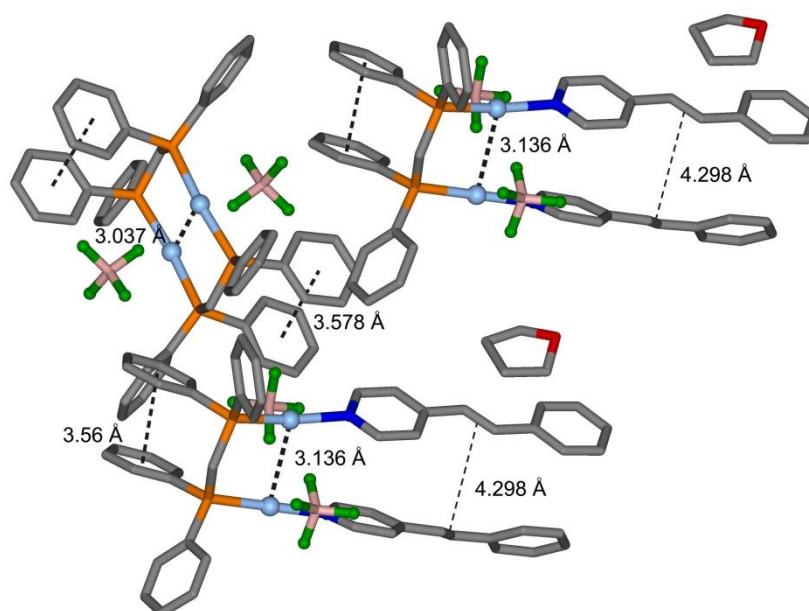
Figure 6.15 Two discrete cationic moieties $[Ag_2(dppm)(4\text{-}SP)_2]^{2+}$ and $[Ag_2(dppm)_2]^{2+}$ in the solid state structure of **42**

The structure of the $[Ag_2(dppm)(4\text{-}SP)_2]^{2+}$ cation is very interesting. Both the Ag(I) atoms are bonded to one P from dppm and one N from 4-SP to have linear geometry with P-Ag-N angles 177.2 and 165.5°. The *cissoid* conformation of dppm clips two Ag(I) closer (Ag···Ag distance 3.14 Å) and as a result the coordinating 4-SP ligands from the other side also are brought closer. However, these two 4-SP ligands are crisscross to each other keeping the distance of 4.3 Å between the centres of C=C bonds (Figure 6.16). Although, the distance is slightly more than the

permitted distance in Schmidt's postulate, this compound was found to be photoreactive as indicated from ^{1}H NMR spectroscopy by the presence of a new peak for cyclobutane protons at δ 4.59 ppm after irradiation under UV light for 35 h. The photodimerization reaction of 4-SP in the solid state in *head-to-head* fashion *viz.* the synthesis of 1,2-bisphenyl-3,4-bis-(4'-pyridyl)cyclobutane was reported before.[8]
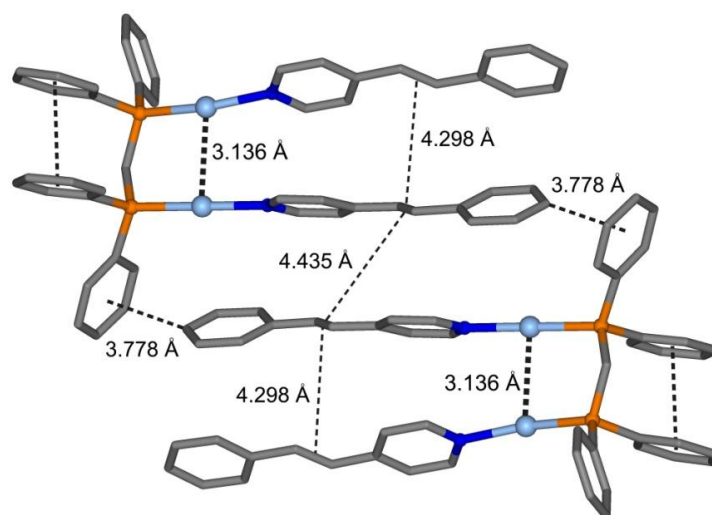
Figure 6.16 The relative dispositions of photoreactive $[Ag_2(dppm)(4\text{-}SP)_2]^{2+}$ cations.

Now if we look at the relative orientations of the photoreactive $[Ag_2(dppm)(4\text{-}SP)_2]^{2+}$ cations, we can see the infinite parallel and crisscross arrangements of 4-SP ligands both in *head-to-head* and *head-to-tail* fashion. The distances between C=C bonds of two consecutive molecules (centroid-to-centroid distances) forming the pair may be important to rationalize the observed photoreactive behaviour. The distancefor HT-pair is 4.44 Å which is beyond Schmidt's distance criteria; whereas, the same for HH-pair is 4.3 Å which is just beyond but can be considered at the borderline. Therefore, it is most likely that would undergo photodimerization in HH-fashion. On the other hand relative orientations of the C=C bonds may also be important. In the intramolecular pair, the C=C bonds are crisscrossed but the intermolecular 4-SP pairs are slip-stacked. The phenyl ring of 4-SP ligand is C-H···π bonded to one of the dppm phenyl rings (Figure 6.16). This appears to hinder the

lateral movements of the 4-SP ligands thus prevent these C=C bonds to dimerize to yield HT dimerized product. By comparing the chemical shift and splitting pattern of the peak(s) for cyclobutane protons as reported in literature,[9] we have confirmed that it, in fact, underwent photodimerization in HH-fashion (Figure 6.17).
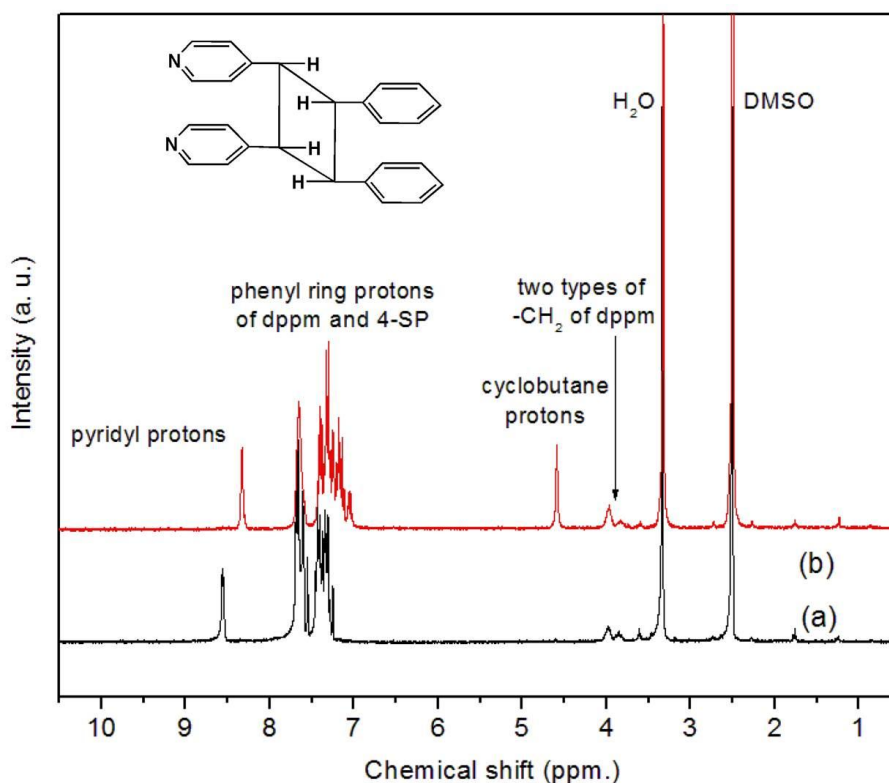
Figure 6.17 ^{1}H NMR spectra of **42**, before (a) and after (b) UV irradiation

6.3 Comparative Discussion on 35 - 42

In the series of the above compounds, we have obtained 0D, 1D, 2D and 3D silver based coordination compounds and polymers. When Ag(I) salt was allowed to react with Na-salt of 4-PA and monodentate PPh$_3$, a two-dimensional coordination polymer **35** was obtained whose topology was determined to be (4, 4) connected uninodal sql/Shubnikov tetragonal plane net. In this compound Ag(I) was found to have a distorted tetrahedral geometry and formed Ag$_2$O$_2$ core that contributes as the node for the 4-connected tetragonal net. When monodentate terminal PPh$_3$ ligand was replaced by the bridging dppe ligand, a coordination polymer **37** was obtained. Ag$_2$O$_2$

core was found to form in **38** with similar coordination environment and geometry around Ag(I). The phosphine derived ligand dppe being able to bridge between two of such Ag_2O_2 cores, resulted in three periodic network structure whose topology was determined to be 6-connected, uninodal, α-Po primitive cubic (pcu) net. When the chain length of the diphosphine ligand was increased with dppp, the coordination polymer **38** obtained was found to contain similar Ag_2O_2 core as in **35** and **37**, having similar coordination number and geometry around Ag(I). **38** was found to have same topology as in **37**, although they are not isostructural. Therefore, in all the compounds where 4-PA was used as spacer ligand, Ag_2O_2 core was constructed by $\mu_{1,1}$ bridging mode of 4-PA and the coordination environments and geometries were found similar. When an angular spacer 3-PA was introduced along with dppp instead of linear 4-PA, a 1D coordination polymer **39** was obtained. Instead of forming an Ag_2O_2 core, here Ag(I) was found to have coordination number of 3 with distorted flattened pyramidal geometry where carboxylate groups coordinate in monodentate fashion instead of bridging mode. When a relatively shorter bridging diphosphine dppm was used the macrocyclic compound **36** was obtained where two Ag(I) are brought closer by the 'U' shaped conformation of dppm leading to stronger ligand supported argentophilic interaction. Although, similar building unit $Ag_2O_2P_4$ was observed for **36** and **40**, the polymeric zigzag chain resulted in **40** in contrast to macrocyclic ring in **36** due to the stoichiometry of dppm and Ag(I) in the product. In **37** and **38**, we find the macrocyclic rings containing four Ag(I) composed of both the bridging 4-PA, diphosphine ligands. On the other hand, 3-PA being an angular spacer, can form rings containing Ag(I) alone, as can be observed in **36** and **39**.

So far we have discussed, there are no macrocycle or polymers where these pyridylcarboxylates were found in parallel orientation within a distance allowed for [2 + 2] cycloaddition reaction and in fact, none of these compounds (**35** − **40**) underwent the same. We anticipate that the formation of macrocyclic structure, as

....

discussed in the Scheme 6.1, is not easy as it is difficult to control the coordinative modes of carboxylate 'O's to Ag(I). The carboxylate group, having higher affinity to metal ions with negatively charged 'O' donor, coordinate to Ag(I) in various ways like monodentate, $\mu_{1,1}$ bridging, $\mu_{1,3}$ bridging and so on. We therefore have chosen 4-SP as monodentate ligand with pyridyl 'N' donor site.

The formation of macrocyclic structure is restricted for 4-SP as it is a monodentate terminal ligand. However, we expected it to furnish 'U' shaped discrete, cationic complexes where we might find parallel arrangement of 4-SP due to argentophilic interaction. We have obtained two discrete cationic complexes **41** and **42** with dppe and dppm as auxiliary ligand respectively. However, we have obtained the desired 'U shaped conformation of dppm in **42** where we have found Ag(I) to exert argentophilic interaction (Ag···Ag distance is 3.136 Å). The 4-SP ligand was found to orient crisscross in *head-to-head* fashion and the compound was found to be photoreactive. The structure can be correlated with parallel arrangement of nicotinic acid and isonicotinic acid in Au(I)-dppm complexes via aurophilic interaction, reported by Hor and coworkers.[6c]

Now, if we consider the compounds containing dipyridyl bridging ligands, the *cissoid* conformation and hence argentophilic interactions were observed only for compounds containing dppm (compounds **36**, **40** and **42**) bridging ligand. In both the compounds **37** and **41**, due to the transsoid conformation of dppe bridging ligand, Ag(I) are far away from each other having no scope for exerting aregntophilic interaction. Among two analogous compounds **41** and **42**, the *cissoid* conformation of dppm in **42** lead to parallel orientation of 4-SP which underwent photodimerization. However, due to *transsoid* conformation of dppe in **41**, 4-SP had no scope of parallel arrangement. Although, in case of longer dppp *cissoid* type conformation was observed in **38** and **39**, they were found photostable as Ag(I) centres are far away from each other having no scope of exerting argentophilic interaction. These

Chapter 6

....

observations certainly demonstrate the roles chain length of diphosphine bridging ligands for the parallel orientation of olefins via argentophilic interaction.

6.4 Summary

In this chapter several Ag(I) based coordination compounds containing certain pyridyl, pyridyl carboxylate and phosphine derived ligands in the context of solid state structure and photoreactivity have been presented. Variable coordination numbers and geometries around Ag(I) have been accounted by different shapes of the pyridyl carboxylates and length of the diphosphine ligands. It has been observed that the coordination environments and geometries around Ag(I) are highly dependent on the coordination mode of carboxylate 'O', whether monodentate or $\mu_{1,1}$ bridging or $\mu_{1,3}$ bridging. On the other hand, the dimensionality of the coordination polymers depends on the bridging diphosphine ligands and shape of the pyridyl carboxylates. We conclude that the formation of macrocycles of Ag(I), suitable for photodimerization reaction, with pyridylcarboxylate ligands may be difficult to accomplish compared to monodentate pyridyl ligands.

6.5 Syntheses and Characterizations

3-PAH, 4-SP, Ag-TFA, AgBF$_4$, dppm, dppe and dppp were purchased from common commercials sources and were used as received without any further purification. 4-PAH[10] and HPVBA[11] were synthesized according to modified literature reported procedure. Generally, all these compounds were synthesized from aqueous THF and then the single crystals were grown by following various techniques as described below.

[Ag$_2$(4-PA)$_2$(PPh$_3$)$_2$]·(Et$_2$O)(0.5CH$_3$CN)(2.5H$_2$O) (35)

Ag-TFA (22 mg, 0.1 mmol) and PPh$_3$ (27 mg, 0.1 mmol) were stirred in 6 mL THF for an hour. Then 4-PAH (15 mg, 0.1 mmol) neutralised with equivalent amount

....

of NaOH (aq.) in 3 mL water was added drop wise. White precipitate was formed and the mixture was continued stirring for another hour. White ppt was filtered off and washed with water and THF. The dried ppt was dissolved in 10 mL 1:1 mixture of water and acetonitrile and then diethyl ether was layered over this solution. Diffraction quality single crystals were obtained after a few days. Yield 70%.

^{1}H NMR (300 MHz, d_6-DMSO, 298K): δ_H = 8.54 (d, Py-H), 7.54-7.49 (m, Ar-H, PPh3 and Py-H), 7.24 (d, CH=CH), 6.77 (d, CH=CH). The observed solvent loss 5.6% in TGA experiment was compared with calculated value 5.9% for the composition $C_{53}H_{48.5}Ag_2N_{2.5}O_{6.5}P_2$ (excluding diethylether molecules and adding hydrogen atoms for water molecules to the formula unit). Analysis found (%): C 57.70, H 4.65, N 2.68; $C_{53}H_{48.5}Ag_2N_{2.5}O_{6.5}P_2$ requires C 57.76, H 4.44, N 3.18.

$[Ag_2(3\text{-}PA)(dppm)_2]BF_4 \cdot (2CH_3CN)$ (36)

AgBF$_4$ (19 mg, 0.1 mmol) and dppm (19 mg, 0.05 mmol) were stirred in 6 mL THF for an hour and then 3-PAH (15 mg, 0.1 mmol) neutralised with equivalent amount of NaOH (aq.) in 3 mL water was added drop wise. The mixture was continued stirring for another hour. White ppt formed was filtered off, washed and dried. The dried ppt was dissolved in 8 mL 1:1 mixture of water and acetonitile. The diffraction quality single crystals were obtained by evaporating this solution slowly. Yield 62%.

^{1}H NMR (300 MHz, d_6-DMSO, 298K): δ_H = 8.84 (s, Py-H), 8.53 (d, Py-H), 8.15 (d, Py-H), 7.69-7.63 (m, Ar-H, dppm), 7.55 (d, CH=CH), 7.44 (dd, Py-H), 7.39 – 7.16 (m, Ar-H, dppm), 6.86 (d, CH=CH). Analysis calculated (%): C 53.49, H 3.67, N 1.42; found: C 55.13, H 3.86, N 3.22. No solvent loss was observed in TGA experiment.

....

[Ag$_2$(4-PA)$_2$(dppe)]·CH$_3$CN (37)

Ag-TFA (22 mg, 0.1 mmol) and dppe (20 mg, 0.05 mmol) were stirred in 6 mL THF for an hour and then 4-PAH (15.0 mg, 0.1 mmol), neutralised in 4mL water by NaOH (aq.), was added dropwise. The mixture was stirred for another 1 h before the white precipitate was filtered, washed and dried. The dried ppt was dissolved in 8 mL 1:1 mixture of water and acetonitrile. Diffraction quality single crystals were obtained by layering diethyl ether over it. Yield 65%.

^{1}H NMR (300 MHz, d_6-DMSO, 298K): δ_H = 8.59 (d, Py-H), 7.74 − 7.67 (m, Ar-H, dppe), 7.61 (d, Py-H), 7.56 − 7.42 (m, Ar-H, dppe) ~2.6 (s, CH-CH, dppe). Analysis calculated (without solvent, %): C 55.54, H 4.13, N 4.42; found: C 55.44, H 5.10, N 3.75. No solvent loss was observed in TGA experiment.

[Ag$_2$(4-PA)$_2$(dppp)]·(3H$_2$O)(0.5Et$_2$O) (38)

AgBF$_4$ (19 mg, 0.1 mmol) and dppp (21 mg, 0.05 mmol) were stirred in 6 mL THF for an hour and then 15 mg (0.1 mmol) 4-PAH neutralised with equivalent amount of NaOH (aq.) in 3 mL water was added dropwise. The mixture was stirred for another 1 h before the white precipitate was filtered, washed and dried. The dried ppt was dissolved in 8 mL 1:1 mixture of water and acetonitrile. Diffraction quality single crystals were obtained by layering diethyl ether over it. Yield 70%.

^{1}H NMR (300 MHz, d_6-DMSO, 298K): δ_H = 8.57 (d, Py-H), 7.65 (m, Ar-H, dppp), 7.57 (d, Py-H), 7.46-7.36 (m, Ar-H, dppp and CH=CH), 6.80 (d, CH=CH), 2.58 (m, CH-CH), 1.75 (m, CH-CH). Analysis found (%): C, 53.56, H, 4.26, N, 2.77; C$_{45}$H$_{43}$Ag$_2$N$_2$O$_{7.5}$P$_2$ requires C, 53.54, H, 4.29, N, 2.77. The observed weight loss 5.9% in TGA can be matched with the calculated value 5.5% (excluding diethyl ether).

....

[Ag(3-PA)(dppp)$_{0.5}$]·H$_2$O (39)

AgBF$_4$ (19 mg, 0.1 mmol) and dppp (21 mg, 0.05 mmol) were stirred in 5 mL THF for an hour and then 3-PAH (15 mg, 0.1 mmol) neutralised with equivalent amount of NaOH (aq.) in 3 mL water was added dropwise. The mixture was stirred for another hour. The white precipitate was filtered, washed with water and THF and then was dried. The dried ppt was dissolved in 8 mL 1:1 mixture of water and acetonitrile. Diffraction quality single crystals were obtained by layering diethyl ether over it. Yield 70%.

^{1}H NMR (300 MHz, d_6-DMSO, 298K): δ_H = 8.74 (s, Py-H), 8.50 (d, Py-H), 8.03 (d, Py-H), 7.69 (m, phenyl), 7.41 (m, phenyl), 7.38 (m, Py-H), 7.35 (d, CH=CH), 6.69 (d, CH=CH). Analysis found (%): C 52.19, H 4.00, N 2.75. The observed water loss in TGA experiment was found 6.1% which can be matched by adding one extra mole of water in the formula unit (calculated value 5.5%) which support the analysis data. C$_{43}$H$_{44}$Ag$_2$N$_2$O$_7$P$_2$ requires C 52.78, H 4.53, N 2.86.

[Ag$_4$(dppm)$_4$(PVBA)$_2$](TFA)$_2$ (40)

Ag-TFA (22 mg, 0.1 mmol) and dppm (38 mg, 0.1 mmol) were stirred in 6 mL THF for an hour and then HPVBA (22 mg, 0.1 mmol) neutralised with equivalent amount of NaOH (aq.) in 4 mL water was added dropwise. The mixture was stirred for another hour. The white ppt was filtered, washed with water and THF and was then dried. The dried powder was dissolved in 8 mL 1:1 mixture of water and CH$_3$CN. Diffraction quality single crystals were grown by slowly evaporation. Yield 78%.

^{1}H NMR (300 MHz, d_6-DMSO, 298K): δ_H = 8.60 (d, Py-H), 8.20 (d, Ar-H), 7.81 (d, Py-H), 7.41 (d, CH=CH), 7.66 (m, Ar-H, dppm), 7.27 (m, Ar-H, PVBA, dppm) 7.12 (m, CH=CH, Ar-H, dppm), 3.85 (m, CH$_2$, dppm). No solvent loss was observed in TGA experiment.

....

[Ag$_2$(4-SP)$_2$(dppe)(TFA)$_2$] (41)

Ag-TFA (22 mg, 0.1 mmol), 4-SP (18 mg, 0.1 mmol) and dppe (20 mg, 0.05 mmol) were stirred in 6 mL THF for 1 h. No ppt was formed. Diffraction quality single crystals were obtained by diffusing hexane over this clear solution. Yield 64%.

^{1}H NMR (300 MHz, d_6-DMSO, 298K): δ_H = 8.56 (4H, d, Py-H), 7.68 − 7.25 (38H, m, Ph (dppe), Ph (4-SP), CH=CH), 3.58 (4H, m CH$_2$-dppe). Analysis found (%): C 56.03, H 3.46, N 2.51; C$_{56}$H$_{46}$Ag$_2$F$_6$N$_2$O$_4$P$_2$ requires C 55.93, H 3.86, N 2.33. No solvent loss was observed in TGA experiment.

[Ag$_2$(dppm)(4-SP)$_2$][Ag$_2$(dppm)$_2$]$_{0.5}$(BF$_4$)$_3$·(2THF) (42)

AgBF$_4$ (19 mg, 0.1 mmol), 4-SP (18 mg, 0.1 mmol) and dppm (19 mg, 0.05 mmol) were stirred in 6 mL THF for an hour. No significant ppt was formed. Diffraction quality single crystals were obtained by diffusing either hexane or ether over this clear solution. Yield 70%.

^{1}H NMR (300 MHz, d_6-DMSO, 298K): δ_H = 8.55 (4H, d, Py-H), 7.68 − 7.24 (58H, m, Ph-H of 4-SP and dppm, Py-H and CH=CH of 4-SP), 3.97 and 3.84 (m, 4H, CH$_2$, dppm). Analysis found (%): C 54.36, H 4.25, N 1.91; C$_{84}$H$_{82}$Ag$_3$B$_3$F$_{12}$N$_2$O$_2$P$_4$ requires C 54.26, H 4.44, N 1.51. The calculated weight loss for this compound is 0.77 %, where ~1 % weight loss was observed in TGA experiment.

After UV irradiation, ^{1}H NMR (300 MHz, d_6-DMSO, 298K): δ_H = 8.32 (4H, d, Py-H), 7.71 − 7.01(50H, m, Ph-H and Py-H of dimer of 4-SP and Ph-H of dppm), 4.59 (s, 4H, CH-CH of dimer of 4-SP), 3.98 and 3.83 (m, 4H, CH$_2$ of dppm).

Comment: In some cases, we observe that there is a little discrepancy in analysis. This is because of the solvent content in the crystalline sample. In some cases, the solvents present in crystal structure are in fractions and also sometimes volatile solvents escape from the system partially.

....

Table 6.1 Crystallographic data for **35 – 38**

Compounds	35	36	37	38
Formula	$C_{57}H_{53.5}Ag_2N_{2.5}$ $O_{7.5}P_2$	$C_{124}H_{112}Ag_4B_2$ $F_8N_6O_4P_8$	$C_{88}H_{78}Ag_4N_6$ O_8P_4	$C_{45}H_{43}Ag_2N_2O_7$ $_{.5}P_2$
M	1171.20	2603.06	1902.92	1009.49
T (K)	100(2)	100(2)	100(2)	223(2)
λ (Å)	0.71073	0.71073	0.71073	0.71073
Cryst syst / Space group	Monoclinic / $P2_1/c$	Monoclinic / $C2/c$	Triclinic / $P\bar{1}$	Orthorhombic / $Pnma$
a (Å)	17.1068(15)	34.344(3)	13.001(3)	17.0341(8)
b (Å)	13.1531(10)	12.7549(10)	13.035(3)	21.3551(10)
c (Å)	25.507(2)	27.197(2)	14.361(3)	13.1534(6)
α (°)	90	90	76.405(5)	90
β (°)	109.460(2)	99.349(2)	67.759(4)	90
γ (°)	90	90	64.723(4)	90
Volume (Å^3) / Z	5411.5(8) / 4	11755.4(17) / 4	2029.2(8) / 1	4784.7(4) / 4
D_{calcd} (g/cm^3) / μ (mm^{-1})	1.438 / 0.837	1.471 / 0.833	1.557 / 1.090	1.401 / 0.934
Reflns col. / Ind. Reflns.	37913 / 12400	34114 / 10338	21551 / 7137	27082 / 4340
R_{int} / Goof on F^2	0.0452 / 1.098	0.0552 / 1.023	0.0835 / 1.072	0.0781 / 1.193
Final R[I>2σ]^a R$_1$ / wR2	0.0522 / 0.1099	0.0537 / 0.1269	0.0773 / 0.1793	0.0762 / 0.1732

^{a} R1 = Σ||F_o| − |F_c||/ Σ|F_o|, ^{b} wR2 = [Σw(F_o^2 − F_c^2)^2/Σw(F_o^2)^2]$^{1/2}$

Table 6.2 Crystallographic data for **39 – 42**

Compounds	39	40	41	42
Formula	$C_{43}H_{42}Ag_2N_2O_6P_2$	$C_{132}H_{108}Ag_4F_6N_2O_8P_8$	$C_{56}H_{46}Ag_2F_6N_2O_4P_2$	$C_{84}H_{82}Ag_3B_3F_{12}N_2O_2P_4$
M	960.47	2643.44	1202.63	1859.44
T (K)	100(2)	100(2)	100(2)	100(2)
λ (Å)	0.71073	0.71073	0.71073	0.71073
Cryst syst / Space group	Monoclinic / $C2/c$	Monoclinic / $P2_1/c$	Monoclinic / $P2_1/n$	Triclinic / $P\bar{1}$
a (Å)	16.2454(16)	23.267(3)	12.550(2)	11.776(2)
b (Å)	14.8766(14)	12.9390(14)	13.733(2)	13.134(2)
c (Å)	17.4915(16)	40.085(5)	14.479(3)	25.916(4)
α (°)	90	90	90	90.704(5)
β (°)	111.531(2)	105.310(3)	90.245(5)	91.621(5)
γ (°)	90	90	90	100.084(5)
Volume (Å³) / Z	3932.3(6) / 4	11640(2) / 4	2495.4(8) / 2	3944.2(12) / 2
D_{calcd} (g/cm³) / μ (mm⁻¹)	1.622 / 1.129	1.508 / 0.842	1.601 / 0.921	1.566 / 0.896
Reflns col. / Ind. Reflns.	13693 / 4507	82078 / 26697	17401 / 5718	42660 / 13854
R_{int} / Goof on F^2	0.0398 / 1.072	0.0338 / 1.096	0.0254 / 1.062	0.0637 / 1.230
Final R[I>2σ][a] R_1 / wR2	0.0427 / 0.0988	0.0469 / 0.1114	0.0326 / 0.0836	0.0966 / 0.2077

[a] $R1 = \Sigma ||F_o| - |F_c||/ \Sigma |F_o|$, [b] $wR2 = [\Sigma w(F_o^2 - F_c^2)^2/\Sigma w(F_o^2)^2]^{1/2}$

6.6 References

1.   (a) Brandys, M.-C.; Puddephatt, R. J., *Chem. Commun.* **2001,** (16), 1508-1509; (b) Irwin, M. J.; Vittal, J. J.; Yap, G. P. A.; Puddephatt, R. J., *J. Am. Chem. Soc.* **1996,** *118* (51), 13101-13102.

2.   Nagarathinam, M.; Peedikakkal, A. M. P.; Vittal, J. J., *Chem. Commun.* **2008,** (42), 5277.

3.   (a) Brandys, M.-C.; Jennings, M. C.; Puddephatt, R. J., *J. Chem. Soc., Dalton Trans.* **2000,** (24), 4601-4606; (b) Irwin, M. J.; Rendina, L. M.; Vittal, J. J.; Puddephatt, R. J., *Chem. Commun.* **1996,** (11), 1281-1282.

4.   (a) Li, C.-P.; Chen, J.; Yu, Q.; Du, M., *Cryst. Growth Des.* **2010,** *10* (4), 1623-1632; (b) Sun, D.; Wei, Z.-H.; Yang, C.-F.; Wang, D.-F.; Zhang, N.; Huang, R.-B.; Zheng, L.-S., *CrystEngComm* **2011,** *13* (5), 1591; (c) Wu, H.; Dong, X.-W.; Ma, J.-F.; Liu, H.-Y.; Yang, J.; Bai, H.-Y., *Dalton Trans.* **2009,** (17), 3162-3174; (d) Liu, D.; Li, H.-X.; Ren, Z.-G.; Chen, Y.; Zhang, Y.; Lang, J.-P., *Cryst. Growth Des.* **2009,** *9* (10), 4562-4566.

5.   (a) Chen, C.; Kang, B.; Su, C., *Aust. J. Chem.* **2006,** *59* (1), 3-18; (b) Pascu, M.; Tuna, F.; Kolodziejczyk, E.; Pascu, G. I.; Clarkson, G.; Hannon, M. J., *Dalton Trans.* **2004,** (10), 1546-1555; (c) Steel, P. J.; Fitchett, C. M., *Coord. Chem. Rev.* **2008,** *252* (8-9), 990-1006; (d) Wang, Y.-L.; Liu, Q.-Y.; Xu, L., *CrystEngComm* **2008,** *10* (11), 1667-1673; (e) Wu, D.-D.; Mak, T. C. W., *J. Chem. Soc., Dalton Trans.* **1995,** (16), 2671-2678.

6.   (a) Puddephatt, R. J., *Chem. Commun.* **1998,** (10), 1055-1062; (b) Che, C.-M.; Tse, M.-C.; Chan, M. C. W.; Cheung, K.-K.; Phillips, D. L.; Leung, K.-H., *J. Am. Chem. Soc.* **2000,** *122* (11), 2464-2468; (c) Teo, P.; Wang, J.; Koh, L. L.; Hor, T. S. A., *Dalton Trans.* **2009,** (25), 5009; (d) Deak, A.; Tunyogi, T.; Tarkanyi, G.; Kiraly, P.; Palinkas, G., *CrystEngComm* **2007,** *9* (8), 640-643.

7.   (a) Blatov, V. A. *TOPOS 4.0 Professional*, Commission on Crystallographic Computing, IUCr: 2006; (b) TOPOS is available at http://www.topos.ssu.samara.ru.

8.   Chu, Q.; Swenson, D. C.; MacGillivray, L. R., *Angew. Chem. Int. Ed.* **2005,** *44* (23), 3569-3572.

9.   (a) Mondal, B.; Captain, B.; Ramamurthy, V., *Photochem. Photobiol. Sci.* **2011,** *10* (6), 891-894; (b) Yamada, S.; Nojiri, Y.; Sugawara, M., *Tetrahedron Lett.* **2010,** *51* (18), 2533-2535; (c) Yamada, S.; Tokugawa, Y., *J. Am. Chem. Soc.* **2009,** *131* (6), 2098-2099.

10.   Marvel, C. S.; Coleman, L. E.; Scott, G. P., *J. Org. Chem.* **1955,** *20* (12), 1785-1792.

11.   (a) Gimeno, N.; Ros, M. B.; Serrano, J. L.; de la Fuente, M. R., *Angew. Chem. Int. Ed.* **2004,** *43* (39), 5235-5238; (b) Kashida, H.; Ito, H.; Fujii, T.; Hayashi, T.; Asanuma, H., *J. Am. Chem. Soc.* **2009,** *131* (29), 9928-9930.

Chapter 7

Crystal Engineering Studies on Functional

Cyclobutane Derivatives for making Co-crystals and
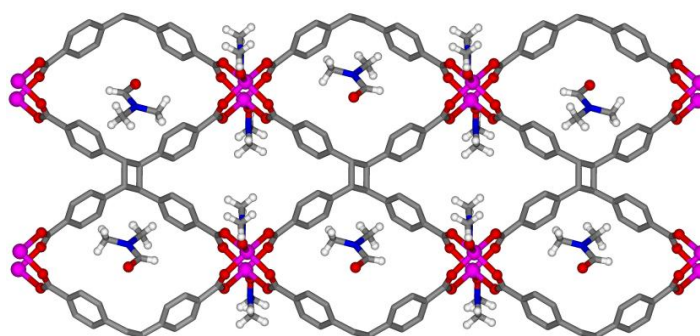
Coordination Polymers[*]

7.1 Introduction

In each of the previous chapters, the solid state photodimerization reaction of several linear spacers containing C=C bond viz. the syntheses of several cyclobutane derivatives with different functional groups have been discussed. It is shown in Chapter 1 that co-crystals and polymorphs have a huge impact in pharmaceutical industries; whereas coordination polymers/MOFs find potential application in gas storage[1], separation[2], catalysis[2b, 3], drug delivery[4] and so on. It is also known in the past that cyclobutane derivatives with pyridyl functionality can be used as potential ligands for synthesizing coordination polymers. MacGillivray *et al.* employed *rctt*-tpcb as four connected square planar ligand to construct 1D and 2D metal organic polyhedra and polygons.[5] Different cyclobutane derivatives (*e.g. rctt*, *rcct*, *rtct* etc) having different geometry, lead to a variety of network topologies in coordination polymers and co-crystals. For example, *rctt*-tpcb has nearly a square planar geometry where as *rtct*-tpcb has an idealized tetrahedral geometry which can furnish different network topologies.[6] Several coordination polymers containing these isomers of cyclobuatne ligands have been reported in the past from our laboratory.[6-7] So far, the research has been focused on the utilization of cyclobutane derivatives made of either pyridyl or carboxylic acid. The ligands with hetero-functionality are expected to provide flexibility and moderate stability in the systems compared to the homo functionality which are often suitable for various properties.

Cyclobutane derivatives *e.g.* TCCB from H₂SDC, HH- & HT-4,4-BPCD from 4-PAH, HH- & HT-3,3-BPCD from 3-PAH and HH- & HT-BPBCCB from HPVBA etc have been synthesized in large scale by solid state photodimerization reaction of molecular salts. This chapter is meant for the crystal engineering studies on these cyclobutane derived compounds exploiting them as ligands for making co-crystals and coordination polymers. The study of sorption properties of porous coordination polymers has also been aimed whenever applicable.

....

7.2 Crystal Engineering Studies on TCCB

7.2.1 Co-crystal of TCCB with 4,4'-Bipyridine (43)

A co-crystal of composition (TCCB)(4,4'-bpy)$_2$·(2DMF) (**43**) using TCCB and 4,4'-bpy was synthesized by dissolving stoichiometric amount of TCCB and 4,4'-bpy (1 : 2) in DMF and the single crystals were grown by evaporating the solution slowly. X-ray crystallography reveals that there are one TCCB, two 4,4'-bpy and two DMF molecules in the asymmetric unit. From the observed values of C=O distances for four carboxylic acid groups [C=O distances are 1.22(8), 1.19(8), 1.22(8) and 1.21(2) Å and corresponding C–OH distances are 1.34(7), 1.33(7), 1.31(7), 1.30(8) Å respectively], it can certainly be called as co-crystal and not a salt. The four carboxylic acid groups of TCCB donates four hydrogen bonding to four different 4,4'-bpy acceptors in $\mathbf{R}_2^2(7)$ fashion. The hydrogen bonding parameters are listed in Table 7.1. Each of the 4,4'-bpy bridges two carboxylic acid groups of two TCCB molecules via H-bonding (Figure 7.1). DMF molecules present in the crystal are found not to participate in H-bonding instead to fill up the void space. There are two types of 4,4'-bpy molecules. One type is almost planar (torsional angle is 5.7° and central C-C bond length is 1.49 Å) and another type is staggered (torsional angle is 31.5° and central C-C bond length of 1.48 Å) and that make two different distances between centroids of cyclobutane rings of 26.525 Å and 25.698 Å respectively. Instead of making a two dimensional sheet-like structure composed of closed circuit hydrogen bonded square nets, the H-bonding propagates with helical segment to form an interpenetrated three dimensional networks (Figure 7.2). The pitch of these helical segments contains four TCCB and four 4,4'-bpy units and propagates along the *b*-direction with the pitch-length of 12.606 Å which is also equal to the unit cell parameter *b*.

Table 7.1 The hydrogen bonding parameters for **43**

D-H⋯A	D(D-H) (Å)	D(H⋯A) (Å)	D(D⋯A) (Å)	<(DHA) (°)	Symmetry Operator
O1-H1⋯N1	0.84	1.85	2.683(7)	173	
O3-H3⋯N4	0.84	1.85	2.686(7)	172	x-1/2, -y+1/2, z
O5-H5⋯N3	0.84	1.83	2.671(7)	174	-x-1/2, y+1/2, z+1/2
O7-H7⋯N2	0.84	1.84	2.675(7)	175	-x+3/2, y-1/2, z+1/2
C37-H37⋯O2	0.95	2.48	3.183(9)	131	
C42-H42⋯O8	0.95	2.57	3.239(8)	128	3/2-x, 1/2+y, -1/2+z
C47-H47⋯O6	0.95	2.50	3.214(8)	132	-1/2-x, -1/2+y, -1/2+z
C48-H48⋯O4	0.95	2.46	3.170(7)	131	1/2+x, 1/2-y, z
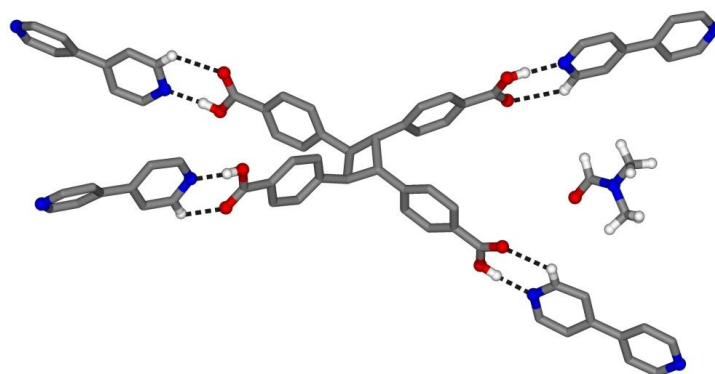
Figure 7.1 The H-bonding pattern in co-crystal **43** is shown.

The degree of interpenetration and the topology of the network was analysed by TOPOS[8] and we found it as a 5-fold interpenetrated 'dmp' network (Figure 7.3 and 7.4).[9] To the best of my knowledge, a maximum of 3-fold interpenetration is reported with organic systems as 'dmp' networks till to date.[10] Therefore, this is the highest degree of interpenetration we have found in this co-crystal. 'dmp' topology was first described by Davide M. Proserpio and thus the name is given. It is similar to diamondoid (dia) topology but the difference arises from the distances, the angles

between the nodes and the presence of additional 2-connected nodal position between each two 4-connected nodes. We know that for an ideal diamondoid net the distances between all nodes are equal and the angle is 109.5°. For this co-crystal, two unequal distances between the nodes are 25.698 and 26.525 Å and the unequal angles around the four connected node are 50.1°, 56.6°, 128.6°, 128.7°, 166.1° and 166.4°.
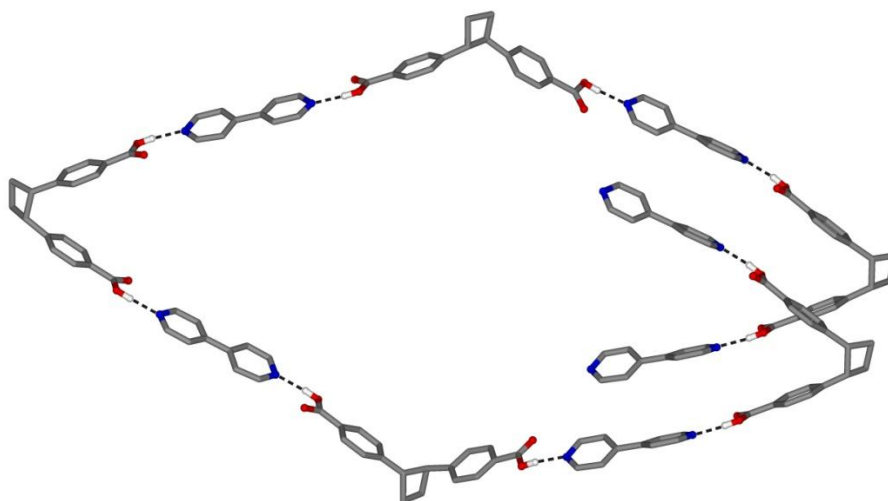
Figure 7.2 Instead of forming 4-connected square net, it forms helical segment (only O-H···N hydrogen bonding is shown).
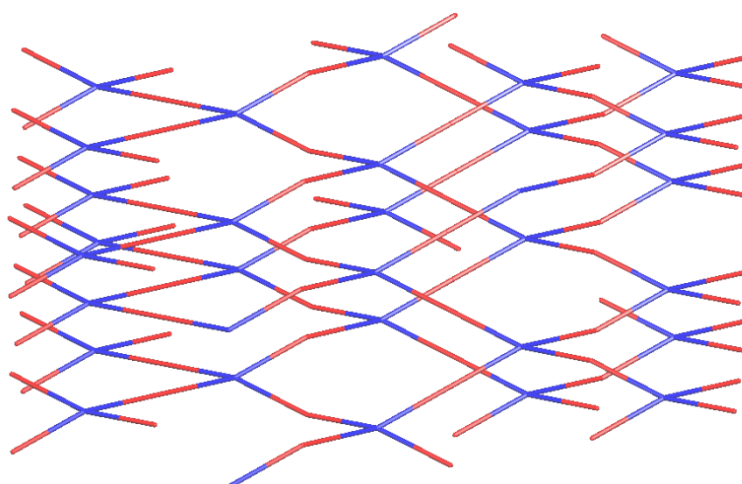
Figure 7.3 A single 'dmp' net, found in **43**
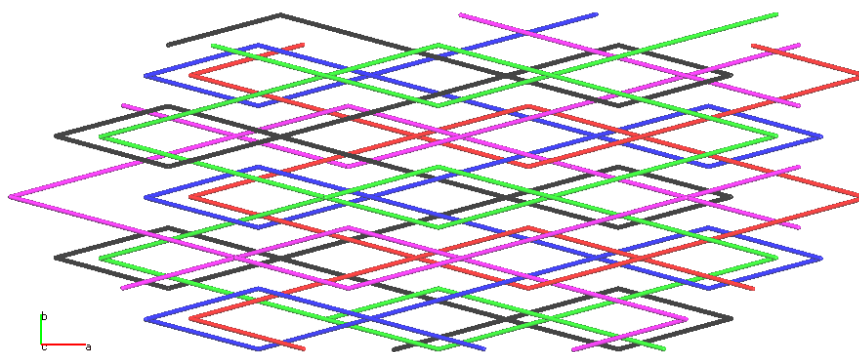
Figure 7.4 5 Different interpenetrated 'dmp' nets are shown in 5 different colours.

7.2.2 Co-crystal of TCCB with 4,4'-bpe (44)

Another co-crystal containing TCCB of composition (TCCB)(4,4'-bpe)·MeOH (**44**) was synthesized by dissolving with 4,4'-bpe in methanol. The asymmetric unit of this co-crystal contains one molecule of TCCB, two halves of 4,4'-bpe (one of which is disordered) and one disordered CH_3OH. From the observed values of C=O bond distances for four carboxylic acid groups [C=O distances are 1.2(3), 1.2(3), 1.2(4) and 1.2(2) Å and corresponding C–OH distances are 1.3(3), 1.3(3), 1.3(4), 1.3(2) Å respectively], it can certainly be called as co-crystal and not a salt. Three kinds of supramolecular synthons namely centrosymmetric carboxylic acid dimer, carboxylic acid dimer via methanol molecule and carboxylic acid-pyridyl H-bonding (Figure 7.5) play principal role to construct two dimensional nets. Each of 4,4'-bpe molecules bridges two carboxylic acid groups of two TCCB molecules and also by H-bonding of carboxyl dimer via methanol molecule form (4,4) connected 2D nets. The hydrogen bonding parameters are listed in Table 7.2. Various types graph set notations of the hydrogen bonded motifs are shown in Figure 7.6 which are $\mathbf{C}(2)$, $\mathbf{R}_2^2(7)$, $\mathbf{R}_2^2(8)$, $\mathbf{R}_4^4(12)$. The four sides of each quadrilateral window of the net are unequal and which are measured as 28.41, 19.49, 28.75 and 16.72 Å. These two dimensional 4-connected uninodal nets are found to stack parallel with a distance of separation 4.44 Å and then further involve in diagonal/diagonal inclined

interpenetration (also known as polycatenation)[11] to generate overall three dimensional network structure with an angle of 61.8° between inclined nets. There are two nodes of two parallel nets on each window of the interpenetrating nets. The nodes of the nets are puckered due to the non-planar geometry of the dimer as shown in Figure 7.7.
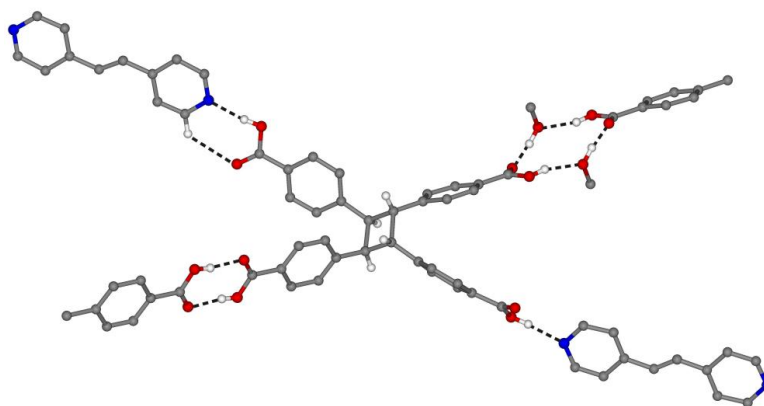
Figure 7.5: A part of the connectivity in the co-crystal **44**

Table 7.2 The hydrogen bonding parameters for **44**

D-H⋯A	D(D-H) (Å)	D(H⋯A) (Å)	D(D⋯A) (Å)	<(DHA) (°)	Symmetry Operator
O1-H1⋯N1	0.83	1.82	2.6(2)	172	
O6-H6...O1S	0.83	1.83	2.6(4)	164	
O6-H6⋯O2S	0.83	2.01	2.8(2)	157	
O7-H7⋯N2X	0.83	1.82	2.6(4)	170	
O7-H7⋯N2	0.83	1.84	2.7(4)	171	
O1S-H1S⋯O5	0.83	2.03	2.7(5)	144	-x+2, -y+2, -z+2
O2S-H2S⋯O5	0.83	1.96	2.6(1)	137	-x+2, -y+2, -z+2
O2S-H2S⋯O2S	0.83	2.09	3(2)	122	-x+2, -y+2, -z+2
C37-H37⋯O2	0.96	2.61	3.3(4)	129	
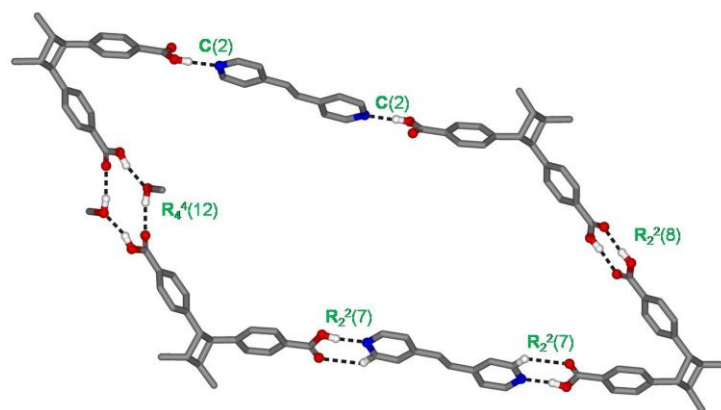
Figure 7.6 The supramolecular synthons that construct the solid state architecture in the co-crystal **44** and the H-bonded motifs are shown.
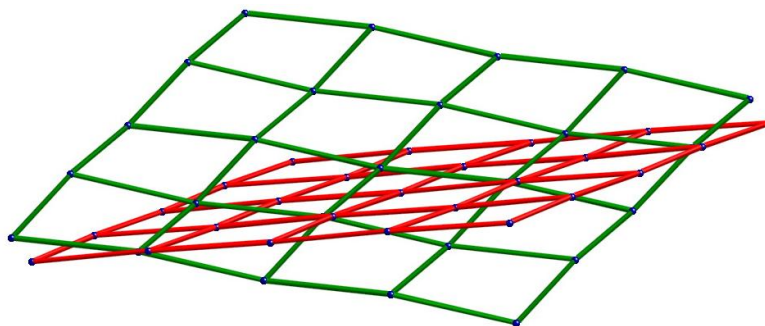
Figure 7.7 (4, 4) connected puckered nets showing diagonal/diagonal inclined interpenetration in the co-crystal **44**.

7.2.3 Co-crystal of TCCB with *trans*-1,2-Bis(4'-pyridyl)ethane (4,4'-bpethane)

Another co-crystal of composition (TCCB)(4,4'-bpethane)·(2DMA)·H$_2$O (**45**) was synthesized by dissolving with 4,4'-bpethane in N,N-dimethylacetamide (DMA) and then by slow evaporation. The asymmetric unit of this co-crystal contains half of the molecule TCCB, half a molecule of 4,4'-bpethane, one DMA and half a water molecule. From the observed values of C=O distances for two carboxylic acid groups in the asymmetric unit [C=O distances are 1.22(3) and 1.20(4) Å and corresponding C–OH distances are 1.3(3) and 1.33(4) Å respectively], it can certainly be called as co-crystal and not a salt. Two diagonally opposite carboxylic acid groups of TCCB donate H-bonding to two 4,4'-bpethane molecules in **R**$_2^2$(7) fashion. The other two

carboxylic acid groups donate H-bonding to DMA molecules and the H-bonding further continues to propagate via water and another DMA molecules to connect finally to a carboxylic acid group of another TCCB (Figure 7.8). Therefore, the growth of the H-bonded network results in (4,4) connected two dimensional network as was observed for **44**. Instead of interpenetrating each other, these two dimensional tetragonal sheets stack parallel in ABAB fashion, perpendicular to b-axis. Two side lengths of these tetragonal nets are 16.76, 27.47 Å and the distance of separation is 5.39 Å which is half of the unit cell parameter *b*. The geometric parameters for hydrogen bonding are listed in Table 7.3.

We attempted to grow single crystals by slowly evaporating DMF solution as described for **45**, which has shown to non-interfere in H-bonding and may lead to a different topology. But the rod-like single crystals obtained were unable to diffract X-ray beam.
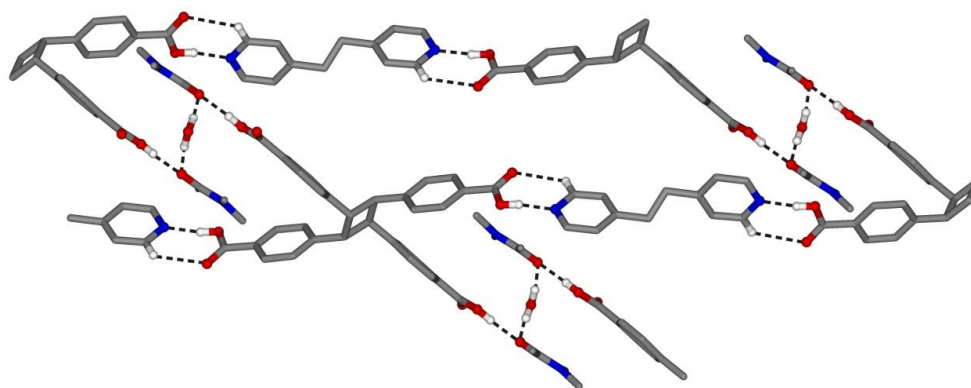
Figure 7.8 The hydrogen bonded connectivity in the co-crystal **45**
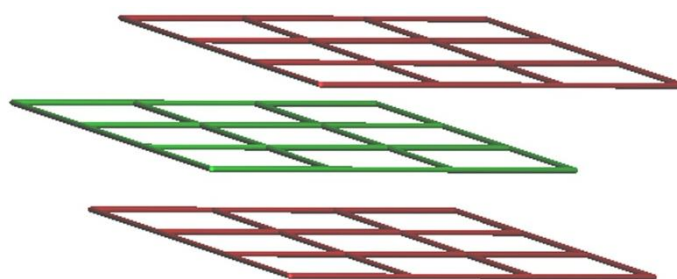
Figure 7.9 The parallel stacking of (4,4) connected tetragonal nets in **45**, perpendicular to *b*-axis.

....

Table 7.3 The hydrogen bonding parameters for **45**

D-H⋯A	D(D-H) (Å)	D(H⋯A) (Å)	D(D⋯A) (Å)	<(DHA) (°)	Symmetry Operator
O1-H1⋯N1	0.84	1.73	2.560(3)	172	x, -1+y, -1+z
O1W-H1WA⋯O5	0.91	1.96	2.855(5)	168(4)	1-x, y, 1/2-z
O3-H3⋯O5	0.84	1.76	2.594(3)	172	1-x, y, 1/2-z
C17-H17⋯O2	0.95	2.57	3.260(4)	130	x, 1+y, 1+z
C20-H20⋯O4	0.95	2.57	3.340(4)	138	1-x, y, 3/2-z

7.2.4 Co-crystal of TCCB with 1,4-Bis(4'-pyridyl)-2,3-diaza-1,3-butadiene (4,4'-bpdb)

Another co-crystal of composition (TCCB)(4,4'-bpdb)·MeOH **(46)** was grown from methanol by dissolving TCCB and 4,4'-bpdb in 1:1 ratio. X-ray crystallography revealed that the asymmetric unit contains one molecule of TCCB, two halves of the compound 4,4'-bpbd and one methanol solvent molecules. The observed values of C=O distances for four carboxylic acid groups [C=O distances are 1.22(3), 1.22(3), 1.22(3) and 1.22(3) Å and corresponding C–OH distances are 1.33(3), 1.33(3), 1.32(4), 1.32(2) Å respectively], confirm it to be a co-crystal and not a salt. Three types of supramolecular synthons *viz.* centrosymmetric carboxylic acid dimer, carboxylic acid dimer via methanol molecule and carboxyl pyridyl H-bonding (Figure 7.10), play principal role to construct two dimensional nets. The graph set notations of the hydrogen bonded motifs present in this co-crystal are $C(2)$, $R_2^2(7)$, $R_2^2(8)$, $R_4^4(12)$ as shown in Figure 7.10. Each 4,4'-bpdb molecule bridges carboxylic acid groups of two TCCB molecules and the connectivity of two methanol molecules hydrogen bonded to two carboxylic acids led to the formation of (4,4) connected 2D nets. The parameters for hydrogen bonding are listed in Table 7.4. The four sides of each quadrilateral window of the net are unequal and measured to be 30.55, 19.42, 30.55 and 16.94 Å. These two dimensional 4-connected nets are found to stack

....
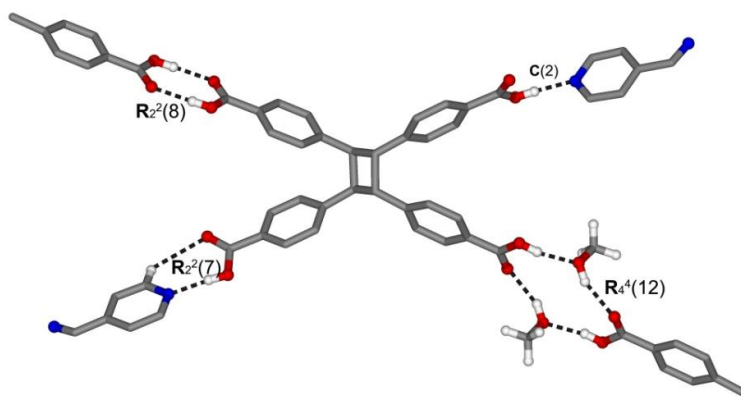
Figure 7.10 A part of the connectivity in **46** which is isostructural with **44**.

Table 7.4 The hydrogen bonding parameters for **46**

D-H⋯A	D(D-H) (Å)	D(H⋯A) (Å)	D(D⋯A) (Å)	<(DHA) (°)	Symmetry Operator
O1S-H1S⋯O3	0.84	1.95	2.735(2)	156	x+1/2, -y+1/2, z+1/2
O8-H8⋯O7	0.84	1.84	2.669(2)	172	-x, -y+1, -z+1
O6-H6⋯N3	0.84	1.80	2.638(3)	175	x-1, y-1, z
O4-H4⋯O1S	0.84	1.83	2.657(2)	169	-x+1/2, y-1/2, -z+1/2
O2-H2⋯N1	0.84	1.79	2.628(3)	176	
C27-H27⋯O2	0.95	2.45	3.313(3)	151	1/2-x, -1/2+y, 1/2-z
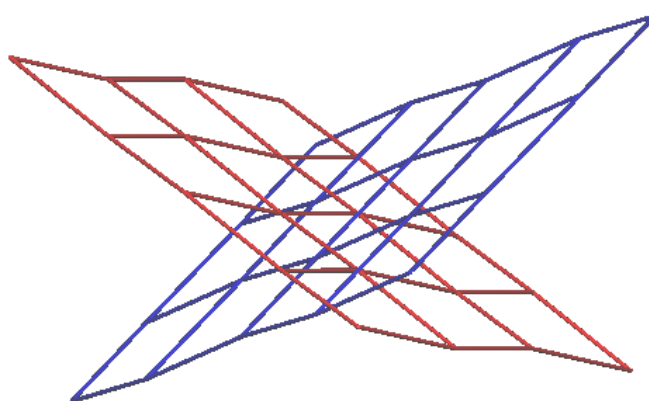
Figure 7.11 Inclined interpenetration of puckered (4,4) nets in **46**

parallel with a distance of separation 4.38 Å and then further undergo diagonal/diagonal inclined interpenetration (also known as polycatenation)[11] to result

an overall three dimensional network. The angle on inclination is 60.7° and there are
two nodes of two parallel nets on each window of the interpenetrating net. The nodes
of the nets are puckered, as shown in Figure 7.11, and the topology of this co-crystal
is found to be the same as in **44**.

7.2.5 Comparative Discussion on the Co-crystals of TCCB

Among the four co-crystals discussed above, only **43**, where TCCB is present
with 4,4'-bpy in 1:2 ratio, has hydrogen bonded three dimensional architecture. Other
three co-crystals **44 – 46** of TCCB with 4,4'-bpe, 4,4'-bpethane and 4,4'-bpdb
respectively in 1:1 ratio, have two dimensional hydrogen bonded structures. **44** and
46 have the same topology and show inclined interpenetration (polycatenation) of
puckered (4,4) sheets. On the other hand, no interpenetration was found in **45**.
Although during crystallization the ratio of TCCB with dipyridyl spacers was
maintained as 1:2, the isolation of 1:1 co-crystal may be driven by their kinetic
stabilities under the experimental conditions. DMF molecules present in the crystal of
43, do not participate in hydrogen bonding to form (4,4) net. On the other hand, in
each of the other three co-crystals, solvents molecules interfere in hydrogen bonding
and take part in the formation of (4,4) nets. Methanol molecules bridge two
carboxylic acid groups via hydrogen bonding. DMA molecules along with water also
bridge between two carboxylic acid groups but in a peculiar way. The reason behind
the diversity in the overall hydrogen-bonded networks may be the role of solvents and
the different ratios of TCCB with dipyridyl spacers that the systems have taken up
(i.e. kinetic factors).

7.2.6 MOF of TCCB with Zn(II)

TCCB was allowed to react with $Zn(NO_3)_2$ in the presence of H_2O_2 in hot DMF
to result single crystals of a MOF of composition
$[Zn_2(C_{32}H_{20}O_8)(C_2H_7NO)_2]\cdot(2DMF)$ (**47**). The structure was refined into the

....

orthorhombic space group, *Pbam* where the ligands and DMF molecules are found to be disordered. The large extent of disorders prevented to arrive at a good structural model. Large extent of restraints, including bond lengths and thermal parameters, were applied. But the connectivity in the structure is proved beyond any doubt despite the disordered structure. In the building unit, four carboxylate units of different but symmetrically equivalent TCCB^{4-} ligands bridge two zinc atoms to provide a paddle-wheel structure. Each Zn(II) is also coordinated by an unusual dimethylamine oxide ligand to furnish an overall arrangement that is reminiscent to this type of carboxylate bridged molecular building blocks (Figure 7.12). The origin of dimethylamineoxide may have stemmed from the oxidation of DMF by H_2O_2 during solvothermal synthesis.
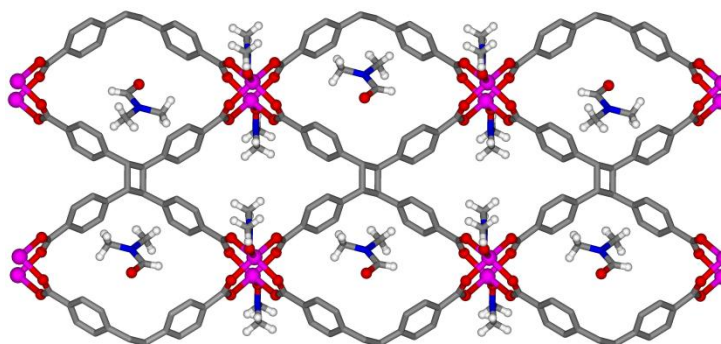
Figure 7.12 Two dimensional sheet structure of **47**. Disordered atoms are not shown for clarity.

The structure was analysed as parallel stacking of binodal (4,4) connected two dimensional nets with equal side length of 9.19 Å in ABAB sequence with a separation of 7.08 Å (Figure 7.13). The total potential solvent accessible volume in the framework is 1065 Å^3, excluding the solvent molecules, which is 45.9% of the unit cell volume as calculated by PLATON.[12] This result promptly led us to study its sorption properties. In recent years, the sorption of CO_2 has gain immense interest of the scientific community because of global warming. Coordination polymeric networks with channels or pores have been explored for this purpose in the past and

....

most of them have been reported at high pressure and low temperature.[13] However, selective sorption of CO_2 in presence of other gases (*e.g.* industrial flue gas contains N_2, CH_4, water vapour etc along with CO_2) at ambient temperature and pressure still remains a challenge.

It did not show any promising result on the sorption of N_2 or methane but it showed very interesting behaviour for CO_2 sorption. It reversibly uptake about 8 wt% of CO_2 which is similar to the other MOFs have been studied recently (Figure 7.14).[14] This was measured by our collaborator at the Pacific Northwest National Laboratory, USA.
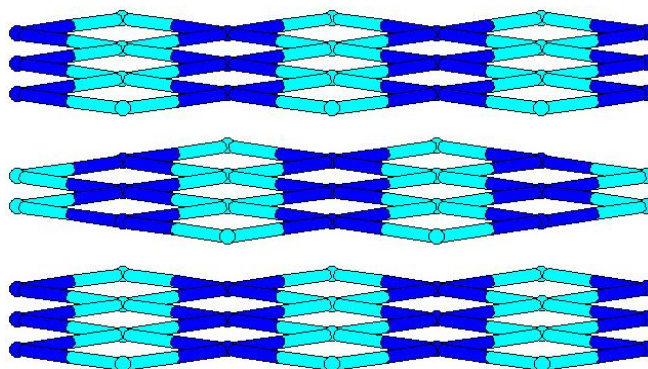
Figure 7.13 Binodal (4,4) connected two dimensional nets found in **47** are stacked in ABAB sequence.
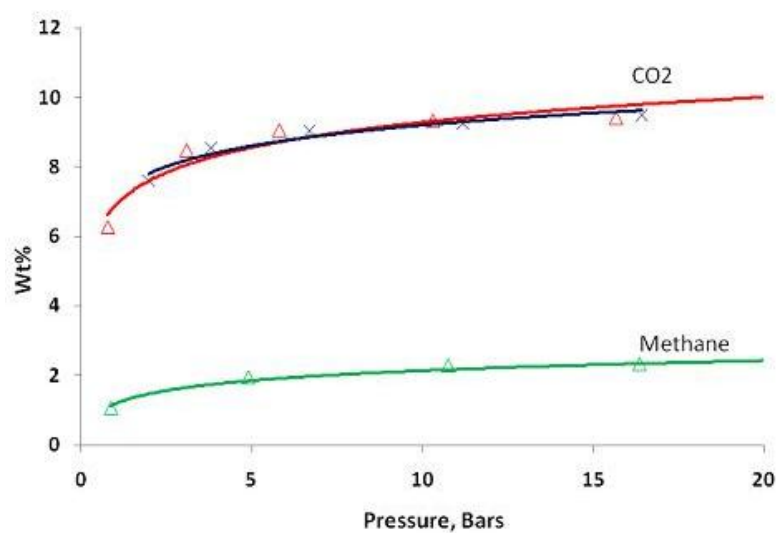
Figure 7.14 Sorption behaviour of MOF **47**

....

7.3 Coordination Polymer of HH-4,4-BPCD with Ag(I)

The compound [Ag$_2$(HH-4,4-BPCD)(H$_2$O)]·(2H$_2$O)·(0.5MeOH) (**48**) was synthesized by reacting AgBF$_4$ with Na-salt of HH-4,4-BPCD in water, MeOH and CH$_3$CN. The asymmetric unit contains one formula unit of the complex. There are two types Ag(I) ions of which the Ag1 has a linear coordination geometry comprising one N from a pyridyl group and one O from the carboxylate group of another ligand with N-Ag-O angle of 178.3°. The Ag2 has distorted trigonal geometry with a N from a pyridyl group, one O from the carboxylate group of the neighboring ligand and one O from a coordinated water molecule (aqua ligand) where Ag(I) occupies 0.401 Å above the O$_2$N plane. Since each of the HH-4,4-BPCD ligand is bonded to four different Ag(I) ions, this gives rise to two-dimensional polymeric structure as shown in Figure 7.15.
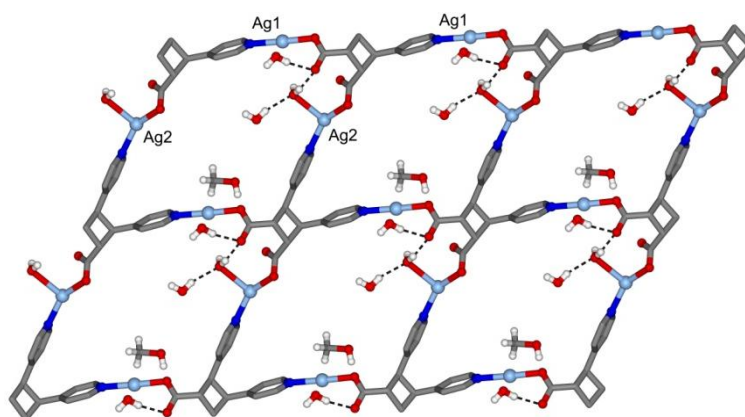
Figure 7.15 Two dimensional polymeric network of **48**

Apart from a coordinated water molecule, two non-coordinated water molecules and half MeOH are present in the lattice to fill in the empty space. The coordinated and non-coordinated water molecules form hydrogen bonds with the O atoms of the carboxylate group of the ligand as shown in Figure 7.15. The parameters for hydrogen bonding are listed in Table 7.5. MeOH molecules in the lattice are situated close to a crystallographic inversion and not involved in any hydrogen bonds. The

connectivity of the two-dimensional polymeric sheets consist of rhomboids (considering the centre of the cyclobutane rings) and this is commonly known as (4,4) grids. Two such (4,4) sheets are further assembled through argentophilic interactions with a distance between Ag1 and Ag2 of 3.11 Å as shown in Figure 7.16. In this assembly, the pyridyl rings of this cylclobutane are found to stack parallel with a distance of 3.83 Å.
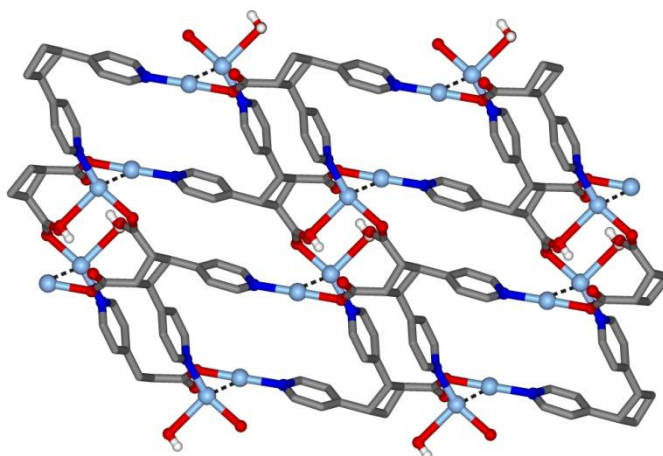
Figure 7.16 The two-dimensional sheets are stacked by argentophilic interaction (non-coordinated solvents are removed for clarity).

Interestingly the Ag···Ag contacts create 16, 20 and 24-membered metallo-macrocycle rings as shown in Figure 7.17a. It appears that such argentophilic interactions assisted metallo-macrocyclic ring is very rare. Each 16-membered macrocyclic ring contains four carbonyl oxygen atoms and all these oxygen atoms are hydrogen bonded to the water molecules. A thorough perusal to the structure reveals that these coordinated and non-coordinated water molecules form hydrogen bonded water cluster ring along with the keto oxygen of HH-4,4-BPCD. The graph set notation of such rings can be denoted as $\mathbf{R}_6^4(12)$ as shown in Figure 7.17b and the geometric parameters for hydrogen bonding are listed in Table 7.5 below.

Table 7.5 The hydrogen bonding parameters for **48**

D-H···A	D(D-H) (Å)	D(H···A) (Å)	D(D···A) (Å)	<(DHA) (°)	Symmetry Operator
O1W-H1W···O3	0.72	1.97	2.696(4)	174(6)	
O1W-H2W···O2	0.76	2.07	2.822(4)	169(5)	-x+1, -y+1, -z+1
O2W-H2WA···O2	0.81	2.05	2.848(4)	167(6)	x+1, y, z
O2W-H2WB···O1W	0.78	2.08	2.846(4)	164(6)	
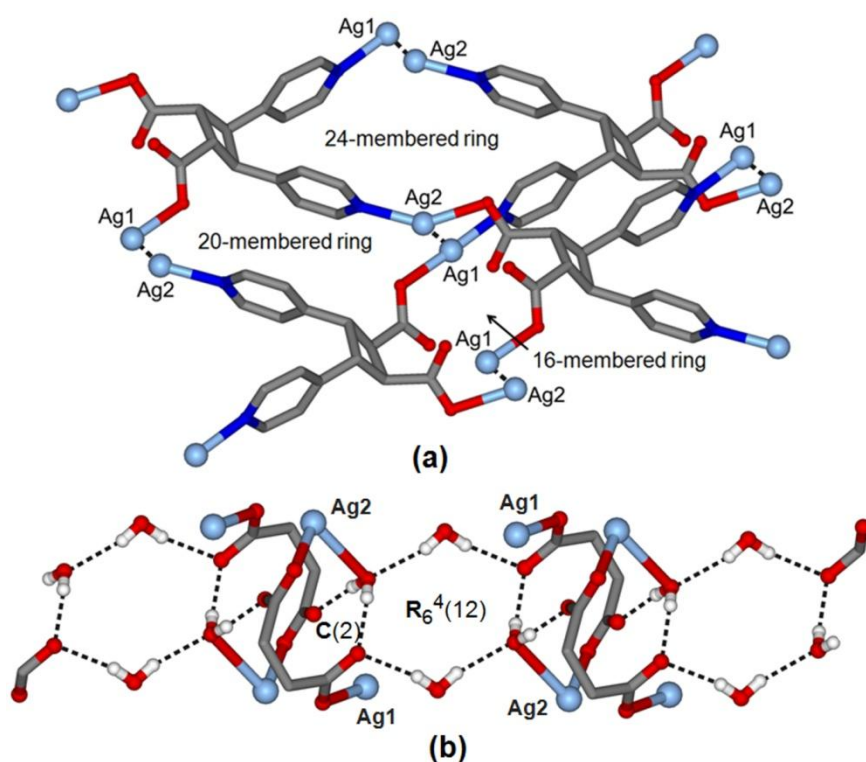
Figure 7.17 Various metallo-macrocycles formed by argentophilic interaction (a), 12-membered water cluster ring inside the macrocycles (b).

7.4 Co-crystal of HT-4,4-BPBCCB with 4,4'-bpe (49)

Another new cyclobutane compound HT-4,4-BPBCCB was also employed for making co-crystals with 4,4'-bpe. An equimolar solution of 4,4'-bpe and HT-4,4-BPBCCB in 1:4 DMF and methanol mixture was allowed to evaporate slowly to grow single crystals. Single crystal X-ray diffraction analysis revealed that HT-4,4-

BPBCCB adopted *rctt*-conformation in the co-crystal of composition (HT-4,4-BPBCCB)(4,4'-bpe)(MeOH)$_{0.75}$(H$_2$O)$_2$ (**49**). From the observed values of C=O distances for two carboxylic acid groups [C=O distances are 1.23(5) and 1.21(5) Å respectively and both the corresponding C–OH distances are 1.32(5) Å], it can certainly be called as co-crystal and not a salt. The two carboxylic acid groups donate H-bonding to two pyridyl groups in $\mathbf{R}_2^2(7)$ and $\mathbf{C}(2)$ fashion as shown in Figure 7.18. The keto oxygen of carboxylic acid group interacts with methanol molecules with O···O distance of 2.946 Å but with O-H···O angle of 115.6°, this may not be significant for H-bonding. One pyridyl group accepts H-bonding from a methanol molecule with N···O distance of 2.765 Å and N···H-O angle of 137.2°. While the other pyridyl group has interaction with water molecule maintaining N···O distance of 2.86 Å, but these interactions may not be significant as the N···H-O angles are 87.7° and 75.9°. Similarly, the distance between two water molecules (O···O distance of 2.88 Å) suggest bonding interaction, but the positions of H atoms do not. Among two water molecules present, the hydrogen atoms of one could not be located. As the growth of H-bonded network is interrupted by the solvent molecule, the overall structure of this co-crystal was determined to be one dimensional.
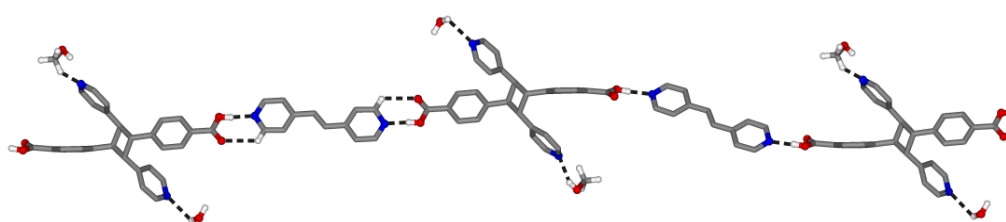
Figure 7.18 One dimensional hydrogen bonded chain of **49**

Table 7.6 The hydrogen bonding parameters for **49**

D-H⋯A	D(D-H) (Å)	D(H⋯A) (Å)	D(D⋯A) (Å)	<(DHA) (°)	Symmetry Operator
O1-H1⋯N4	0.84	1.79	2.625(5)	177	-x+1/2, y+1/2, -z+1/2
O3-H3⋯N3	0.84	1.73	2.569(4)	175	x+1, y, z
O1W-H1WB⋯O2W	0.85	2.36	2.794(8)	112(5)	x+1, y, z
O1S-H1S⋯N2	0.84	2.09	2.764(8)	137	-x+3/2, y+1/2, -z+1/2
O1S-H1S⋯O4	0.84	2.48	2.945(8)	116	x-1, y, z

7.5 Summary

In this chapter, the cyclobutane derived compounds containing only carboxylic acid and mixed pyridyl and carboxylic acid functionality have been shown to be the potential ligands for making co-crystals and MOFs. The tetradentate compounds always have the tendency to form 4-connected square/tetragonal grid structure in the co-crystals and MOFs. The detailed investigation on the packing pattern of the obtained crystals **44** – **46** and **49** reveals that the solvent molecules present in the co-crystals also play important role in forming such (4,4) nets. For example, 1D chain instead of 2D sheet due to the interruption of H-bonding by solvent molecules was observed in **49**. Two dimensional coordination polymeric sheets of $[Zn_2(C_{32}H_{20}O_8)(C_2H_7NO)_2]\cdot 2DMF$ (**47**) absorbs about 8% CO_2 gas, implying that MOFs obtained from these cyclobutane compounds can be used for various potential applications. In the Ag(I) coordination polymer $[Ag_2(HH-4,4-BPCD)(H_2O)]\cdot(2H_2O)(0.5MeOH)$ (**48**), the argentophilic interaction assisted various metallo-macrocycle ring hosting hydrogen bonded water cluster rings have been identified, which appears to be very rare in the literature.

....

7.6 Syntheses and Characterizations

(TCCB)(4,4'-bpy)$_2$·2DMF (43)

TCCB (27 mg) and 4,4'-bipyridyl (16 mg) were dissolved in 4 mL DMF and the resulting solution was kept for slow evaporation. Diffraction quality block shaped single crystals were obtained after a week. Yield 72%.

^{1}H NMR (300 MHz, d_6-DMSO, 298K): δ_H = 12.78 (s, 4H, -CO$_2$H), 8.72 (d, 8H, Ar-H), 7.95 (s, 2H, alde-DMF), 7.83 (d, 8H, Ar-H), 7.72 (d, 8H, Ar-H), 7.33 (d, 8H, Ar-H), 4.71 (s, 4H, CH-CH), 2.89 (s, 6H, CH$_3$-DMF), 2.73 (s, 6H, CH$_3$-DMF). Analysis found (%): C 69.87, H 5.36, N 8.35; C$_{58}$H$_{54}$N$_6$O$_{10}$ requires C 70.01, H 5.47, N 8.45. The observed solvent (DMF) loss 15.8% in TGA experiment compared with the calculated value 14.7%.

(TCCB)(4,4'-bpe)·MeOH (44)

Methanolic solution of 4,4'-bpe (18 mg, 0.1 mmol in 2 mL) was carefully layered over TCCB (27 mg, 0.05 mmol in 6 mL methanol) in a test tube. Diffraction quality block shaped single crystals were separated on the next day. Even though the ratio of 4,4'-bpe and TCCB used was 2:1, the co-crystal of composition 1:1 was always obtained. Yield 68%.

^{1}H NMR (300 MHz, d_6-DMSO, 298K): δ_H = 12.78 (s, 4H, -CO$_2$H), 8.60 (d, 4H, Ar-H), 7.71 (d, 8H, Ar-H), 7.60 (d, 4H, Ar-H), 7.53 (s, 2H, CH=CH), 7.33 (d, 8H, Ar-H), 4.71 (s, 4H, CH-CH), 4.08 (s, MeOH), 3.17 (s, CH$_3$OH). Analysis found (%): C 71.73, H 5.06, N 3.71; C$_{45}$H$_{38}$O$_9$N$_2$ requires C 71.99, H 5.10, N 3.73. The observed solvent loss 4.15 % in TGA experiment was matched with the calculated solvent loss of 4.26%.

....

(TCCB)(4,4'-bpethane)·(2DMA)·H$_2$O (45)

The mixture of 4,4'-bpethane (20 mg, 0.1 mmol) and TCCB (27 mg, 0.05 mmol) were dissolved in 3 mL DMA and the resulting solution was allowed to evaporate slowly. Block shaped diffraction quality single crystals were obtained after a week. Regardless the ratio of 4,4'-bpethane and TCCB in the mixture, co-crystal of composition 1:1 was obtained every time. Yield 60%.

^{1}H NMR (300 MHz, d_6-DMSO, 298K): δ_H = 12.8 (s, 4H, -CO$_2$H), 8.44 (d, 4H, Ar-H), 7.71 (d, 8H, Ar-H), 7.33 (d, 8H, Ar-H), 7.25 (d, 4H, Ar-H), 4.71 (s, 4H, CH-CH), 2.94 (s, 10H, CH-CH of 4,4'-bpethane and CH$_3$ of DMA together), 2.78 (s, 6H, CH$_3$ DMA), 1.95 (s, 6H, CH$_3$ DMA). Analysis found (%): C 68.85, H 6.18, N 6.05; C$_{52}$H$_{56}$N$_4$O$_{11}$ requires: C 68.41, H 6.18, N 6.14. The weight loss observed at 285 °C in the TGA experiment is 40.7% which can be matched with the sum of solvent loss (21.05%) and weight loss due to decarboxylation of TCCB (19.27%).

(TCCB)(4,4'-bpdb)·MeOH (46)

4,4'-Bpdb (21 mg, 0.1 mmol in 3 mL methanol) was layered over of TCCB (27 mg, 0.05 mmol in 5mL methanol). Diffraction quality single crystals were obtained after two days. Although 4,4'-bpdb and TCCB were mixed in 2:1 ratio, the co-crystal of composition 1:1 was resulted. The same co-crystal was also resulted by slowly evaporating the above methanolic solution. Yield 85%

^{1}H NMR (300 MHz, d_6-DMSO, 298K): δ_H = 12.78 (s, 4H, -CO$_2$H), 8.75 (d, 4H, Ar-H), 8.70 (s, 2H, C-H, 4,4'-bpdb), 7.81 (d, 4H, Ar-H), 7.71 (d, 8H, Ar-H), 7.34 (d, 8H, Ar-H), 4.72 (s, 4H, CH-CH), 4.1 (s, MeOH), 3.17 (s, CH$_3$OH). Analysis found (%): C 69.80, H 5.13, N 7.46; C$_{45}$H$_{38}$N$_4$O$_9$ requires C 69.40, H 4.92, N 7.19. The observed weight loss in TGA experiment is 5.1%, whereas the calculated value is 4.1%.

....

[Zn$_2$(C$_{32}$H$_{20}$O$_8$)(C$_2$H$_7$NO)$_2$]·(2DMF) (47)

TCCB (27 mg, 0.05 mmol), Zn(NO$_3$)$_2$.6H$_2$O (30 mg, 0.1 mmol) and a few drops of H$_2$O$_2$ in 8mL DMF were heated at 105 °C in a scintillation vial for 30 h and then were cooled very slowly for 15 h. Colourless single crystals were separated by filtration. Yield 69%.

Analysis found for the dried sample (%): C 53.85, H 4.61, N 3.63; Zn$_2$(C$_{32}$H$_{20}$O$_8$)(C$_2$H$_6$NO)$_2$ requires C 55.19, H 4.11, N 3.57%. A small discrepancy in the elemental analysis may be attributed to the incomplete removal of DMF on drying. In TGA experiment with dried sample, 16.3% solvent loss was observed where the calculated weight loss for the composition Zn$_2$(C$_{32}$H$_{20}$O$_8$)(C$_2$H$_6$NO)$_2$ is 15.4%.

[Ag$_2$(HH-4,4-BPCD)(H$_2$O)]·(2H$_2$O)(0.5MeOH) (48)

AgBF$_4$ (21 mg, 0.1 mmol in 2 mL methanol) was carefully layered over aqueous solution of Na-salt of HH-BPCD (15 mg, 0.1 mmol in 3 mL water) using CH$_3$CN (2 mL) as buffer layer. Block shaped single crystals were separated after a week. Yield 72%.

Elemental analysis found (%): C 34.50, H 3.19, N 5.09, calculated for C$_{16.5}$H$_{18}$Ag$_2$N$_2$O$_{7.5}$: C 34.16, H 3.13, N 4.83. The calculated total solvents loss including MeOH, coordinated and non-coordinated water molecules is 12.1% where the found total solvent loss in TGA experiment is 12.7%.

(HT-4,4-BPBCCB)(4,4'-bpe)(MeOH)$_{0.75}$(H$_2$O)$_2$ (49)

4,4'-Bpe (9 mg, 0.05 mmol) and HT-BCBPCB (45 mg, 0.1 mmol) were dissolved in 4 mL methanol and 1 ml DMF. The resulting solution was kept for slow evaporation and diffraction quality block shaped single crystals were obtained after a few days. Yield 80%.

....

^{1}H NMR (300 MHz, d_6-DMSO, 298K): δ_H = 12.82 (s, 2H, -CO$_2$H), 8.60 (d, 4H, Ar-H), 8.31 (d, 4H, Ar-H), 7.73 (d, 4H, Ar-H), 7.61 (d, 4H, Ar-H), 7.54 (s, 2H, CH=CH), 7.35 (d, 4H, Ar-H), 7.21 (d, 4H, Ar-H), 4.69 (s, 4H, CH-CH). Analysis found (%): C 70.87, H 5.13, N 8.17; $C_{40.75}H_{37}N_4O_{6.75}$ requires: C 70.65, H 5.67, N 8.09. In TGA experiment 7.5% solvent loss was observed, where the calculated value is 8.6%.

Table 7.7 Crystallographic data for compounds **43** – **46**

Compounds	43	44	45	46
Formula	$C_{58}H_{54}N_6O_{10}$	$C_{45}H_{38}N_2O_9$	$C_{52}H_{56}N_4O_{11}$	$C_{45}H_{38}N_4O_9$
M	995.07	750.77	913.01	778.79
T (K)	100(2)	223(2)	100(2)	100(2)
λ (Å)	0.71073	0.71073 Å	0.71073	0.71073
Cryst syst / Space group	Orthorhombic / $Pna2_1$	Monoclinic / $P2_1/n$	Monoclinic / $C2/c$	Monoclinic / $P2_1/n$
a (Å)	18.6545(8)	10.4208(6)	28.787(3)	11.0252(9)
b (Å)	12.6058(5)	10.3302(6)	10.7716(12)	10.1233(7)
c (Å)	21.7602(9)	34.5404(19)	14.7431(16)	34.861(3)
α (°)	90	90	90	90
β (°)	90	94.195(2)	95.240(3)	98.614(3)
γ (°)	90	90	90	90
Volume (Å^3) / Z	5117.0(4) / 4	3708.3(4) / 4	4552.5(9) / 4	3847.0(5) / 4
D_{calcd} (g/cm^3) / μ (mm^{-1})	1.292 / 0.089	1.345 / 0.094	1.331 / 0.094	1.345 / 0.095
Reflns col. / Ind. Reflns.	29348 / 7250	21057 / 6533	15946 / 5201	27133 / 8825
R_{int} / Goof on F^2	0.0406 / 1.632	0.0498 / 1.030	0.0504 / 1.036	0.0627 / 1.015
Final R[I>2σ]^a R$_1$ / wR2	0.1443 / 0.3535	0.0741 / 0.1636	0.0707 / 0.1716	0.0647 / 0.1333

^{a} R1 = Σ||F_o| − |F_c||/ Σ|F_o|, ^{b} wR2 = [Σ$w(F_o^2 − F_c^2)^2$/Σ$w(F_o^2)^2$]$^{1/2}$

Table 7.8 Crystallographic data for compounds **47** - **49**

Compounds	47	48	49
Formula	$C_{42}H_{48}N_4O_{12}Zn_2$	$C_{16.5}H_{18}Ag_2N_2O_{7.5}$	$C_{40.75}H_{39}N_4O_{6.75}$
M	931.58	580.07	692.76
T (K)	193(2)	293(2)	100(2)
λ (Å)	0.71073	0.71073	0.71073 Å
Cryst syst / Space group	Orthorhombic / $Pbam$	Triclinic / $P\bar{1}$	Monoclinic / $P2_1/n$
a (Å)	11.360(4)	9.1159(8)	10.1643(11)
b (Å)	14.155(4)	9.6256(8)	10.1819(10)
c (Å)	14.435(4)	12.3162(11)	34.305(4)
α (°)	90	106.127(2)	90
β (°)	90	106.549(2)	95.067(3)
γ (°)	90	99.865(2)	90
Volume (Å^3) / Z	2321.2(12) / 2	957.65(14) / 2	3536.4(6) / 4
D_{calcd} (g/cm^3) / μ (mm^{-1})	1.333 / 1.094	2.012 / 2.089	1.297 / 0.089
Reflns col. / Ind. Reflns.	14072 / 2767	12652 / 4385	20322 / 6205
R_{int} / Goof on F^2	0.0460 / 1.102	0.0270 / 1.049	0.0839 / 1.072
Final R[I>2σ][a]	0.0847 / 0.2526	0.0363 / 0.0882	0.0861 / 0.2053
R_1 / wR2			

[a] R1 = $\Sigma||F_o| - |F_c||/ \Sigma|F_o|$, [b] wR2 = $[\Sigma w(F_o{}^2 - F_c{}^2)^2/\Sigma w(F_o{}^2)^2]^{1/2}$

....

7.7 References

1.   (a) Ma, L.; Lee, J. Y.; Li, J.; Lin, W., *Inorg. Chem.* **2008,** *47* (10), 3955-3957; (b) Rosi, N. L.; Eckert, J.; Eddaoudi, M.; Vodak, D. T.; Kim, J.; O'Keeffe, M.; Yaghi, O. M., *Science* **2003,** *300* (5622), 1127-1129; (c) Dincă, M.; Long, J. R., *Angew. Chem. Int. Ed.* **2008,** *47* (36), 6766-6779.

2.   (a) Cheon, Y. E.; Suh, M. P., *Chem, Eur. J.* **2008,** *14* (13), 3961-3967; (b) Seo, J. S.; Whang, D.; Lee, H.; Jun, S. I.; Oh, J.; Jeon, Y. J.; Kim, K., *Nature* **2000,** *404* (6781), 982-986.

3.   (a) Hasegawa, S.; Horike, S.; Matsuda, R.; Furukawa, S.; Mochizuki, K.; Kinoshita, Y.; Kitagawa, S., *J. Am. Chem. Soc.* **2007,** *129* (9), 2607-2614; (b) Sawaki, T.; Aoyama, Y., *J. Am. Chem. Soc.* **1999,** *121* (20), 4793-4798.

4.   Horcajada, P.; Serre, C.; Maurin, G.; Ramsahye, N. A.; Balas, F.; Vallet-Regí, M. a.; Sebban, M.; Taulelle, F.; Férey, G. r., *J. Am. Chem. Soc.* **2008,** *130* (21), 6774-6780.

5.   (a) Hamilton, T. D.; Bucar, D.-K.; Atkinson, M. B. J.; Papaefstathiou, G. S.; MacGillivray, L. R., *J. Mol. Struct.* **2006,** *796* (1-3), 58-62; (b) Papaefstathiou, G. S.; MacGillivray, L. R., *Angew. Chem. Int. Ed.* **2002,** *41* (12), 2070-2073.

6.   Peedikakkal, A. M. P.; Peh, C. S. Y.; Koh, L. L.; Vittal, J. J., *Inorg. Chem.* **2010,** *49* (15), 6775-6777.

7.   (a) Peedikakkal, A. M. P.; Koh, L. L.; Vittal, J. J., *Chem. Commun.* **2008,** (4), 441-443; (b) Mir, M. H.; Koh, L. L.; Tan, G. K.; Vittal, J. J., *Angew. Chem. Int. Ed.* **2010,** *49* (2), 390-393.

8.   (a) Köhler, T.; Seidel, D.; Lynch, V.; Arp, F. O.; Ou, Z.; Kadish, K. M.; Sessler, J. L., *J. Am. Chem. Soc.* **2003,** *125* (23), 6872-6873; (b) Blatov, V. A. *TOPOS 4.0 Professional*, Commission on Crystallographic Computing, IUCr: 2006.

9.   Blatov, V. A.; Carlucci, L.; Ciani, G.; Proserpio, D. M., *CrystEngComm* **2004,** *6* (65), 377-395.

10.   (a) Sarmah, M. P.; Shashidhar, M. S.; Sureshan, K. M.; Gonnade, R. G.; Bhadbhade, M. M., *Tetrahedron* **2005,** *61* (18), 4437-4446; (b) Chao, W.; Waldman, J. H.; Weinreb, S. M., *Org. Lett.* **2003,** *5* (16), 2915-2918; (c) Sakamoto, J.; Nakagawa, T.; Kanehisa, N.; Kai, Y.; Katsura, M., *Acta Crystallogr. Sect. C* **2000,** *56* (10), e485-e486; (d) Meyers, C. Y.; Lutfi, H. G.; Kolb, V. M.; Robinson, P. D., *Acta Crystallogr. Sect. C* **1994,** *50* (12), 1925-1928; (e) Rozycka-Sokolowska, E.; Marciniak, B.; Pavlyuk, V., *Acta Crystallogr. Sect. E* **2005,** *61* (1), o114-o115; (f) Bianchi, R.; Gervasio, G.; Viscardi, G., *Acta Crystallogr. Sect. B* **1998,** *54* (1), 66-72.

11.   (a) Batten, S. R., *CrystEngComm* **2001,** *3* (18), 67-72; (b) Zaworotko, M. J., *Chem. Commun.* **2001,** (1), 1-9; (c) Proserpio, D. M., *Nat. Chem.* **2010,** *2* (6), 435-436.

12.   Spek, A., *J. Appl. Crystallogr.* **2003,** *36* (1), 7-13.

13.   (a) Kitaura, R.; Seki, K.; Akiyama, G.; Kitagawa, S., *Angew. Chem. Int. Ed.* **2003,** *42* (4), 428-431; (b) Millward, A. R.; Yaghi, O. M., *J. Am. Chem. Soc.* **2005,** *127* (51), 17998-17999; (c) Llewellyn, P. L.; Bourrelly, S.; Serre, C.; Vimont, A.; Daturi, M.; Hamon, L.; De Weireld, G.; Chang, J.-S.; Hong, D.-Y.; Kyu Hwang, Y.; Hwa Jhung, S.; Férey, G. r., *Langmuir* **2008,** *24* (14), 7245-7250.

14.   (a) Caskey, S. R.; Wong-Foy, A. G.; Matzger, A. J., *J. Am. Chem. Soc.* **2008,** *130* (33), 10870-10871; (b) Choi, H.-S.; Suh, M. P., *Angew. Chem. Int. Ed.* **2009,** *48* (37), 6865-6869; (c) D'Alessandro, D. M.; Smit, B.; Long, J. R., *Angew. Chem. Int. Ed.* **2010,** *49* (35), 6058-6082; (d) Wang, B.; Cote, A. P.; Furukawa, H.; O'Keeffe, M.; Yaghi, O. M., *Nature* **2008,** *453* (7192), 207-211; (e) Zheng, B.; Bai, J.; Duan, J.; Wojtas, L.; Zaworotko, M. J., *J. Am. Chem. Soc.* **2010,** *133* (4), 748-751.

Chapter 8

Conclusion and Suggestions for Future Work

8.1 Conclusion

The research work presented in this thesis has dealt with the syntheses and characterizations of several types of molecular salts and silver(I) coordination complexes and polymers exploiting the crystal engineering principles. The photochemical [2 + 2] cycloaddition reaction of these molecular salts and Ag(I) compounds have resulted handful of functional cyclobutane derived compounds and their isomers.

Photostable H_2SDC has been made photoreactive in its salts with 1,3-diaminopropane, ammonia and 3,3′-dipropylamino amine. Other salts of various homologous amines were found not to undergo photodimerization. The supramolecular synthons and hydrogen bonded motifs constructing the solid state architecture in these salts have been identified and accounted to understand if there is any design strategy involved for aligning C=C bonds in the ammonium-carboxylate salts. The corresponding dimer, 1,2,3,4-tetrakis(4'-carboxyphenyl)cyclobutane has been synthesized in gram scale by following solventless, mechanochemical green route.

Photostable and asymmetric olefin 4-PAH has been made photoreactive by making its salts with various strong acids exploiting its pyridyl functionality. It has been shown for the first time that the anions present in these salts play key role in constructing the solid state structure and it can be tuned by changing the anion. The corresponding *head-to-tail* photodimer viz. HT-4,4-BPCD has been obtained in quantitative yields using $CF_3CO_2^-$, ClO_4^-, BF_4^-, Cl^- etc anions. On the other hand, the *head-to-head* photodimer viz. HH-4,4-BPCD can be obtained from sulphate-bisulphate salt where the quantitative yield has been achieved by grinding the salt prior to the photochemical reaction. It was witnessed that the absorption of moisture induced by mechanochemical force, which triggered structural transformation, led to

the proper alignment and hence the quantitative conversion was achieved. 3-PAH, which is photoreactive in *head-to-head* fashion and whose *head-to-tail* aligned polymorph is not known, has been aligned in *head-to-tail* fashion by using $HClO_4$ as salt former and the synthesis of HT-3,3-BPCD has become possible for the first time and in quantitative yield. It has been anticipated that the parallel alignment in *head-to-tail* fashion is quite common and more stable due to cation-π interaction, compared to the same in *head-to-head* fashion where bivalent anions like sulphate is necessary to balance the cation-cation repulsion. The strategy of salt formation exploiting both the pyridyl and carboxylic acid functionality was extended to HPVBA and the corresponding HH- and HT-photodimers were synthesised. It has been revealed in this thesis that the strategy of salt formation works well and might be a preferred route to access the functional cyclobutane derivatives. But the predictability of the solid state packing of the salt is low due to the presence of less directional charge assisted hydrogen bonding.

Argentophilic interaction has been investigated in a series of silver(I) coordination complexes in the context of their photoreactivity. It has been shown that the parallel alignment of photoreactive C=C bonds is the result of cooperation between the argentophilic interaction and other supramolecular interactions collectively. The coordination behaviour of 'N', 'O' and 'P' donor sites of the pyridyl carboxylate (mixed functionality) and phosphine derived ligands and only 'N' donor for neutral ligands toward Ag(I) have been utilized to synthesize several multidimensional coordination polymers.

All the 4-pyridyl substituted cyclobutane derivatives have been studied for their isomerisation in presence of H^+ from *rctt*-form to *rctc*-form and a probable mechanism has been proposed which is also able to explain the inertness of 3-pyridyl substituted cyclobutane compounds to such isomerisation.

....

All the cyclobutane derivatives have been employed as tetratopic ligands for making co-crystals and coordination polymers. They always tend to form (4,4) square grid networks because of their inherent geometry of the cyclobutane isomer. One such coordination polymer/MOF has been investigated for sorption properties and was found to adsorb 8 wt% CO_2 gas at 1 bar pressure reflecting suitable for potential application.

8.2 Scopes for Future Research

The strategy of salt formation developed in this thesis can be employed to any olefin containing molecule with moderately strong acidic or basic functionality and especially when difficulty in co-crystallization is encountered. The pyridyl groups of 4-PAH and 3-PAH have been exploited for making salts with strong acids. The carboxylic acid groups can further be exploited for making photoreactive salts with amines, as has been done for H_2SDC and HPVBA.

Although, the photochemical [2 + 2] cycloaddition reaction of 3-PAH and 4-PAH has been carried out but 2-PAH has not been explored. According to the proposed mechanism of acid catalysed isomerisation of cyclobutane compounds, both the HH- and HT-photodimer should exhibit such isomerisation in similar condition. Therefore, further research can be extended for the selective syntheses of HH- and HT-2,2-BPCD from 2-PAH either via molecular salts or Ag(I) coordination compounds and their acid catalysed isomerisation can be investigated. Similarly, research can be extended with HPVBA analogues containing 2- and 3-substituted pyridyl moieties.

Two-dimensional MOF with parallel layered structure, obtained from Zn(II) and TCCB, has been demonstrated with CO_2 gas sorption properties. However, the synthesis of 3D MOF with this tetracarboxylate and dipyridyl linear spacer ligands

having pillared-layer structure, can be attempted for better porosity and thus for better

sorption properties.

The photochemical [2 + 2] cycloaddition reaction is known to be reversible, yet the formation of olefins back from cyclobutane compounds is not well explored. If HT-photodimers undergo cleavage, the cyclobutane ring is expected to revert back the olefin monomer in *trans-* or *cis*-forms. On the other hand, the HH-photodimers may cleave the cyclobutane ring in two pathways. For example, HH-4,4-BPCD may cleave to produce only 4-PAH back or alternatively it may produce an equimolar mixture 4,4'-bpe and fumaric acid. It would be very interesting to study such reversible cycloaddition reaction where the systems follow the second pathway. Therefore, the future research can be directed to establish this reversibility and the process is desired to follow in SCSC manner where the crystal engineering principle can contribute a lot.

Appendix I

A Few Representative Spectroscopic Data for Characterization of Different Compounds

Experimental Details

The NMR spectra were recorded with a Bruker ACF 300FT-NMR spectrometer with TMS as internal reference. ESI-MS spectra were recorded with aqueous or alcoholic solution (< 50 $\mu g.mL^{-1}$) with Finnigan MAT LCQ Mass Spectrometer by the syringe-pump method. Thermogravimetric analyses (TGA) were recorded on a TA Instrument SDT 2960 TGA Thermal Analyzer. The samples were heated at a constant rate of 5 °C min^{-1} from room temperature and the atmosphere was maintained with continuous flow of nitrogen. Elemental analyses were performed in the Micro Analytical Laboratory, Department of Chemistry, National University of Singapore. Powder X-ray diffraction (PXRD) patterns were obtained by using a D5005 Bruker X-ray diffractometer equipped with Cu Kα radiation. The accelerating voltage and current were 40 KV and 40 mA respectively.

UV irradiation:

The UV irradiation experiments were conducted by using Luzchem photoreactor (wavelength 350 nm, Intensity ∼ 1.75 mW-cm^{-2}). ∼ 20 mg of the samples (finely powdered sample or single crystals) were packed gently between two pyrex glass slides and the UV irradiations were completed by flipping the packed glass slide pairs for each sample in half of their irradiation time interval to ensure uniform irradiation. For studying '% Conversion *vs.* Time' plot, the samples were collected from UV chamber in different time interval and ^{1}H NMR spectra were acquired to determine the percentage of dimer compounds formed from integration values.

X-ray Crystallography:

Single Crystals suitable for data collection were chosen under an optical microscope, mounted on glass fibre, and frozen under a stream of cryogenic nitrogen gas before data collection. Intensity data were collected on a Bruker APEX diffractometer attached with a CCD detector and graphite-monochromated MoKα (λ = 0.71073 Å) radiation. Empirical absorption corrections were applied with the data

Appendix I

....

using the program SADABS and the crystallographic package SHELXTL was used for all calculations.
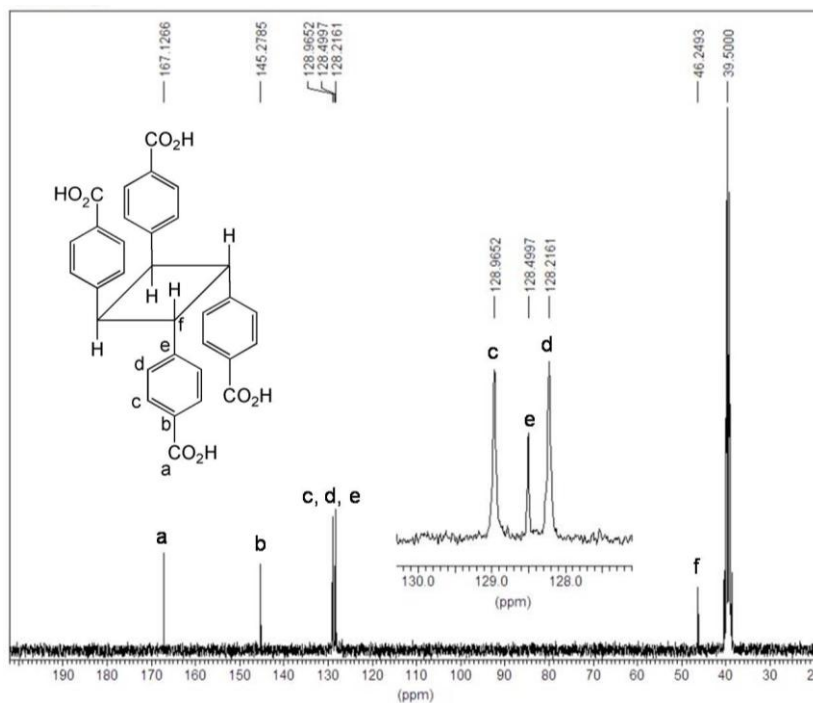

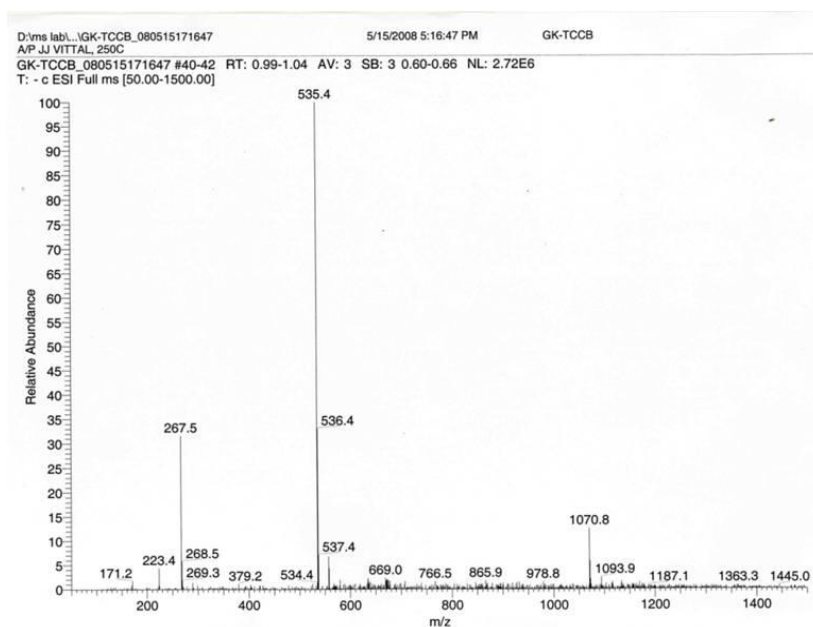Figure A1: ^{13}C-NMR (75 MHz, d_6-DMSO, 298K) spectrum of *rctt*-TCCB.

Figure A2: ESI-Ms spectrum of TCCB [m/z 535.4 represents (M-1) peak].
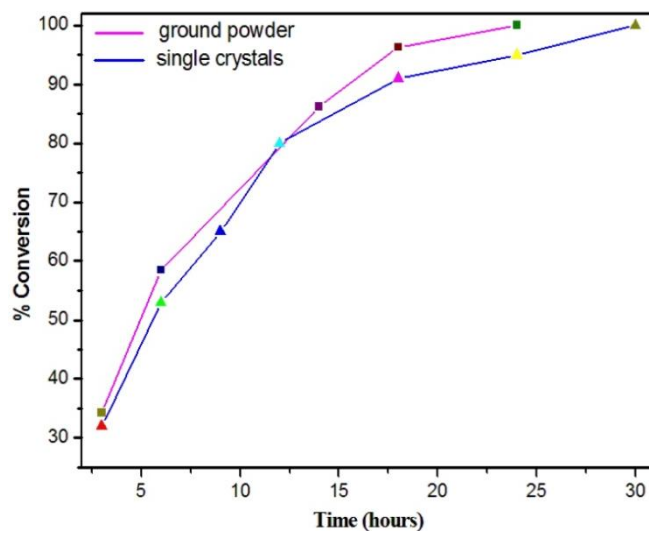
Figure A3: Percentage conversion *vs.* time plot for single crystals and powdered sample of **11**.
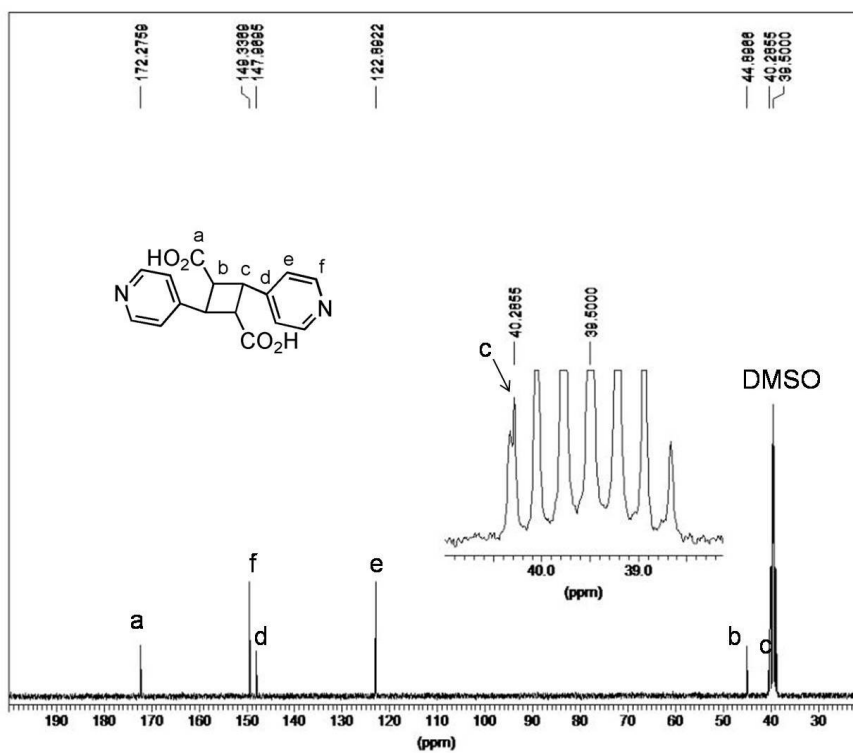
Figure A4: ^{13}C-NMR (300 MHz, d_6-DMSO, 298K) spectrum of *rctt*-HT-BPCD

Figure A5: ^{13}C-NMR(75 MHz, D$_2$O, 298K) spectrum of *rctc*-HT-BPCD (as CF$_3$CO$_2^-$ salt). There are three different types of cyclobutane carbons instead of two for *rctt*-form. Asterisk mark show the presence of small percent of *rctt*-form is present (as isomerisation is not quantitative).
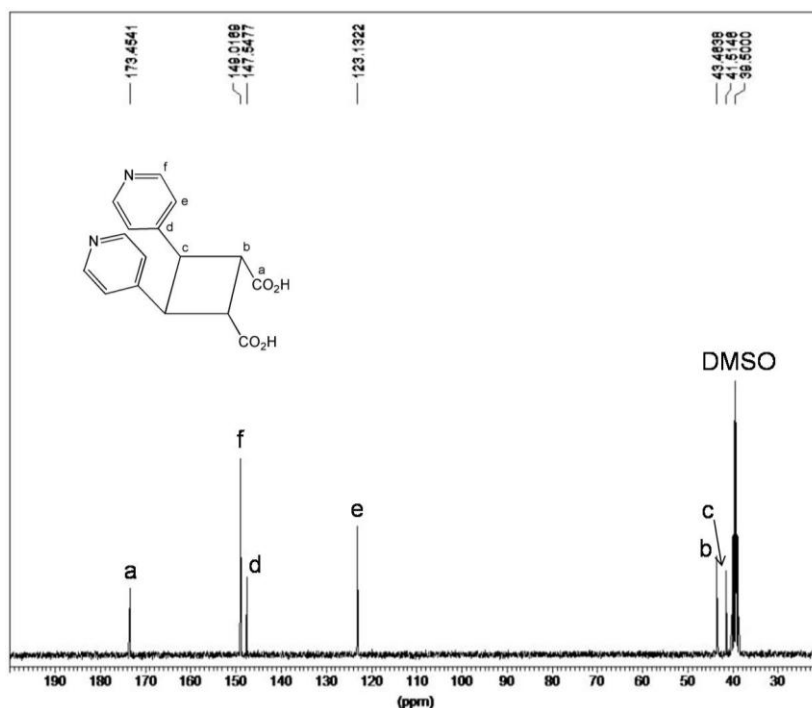
Figure A6: ^{13}C-NMR (75 MHz, d_6-DMSO, 298K) spectrum of *rctt*-HT-BPCD
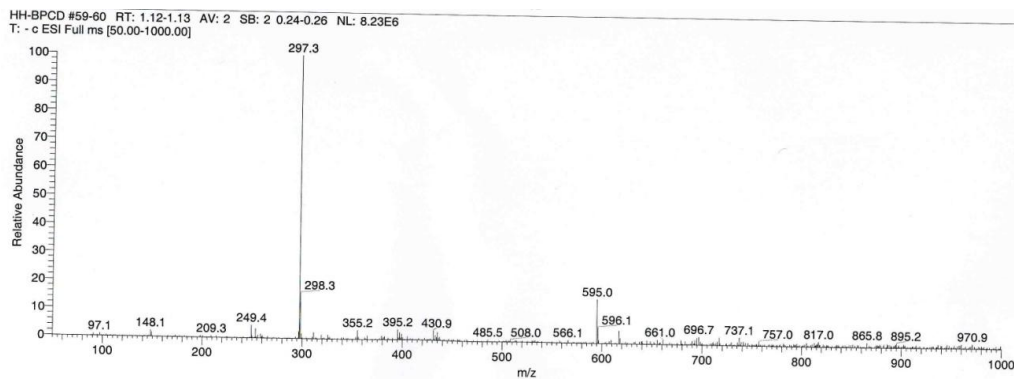
Figure A7: ESI-Ms spectrum of HH-BPCD
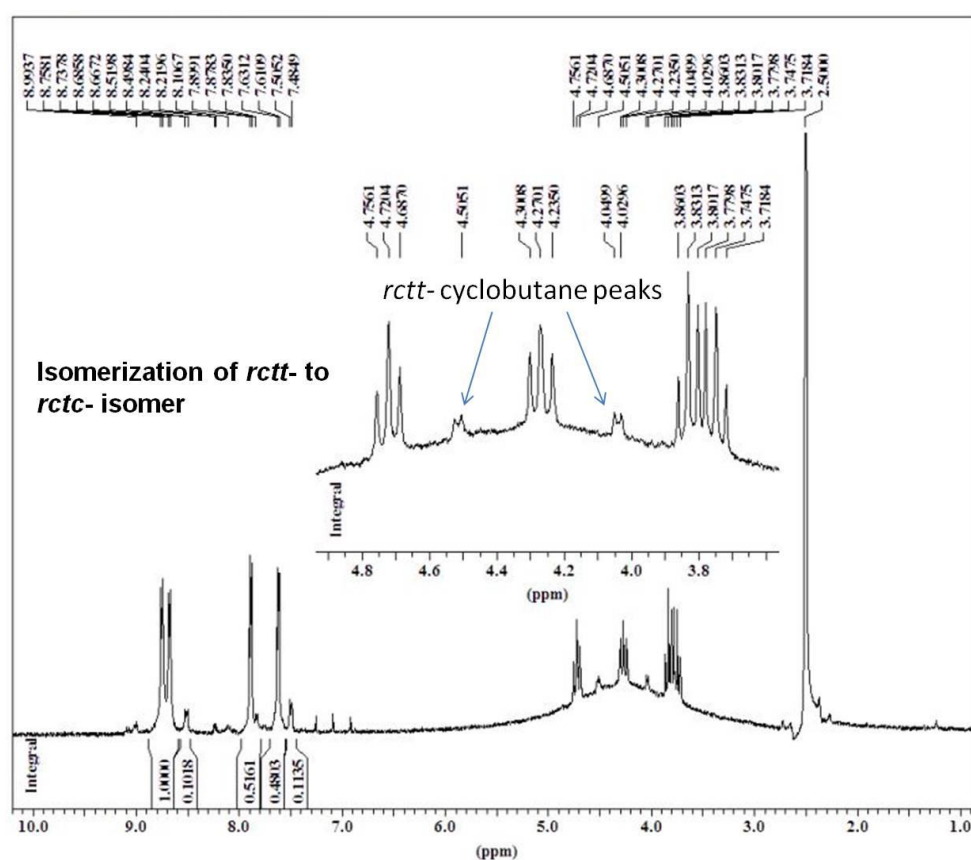
Figure A8: ^{1}H NMR (300 MHz, d_6-DMSO, 298K) spectrum shows the isomerisation of *rctt*-HH-BPCD to *rctc*-HH-BPCD. There are four different types of cyclobutane protons instead of two for *rctt*-form. This isomerisation is also not quantitative as *rctc*-form is less stable than *rctt*-form.
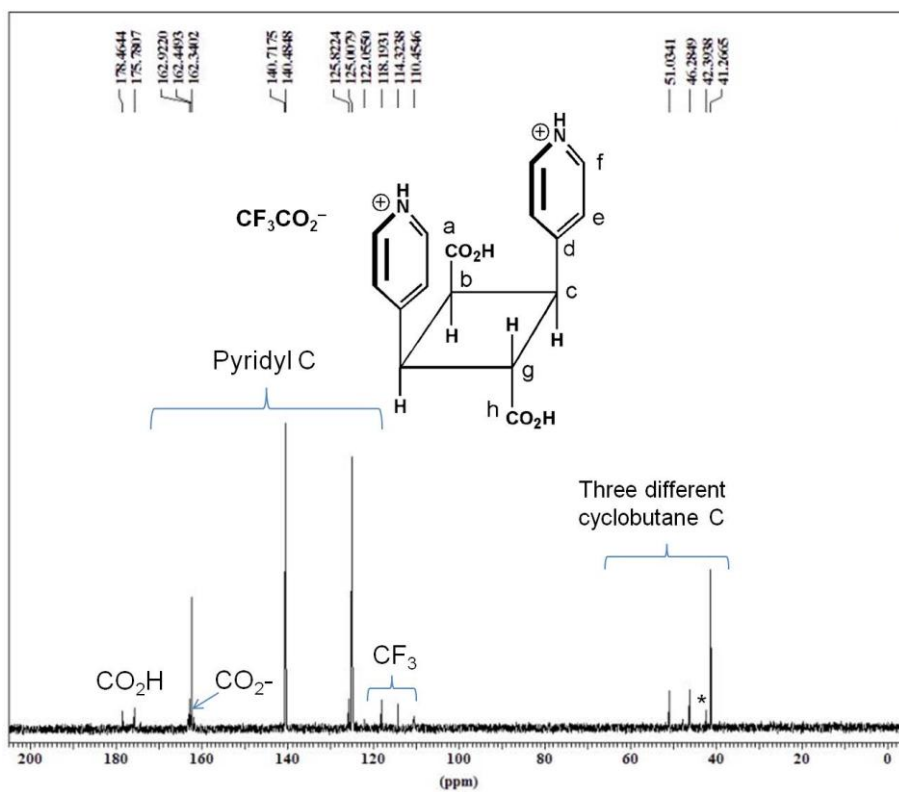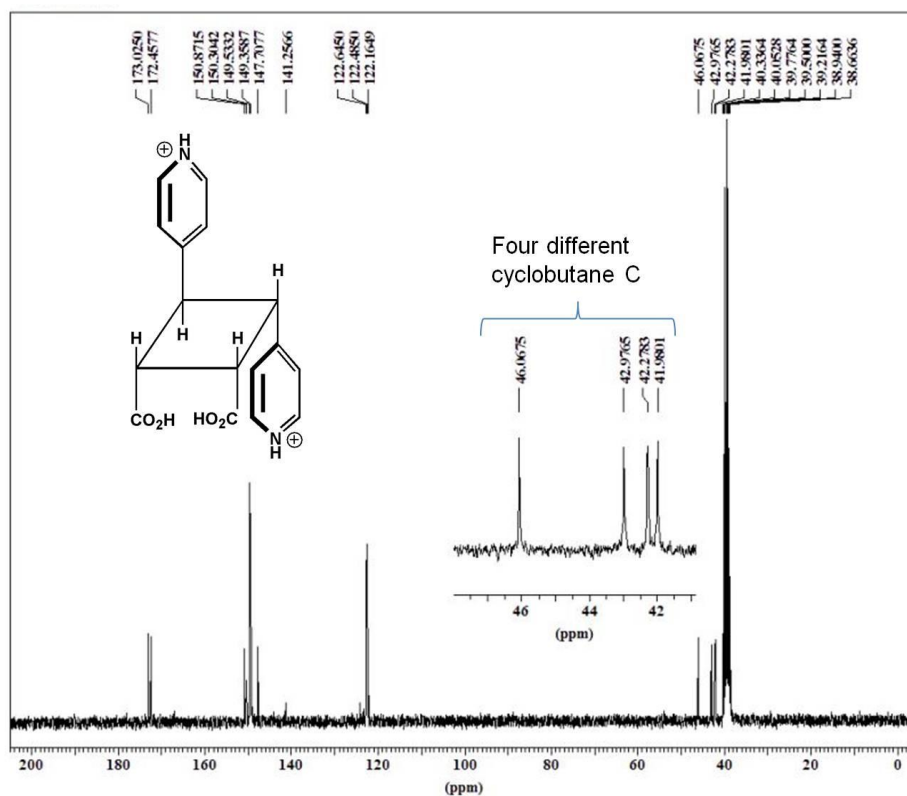
Figure A9: ^{13}C-NMR (75 MHz, d_6-DMSO, 298K) spectrum of *rctc*-HH-BPCD salt. There are four different types of cyclobutane carbons instead of two for *rctt*-form.
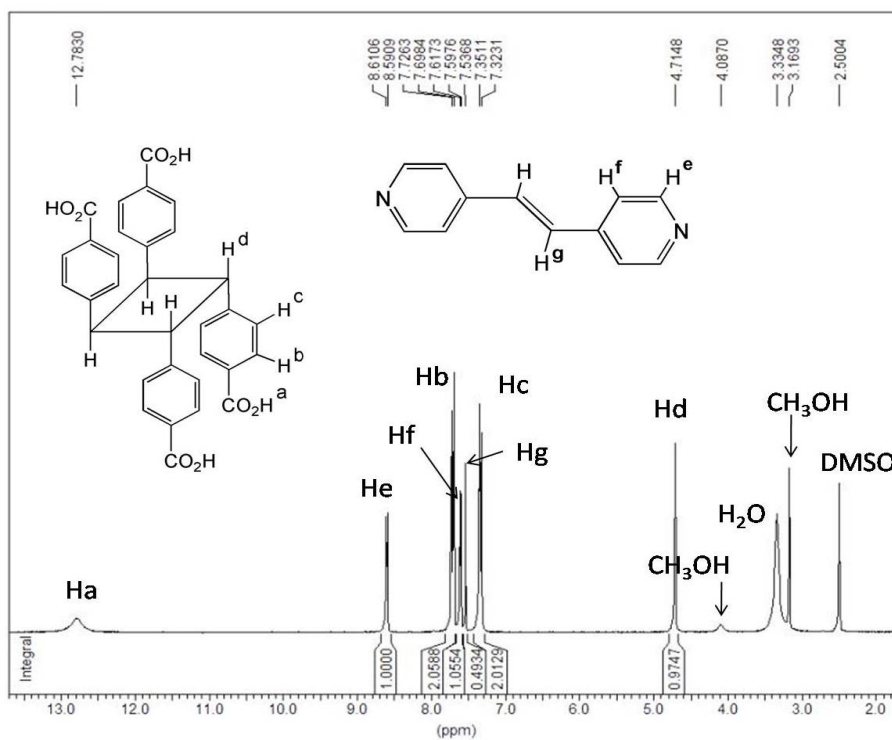
Figure A10: ^{1}H NMR (300 MHz, d_6-DMSO, 298K) spectrum of the co-crystals **44**. Integral values show the ratio of TCCB and 4,4'-bpe is 1:1.
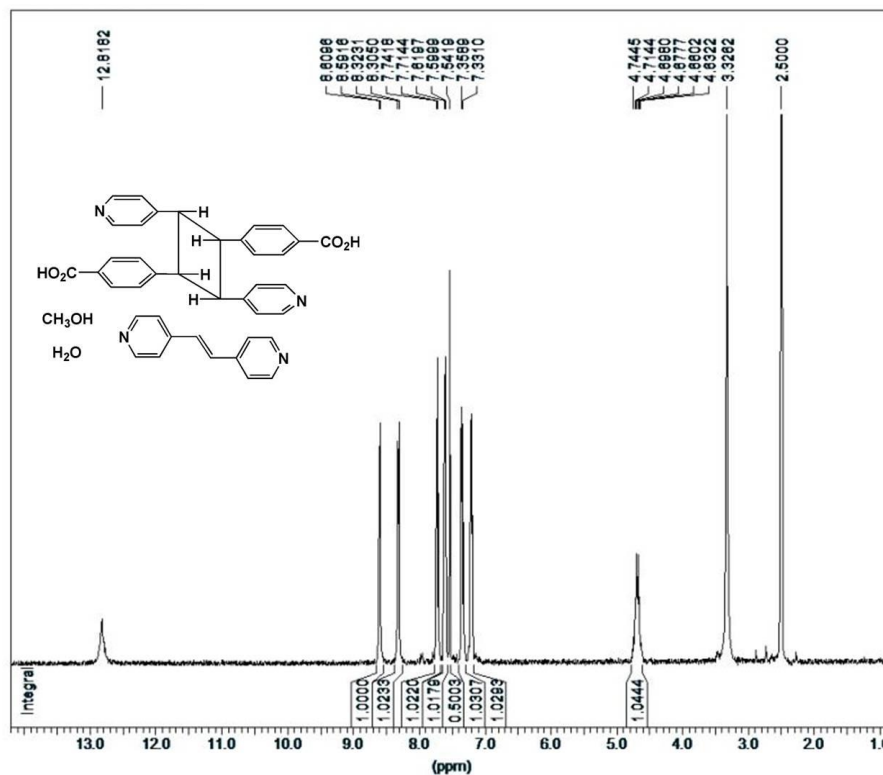
Figure A11: ^{1}H NMR (300 MHz, d_6-DMSO, 298K) spectrum of the co-crystals **49**. Integral values show the ratio of HT-4,4-BPBCCB and 4,4'-bpe is 1:1.

<div align="center">

Appendix II

</div>

A part of my work during this candidature was published in *New Journal of Chemistry* as a part the themed issue 'Coordination polymers: structure and function'. The work is not included in this thesis and therefore, the published materials are given in this appendix.

Solvent-free porous framework resulted from 3D entanglement of 1D zigzag coordination polymer†

Goutam Kumar Kole [a], Amy J. Cairns [b], Mohamed Eddaoudi *[bc] and Jagadese J. Vittal *[a]

[a]*Department of Chemistry, National University of Singapore, 3 Science Drive 3, Singapore-117543. E-mail: chmjjv@nus.edu.sg; Fax: +65 6779 1691; Tel: +65 6516 2975*

[b]*Department of Chemistry, University of South Florida, 4202 East Fowler Avenue (CHE205), Tampa, Florida 33620, USA*

[c]*KAUST Advanced Membranes & Porous Materials Center, Chemical and Life Sciences and Engineering Division, King Abdullah University of Science and Technology, Thuwal 23955-6900, Kingdom of Saudi Arabia. E-mail: mohamed.eddaoudi@kaust.edu.sa*

A solvent-free porous metal organic framework is constructed by the 3D entanglement of 1D zigzag coordination polymeric chains. The role of solvents and the effect of reaction conditions on such unique entanglement are addressed.

Porous coordination polymers (PCPs) or metal organic frameworks (MOFs) have now become a fascinating class of materials[1] from both the fundamental and application point of view.[2] The very interesting topologies of the frameworks inspire the creative minds of the researchers to enrich the field with new materials of versatile topologies. These materials serve various potential applications including gas storage,[3] separation,[4] ion exchange,[5] catalysis[6] and drug delivery.[7] The self-assembly of metal-ion centers bridged through multi-dentate ligands often reveals extended polymeric networks with void spaces that are ideally suited for such applications. However, the available free volume is often occupied by solvent and/or guest molecules, which must be exchanged in order to exploit the porous features of these materials. The desolvated MOFs may or may not retain the crystallinity, leave alone the single crystal nature of the material.[2a–c,8] Hence, only a few examples are

known in the literature for solvent-free single crystals which have been obtained after the removal of the solvents from solvent -filled MOFs. Thus designing a PCP without any solvent molecule in its pores has proven to be a continuous challenge, as '*nature abhors void space*'. Interpenetration often occurs during the propagation of the network to obstruct the formation of the void space in the materials.[9] Using chelating ligands along with the spacers is a well-known strategy to stop the interpenetration to take place but it often reduces the dimensionality of the frameworks. Although the sorption properties of 2- and 3-periodic frameworks have been extensively studied, the use of one periodic framework materials for this purpose is scarce,[10] as single chains tend to pack separately and fail to form porous channels. Despite forming porous channels completely filled with solvent molecules, the frameworks collapse upon removal of the solvent, thus devoid of any gas/solvent exchange application. The formation of porous channels in 1D zigzag coordination polymer is only possible when three or more single chains propagate in different and non-coplanar directions to undergo rare 3D entanglements. 'Warp-and-woof' like interwoven molecular fabric structures are known to form via the 2D entanglement of 1D coordination polymeric strands.[11] Entanglement via H-bonding, extensive interchain π–π stacking and C–H$\cdots\pi$ interactions often enhances the robustness of the networks upon guest removal.[12–14]

Recently, Gao and co-workers have documented the first example of '*hierarchical entanglement*' of 1D zigzag chain that resulted in a robust microporous framework.[13] The 1D zigzag coordination chains of **1**·DMSO (**1** = [Zn(phen)(SDC)]$_n$, where phen = 1,10-phenanthroline, H$_2$SDC = *trans*-4,4′-stilbenedicarboxylic acid) were found to propagate in four different directions to undergo 3D entanglement via π–π interactions. Accordingly, this led to the formation of a rare 3D interwoven framework. Wang and co-workers reported 1D zigzag chains of same composition, synthesized by hydrothermal method , with a different structure where the zigzag chains propagate in two non-coplanar directions that resulted in three-dimensional polycatenated network.[14] The authors who reported **1**·DMSO[13] had anticipated that DMSO might have played the role of a template in that reaction condition to result such unique 3D entanglement that resulted in a microporous framework. It is well known that experimental conditions influence the nature of overall topology. Hence, we have revisited the system to investigate the role of DMSO in this 3D-entanglement.

We have successfully synthesized§ [Zn(phen)(SDC)]$_n$, **2**, the same 1D zigzag chains (Fig. 1) with the same connectivity and entanglement as in **1** but from a

different reaction condition without any lattice solvent molecule. The structure was refined in the tetragonal space group,[¶] *P4/ncc* where the Zn(II) ion occupies a distorted octahedral centre and coordinated by a chelating phen ligand and two chelating carboxylate groups from two different SDC ligands. The SDC ligand lies about an inversion centre and a 2-fold axis passes through Zn(II) bisecting phen. The chelate modes of SDCs are highly asymmetric with unequal Zn···O distances 1.960(4) and 2.598(4) Å. The coordination geometry around Zn can be described as a distorted trigonal prism where the corner angle is 118.2°.
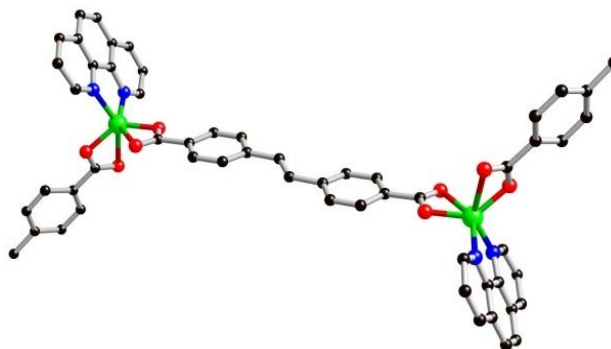

Fig. 1 A fragment of the 1D zigzag coordination chain in **2**

The zigzag chains of the coordination polymer propagate in four different non-coplanar directions around the crystallographic four-fold axes in the [001] direction to generate an interwoven framework (see ESI†). The chains are entangled via strong π–π interactions between the aromatic rings of the phen and SDC ligands that lead to the formation of a robust microporous framework. The total potential solvent area volume is 797.4 Å^3 (15.8% per unit cell volume), as calculated by PLATON.[15] The void channels of diameter 6 Å (distance between the centers of the diagonal hydrogen atoms in the channel) that are readily available to host gases or solvents (Fig. 2) are passing through the [001] direction. The absence of solvent or guest molecules in **2** was also confirmed by thermogravimetry which shows no weight loss from room temperature up to 350 °C. A quick comparison between the structures of **1**·DMSO and **2** reveals that the diameter of the channel is reduced from 6.304 to 6.056 Å while the Zn–O1 distance increased from 1.939(3) to 1.960(4) Å upon removal of the solvent. Since the data collections for the two structures were done at two different temperatures (293 and 223 K respectively) these differences may not mean much.
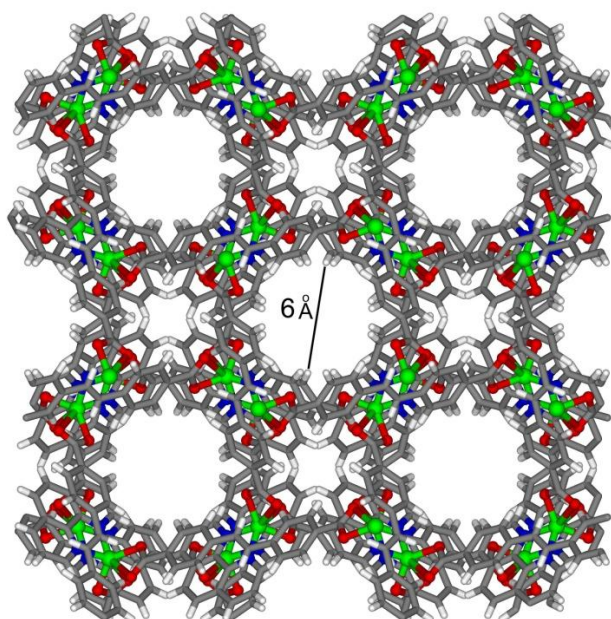
Fig. 2 Solvent-free porous channels along [001] direction

When the sample **2** was immersed in DMSO for 3 days, one equivalent of the solvent was sorbed into the channels, that was measured by thermogravimetric analysis. The PXRD pattern after DMSO sorption of the samples exactly matches with the simulated pattern for **1**·DMSO (Fig. 3). Although the attempt to observe the process via single-crystal to single-crystal failed, the conversion from **2** to **1**·DMSO was found to be complete and reversible. The observed cell data‖ after 12 h immersion of the sample **2** in DMSO clearly indicate the contraction of *a* and *b* values and the expansion of *c* value. When the sample **2** was immersed in DMF, 0.5 equivalent DMF was found to be sorbed in after 4 days as indicated by the TGA experiment (see ESI†). Xylene is bulkier than toluene but the data shows higher uptakes for xylene (any noticeable changes in the PXRDs). The hydrophobic channels in **2** were also found to sorb small guest molecules like 1.8 equivalent of cyclohexane, 1.8 equivalent of benzene, 2.3 equivalent of toluene and 3.5 equivalent of xylene upon immersing the sample in respective solvents, as estimated by TGA experiment (see ESI†). However, **2** was found not to sorb any water, methanol and ethanol molecules in its channels. This could be due to the hydrophobic nature of the channels, or the solvent molecules trapped initially may have escaped rapidly when the crystals were taken out of the mother liquor.
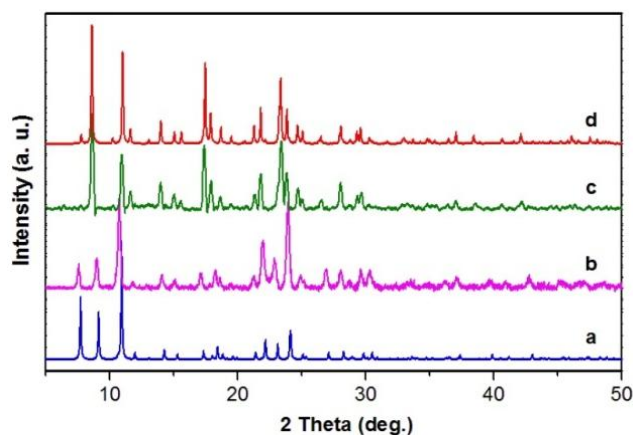
Fig. 3 PXRD patterns: (a) simulated pattern for **2**; (b) observed pattern for as-synthesized sample **2**; (c) for **2**·DMSO after **2** was immersed in DMSO for 3 days; (d) simulated pattern for **1**·DMSO[13a]

The presence of narrow open channels in **2** prompted us to evaluate its potential gas sorption properties. The solvent-free as-synthesized compound was initially evacuated at room temperature for 24 h and subsequently heated to 100 °C for 8 h. The permanent microporosity of **2** was confirmed from the argon type I adsorption isotherm which revealed an apparent BET and Langmuir surface areas of 220 and 349 $m^2 g^{-1}$, respectively (see ESI†). The estimated experimental pore volume was determined to be 0.10 $cm^3 g^{-1}$, as obtained using the Dubinin–Radushkevich (D–R) equation. The hydrogen capacity at 77 K (0.49 wt%) is low (Fig. 4); however, this creates a new landmark for the sorption studies on the 1D zigzag coordination polymers. The creation of solvent free porous channels by a complicated 3D entanglement of single zigzag chains is unique.

Interestingly, the isosteric heat of adsorption has an estimated value of 7.0 kJ mol^{-1} at the lowest coverage and remains constant until approximately 0.2 wt% (see ESI†). This observation can be explained by the presence of narrow pores which promote stronger adsorbate–adsorbent interactions because the adsorption potentials of neighboring walls overlap. On the other hand, at higher loadings these sites are occupied and weaker adsorbate–adsorbate interactions are predominate, hence the slight decrease in the isosteric heat of adsorption.
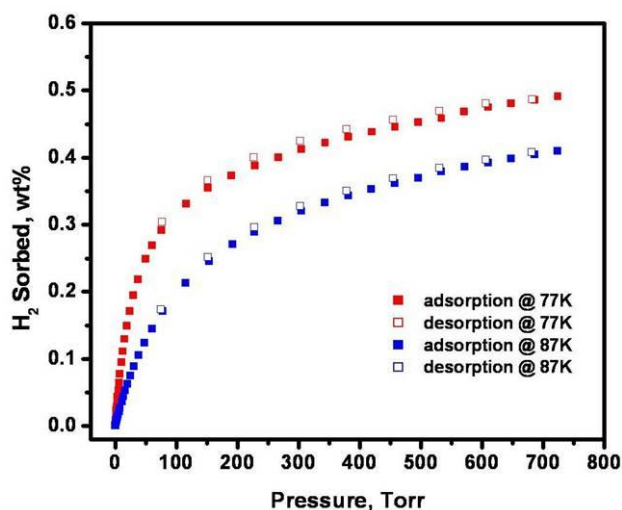
Fig. 4 H_2 adsorption isotherm at 77 and 87 K

In another experiment, equivalent amount of reactants were mixed and stirred in a mixture of solvents water, ethanol and methanol for an hour at room temperature.** The resulting product (here we denote **3**) has the same structure as **2**, as was evidenced by PXRD patterns (see ESI†). When the same reactants are mixed and stirred in DMSO at room temperature, the PXRD pattern of the resulting compound matches with **1**·DMSO (see ESI†). These observations conclude that the 3D entanglement that leads to microporosity in the aforementioned system can be achieved simply by mixing the reactants in stoichiometric amounts. We anticipate that neither the reaction condition (temperature and pressure in solvothermal method) nor the solvent played any template effect for the entanglement. It might be the Nature's selection for this particular system as none other 1D zigzag coordination polymer obtained from SDC shows this property.[16]

The results presented herein raise two important and interesting questions: (1) is it possible to synthesize solvent-free PCPs in general or is this observation an isolated special case? (2) Is there any restriction to the pore size that can still exist without guest molecule? Research is in progress towards understanding these issues in the formation of solvent-free PCPs. In conclusion, we have presented a very unique 1D zigzag coordination polymer with solvent-free porous channels for the first time, constructed by 3D entanglement and stabilized by interchain π–π stacking interactions. The solvent and gas sorption properties are thus discussed.

Notes and references

† Electronic supplementary information (ESI) available: Additional structural diagrams, TGA, and PXRD patterns. CCDC reference number 770990. For ESI and crystallographic data in CIF or other electronic format see DOI: 10.1039/c0nj00217h.

‡ This article is part of a themed issue on Coordination polymers: structure and function.

§ Synthesis of **2**: triethyl amine salt of H_2SDC (0.0134 g, 0.05 mmol) in ethanol was carefully layered over 1 : 1 mixture of $Zn(NO_3)_2$ (0.0149 g, 0.05 mmol in 0.5 ml H_2O) and 1,10-phenanthroline monohydrate (0.0099 g, 0.05 mmol, 0.5 ml MeOH) using methanol as buffer layer in a long test tube. Octahedral shaped, colourless single crystals were obtained after 2 days and were used for X-ray diffraction analysis. Yield 0.02 g, 78%. Analysis found: C, 65.58; H, 3.48; N, 5.69, $C_{56}H_{36}N_4O_8Zn_2$ requires: C, 65.70; H, 3.54; N, 5.47%.

¶ Crystal data for **2** at 223 K: $C_{28}H_{18}N_2O_4Zn$, $M = 511.83$, tetragonal, space group $P4/ncc$, $a = 16.1598(4)$, $c = 19.3303(11)$ Å, $V = 5047.9(3)$ Å^3, $Z = 8$, $D_{calc} = 1.347$ g cm^{-3}, $\mu = 1.008$ mm^{-1}, GOF = 1.047, Final $R_1 = 0.0784$, w$R_2 = 0.2385$ [for 2221 data $I > 2\sigma(I)$].

|| The observed cell data after 12 h immersion of **2** into DMSO (incomplete conversion) were as: $a = 16.129$, $c = 19.547$ Å, and $V = 5085.2$ Å^3. The contraction in a and b but the expansion in c and V clearly indicate that **2** slowly converted to **1**·DMSO.

** Synthesis of **3**: H_2SDC (0.268 g, 1 mmol) was dissolved in 8 ml water with the addition of triethyl amine and then was mixed with a mixture of $Zn(NO_3)_2$ (0.298 g, 1 mmol in 12 ml ethanol) and 1,10-phenanthroline (0.198 g, 1 mmol in 12 ml methanol). The resulting mixture was stirred for an hour and then the white powder was collected by filtration and dried. The structure was determined by comparing PXRD patterns with **2**

1   K. Biradha, A. Ramanan and J. J. Vittal, *Cryst. Growth Des.*, 2009, **9**, 2969.

2   Some reviews: (*a*) S. Kitagawa and K. Uemura, *Chem. Soc. Rev.*, 2005, **34**, 109; (*b*) S. Kitagawa, R. Kitaura and S. Noro, *Angew. Chem., Int. Ed.*, 2004, **43**, 2334; (*c*) S. Kitagawa and R. Matsuda, *Coord. Chem. Rev.*, 2007, **251**, 2490; (*d*) J. L. C.

Rowsell and O. M. Yaghi, *Microporous Mesoporous Mater.*, 2004, **73**, 3; (*e*) N. L. Rosi, M. Eddaoudi, J. Kim, M. O'Keeffe and O. M. Yaghi, *CrystEngComm*, 2002, **4**, 401.

3   (*a*) M. Eddaoudi, J. Kim, N. Rosi, D. Vodak, J. Wachter, M. O'Keeffe and O. M. Yaghi, *Science*, 2002, **295**, 469; (*b*) N. L. Rosi, J. Eckert, M. Eddaoudi, D. T. Vodak, J. Kim, M. O'Keeffe and O. M. Yaghi, *Science*, 2003, **300**, 1127; (*c*) H. Chun, D. N. Dybtsev, H. Kim and K. Kim, *Chem.–Eur. J.*, 2005, **11**, 3521; (*d*) L. Ma, D. J. Mihalcik and W. Lin, *J. Am. Chem. Soc.*, 2009, **131**, 4610; (*e*) M. Dincă and J. R. Long, *Angew. Chem., Int. Ed.*, 2008, **47**, 6766; (*f*) A. C. McKinlay, B. Xiao, D. S. Wragg, P. S. Wheatley, I. L. Megson and R. E. Morris, *J. Am. Chem. Soc.*, 2008, **130**, 10440; (*g*) J. Luo, H. Xu, Y. Liu, Y. Zhao, L. L. Daemen, C. Brown, T. V. Timofeeva, S. Ma and H.-C. Zhou, *J. Am. Chem. Soc.*, 2008, **130**, 9626; (*h*) L. J. Murray, M. Dincă and J. R. Long, *Chem. Soc. Rev.*, 2009, **38**, 1294; (*i*) J. Moellmer, E. B. Celer, R. Luebke, A. J. Cairns, R. Staudt, M. Eddaoudi and M. Thommes, *Microporous Mesoporous Mater.*, 2010, **129**, 345; (*j*) F. Nouar, J. F. Eubank, T. Bousquet, L. Wojtas, M. Zaworotko and M. Eddaoudi, *J. Am. Chem. Soc.*, 2008, **130**, 1833.

4   (*a*) D. N. Dybtsev, H. Chun, S. H. Yoon, D. Kim and K. Kim, *J. Am. Chem. Soc.*, 2004, **126**, 32; (*b*) D. Bradshaw, T. J. Prior, E. J. Cussen, J. B. Claridge and M. J. Rosseinsky, *J. Am. Chem. Soc.*, 2004, **126**, 6106.

5   (*a*) K. S. Min and M. P. Suh, *J. Am. Chem. Soc.*, 2000, **122**, 6834; (*b*) O. M. Yaghi and H. Li, *J. Am. Chem. Soc.*, 1996, **118**, 295; (*c*) F. Nouar, J. Eckert, J. F. Eubank, P. Forster and M. Eddaoudi, *J. Am. Chem. Soc.*, 2009, **131**, 2864; (*d*) T. K. Maji, R. Matsuda and S. Kitagawa, *Nat. Mater.*, 2007, **6**, 142.

6   (*a*) J. S. Seo, D.-M. Whang, H.-Y. Lee, S. I. Jun, J.-H. Oh, Y.-J. Jeon and K. Kim, *Nature*, 2000, **404**, 982; (*b*) T. Sawaki and Y. Aoyama, *J. Am. Chem. Soc.*, 1999, **121**, 4793; (*c*) M. Fujita, Y.-J. Kwon, S. Washizu and K. Ogura, *J. Am. Chem. Soc.*, 1994, **116**, 1151; (*d*) J. Y. Lee, O. K. Farha, J. Roberts, K. A. Scheidt, S. T. Nguyen and J. T. Hupp, *Chem. Soc. Rev.*, 2009, **38**, 1450.

7   (*a*) P. Horcajada, C. Serre, G. Maurin, N. A. Ramsahye, F. Balas, M. Vallet-Regí, M. Sebban, F. Taulelle and G. Férey, *J. Am. Chem. Soc.*, 2008, **130**, 6774; (*b*) P. Horcajada, T. Chalati, C. Serre, B. Gillet, C. Sebrie, T. Baati, J. F. Eubank, D. Heurtaux, P. Clayette, C. Kreuz, J.-S. Chang, Y. K. Hwang, V. Marsaud, P.-N.

Bories, L. Cynober, S. Gil, G. Ferey, P. Couvreur and G. Ruxandra, *Nat. Mater.*, 2010, **9**, 172; (*c*) A. C. McKinlay, B. Xiao, D. S. Wragg, P. S. Wheatley, I. L. Megson and R. E. Morris, *J. Am. Chem. Soc.*, 2008, **130**, 10440.

8   (*a*) T. Min, B. Zheng, J. Bai, R. Sun, Y. Li and Z. Zhang, *CrystEngComm*, 2010, **12**, 70; (*b*) R. Sun, S. Wang, H. Xing, J. Bai, Y. Li, Y. Pan and X. You, *Inorg. Chem.*, 2007, **46**, 8451; (*c*) S. Hasegawa, S. Horike, R. Matsuda, S. Furukawa, K. Mochizuki, Y. Kinoshita and S. Kitagawa, *J. Am. Chem. Soc.*, 2007, **129**, 2607.

9   (*a*) C. A. Bauer, T. V. Timofeeva, T. B. Settersten, B. D. Patterson, V. H. Liu, B. A. Simmons and M. D. Allendorf, *J. Am. Chem. Soc.*, 2007, **129**, 7136; (*b*) O. M. Yaghi, *Nat. Mater.*, 2007, **6**, 92; (*c*) S. R. Batten and R. Robson, *Angew. Chem., Int. Ed.*, 1998, **37**, 1460.

10 (*a*) E. Y. Lee and M. P. Suh, *Angew. Chem., Int. Ed.*, 2004, **43**, 2798; (*b*) H. R. Moon, J. H. Kim and M. P. Suh, *Angew. Chem., Int. Ed.*, 2005, **44**, 1261; (*c*) C.-D. Wu and W. Lin, *Dalton Trans.*, 2006, 4563; (*d*) S. Takamizawa, E.-I. Nakata, H. Yokoyama, K. Mochizuki and W. Mori, *Angew. Chem., Int. Ed.*, 2003, **42**, 4331; (*e*) S. Hu, K.-H. He, M.-H. Zeng, H.-H. Zou and Y.-M. Jiang, *Inorg. Chem.*, 2008, **47**, 5218; (*f*) G. Li, C. Zhu, X. Xi and Y. Cui, *Chem. Commun.*, 2009, 2118; (*g*) S. Noro, D. Tanaka, H. Sakamoto, S. Shimomura, S. Kitagawa, S. Takeda, K. Uemura, H. Kita, T. Akutagawa and T. Nakamura, *Chem. Mater.*, 2009, **21**, 3346.

11 (*a*) A. M. P. Peedikakkal and J. J. Vittal, *Cryst. Growth Des.*, 2008, **8**, 375; (*b*) L. Carlucci, G. Ciani, A. Gramaccioli, D. M. Proserpio and S. Rizzato, *CrystEngComm*, 2000, **2**, 154; (*c*) Y.-H. Li, C.-Y. Su, A. M. Goforth, K. D. Shimizu, K. D. Gray, M. D. Smith and H.-C. zur Loye, *Chem. Commun.*, 2003, 1630.

12 (*a*) L. Han and Y. Zhou, *Inorg. Chem. Commun.*, 2008, **11**, 385; (*b*) H.-D. Guo, D.-F. Qiu, X.-M. Guo, G.-L. Zheng, X. Wang, S. Dang and H.-J. Zhang, *CrystEngComm*, 2009, **11**, 2425.

13 (*a*) A.-L. Cheng, N. Liu, Y.-F. Yue, Y.-W. Jiang, E.-Q. Gao, C.-H. Yanb and M.-Y. He, *Chem. Commun.*, 2007, 407; (*b*) A.-L. Cheng, Y. Ma, J.-Y. Zhang and E.-Q. Gao, *Dalton Trans.*, 2008, 1993.

14 X.-L. Wang, C. Qin, E.-B. Wang and L. Xu, *Cryst. Growth Des.*, 2006, **6**, 2061.

15 A. L. Spek, *PLATON, a multipurpose crystallographic tool*, University of Utrecht, Utrecht, The Netherlands, 2003.

16 (*a*) X.-L. Wang, C. Qin, E.-B. Wang, L. Xu, Z.-M. Su and C.-W. Hu, *Angew. Chem., Int. Ed.*, 2004, **43**, 5036; (*b*) Y. Ma, A.-L. Cheng, J.-Y. Zhang, Q. Yue and E.-Q. Gao, *Cryst. Growth Des.*, 2009, **9**, 867; (*c*) H.-Y. Wang, S. Gao, L.-H. Huo and J.-G. Zhao, *Acta Crystallogr., Sect. E: Struct. Rep. Online*, 2006, **62**, m3395.